Graduate Theses, Dissertations, and Problem Reports

2001

Effect of pretreatment on the performance of metal contaminated commercial FCC catalyst

Oguz Bayraktar
West Virginia University

Follow this and additional works at: https://researchrepository.wvu.edu/etd

EFFECT OF PRETREATMENT
ON
THE PERFORMANCE OF METAL CONTAMINATED
COMMERCIAL FCC CATALYST

Oguz Bayraktar

Dissertation submitted to the
College of Engineering and Mineral Resources
at West Virginia University
in partial fulfillment of requirements
for the degree of

Doctor of Philosophy
in
Chemical Engineering

Edwin L. Kugler, Ph.D., Chair.
Dady B. Dadyburjor, Ph.D.
Howard F. Moore, M.S.
Alfred H. Stiller, Ph.D.
John H. Penn, Ph.D.

Department of Chemical Engineering

Morgantown, West Virginia
2001

Keywords: FCC catalyst, TPR, TPO, pretreatment, coke characterization, AFM

ABSTRACT

EFFECT OF PRETREATMENT
ON
THE PERFORMANCE OF METAL CONTAMINATED
COMMERCIAL FCC CATALYST

Oguz Bayraktar

The performance of fluid catalytic cracking (FCC) catalyst decreases due to the severe negative effects of metal contaminants (e.g., nickel, vanadium and iron) deposited on the catalyst from the hydrocarbon feed. The metal contaminants cause an increase in the production of gas and coke at the expense of gasoline.

In this work the effect of pretreatment with hydrogen and methane gases on the performance of commercial, metal-contaminated, FCC equilibrium catalysts was investigated. Cracking reactions of both sour imported heavy gas oil (SIHGO) and n-hexadecane were carried out in a microactivity test (MAT) unit using three commercial equilibrium catalysts with different metals concentrations. These catalysts were also characterized by temperature-programmed reduction (TPR), temperature-programmed oxidation (TPO), surface area measurements (BET/T-Plot), atomic force microscopy (AFM), and scanning electron microscopy in combination of elemental analysis by EDX (SEM-EDX). The characterization data were used in the interpretation of the MAT results.

MAT results have shown that pretreatment of catalysts with hydrogen and methane prior to cracking reactions decreases the yields of hydrogen and coke from gas oil cracking with a significant increase in gasoline yield. The effect of pretreatment was found to be more pronounced with highly contaminated equilibrium catalyst, as compared to the catalysts with low metal concentrations. The decrease in hydrogen and coke yields with pretreatment was attributed to the lower dehydrogenation activity of reduced vanadium compared to oxidized vanadium.

TPR results helped to explain the effect of pretreatment on the catalyst activity. The observed TPR spectra of commercial equilibrium catalysts were deconvoluted into three peaks. The reduction of NiO and V_2O_5 contributed mainly to the low temperature peak at around 525 °C whereas nickel aluminate and silicate type compounds contributed to the high temperature peak at around 820 °C. The intermediate peak at around 690 °C was attributed to the reduction of excess vanadium oxides on the catalyst. Enhancement of catalyst performance coincides with the disappearance of peak at around 690 °C in the TPR profile, after pretreatment with hydrogen at 700 °C. This suggests that the vanadium oxides represented by this intermediate peak have high dehydrogenation activities during cracking reactions.

TPO experiments were carried out to determine the nature, location and composition (carbon and hydrogen content) of the coke on the spent catalysts. TPO profiles of spent equilibrium catalysts from the cracking of SIHGO were deconvoluted into four peaks (Peak K, L, M and N). The location of TPO peaks shifted to lower temperatures with increasing metal concentrations on the catalyst. This was due to the catalytic effects of metals (e.g., vanadium and nickel) on the

oxidation reaction. Peak L in the TPO spectrum was assigned to the "contaminant" coke in the vicinity of metals.

TPO spectra of the spent highly contaminated catalyst pretreated with hydrogen and methane prior to cracking reactions have shown that the size of the Peak L decreases significantly, as compared to the same non-pretreated catalyst. However, the changes in the sizes of the Peak L were not significant for the catalysts with low metal concentrations. This further explains the improvement of catalyst performance with pretreatment by reducing the "contaminant" coke.

The surface area measurements before and after cracking reactions identified the location of coke on spent catalyst. Surface area measurements indicated that the coke formed during cracking reactions preferentially deposits in the micropores of the catalyst without blocking the larger pores of catalyst.

Surface characteristics of catalysts were studied using AFM. Roughness of surface decreased with increasing metal concentrations on the catalyst. AFM images have revealed the presence of debris on the catalyst surface. Iron was detected in some of these debris using SEM-EDS analysis. Additional work should be done to identify the exact nature of these surface structures.

ACKNOWLEDMENTS

I would like to express my special thanks to the following people:

- Dr. Edwin L. Kugler, my research advisor, for his advice, guidance, criticism, valuable corrections, and support throughout this study.

- Mr. Howard F. Moore, Ashland Marathon LLC, for his helpful discussions and for providing the equilibrium FCC catalyst samples used in this study.

- Dr. Nigel Clark, Dr. Alfred H. Stiller, Dr. Aubrey L. Miller, Dr. John H. Penn and Dr. Dady B. Dadyburjor for their academic expertise, constructive comments and suggestions.

- Mr. James Hall for his technical assistance in almost every stage of the project.

- My family for their support and encouragement throughout the course of my education.

TABLE OF CONTENTS

LIST OF TABLES

LIST OF FIGURES

1.0 INTRODUCTION

The fluid catalytic cracking (FCC) process is used for the conversion of relatively high - boiling hydrocarbons to lighter hydrocarbons boiling in the heating oil and gasoline (or lighter) range. In recent years, to take full advantage of today's marketing opportunities, some refiners are blending residua with their gas oil feed stock (Gall et al., 1982; Logwinuk et al., 1981). In fact, the majority of recent cracking expansions have been designed to process residual oil exclusively. In response to the demand for catalyst for these crackers, manufacturers are designing and developing specific catalyst that have good hydrothermal stability, high metal tolerance, and good bottoms upgrading (Woltermann et al., 1996).

A common problem in FCC processing is the gradual deterioration of the catalyst due to the deposition of metal contaminants, such as nickel, vanadium and iron, contained in the hydrocarbon feed on the catalyst. FCC when combined with effective catalyst demetalization provides a profitable means of converting the bottom of the barrel to useful products. High metal content crude oils can be processed without economic penalty. This greatly extends the range of crude oils, which can be used by refiners. Various factors such as changing crude sources, residual oil price structures, and shifts in product market demand have made residual conversion to lighter products an economically attractive option for many refiners. When residual oil is added to an FFC unit, the severe negative effects of metal poisoning of cracking catalyst are observed. For example, gasoline yield decreases while the yields of coke and gas increase. The effects of nickel, vanadium and other heavy metals on activity and selectivity of FCC catalysts are discussed in detail by Cimbalo et al. (1972).

In the catalytic cracking of hydrocarbon feedstocks, particularly heavy feedstocks, vanadium, nickel and/or iron become deposited as a nonvolatile compound on the cracking catalyst

1

promoting excessive hydrogen and coke makes. These deposited metal contaminants are not removed during conventional catalyst regeneration operations during which coke deposits on the catalyst are converted to CO and CO_2. While it would be ideal to remove these contaminants, such procedures are usually quite elaborate and expensive. A simpler approach is to neutralize or passify the metals present on the catalyst. Such a procedure does not necessarily restore the full clean catalyst activity (since metals may still block a percentage of the catalyst sites), but is quite helpful in lowering hydrogen gas production which can overload gas compressors and in reducing coke on the catalyst resulting from active metal influences.

The major objective of this research is to understand the effect of pretreatment on commercial, metals-contaminated, FCC equilibrium catalysts. We are interested in the differences in activity and product distribution between catalyst that was reduced prior to contacting feed and catalyst that has been fully oxidized during regeneration. The experiments involve the pretreatment of equilibrium catalyst with hydrogen or methane prior to gas oil cracking to see the effect of hydrogen and methane as a reducing gas on catalyst performance. The goals of this study can be summarized as follows:

1- To characterize the reduction of FCC catalyst using hydrogen or methane gases.

2- To determine the effect of catalyst reduction on cracking activity and selectivity.

2.0 LITERATURE REVIEW

2.1 Catalytic Cracking

2.1.1 History of Catalytic Cracking

Catalytic cracking -- conversion of large petroleum molecules into smaller hydrocarbons primarily in the gasoline, light, and heavy cycle oil ranges -- is one of the largest scale catalytic processes practiced. Catalytic cracking started around 1936 by utilizing chemically treated natural clays as catalysts (Reichle, 1988). The most important development in cracking technology has been the introduction of zeolite containing catalyst, mainly the wide pore faujasite family (X- and Y-type) in the early 1960's. This catalyst development increased reaction rates and improved selectivities to gasoline and $C_3 - C_4$ hydrocarbons. Catalyst and process configuration as well as the economics of the process has changed. The old fashion fixed-bed technology was replaced by the more modern and highly efficient fluidized-bed technology. Numerous FCC process changes such as shorter contact time (vertical riser reactor) and higher reactor temperature to take full advantage of the improved catalyst activity and thermal stability were implemented.

A typical FCC complex may be divided into three main sections; a) Reactor-riser, b) Regenerator-flue gas handling, and c) Product Fractionation. Figure 2.1 presents a FCC complex and Figure 2.2 shows the location of the FCC unit in a typical refinery scheme (Venuto et al., 1979). Almost any crude fraction can be feed to a FCC unit. However, in Figure 2.1 the feed to the FCC unit consists mainly of heavy straight run naphtha, heavy vacuum gas oil, and hydro-treated, solvent-deasphalted, vacuum residue. Cracked products of FCC unit are mainly
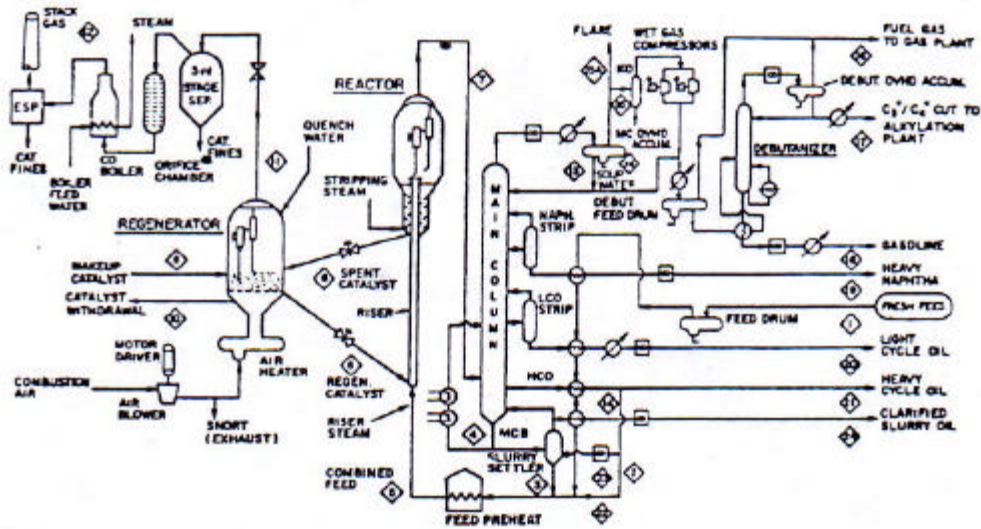
Figure 2.1 Modern Short Contact Time Riser FCC Complex (Venuto et al., 1979)
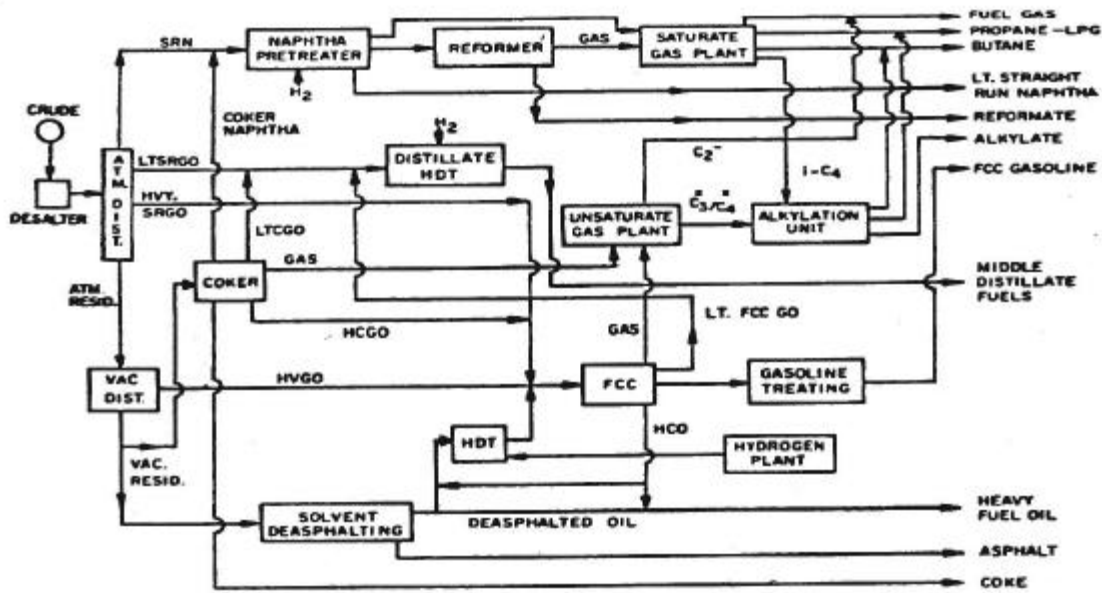
Figure 2.2 Conceptual Gasoline-oriented Refinery Featuring Catalytic Cracking and Alkylation (Venuto et al., 1979)

gasoline, heavy cycle oil, light gas oil, and C_5^- gaseous hydrocarbons along with hydrogen. The coke deposited on the catalyst is utilized as an energy source to maintain the heat balance of the FCC unit. This is carried out in the regenerator, so that the catalyst activity is restored and heat is produced.

2.1.2 Chemistry of Catalytic Cracking

A series of complex reactions are involved in catalytic cracking operations. These reactions include carbon-carbon bond scission, as well as isomerization, alkylation, dehydrogenation, etc. The complex chemistry of catalytic cracking is caused by several factors, such as feed composition and contaminants, catalyst formulations, the type of reaction under certain FCC conditions (e.g., cracking, dimerization, oligomerization, hydrogen transfer), and the operating conditions. Final product distribution is significantly determined by the secondary reactions, such as isomerization (isoolefin formation), hydrogen transfer, and alkyl group transfer. For example, cracking catalyzed by silica-alumina gives much lower yields of olefins compared to cracking catalyzed by zeolite catalysts. This is explained by the hydrogen transfer reactions rapidly converting olefins to paraffins and cyclo-paraffins to aromatics. Hydrogen transfer also influences the coke formation and catalyst deactivation (Gates et al., 1979).

A carbenium ion mechanism is usually accepted for the catalytic reactions (Derouane, 1986) in the presence of the cracking catalyst, which is acidic material having Bronsted and Lewis acid sites. Various kinds of carbenium ions having different stabilities can be formed during the FCC process. These ions are primary, secondary and tertiary. Their stability increases from primary to tertiary. After being formed in the feed, carbenium ions can react in several ways; a) crack to smaller molecules, b) react with other molecules, c) isomerize to other forms,

and d) react with catalyst to stop the chain. The chain of carbenium ion reactions is presented in

Figures 2.3 and 2.4 (Dawoud et al., 1992).

1 CRACKING

$$RC_A^H \cdot CH_2 \cdot CH_2 CH_2 R' \rightleftharpoons RC^H = CH_2 + CH_2 CH_2 R'$$

β-SCISSION $CH_2 CH_2 R \rightleftharpoons CH_2 CHR$

2 ISOMERIZATION

3 TERMINATION

$RCH_2 \cdot C \cdot CH_3$ $\xrightarrow[\text{H-TRANSFER}]{\text{H}^- \text{ donor}}$ $RCH_2 \cdot CH \cdot CH_3$

H^- ⟵ donor can be another paraffin (or naphthene or coke)
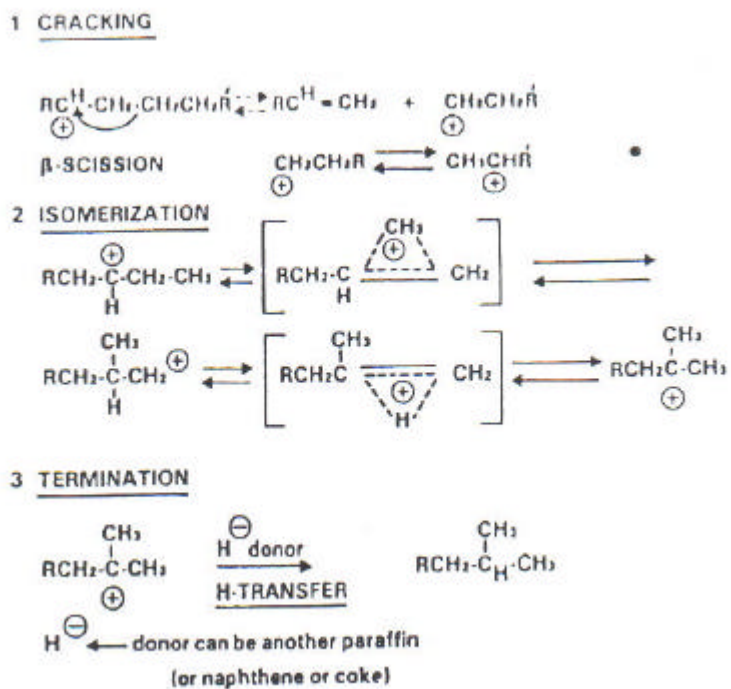
Figure 2.3 Formation of Carbonium Ions (Dawoud et al., 1992)

6
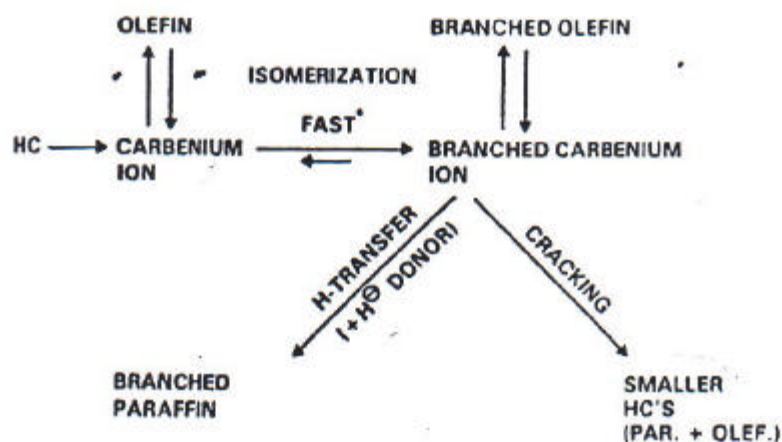
Figure 2.4 Reactions of Carbonium Ions (Dawoud et al., 1992)

2.2 Cracking Catalysts for FCC Process and Their Characteristics

There are two groups of cracking catalysts: amorphous (silica-alumina) catalysts and crystalline (zeolite) catalysts. Amorphous catalyst used in catalytic cracking is a co-gelled mixture of silica and alumina with a relatively high amount of silica. Modern commercial FCC catalysts contain mainly two components; a zeolite "molecular sieve" component and a non-zeolite (amorphous or matrix) component. Both components affect the overall performance of a FCC catalyst and can be present in different proportions (Ritter et al., 1984; Maselli et al., 1984). A tetrahedron having four oxygen anions surrounding a smaller silicon or aluminum ion comprises the fundamental building block of all zeolites. Each of the four oxygen anions is shared with another silica or alumina tetrahedron. The arrangement of the tetrahedral gives zeolites an open framework structure with a well-defined pore structure and high surface area. Rings of oxygen atoms determine the pore diameters in all zeolites. These pores cause diffusional limitations in zeolites. The sodalite units (or the truncated octahedral units) having the silica alumina tetrahedra

7

are the secondary building block of the zeolites used for catalytic cracking. Molecules pass through the twelve membered oxygen rings into these units. Figure 2.5 shows a typical sodalite cage (Gates et al., 1979). The interactions between the zeolite and surrounding matrix are responsible for the higher activity for gas-oil cracking and better selectivity for gasoline production than the silica-alumina catalysts (Gates et al., 1979). The unit cell size and the surface area of zeolite are important parameters in the determination of FCC catalyst activity and product distribution characteristics.

Matrix component consisting of mainly amorphous silica-alumina functions as a selective matrix which works with the molecular sieve portion of the catalyst. The matrix can also be used as "metal trap" for vanadium and nickel present in FCC feed in order to minimize undesirable catalytic effects of these contaminant metals. The matrix is responsible for cracking large molecules, which are too large to fit into the zeolite pores.
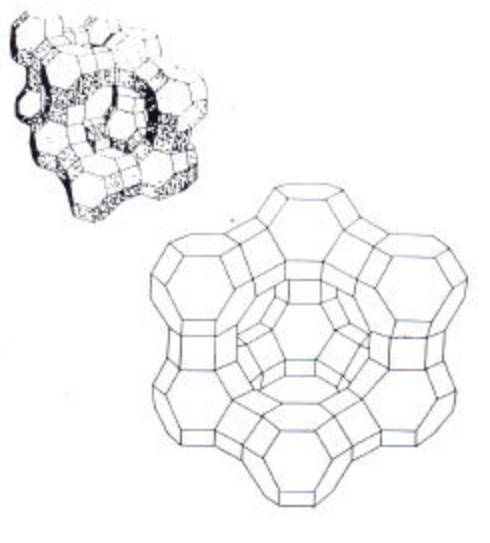
Figure 2.5 Typical Sodalite Cage (Gates et al., 1979)

2.3 Evaluation and Properties of Equilibrium FCC catalysts

Activity of catalyst can be defined as the capability of converting a given feed stock to desired products under certain operating conditions. Catalyst activity decreases due to the losses in surface area, pore volume, and zeolite crystallinity (Baker et al., 1968; Letzsch et al., 1976; Ciapetta et al., 1967). Although the primary measure of performance evaluation is the activity/selectivity pattern, certain physical properties, including pore size distribution, are desirable (Letzsch et al., 1976). Any effects of contaminant metals (or the coke derived therefrom) must also be taken into account. It should be remembered that in commercial equilibrium catalysts there is a distribution of deactivations (due to distribution in age), while with lab-steamed catalyst samples are uniformly deactivated.

Catalyst manufacturers and refiners usually work together to optimize the operations of cat crackers by using the equilibrium catalyst reports which are most useful as a trend indicator.

2.3.1 Catalytic Properties

Micro-activity test (MAT) runs are widely performed by refiners for comparing catalyst performances, and choosing the most suitable ones under certain operating conditions. In this test, a sample of regenerated equilibrium catalyst is placed in a laboratory reactor. A typical FCC feed is passed over a fixed catalytic bed at cracking conditions and the results are analyzed. The MAT test highly depends on maintaining isothermal conditions; feedstock differences affect the catalyst performance. MAT test runs have been published that evaluate the performance characteristics of a zeolite catalyst by changing catalyst-to-oil ratios between two-to-ten at temperatures of 900 , 1000 and 1100 °F (Venuto et al., 1979). In this study, conversion has increased with increasing catalyst-to-oil ratio and temperature. However, the rate of increase in conversion has been found to be

9

smaller at 1100 °F compared to lower temperatures. The authors attributed this to large size of certain molecules that cannot diffuse and enter the zeolite framework, where most reaction takes place.

2.3.1.1 Activity

The value known as activity is the conversion obtained on a decoked sample at standard test conditions in MAT. Therefore any change in activity is due to catalyst changes. MAT activity data allows the refiner to exclude the catalyst effect from the process and feed effect. To minimize the variability in the MAT value, each sample is tested in duplicate and sometimes in triplicate. Feed metals contamination decreases catalyst activity. A total metals level of less than 1000 ppm has little effect upon equilibrium catalyst activity. Activity then begins to drop off rapidly as the metals level exceeds 2000 ppm. The combined action of steam and high temperatures can also reduce catalyst activity. This process is known as hydrothermal deactivation. At regeneration temperatures in the region of 650 – 700 °C, exposure to a steam atmosphere equivalent to 160-200 mm Hg water partial pressure destroys a large portion of catalyst matrix (40-60 %) and a smaller portion of the molecular sieve (25 %) after a few cycles through the regenerator. Then the catalyst becomes stable and no further destruction is observed in the matrix, however the molecular sieve portion is destroyed slowly at a rate of less than 0.5 % per day. At higher regenerator temperatures, hydrothermal destruction of the molecular sieve increases rapidly with a corresponding loss of equilibrium catalyst activity. For example, increasing regenerator temperature from 700 °C to 725 °C can sufficiently deactivate a typical commercial cracking catalyst to cause a 4-6 number drop in MAT activity (Upson, 1981). Then, fresh catalyst makeup rate is doubled to keep the same system activity. At extremely high temperatures (>1000 °C)

matrix collapse can occur along with sieve destruction. This is known as thermal deactivation. This results in loss of surface area for both the sieve and matrix components and shrinkage of the matrix component, which causes a loss of equilibrium catalyst pore volume and increase in bulk density. Therefore, when a large drop in catalyst activity is noted, physical properties of the equilibrium catalyst should be measured to define the reason of this problem.

2.3.1.2 Catalyst Selectivity

Catalytic selectivity information in an equilibrium catalyst test report can be expressed as a Coke Factor (CF), a Gas Factor (GF), and a H_2/CH_4 molar ratio.

CF can be described as the coke making characteristics of the equilibrium catalyst relative to the coke-making characteristics of some standard catalyst at the same conversion (Cimbalo et al., 1972). The type of fresh catalyst used and the metals in the feed affect CF. Coke yield gives an instantaneous response to metals deposition on the catalyst. Total metals (Ni + V) as low as 500 ppm can produce CF values 10-30 % above fresh catalyst values (Upson, 1981).

GF can be described as the light hydrocarbon production (C_1 - C_4) of the equilibrium catalyst relative to the C_1 - C_4 production of a standard catalyst at the same conversion. The GF, like CF, is a function of the type of fresh catalyst used and of the contaminant metals deposited on the catalyst. However, GF is much less sensitive than the CF. GF is more an indicator of the type of catalyst used than it is of metals contamination. GF is useful to evaluate FCCU gas plant operating problems (e.g., gas compressor, absorber, stripper. etc.) (Upson, 1981).

Hydrogen production is measured to have an idea about the catalytic effects upon total gas yield. H_2 yields have usually been reported by using H_2/CH_4 ratio. Hydrogen production is considered to be very sensitive to catalyst metals contamination (Pohlenz, 1963; Cimbalo et al.,

1972). At low catalyst metals levels (<1000 ppm Ni + V) H_2/CH_4 ratios of less than 1.0 are typical. At metals level of 1000-1500 ppm, which is the normal level for many FCC units, H_2/CH_4 ratios of 1-2 are typical. For the case of severe metals contamination when the Ni + V levels have risen above 5000 ppm, H_2/CH_4 ratios of 10 or higher would be expected with typical cracking catalysts available today (Upson, 1981).

2.3.2 Properties of Equilibrium FCC Catalysts

Table 2.1 gives a representative comparison of the properties of fresh and equilibrium zeolite and amorphous FCC catalysts. Relatively low levels of sodium and high levels of iron and contaminant metals such as nickel, and vanadium are present on the equilibrium catalysts. Typical vanadium-to-nickel ratio of 1.5 is observed in contaminated catalyst. Surface areas and pore volumes are lower in equilibrium catalyst compared to fresh catalyst. Conversions are higher, and coke (CF) and hydrogen factors are lower for the zeolite, as expected.

Table 2.1 Comparison of Properties of Fresh and Equilibrium FCC Catalysts (Venuto et al., 1979)

	Amorphous high alumina		Zeolite XZ-2	
	Fresh	Equi-librium	Fresh	Equi-librium
Chemical analysis (dry basis), wt%				
Alumina[b]	28	21.5	31	25.4
Carbon	0	0.20	0	0.25
Sulfate	0.7	0.1	0.3	0.1
Sodium	0.03	0.02	0.04	0.04
Iron (ppm)	300	3900	700	3700
Metals (ppm of V + Ni + Cu)	0	162	0	259
Physical properties				
Surface area, m^2/g	415	140	335	97
Pore volume, cm^3/g	0.88	0.43	0.60	0.45
Average bulk density, g/cm^3	0.39	0.70	0.52	0.68
Particle size, micromesh sieves, wt%				
0 to 20 μm	2	0	2	0
0 to 40 μm	17	8	19	6
0 to 80 μm	68	69	75	75
Average particle size, μm	65	63	62	62
Catalytic activity				
Microactivity, vol% conversion	60[c]	59[c]	85	73
Carbon factor	1.0	1.1	0.6	0.6
Hydrogen factor	1.0	1.1	0.2	0.7

[a]Data from Ref. 124 for same commercial unit.
[b]Equilibrium values are lower due to presence of some residual low alumina of long age.
[c]After 24 hr/1050° F/60 psig, 100% steam.

2.4 Factors Affecting Overall Process Performance

The overall performance of the FCC process, including gasoline yield and gasoline octane, is affected by several factors including: feed stock compositions, feed stock contaminants, process operating conditions, and catalyst characteristics.

2.4.1 Feed Stock Compositions

Feeds to the FCC unit contains different types of compounds which consist of various numbers of carbon atoms ranging between approximately C_7 and C_{60}. These compounds are usually categorized into paraffins, naphthenes, and aromatics. The smaller ones up to C_4 are present in the form of dissolved gases. The linear paraffins from C_{18} and higher are called paraffin waxes. The major classes of hydrocarbons in crude are paraffins, cycloparaffins, and aromatics. Olefins usually are not present. The relative fraction of paraffins decreases with increasing boiling points, whereas the amount of aromatics increases. The high boiling fractions consists of large portions of polynuclear aromatics. Cracking ability of hydrocarbons decreases from paraffins to aromatics through naphthenes (Ginzel, 1985). Voge (1958) suggested that in general the following order might exist in catalytic cracking reaction: Olefins > aromatics with C_3 or higher alkyl substituents > naphthenes > polymethylaromatics > paraffins > aryl rings > polynuclear aromatics.

Although feeds may have similar global properties, catalytic-cracking-conversion results may differ due to different feed molecular properties. Effect of molecular type, size and shape on catalytic cracking performance has been studied in detail by Subramanian, (1993). In a recent study, Lerner et al. (1997) have also shown that it is possible to select the proper catalyst for maximizing the conversion towards favorable products and minimizing coke and gas production by understanding the molecular characteristics of a residual oil.

2.4.2 Feed Contaminants

Organic sulfur and nitrogen compounds as well as organo-metallic compounds of vanadium, and nickel are considered as feed contaminants. The damage of sulfur and nitrogen compounds to catalyst is small but they may affect the catalyst activity and selectivity. These types

of contaminants are eliminated from the FCC process in the form of their oxides and hydrides. On the other hand, organo-metallic compounds decompose and leave metals on the catalyst.

2.4.2.1 Metal Contaminants

Supplying feedstock to the FCC process substantially free of metal contaminants is very important for petroleum refiners. The metals present in the feedstock are deposited along with the coke on the cracking catalyst. Unlike the coke, these deposited metals are not removed by regeneration. Therefore, they accumulate on the catalyst and act as a catalyst poison. Depending on the metals level on the catalyst, the catalyst activity decreases as the production of coke, hydrogen, and dry gas increase at the expense of gasoline and/or fuel oil.

Various petroleum stocks have been known to contain at least traces of many metals. The principal metal contaminants in crude petroleum oils are nickel and vanadium, with the relative amounts varying with the type of crude. In general, a crude oil can contain from about 5 to 500 ppm nickel and from about 5 to 1500 ppm vanadium (Venuto et al., 1979). It is obvious that the higher the metal level in the feed, the more quickly a given catalyst will be poisoned and consequently, the more often or more effective the demetallization of that catalyst must be performed.

Iron and small amounts of copper also may be present. Trace amounts of zinc and sodium are sometimes found. In addition to metals naturally present in petroleum, petroleum stocks also have a tendency to pick up tramp iron from transportation, storage and processing equipment. Most of these tramp metals deposit in a relatively non-volatile form on the catalyst during the conversion processes.

Among various metals found in a representative hydrocarbon feedstock, some like the alkali metals only deactivate the catalyst without changing the product distribution; therefore, they

might be considered true poisons. Others such as iron, nickel, vanadium and copper significantly alter the selectivity and activity of cracking reactions if allowed to accumulate on the catalyst. Since they affect process performance, they are considered as "poisons" as well.

The Engineers concerned with FCC process refer to metal content of feedstock in several ways. One of these is "metals factor", designated F_m. This factor is expressed in the following equation:

$$F_m = \text{ppm Fe} + \text{ppm V} + 10 \,(\text{ppm Ni} + \text{ppm Cu}) \qquad \text{(Zrinscak et al., 1979)}$$

A feedstock with a "metals factor" greater than 2.5 is considered to be poisonous for cracking catalyst. With this factor the negative effect of nickel is taken into account more seriously than that of vanadium and iron present in equal concentrations with the nickel. Another way of expressing the metals content of a feedstock is as "ppm Nickel equivalent", which is defined as

$$\text{ppm Nickel Equivalent} = \text{ppm Nickel} + 0.25 \text{ ppm vanadium} \quad \text{(Zrinscak et al., 1979)}$$

In this expression copper is not taken into consideration, since this metal usually is not present to any significant extent. However, if it is present in significant concentration, it is should be included in the computation of Nickel Equivalent and weighted as nickel.

It is current practice in FCC technology to control the metals content of the feedstock so that it does not exceed about 0.25 ppm Nickel Equivalent. Metal content of the feedstock may vary from day to day without serious disruption, provided that the weighed average of the metals content does not exceed about 0.25-ppm nickel equivalent of metal.

A persistent increase in metals content of the circulating inventory of catalyst determines the performance of the FCC unit. In fact, circulating inventory of catalyst, by its metals content, provides a time-average value of the metals content of the charge stock.

In fluid catalytic cracking of a metal-contaminated feedstock, the yield of the desirable products drops as the amount of metal contaminant increases. For instance, James (1989) has shown that increasing the amount of nickel on the catalyst from 55 ppm to 645 ppm and the amount of vanadium from 145 ppm to 1480 ppm decreases the yield of butanes, butylenes, gasoline, and coke from 58.5 to 49.6 volume percent. The volume percent was based on converting 60 volume percent of cracking feed to lighter materials. Since coke burning or gas-handling facilities limits many cracking units, increased coke or gas yields require a reduction in conversion or throughput to stay within the unit capacity.

2.4.2.2 Resistance to Metals Poisoning

Some researchers (Grane et al., 1961; Connor et al., 1957) have shown the presence of nonselective cracking induced by metals in amorphous catalysts. Zeolite cracking catalysts have better resistance to contamination by vanadium, nickel, and other heavy metals when compared to amorphous catalysts. In the range of 3000-ppm effective metals, the zeolite catalyst produced less coke than the amorphous silica-alumina catalysts (Masologites et al., 1973). The resistance to poisoning by organic nitrogen compounds was found to be high for faujasite catalysts (Plank et al., 1964, 1967). These properties of zeolites made a trend toward heavy feedstocks processing (Murphy, 1970). Masologites et al. 1973 have observed that total metals level cannot be used as an index of contamination, since each deposited metal produces different amounts of coke and hydrogen. On a weight basis, nickel is four times more effective in coke and hydrogen production than vanadium. Cimbalo et al., 1972 defined contaminant "effective metals" as (4 [ppm Ni] + [ppm V]) * "fraction effectiveness". Fraction effectiveness was claimed to be a function of feed type and throughput; catalyst type, age and history; unit inventory and makeup rate (Cimbalo et al., 1972;

17

Masologites et al., 1973). Although authors mentioned the differences in metal poisoning resistances depending on cracking catalyst and regenerator conditions which may affect rate of metal deactivation, they could come up with a single standard for determination of "effective metal" values for specific catalyst and operating conditions.

The poisoning effect of previously deposited metals subjected to many repeated cycles of oxidation/reduction in the FCC regenerator/reactor unit, have been found to be less significant than those of freshly deposited metals (Montgomery, 1973). However, the effectiveness of metals on zeolites was kept longer compared to amorphous catalysts (Cimbalo et al., 1972)). Higher metal accumulation has been observed in fluid catalysts compared to accumulation in bead types (Morozov et al., 1973), because with bead types significant amounts of surface metals have been removed by the attrition process. Montgomery (1973) has observed higher dehydrogenation activity of metals on a cracking catalyst after being sulfided by the sulfur in FCC feed. However, in short contact time operation, metals contaminants were less effective (Phelps, 1957; Blazek, 1973a). This has been attributed to the metal oxides, which are not sufficiently sulfided in their short stay in the reactor (Blazek, 1973a-b).

2.4.2.3 The Catalytic Effect of Metals

Nickel, copper, vanadium and iron are all catalysts themselves. They are particularly effective in catalyzing hydrogenation and dehydrogenation reactions and they have some cracking activity. Nickel and copper are more effective than vanadium whereas iron is considered to be the least effective among all (Larson et al., 1966; Hildebrand et al., 1973; Chen, 1972).

Nickel and vanadium are found in crude oil in the form of porphyrin complexes (Rothrock, 1957; Speronello et al., 1984; Bencosme et al., 1986). Metal contaminants are centered to these

18

porphyrins in the form of vanadyl (VO^{+2}) and nickel (Ni^{+2}) ions, which are very stable and difficult to remove (Occelli, 1991). Pompe et al. (1984) studied the thermal stability of nickel and vanadium porphyrins. In this study, the decomposition of porphyrins was observed at a temperature range of 400 - 500 °C under reducing atmosphere. However, in oxidizing atmosphere this temperature range lowered to 403 - 470 °C. This decomposition temperature ranges are below the normal operational conditions of a commercial FCC unit. This assures the deposition of the metals on the catalyst after porphyrins are decomposed under cracking conditions (Anderson et al., 1984; Barbi, 1982). In regeneration conditions, coke burns off the catalyst and vanadium oxidizes to the +4 and +5 states. If present at high enough concentration, the oxidized vanadium may be present as V_2O_5 on the catalyst surface.

Some researchers (Jaras, 1982; Chester, 1981) observed that nickel does not migrate, even after aging conditions and stays randomly distributed in the matrix and builds up on the catalyst as catalyst ages. Nickel catalyzes dehydrogenation and condensation reaction --including formation of carbon and hydrogen -- at high temperatures (Germain, 1969). Nickel-catalyzed reactions account for most of the "contaminant" coke and hydrogen formation observed in metals-poisoned cracking systems. Vanadium is believed to destroy the zeolitic structure, and hence increases the amorphous content of the catalyst, which has a negative effect on the catalyst selectivity (Agrawal et al., 1972; Valkoric, 1978; Martinez et al., 1986; Geisler et al., 1988; Tatterson et al., 1988, Armstrong et al., 1972; Speronello et al., 1984).

The commonly accepted mechanism for catalyst deactivation is the migration of vanadium from the matrix where it deposits originally, to the zeolite. Then vanadium forms a rare-earth vanadate by extracting oxygen from the zeolite structure. This leads to the destruction of zeolite. The formation of a volatile vanadium species, vanadic acid, has also been reported as a possible

alternate or additive-deactivating agent (Wormsbecher et al., 1986). Mobile vanadium species, such as vanadic acid, $VO(OH)_3$ are formed by reaction of the oxidized vanadium with steam in the FCC regeneration. Vanadic acid migrates into the catalyst particle and destroys zeolite and reduces catalyst activity (Occelli, 1991). Vanadic acid also can move from particle to particle, which accelerates the deactivation of fresh catalyst particles. Additionally, in the pressure of steam, vanadium may react with rare earth elements in the zeolite, forming rare earth vanadates and further destabilizing the zeolite (Feron et al., 1992).

It can be concluded from the proposed deactivation mechanisms that the presence of oxygen is essential for the vanadium to initiate and complete its destructive action against the active sites of the catalyst.

Tatterson et al. (1988) studied the behavior of nickel and vanadium on the surface of a commercial cracking catalyst. Vanadium was found to interact with nickel in a manner which inhibits the deactivation behavior of nickel. Therefore, it has been suggested that metals resistant cracking catalyst must be evaluated in the presence of both nickel and vanadium. Larocca et al. (1990) also studied deactivation kinetics of cracking catalyst by nickel and vanadium contaminants. They checked and confirmed the adequacy of their laboratory impregnation techniques by using secondary ion mass spectrometry (SIMS). SIMS photographs have shown a uniform distribution of nickel and vanadium through out the catalyst pellet with some tendency to have higher metal concentrations close to the external surface. Their result is also consistent with the result of metal distribution in naturally poisoned catalysts in a commercial unit, showing a higher concentration of metals at the external catalyst surface (Kugler et al., 1988).

2.4.2.4 Effects of Metals Contaminants and Coke Deposits on Activity and Selectivity

Although metal contaminants level is low in FCC feeds, these metals finally accumulate on the cracking catalysts. This causes the reduction of catalyst performance, with serious effects on process efficiency. The high metals levels in FCC feeds is a result of either processing heavier, more asphaltenic, crude oils or major variations in operating practice as shown in Figure 2.6. For example, as the level of active catalyst metals increases, a decrease in conversion and deterioration in selectivity associated with increase in hydrogen and coke, and a decrease in gasoline are observed. An increase in the production of hydrogen and light gas results in a serious load on refinery gas-handling facilities. This can affect the entire system including riser/reactor, main column, condensers, and compressors, and may force a cutback in unit throughput as seen in Figure 2.6.
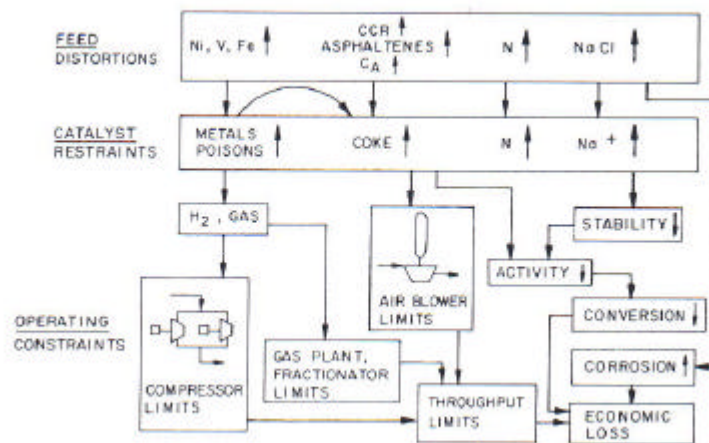
Figure 2.6 Wide Variations in Feed Composition and Operational Upsets Affecting Catalyst Performance and Unit Operations (Venuto et al., 1979)

Heavy secondary products referred as coke typically consists of polyaromatic condensed-ring structure, which approaches the character of graphite. The cracking of paraffinic compounds gives lower coke yields than that of aromatic compounds, and both the rate of cracking and the rate of coke formation increases as the molecular weight of the paraffinic reactant increases (Gates et al., 1979). Polar compounds are very difficult to crack and make high yields of coke (Stratiev et al., 1997). Habib et al. (1977) categorize the coke formed during FCC into four groups depending on the classification by Cimbalo et al. (1972). These are:

1. "Catalytic" coke, which is formed during the acid-catalyzed cracking, increases exponentially with conversion.

2. "Contaminant" coke, which is caused by the catalytic dehydrogenation activity of metals poisons such as nickel, vanadium, etc.

3. "Additive" coke (or carbon) is independent of the C/O ratio or catalyst type. It can be correlated with the basic nitrogen and average molecular weight of the feed stock as well as

22

Conradson Carbon Residue (residual portion of single-stage atmospheric distillation or two-stage atmospheric/vacuum distillation, which forms the resinous or tar-like compounds on cracking catalysts without substantial conversion.)

4. "Cat-to-oil" coke, which is a measure of unstripped hydrocarbons. They are formed as a result of non-ideal stripping in the commercial process.

Brevoord et al. (1996) experimentally determined the individual components of coke on catalytic cracking catalyst.

Coke formed during catalytic cracking has both negative and positive effect. The advantage is the heat provided by the coke combustion in regenerator; this heat is used for the endothermic cracking reactions. The amount of coke on the catalyst is affected by metals contamination level. It is also known that metal contaminants play an important role in the production of carbon dioxide during the regeneration of cracking catalysts (Doolin et al., 1991). Direct conversion of carbon to carbon dioxide in regenerator was catalyzed by nickel. The metals deposited on the zeolitic cracking catalyst increased carbon dioxide production during regeneration. This effect increased from iron to vanadium to nickel. Doolin et al. (1991) observed a decrease in CO_2/CO ratio during regeneration with increasing supported carbon levels in the presence of nickel. This was explained by the theory of nickel being "encapsulated in carbon" (Bernardo et al., 1979). Coke is also known as a source of hydrogen for stabilizing valuable lower-molecular-weight hydrocarbon products.

The disadvantage of coke formed during catalytic cracking is the loss of activity and selectivity for zeolite-containing FCC catalysts. In this aspect, zeolites, in short-contact-time riser operation, seem to be more severely affected by residual catalyst carbon level than conventional amorphous materials (Ritter, 1975; Venuto et al., 1979). Decrease in conversion and increase in coke, C_3-and-lighter gas, and butanes at the expense of C_5 + gasoline were reported by Wachtel et

al. (1971). Wachtel et al. (1971) attributed the loss in gasoline selectivity with increasing coke content to blockage of zeolite sites by carbon. Ritter (1975) suggested that most of the coke is preferentially deposited in and around the active cracking sites of zeolite particles; since most of the cracking is supposed to occur at the zeolite sites, then one would expect a change in selectivity as well as activity.   Therefore, complete removal of residual coke on the catalyst has strongly been suggested for better utilization of zeolite potential (Ritter, 1975, Blazek, 1973a-b).

Recently, Mandal et al. (1993) have shown the effect of coke on regenerated catalyst (CRC) on an FCC unit performance depending upon the operation mode. In the distillate mode (i.e., maximization of the middle distillate yield), they found that increase in CRC level up to an optimal value enhances the middle distillate yield. However, in the gasoline mode (i.e., at high reaction severity, where maximization of gasoline is main concern), increasing the CRC level only overcracks gasoline to LPG (Mandal et al., 1993). However the equilibrium catalyst used in these studies mentioned above had relatively low metal contaminants level. In the case of high metal contamination levels, there may be an optimal CRC level, which may enhance the overall FCC process performance by reducing the negative effects of metal contaminants.

The selectivity of a complex reaction depends on a number of factors, such as the reaction mechanism, operating conditions, catalyst properties and catalyst deactivation. For zeolite catalysts, changes in selectivity can be a result of intrinsic selectivity effects or shape selectivity effects. Shape selectivity effects are crucial in determining the product distribution in zeolite catalysis, and the selectivities depend on a number of factors. Three types of shape selectivities have been identified (Weisz, 1980), i.e., reactant shape selectivity, product shape selectivity, and transition-state shape selectivity. The relative importance of these types depends on the zeolite pore structure, and shape and sizes of the reactant and product molecules, and might be influenced

24

by coke formation. The change in selectivity due to coke formation has been explained by changes in the diffusivity of the molecules or in the zeolite pore volume, with the formation of the coke (Dadyburjor, 1992; Rene Bos et al., 1995; Xu et al., 1995).

2.4.3 Process Operating Conditions

Under steady-state operation, temperatures in the reactor and regenerator are the most important parameters, which affect overall FCC process performance (Yen et al., 1985). In the FCC process, catalyst is subjected to different deactivation processes as it is transferred between reactor, stripper and regenerator. As a result of the severe conditions, catalyst suffers from temporary (coke deposition) and permanent (metal deposition) deactivation in the reactor; partial permanent deactivation (alteration of its composition) in the stripper, and thermal deactivation (destruction of its crystal structure) in the regenerator.

2.5 Techniques Applied to Combat Metals Contaminants in FCC Process

Basic approaches applied to solve this problem are feedstock pretreatment, catalyst management, metal passivation and demetallization of catalyst. The most conventional methods are the careful preparation of feedstock to keep its metal content low and replacement of catalyst to control metal levels on the catalyst (catalyst management).

Catalysts used commercially are the result of years of study and research. The costs in the development of a commercially viable catalyst are not negligible. Therefore, catalyst cost frequently determines the quality of the feed stream to be used in the process. Feedstocks, which are plentiful but which have high metal content, are avoided to prevent the frequent replacement of

expensive catalyst. In commercial catalytic cracking operations, sometimes complete elimination of metal-containing compounds from the feeds is impractical, especially when there is an increasing demand to maintain, or increase, the octane number of the gasoline pool. Therefore, alternative methods such as passivation and demetallization for controlling metal poison concentration on catalysts become very important. These processes reduce the amount of catalyst discarded and allow the use of plentiful, but metal-contaminated, petroleum feedstock.

Passivation processes reduce the harmful metal activity without causing significant reduction in catalyst activity by contacting the catalyst with a passivating agent, which forms relatively harmless complexes with the metal contaminants from the catalyst (Chester et al., 1990). A passivation method reduces the hydrogen and coke formation by decreasing the catalytic effects of metal contaminants on the catalyst, whereas demetallization processes involve the physical removal of the metal contaminants from the catalysts.

2.5.1 Feedstock Treatment

The effects of metals in the feed can be minimized by the appropriate pretreatment of oil such as distillation, solvent extraction, or hydrogenation (Rush, 1981a; Hemler et al., 1973; Hildebrand et al., 1973; Ritter et al., 1974; Arey et al., 1969; McCulloch, 1975; Ritter, 1975; Weisz, 1968). A number of studies reported the effect of hydrotreating severity on FCC process variables, crackability, yields/selectivity, and product quality (Owen et al., 1977; Ritter et al., 1974; Arey et al., 1969; McCulloch, 1975; Huling et al., 1975). Hydrotreating catalysts are designed to tolerate large amounts of deposited metals (i.e., act as a metals sink). Therefore, contamination of the FCC catalyst whose performance is much more sensitive to metals is prevented (Arey et al., 1969).

Sour crudes (oils with high sulfur contents) were projected to constitute an increasing portion of tomorrow's crude supply (Logwinuk et al., 1981; Ritter et al., 1981). To process these crudes, residual oil hydrodesulfurization (HDS) combined with heavy-oil cracking was suggested as an attractive refinery process scheme which maximizes gasoline yields (Rush, 1981b). Besides removing sulfur, HDS also reduces the metals and Conradson Carbon levels while improving the distribution of cracked products.

2.5.2 Catalyst Management:

Catalyst management is a conventional approach to control the contaminant metals level in cracking unit by increasing the makeup rate of fresh catalyst, coupled with an increase in withdrawal of inventory catalyst in order to maintain a constant amount of contaminant metals in the catalyst inventory. The higher the metal content of the feedstock, the greater the makeup rate of fresh catalyst is required, and the greater is the expense. Therefore, the use of the conventional approach to feedstock having high metal contents is not very economical.

2.5.3 Passivation

Benefits of passivation are decrease in the yields of hydrogen and coke with increase in the yields of gasoline because of better cracking selectivity. This will allow a refinery to add low-value residual oil to the feed while still maintaining an acceptable product yield.

2.5.3.1 Metal Passivators

In industrial applications, metal passivators are conventionally added to the hydrocarbon feed as the free metal, or as salts or compounds of the metal (e.g., the metal oxides or an organo-metallic compound) (Dale et al., 1977; English et al., 1984). In several applications, they are either impregnated into the catalyst or added separately to the cracking unit during the cracking process. Several metals and metal oxides were successfully used as passivators. These are antimony - containing compounds such as antimony O,O' - dialkyl phosphorodithioate (Dreiling et al., 1979), antimony di -n- propyl phosphorothioate in hydrocarbon oil (Mark et al., 1982), antimony tris (O,O' -dipropyl phosphorothioate) (Mark et al., 1984), and antimony tris (O,O' - dipropyl dithiophosphates) (Gall et al., 1982).

Many US patents (McKay et al., 1977a-b, 1978, 1979a-b-c and Nielsen et al., 1979) used antimony compounds to passivate the catalytic activity of the iron, nickel and vanadium contaminants deposited on the cracking catalyst. In these patents, contacting the catalyst with antimony selenide, antimony sulfide, antimony sulfate, bismuth selenide, bismuth sulfide, or bismuth phosphate succeeded in passivating the metals. However, use of antimony compounds alone was not sufficient to passivate the metal contaminants when the metal contaminant concentration on the catalyst was relatively high.

Phillips Research and Development used a compound called Phil-Ad® CA, an oil-soluble, antimony-containing additive, by directly injecting into the feed. This agent was antimony trisdipropyldithio-phosphate in a hydrocarbon diluent represented as shown in Figure 2.7. Antimony content was typically 10.5 to 12.5 wt percent. It contained not only antimony but also sulfur (typically a minimum of 17.5 wt. %) and phosphorus (typically a minimum of 7.5 wt. %). In this application, antimony trisdipropyldithio-phosphate demonstrated superior metals passivation

performance compared to other organoantimony compounds such as triphenyl antimony and antimony tritallate (also shown in Figure 2.7) and to an inorganic antimony compound, colloidal antimony pentoxide dispersed in a hydrocarbon.
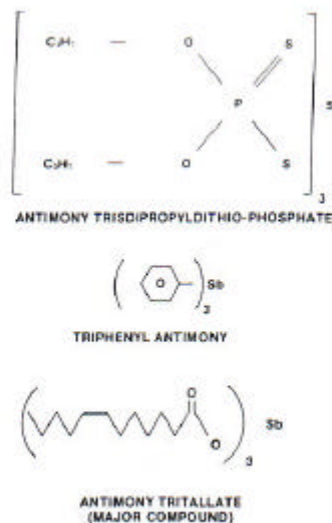
Figure 2.7 Representations of Some Organoantimony Compounds (Gall et al., 1982)

Use of bismuth (Kennedy et al., 1990) or manganese compounds (Readal et al., 1976) as metal passivators is described in US patent literature. These methods eliminated the use of antimony that is on the U.S. Environmental Protection Agency's list of hazardous chemicals. The bismuth also reduced the negative effects of high nickel content in the FCC feed, at a bismuth quantity equal to, or slightly greater than, the amount of antimony previously used. Trouble-free operation of the FCC unit in a Mapco Petroleum Refinery was achieved with a low passivation cost (Heite et al., 1990).

In practice, antimony and bismuth compounds were used to passivate the negative effects of nickel contaminants while tin compounds were employed for vanadium contaminant passivation. Although the effectiveness of antimony in industrial applications was not doubted (Bohmer et al.,

1989; Heite et al., 1990; Dreiling et al., 1979; Mark et al., 1982, 1984; Gall et al., 1982), the effectiveness of bismuth for nickel passivation was questioned (Bohmer et al., 1989).

A variety of tin compounds were also employed. These were elementary tin and/or tin compounds in combination with elementary cadmium and/or cadmium compounds (Bertsch, 1985a-b), stannous dihydrocarbyl phosphorodithioates, stannous di-n-propyl phosphorodithioates (Mark et al., 1982) hexabutyltin, tin chloride (Mitchell et al., 1987) and tetrabutyltin. For example, Martinez et al. (1995) successfully used a single compound containing both antimony and tin by adding it to the feedstock or impregnating it into the catalyst.

In the literature, compounds of the following elements were also proposed as metal passivators: lithium (Tu, 1982), barium (Bertus et al., 1983), phosphorus (Durante et al., 1984), bismuth (Kennedy et al., 1990), boron (Tu, 1981), aluminum (Yoo, 1982), zinc (Hirschberg et al., 1982), and silicon (Yoo, 1982).

Beck et al. (1984) observed benefits of adding metals such as titanium, zirconium, manganese, indium and lanthanum to a cracking unit during the cracking process. Similarly, Occelli et al. (1984) used metal additives for passivating contaminating metals in hydrocarbon feeds. These metal additives were magnesium compounds optionally in combination with a heat-stable metal compound such as an oxide of silicon, aluminum, iron, boron, zirconium, phosphorus and certain clay minerals. The additives used by Occelli et al. (1984) were separate and distinct from the catalyst.

Mitchell et al. (1987) used calcium additive, e.g., calcium carbonate, during catalytic cracking. The calcium additive used may be either a part of the catalyst matrix or introduced separately from the catalyst matrix.

Senn et al. (1995-a) described a method in which a zeolite-containing cracking catalyst is passivated with lithium sulfate and an additional passivating agent (more preferably at least one antimony compound). Similarly, in another U.S. patent a zeolite-containing cracking catalyst is passivated with the compounds of antimony and zirconium and/or tungsten (Senn et al., 1995-b).

Another way of preventing catalyst from being deactivated is to add metal traps to the catalyst during pretreatment step. Farag et al. (1993) reported improved gasoline yield, reduced coke formation and increased gas formation by using vanadium traps. A common vanadium trap contains a basic component which reacts with acidic vanadium compounds to neutralize them (Dougan et al., 1994). A general reaction scheme can be expressed as follows:

$$2\,MeO + 2\,VO\,(OH)_3 \rightarrow Me_2V_2O_7 + 3H_2O$$
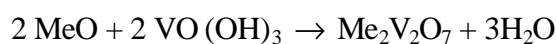
Compounds proposed to react by this mechanism include barium titanate, calcium titanate, calcium carbonate, strontium titanate, and magnesium oxides. The main problem with trap technology is the chemical reaction of trap material with oxides of sulfur (contaminant in FCC feedstock) in competition with vanadium. This sulfur competition prevented previous traps from working commercially. However, Dougan et al. (1994) successfully applied a new, rare-earth based, dual particle trapping technology known as RV+4 to commercial refiners. Although the trap picked up some sulfur, this did not hinder the trap's performance very much. With this technology, vanadium was almost irreversibly trapped along with some of the nickel. Trapped nickel revealed inter-particle Ni mobility, somewhat contrary to current beliefs. This suggested that, while Ni is significantly less mobile than vanadium, nickel can still be mobile under certain FCC conditions (Scherzer, 1990; Gerritsen et al., 1991). A successful vanadium trap should be able to immobilize the vanadium in non-destructive form, and trap capacity must be great enough to remove a

considerable amount of vanadium from the catalyst, after satisfying the conditions for a fast rate of vanadium migration to the trap rather than to zeolite.

2.5.3.2 Gaseous Passivation:

There are many methods of gaseous passivation described in U.S. patent literature. First, Cimbalo et al. (1972) reported the decrease in the catalytic activity of metal contaminants with repeated oxidation and reduction cycles during the use of the catalyst. Then, Tatterson et al., (1981a-b) used the processes in which cracking catalyst was exposed up to 30 minutes of an alternating oxidizing and reducing conditions at elevated temperatures to reduce the hydrogen and coke makes. This led to developments of new processes, which deactivate the metals faster than their natural deactivation in the cracking unit without affecting the cracking function of the catalyst. Another invention was the deactivation of harmful metals on the catalyst with steam under certain conditions. The degree of passivation is controlled by adjusting parameters such as residence time, steam partial pressure and temperature (Chester et al., 1981).

Some studies reported improvements in passivating metal contaminants on the cracking catalyst by using the combination of more than one method. For example, in the method used by Bearden et al. (1983-a) coke production was reduced during the cracking of hydrocarbon feedstock to lower-molecular-weight products in a reaction zone. In this process, catalyst is transferred from a regeneration zone operated under net reducing conditions to the reaction zone through a high temperature reduction zone where catalyst are allowed to stay for a sufficient time to passivate metal contaminants at least partially (see Figure 2.8).
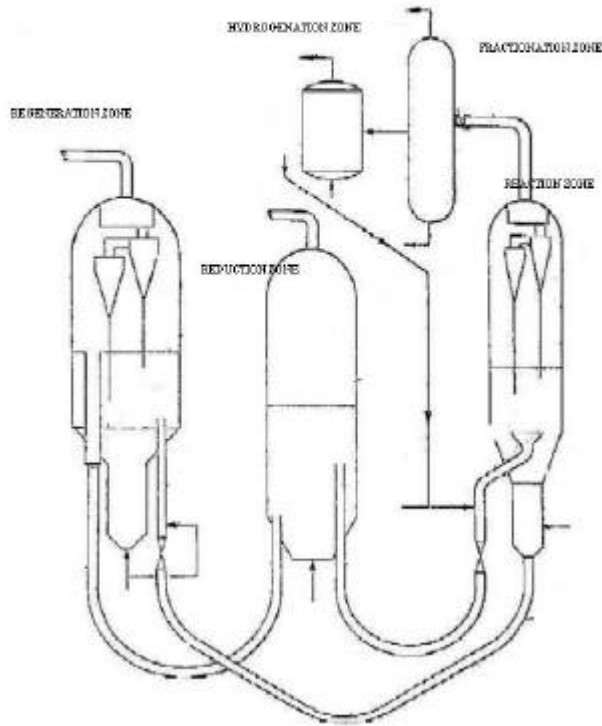
Figure 2.8 Process for Reducing Coke Formation in Heavy Feed Catalytic Cracking (Bearden et al., 1983)

Hydrocarbon feedstock with at least two metal contaminants is fed to the reaction zone having a cracking catalyst. A regeneration gas is used to remove at least a portion of the coke from the catalyst. In this technique, one passage through the reaction and regeneration zones reduces the effectiveness of the reduction zone passivation. Thus, the catalyst from the regeneration zone has to be passed through the reduction zone to passivate the metals on the catalyst on every catalyst regeneration cycle. Effectiveness of reduction zone passivation is diminished less when the regeneration zone is operated under net reducing conditions than when the regeneration zone is

operated under net oxidizing conditions. When the regeneration zone is operated under net oxidizing conditions, the metal contaminants are reactivated unless catalyst is passed through the reduction zone on each cycle. Reduction zone is maintained at a temperature within the range of about 600 °C to about 850 °C in the presence of hydrogen, carbon monoxide or mixtures of these gases. Then, catalyst is passed from the reduction zone to the reaction zone without further processing.

Addition of a hydrogen-donor material to the reaction zone is recommended (Bearden et al., 1983) in order to transport hydrogen to the hydrocarbon feedstock and/or to the cracked lower molecular weight products. The hydrogen donor material is obtained by fractionating the cracked molecular products from the reaction zone. After passing the desired fraction through a hydrogenation zone, it is re-circulated to the reaction zone. Hydrogen donor compounds may include two ring naphthenic compounds such as decahydronaphthalene (decalin) and two ring hydro-aromatic compounds such as tetrahydronaphthalene (tetralin). These compounds take hydrogen in the hydrogenation zone and readily release the hydrogen in the reaction zone.

Some processes employing a passivating zone having a reducing atmosphere maintained at an elevated temperature (Bearden et al., 1983b and Stuntz et al., 1981a-b) have been combined with the use of hydrogen donors to further decrease the hydrogen and coke makes in a process. When the use of a hydrogen donor is combined with the previously described metals passivation processes (see sections 2.5.3.1), this reduces coke still further. Increasing reduction zone temperatures (500 °C - 750 °C) enhances the degree of passivation further.

Some other studies have shown metal contaminants can be passivated by using a reducing gas, such as hydrogen, carbon monoxide, light hydrocarbon gases or mixture of these gases with or without water saturation. All of these methods used reducing atmospheres maintained at elevated

temperatures. For example, Stine et al. (1981) described passivation of contaminant metals on a FCC catalyst by using a reducing gas such as hydrogen saturated with water at certain reduction-reaction conditions. It was found that reducing gas saturated with water causes significant reduction in the formation of hydrogen and coke in the catalytic reactor. Although CO may be used, in most of the applications hydrogen is preferred as a reducing gas. The preferred reduction reaction conditions are temperatures ranging from about 1100 °F to about 1350 °F and pressures from about atmospheric to about 35 psig. The acidity of V_2O_5 was held responsible for its contaminating activity in promoting undesirable reactions such as excessive hydrogen and coke production. After being reduced, less active (if not inactive) basic, lower oxidation states of vanadium are formed. When the nickel is reduced to the zero oxidation state, on the other hand, enhanced agglomeration may serve to reduce its negative effects. It has been postulated that, at least when hydrogen is used as a reducing gas, an amount of hydrogen will become H+ ions on the catalyst during the reduction. Later, H+ acts to minimize the extent of hydrocarbon polymerization in the reactor. Therefore, significant reduction in coke formation is observed. It has been further postulated that saturation of reducing gas with water enhances interaction of the contaminating metal with the amorphous catalyst or amorphous catalyst matrix. This interaction is referred as "spinel formation" which may be exemplified by the reaction of nickel with alumina to form nickel aluminate ($NiAl_2O_4$). The spinel formed tends to be inactive with regard to the promotion of undesirable reactions.

In the method described by McGovern et al. (1979), hot regenerated FCC catalyst is purged with a flue gas containing C_3 and lower-boiling components of a hydrocarbon cracking operation. This patent does not mention contaminating metals or even the particular feedstock employed.

In the processes given by Stuntz et al. (1981a-b), and Bearden et al. (1981), cracking catalyst is passivated under reducing conditions. These processes use gas streams such as cat cracker tail gas, catalytic reformer off-gas, spent hydrogen streams from catalytic hydro-processing, synthesis gas, flue gases and mixtures of these.

Stuntz et al. (1985a) described a method in which metal-contaminated catalysts are passivated in a passivation zone having a reducing atmosphere maintained at elevated temperatures. Reducing gas is passed through a zeolite-containing guard bed to remove the unsaturated hydrocarbons (particularly olefinic compounds such as ethylene which contribute to excessive coke formation on the cracking catalyst). Zeolite used in guard bed is preferably a Cu (I) Y-type zeolite. In another similar application (Stuntz et al., 1985b), the unsaturated hydrocarbon content of reducing gas is decreased before introduction of reducing gas into passivation zone by passing it through a hydrogenation zone instead of a zeolite guard bed.

Castillo et al. (1982a-b), (1983a-b); and Hayes et al. (1984) described a method in which metal-contaminated catalyst is contacted with a hydrocarbon gas or mixture of gases comprising molecules of three carbon atoms or less at passivation reaction conditions prior to the cycling of the catalyst to the cracking zone. It was found that contacting the freshly regenerated FCC catalyst with a light hydrocarbon gas comprising molecules of three carbon atoms or less or a mixture of such gases would significantly decrease the formation of hydrogen and coke in the catalytic reactor. Hydrogen may also be present in the gas. It is advantageous to use light gas saturated with water at ambient pressure and temperature of from about 120 °F to about 212 °F. The use of wet gases further contributes to the passivation of the undesired contaminating metal activity, particularly activity causing coke deposition on the catalyst. Less coke formation is also advantageous with regard to operations of the FCC regenerators, since there will be less undesired

heat made in the regenerator and a smaller amount sulfur carried over from the reactor with the coke. The propane and lighter hydrocarbon gases are usually formed in the FCC reactors and the catalyst is contacted with such gases. There is also usually some amount of steam introduced into the FCC reactor. Therefore, one may think that the light gases and water during the FCC reactions can passivate contaminating metals. However, passivation in this manner does not occur until well after the contaminating metals have been in contact with the heavy hydrocarbons and have had ample opportunity to catalyze the undesirable coke and hydrogen producing reactions. It was found that careful selection of reaction conditions is essential for the complete reduction of the contaminant metals to their free metallic states. It is well known that free metallic states promote undesirable coke-making reactions (Castillo et al., 1982). The catalyst subjected to the complete reduction processes with light hydrocarbon gas acquires a condition for selective carbonization. Then, free metal active sites are selectively carbonized, i.e., they are coated with a layer of carbon which insulates these free metal active sites from subsequent contact with the feedstock, while the desirable acid sites of the catalyst are unaffected. A passivation reaction temperature of about 1300 °F or above was found to be advantageous for a significant passivation (Bearden et al., 1983). The upper limit of the temperature would be determined by the maximum temperature to which the catalyst in question could be exposed without being degraded or destroyed. The composition of the light hydrocarbon gas being used for passivation could be adjusted for the level of metal contamination.

In the applications given by Bertsch et al. (1985a-b), a passivator promoter, such as cadmium, germanium, indium, tellurium, tin or zinc, is used under reducing atmosphere at elevated temperatures.

2.5.4 Demetallization

Some applications for the demetallization of metals-contaminated FCC catalyst are given by Suggitt et al. (1977). The earlier demetallization processes involve the chlorinating of metal-contaminated alumina, silica-alumina and silica catalysts at elevated temperatures.

Before the invention of zeolite cracking catalysts in the early 1960's, many processes were applied for the demetallization of the amorphous silica-alumina type FCC catalyst. These processes can be classified into six general categories (Suggitt et al., 1977);

1. Acid Resin Contact, that is, the pretreatment of the metal contaminated catalyst with sulfuric acid followed by oxidation and contact with aqueous slurry of cationic resin.

2. Acid Complex, in which contaminated catalysts are activated with oxygen, hydrogen sulfide and chlorine, followed by contact with aqueous acid complexing agents such as citric acid.

3. Inorganic Acid Treatment, in which contaminated catalysts are brought into contact with acids such as, H_2SO_4, HNO_3, HCl or H_2SO_3.

4. NH_4OH Treatment, in which metal-contaminated catalysts are precalcined and then contacted with NH_4OH.

5. Volatilization, which pre-reduces the metal-contaminated catalysts, then catalysts are subjected to carbonyl formation with carbon monoxide interaction at low temperature under pressure.

6. Simple abrasion, in which pre-oxidized metal poisoned catalysts are contacted with hydrogen sulfide gas at flow rates high enough to cause abrasion.

The procedures mentioned above were also used for the demetallization of zeolite cracking catalysts. Many of these treatments involving strong acids may cause severe damages to catalysts

containing zeolites. Treatments at low pH should be avoided, or of short duration, to prevent acid destruction of zeolite catalysts. A process dealing with chemical removal of metal poisons from equilibrium catalyst is described by Edison et al. (1976). This process is similar to the acid resin contact process and can be used with zeolite catalysts.

Demetallization processes, which do not primarily include chlorinating the catalyst are given by Burk et al. (1978), (1979a-b). There have been many efforts to effectively demetallize the zeolite-containing catalysts while eliminating the use of chlorinating agents and chlorinated catalyst, which are often corrosive, particularly at elevated temperatures. These processes were thought to be less harmful to the relatively fragile zeolite-containing catalysts. However, in several cases, these "non-chlorinating" processes have been found to be less effective in catalyst demetallization than processes involving catalyst chlorination. Since chlorination techniques are destructive to zeolite-containing catalyst, they have received less and less consideration for commercialization.

2.5.4.1 Demetallation Chemistry:

Nickel is homogeneously distributed throughout the catalyst particle whereas vanadium deposits on the zeolite sites and reacts destructively with zeolite (Jaras, 1982).

Vanadium pentoxide interacts with lanthanum oxide exchanged with zeolite sites for a eutectic mixture (major cause for destruction of zeolite and drastic decline of catalytic activity, surface area, crystallinity and pore volume) (Occelli et al., 1985). The main poison precursor was identified as volatile vanadic acid, H_3VO_3,

$$V_2O_5 \, (s) + 3 \, H_2O \, (v) \longleftrightarrow 2 \, H_3VO_4$$
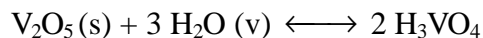
Reduction of V_2O_5 and ammonium metavanadate in a hydrogen atmosphere at 375 °C produced V_2O_3 via homologous oxide intermediates such as $VO_{1.75}$, $VO_{1.80}$, $VO_{1.84}$, $VO_{1.85}$, $VO_{1.87}$ (Sato et al., 1970). The presence of these intermediates under oxidation-reduction situation was also reported by Srivastava et al. (1982).

Many attempts have been made to remove the vanadium oxide(s) from the metal-contaminated FCC catalysts by washing them with various solutions. This includes a dilute solution of complexing agent such as oxalic acid (Beuther et al., 1963), and an ammonial solution containing a chealating agent (Erickson, 1964, 1965), a dilute sulfurous acid with complexing agent such as ammonia cyanide and hydroxycarboxylic acids (Schwartz, 1963) and an acid solution suspended with ion exchange resin (Ozawa et al., 1964).

Among the gas phase reaction approaches, vapor-phase chlorination process (Sandford et al., 1962) and Demet III process developed by Atlantic Richfield Company (Yoo et al., 1986) achieved commercial success. The process called "Demet" is claimed to reduce both fresh catalyst addition and spent catalyst disposal when used with any FCC catalyst. It is considered to be inexpensive, efficient, environmentally safe metals removal system. First, the metals on the catalyst are oxidized, sulfided and chlorinated in the reactor section. Then, volatile iron and vanadium chlorides are vaporized from the catalyst, and the nickel and sodium chlorides are washed from the catalyst.

Without an exception, all of these attempts were concerned with the total metal removal of V, Ni and Fe rather than selective vanadium removal. Yoo et al., (1990) tried selective V removal for effective rejuvenation of catalyst activity, while allowing both Ni and Fe to remain intact on the catalyst surface. They demonstrated that approximately 13 % of vanadium was selectively removed from the regenerated equilibrium FCC catalyst contaminated with metals such as Ni, Fe,

40

and vanadium by simple water wash. The vanadium removal was improved to approximately 28 % by applying reductive wash with an aqueous sulfur dioxide solution followed by the oxidative wash with an aqueous hydrogen peroxide solution to the same regenerated catalyst. A significant fraction of vanadium (50-70 %) was further removed by subjecting the same catalyst to a calcination step at high temperatures (730 – 815 °C) before the reductive and oxidative washing processes. Devanadated catalysts showed a catalytic activity close to that of the virgin catalyst and those achieved by other known demetalation processes removing vanadium, nickel, and iron simultaneously (Yoo et al., 1990). It has been shown that the poisoning effect caused by the vanadium deposition on the FCC catalyst can effectively be reversed by removing vanadium from the catalyst matrix. This warranted additional efforts to validate the idea that vanadium poisoning destroys the zeolite structure permanently.

3.0 MATERIALS AND METHODS

This research consists of three main sections as seen in Figure 3.1. These are catalyst characterization, catalyst pretreatment and catalyst evaluation.

```
┌──────────────────┐    ┌──────────────────┐        ┌──────────────────┐
│    CATALYST      │    │    CATALYST      │        │    CATALYST      │
│ CHARACTERIZATION │    │  PRETREATMENT    │        │   EVALUATION     │
└──────────────────┘    └──────────────────┘        └──────────────────┘


┌──────────────┐      ┌────────────────────┐      ┌──────────────────┐
│              │      │ PRETREATMENT W/ H₂ │      │ MAT UNIT         │
│   TPR/TPO    │◄════►│ OR CH₄             │═════►│ C/O=3, 5, 8      │
│              │      │                    │      │ T=500 °C         │
└──────────────┘      └────────────────────┘      └──────────────────┘

                                   ┌──────────────┐  ┌──────────┐  ┌──────────────┐
                                   │    COKE      │  │   GAS    │  │  SIMULATED   │
                                   │ DETERMINATION│  │ ANALYSIS │  │ DISTILLATION │
                                   └──────────────┘  └──────────┘  └──────────────┘

┌──────────────┐                              ┌──────────────┐
│ SURFACE AREA │                              │  MATERIAL    │
│              │                              │  BALANCE     │
└──────────────┘                              └──────────────┘


┌──────────────┐
│ VISIUALIZATION│
│    (AFM)     │
└──────────────┘
```
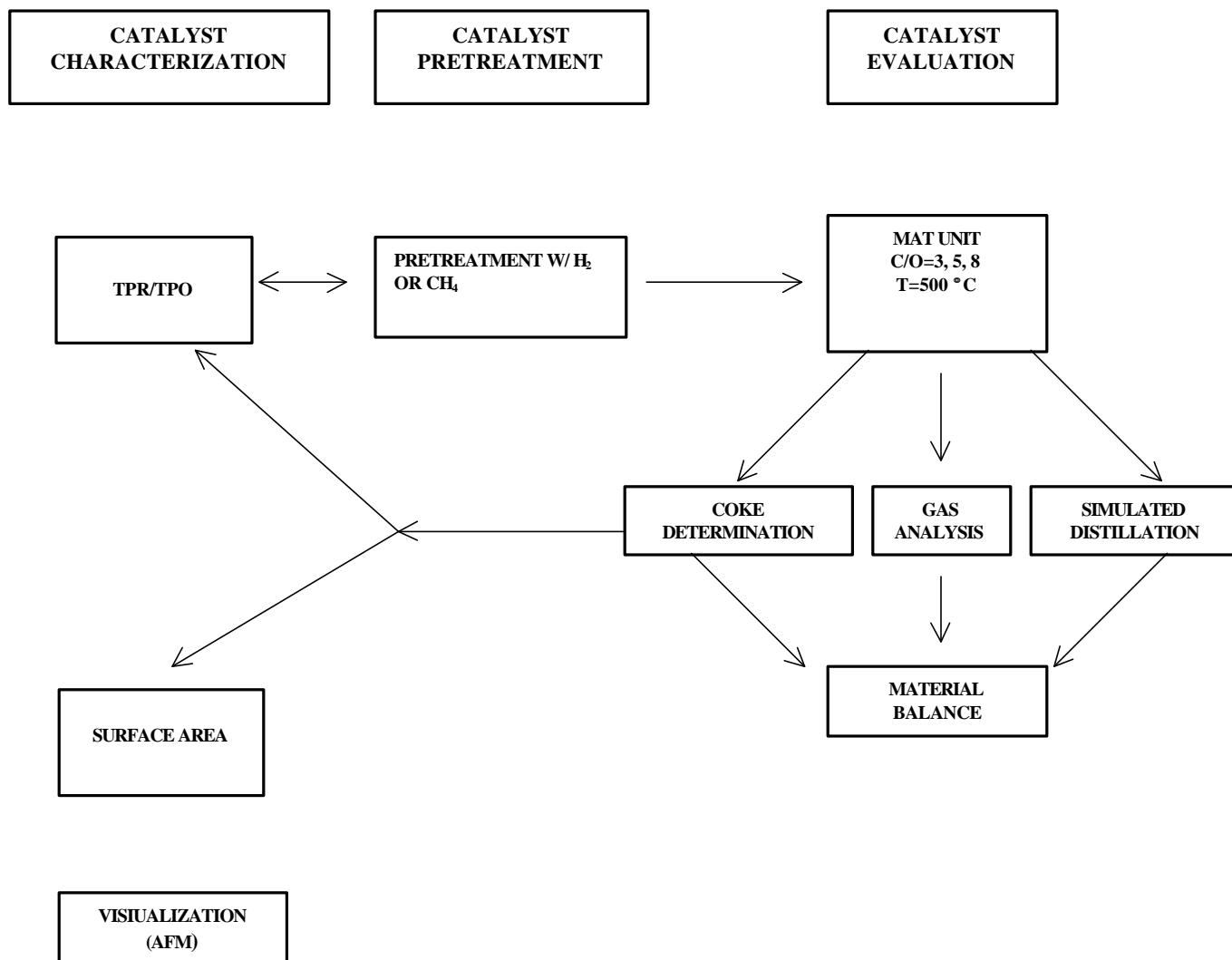
Figure 3.1 General Experimental Scheme

3.1 Catalyst Characterization

Temperature Programmed Reduction (TPR), Temperature Programmed Oxidation (TPO) and surface area measurements were used to characterize the equilibrium FCC catalysts.

3.1.1 Temperature Programmed Techniques

3.1.1.1 Materials

Nickel oxide was prepared in the laboratory by decomposing nickel(ous) nitrate hexahydrate ($Ni(NO_3)_2.6H_2O$, Aldrich Chemical Company) at 500 °C for 4 hours in static air (Chen et al., 1988). Vanadium pentoxide (V_2O_5, 98+ % purity) obtained from Aldrich Chemical Company was used as received. Nickel aluminate ($NiAl_2O_4$, blue in color) was prepared as described in the literature (Murthy et al., 1993) by coprecipitating a stoichiometric mixture of nitrates of nickel and aluminum using 1 N ammonium hydroxide solution to a final pH of 8.2. The precipitated hydroxide precursor was calcined at 800 °C in static air for 24 hours with intermittent grinding.

Gas mixtures, such as 3 % oxygen in helium and 8 % hydrogen in argon were all obtained from Matheson and used as received. Calcium oxalate monohydrate ($CaC_2O_4.H_2O$, 98 %+ purity) used in the calibration of temperature-programmed oxidation apparatus was obtained from Fluka. Methylene chloride (HPLC grade) used for Soxhlet extraction was obtained from Fisher Scientific Company.

3.1.1.2 Catalysts and Catalyst Preparation

In TPR experiments, commercial equilibrium FCC catalysts were supplied by Ashland Oil Company. The properties of these equilibrium catalysts are given in Table 3.1. Nickel and vanadium were doped on Davison Octacat (obtained from Grace and Davison Catalyst Company) and commercial equilibrium FCC catalyst (ECat-LOW from Ashland oil company) by incipient-wetness impregnation method. Aqueous solutions of nickel(ous) nitrate hexahydrate and vanadium pentoxide were used for nickel and vanadium impregnation respectively. After impregnation, catalysts were dried in air at 100 °C overnight, then calcined at 500 °C for 4 hours.

Table 3.1. Nominal Properties of Commercial Equilibrium Catalysts from Ashland Oil Company

Catalyst Type	ECat-LOW	ECat-INT	ECat-HIGH
Surface Area (m^2/g)	178	160	115
Metals (ppm)			
Nickel	300	900	2600
Vanadium	700	1700	6700
Microactivity	71	69	62

In TPO experiments, standard FCC catalysts, RR3 and RR6, and commercial equilibrium FCC catalysts were used. Standard FCC catalysts were obtained from the National Institute for Standards and Technology, with designation RM-8589.

Spent catalysts were prepared by cracking sour imported heavy gas oil (SIHGO) (obtained from Davison Chemical Company), n-hexadecane (99.3 % purity, obtained from Fisher Scientific), and ASTM standard feed (obtained from the National Institute for Standards and Technology, with designation RM-8590) using either calcined or pretreated catalysts. The cracking was performed in a microactivity test (MAT) unit at 500 °C at catalyst-to-oil (C/O) ratios of 3, 5 and 8 (see section 3.3.2 for the details of cracking experiments).

A 1 % platinum-alumina (Pt/Al_2O_3) catalyst, which is used in TPO experiments, was prepared in the laboratory by impregnating platinum chloride hexahydrate ($H_2PtCl_6 \cdot 6H_2O$, obtained from VWR Company) on aluminum oxide (Al_2O_3 12-20 mesh size, obtained from VWR Company). After impregnation, catalysts were dried in air at 100 °C overnight and calcined at 550 °C. Before using, this catalyst was activated with 8 % hydrogen in argon at 500 °C for 6 hours.

3.1.1.3 Temperature-programmed Apparatus: TPR and TPO Modes

The diagram for the combined TPR/TPO apparatus used in temperature-programmed methods is given in Figure 3.2. This apparatus can be used in multiple modes of operations by using different reactant gas mixtures. Temperature-programmed reduction (TPR) mode was successfully used in our laboratory earlier (Feng et al., 2000).

Figure. 3.2 Combined TPR/TPO Apparatus
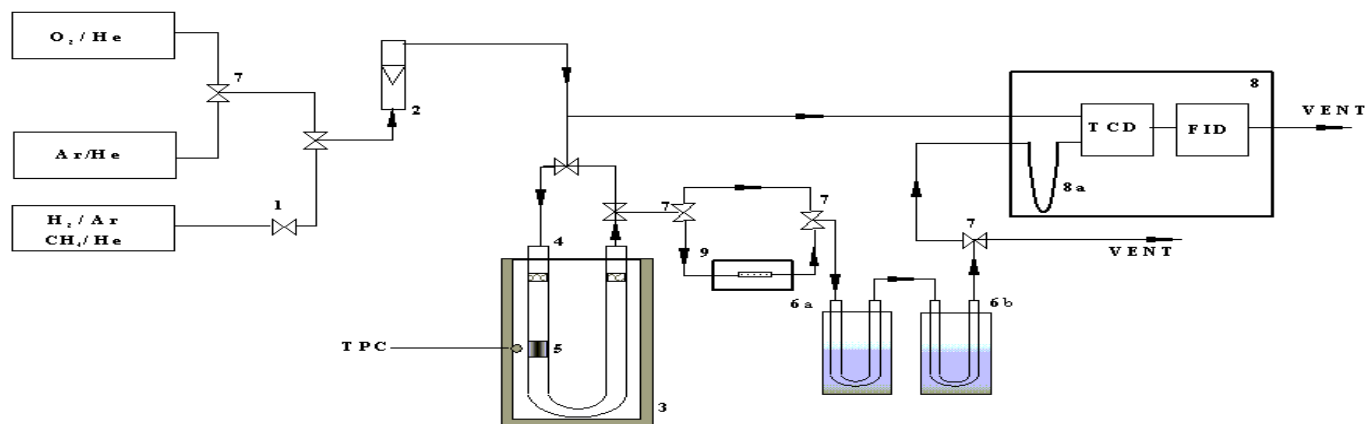
1.	On-Off valve	**6.**	Cold trap (a-mixture of dry ice & acetone, b- liquid N_2)
2.	Rotometer	**7.**	3-way switching valve
3.	Furnace	**8.**	GC
4.	Quartz tube reactor	**9.**	Heated Pt/Al_2O_3 catalyst
5.	Sample		

TCD: Thermal Conductivity Detector
TPC: Temperature Program Controller
FID: Flame Ionization Detector

Briefly, this equipment consists of a Hewlett-Packard 5890 gas chromatograph (with thermal conductivity detector (TCD) and flame ionization detector (FID)) and an external furnace connected to a temperature program controller obtained from Automated Test Systems (Butler, PA). The sample to be analyzed was placed in a quartz U-tube reactor and surrounded with quartz chips. A mixture of 8 % hydrogen in argon flowed through the reactor with a flow rate of 35 cc/min. The exit stream from the reactor passed only through a cold trap filled with a mixture of dry-ice and acetone (to remove water from exit steam), then to TCD and FID detectors connected in series in the gas chromatograph. TCD monitored hydrogen concentration while FID monitored methane and carbon monoxide formation during the TPR experiments. Approximately 250 mg of calcined catalyst was used in each TPR experiment.

In TPO experiments, a mixture of 3 % oxygen in helium flowed with a flow rate of 40 cc/min through the reactor. For TPO the exit stream first passed through the 1 % platinum-alumina catalyst kept at 595 °C, then through traps filled with a dry-ice/acetone mixture (to trap water) and liquid nitrogen (to trap carbon dioxide formed) in series. Platinum-alumina catalyst converted the carbon monoxide formed and any desorbing hydrocarbon to carbon dioxide and water. This arrangement made the quantification of carbon content possible by measuring the carbon dioxide trapped in the liquid nitrogen trap during the TPO run. Approximately 50 mg spent-catalyst samples were used in each TPO experiment.

In all the TPR and TPO experiments, temperature was ramped linearly from room temperature to 865 °C at a rate of 10 °C/min. Then the furnace was held at 865 ºC until the end of analysis. Both TPR and TPO profiles of the samples were analyzed by deconvoluting them using PeakFit software from Jandel Scientific.

The TPO system was calibrated with respect to oxygen and carbon dioxide concentrations by decomposing known amounts of $CaC_2O_4.H_2O$ (obtained from Fluka) under the flow of 3 % oxygen in helium. A typical TPO spectrum from the calibration run with $CaC_2O_4.H_2O$ is given in Figure 3.3a. Thermal decomposition of $CaC_2O_4.H_2O$ under helium flow forms H_2O, CO and CO_2. After the dry ice-acetone mixture at the exit of U-shaped quartz reactor traps H_2O, only CO and CO_2 peaks are detected as seen in Figure 3.3b. During the TPO calibration run, the CO produced by the thermal decomposition of known amount of $CaC_2O_4.H_2O$ is converted into CO_2 at the surface of Pt/Al_2O_3 catalyst located at the exit of reactor. The oxidation of CO causes the oxygen concentration to decrease in the flow stream. Then the flow stream passes through the traps filled with liquid nitrogen and dry-ice/acetone mixture. In these traps H_2O, CO_2 formed by the oxidation of CO and CO_2 produced during the thermal decomposition are trapped during the TPO run. Therefore, only the oxygen consumption in the flow stream is detected by thermal conductivity detector (TCD) and recorded as a negative peak during the experiment (see Figure 1a). At the end of the temperature programming, the liquid nitrogen trap is removed and carbon dioxide evaporates into the carrier gas flow. At this point, the GC column (Carboxen 1000, from Supelco) preceding the TCD comes into the picture. This column holds the carbon dioxide long enough so that the disturbances in TCD signal due to the flow changes created by removing the liquid nitrogen trap do not overlap with the signal created by carbon dioxide. From the areas under these peaks shown in Figure 3.3a, the system is calibrated with respect to oxygen (negative peak) and carbon dioxide (positive peak) concentrations.
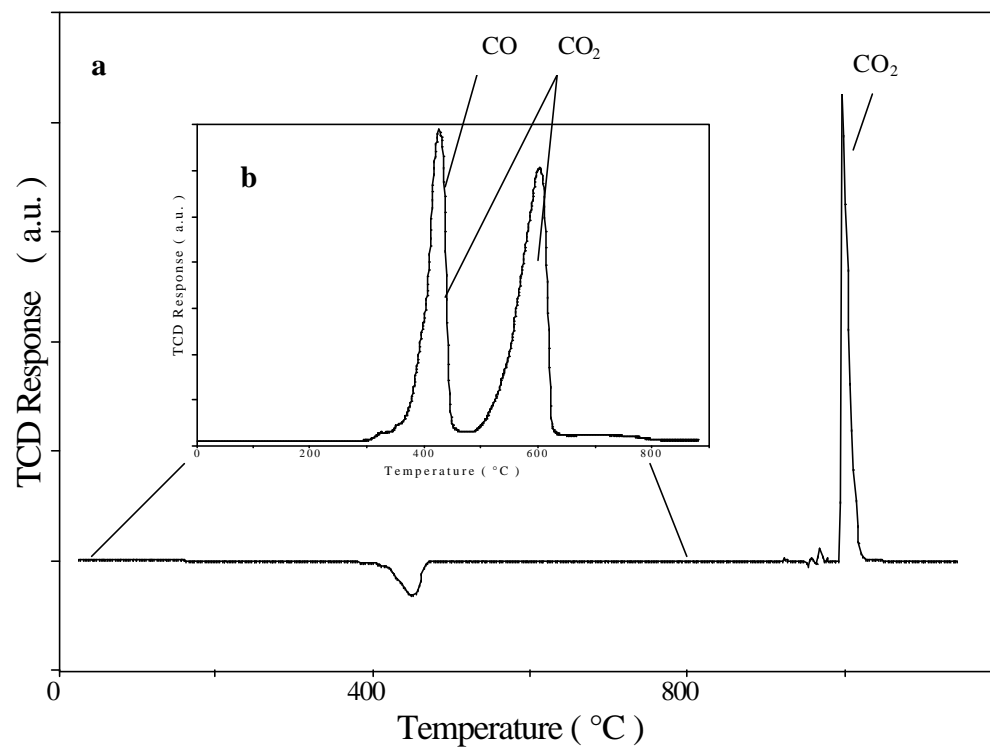
Figure. 3.3 A Typical TPO Spectrum. (a) TPO Spectrum for CaC₂O₄.H₂O with 3% O₂ in He; (b) Thermal Decomposition of CaC₂O₄.H₂O with He

49

After calibration, the carbon and hydrogen contents of spent catalyst samples were determined using our TPO apparatus. To confirm the results from TPO experiments, the same samples were sent to a commercial laboratory (Galbraith Laboratories) for carbon and hydrogen determination. Both results are compared in Table 3.2, and are in good agreement.

Table 3.2 Comparisons of Quantitative Analysis Results from TPO and Commercial Laboratory

Sample Number	TPO Analysis Results		Combustion Analysis Results[c]	
	Carbon (wt. %)	Hydrogen (wt. %)	Carbon (wt. %)	Hydrogen (wt. %)
Sample 1	0.79	0.05	0.83	<0.5
Sample 2	1.21	0.08	1.18	<0.5
Sample 3	1.07	0.09	1.09	<0.5

C: Galbraith Laboratories

3.1.2 Coke Determination

The coke amount on spent catalysts was determined by using thermogravimetric analysis (TGA), temperature programmed oxidation (TPO) and calcination in a muffle furnace.

Three different types of commercial equilibrium FCC catalysts and standard ASTM catalysts were analyzed with the techniques mentioned above. The TGA method was applied to spent standard ASTM catalysts, namely RR3 and RR6 to understand the accuracy of coke determination by weight measurements after calcination.

3.1.2.1 TPO for Carbon and Hydrogen Determination

The coke composition, hydrogen-to-carbon molar ratio (H/C), was determined by measuring the oxygen consumption and carbon dioxide production during the TPO experiment.

3.1.2.1 TGA of Spent Standard Catalysts

TGA analysis was carried out by Dr. Mani Manivannan using a Mettler thermogravimetric analyzer at WVU Physics Department. About 40-50 mg of spent standard catalyst was used in each experiment. The sample was heated in the presence of air at a rate of 20 °C/min from room temperature to 700 °C.

3.1.2.2 Calcination in the Muffle Furnace

To determine the coke amount by calcining in a muffle furnace, fused-quartz crucibles obtained from Fisher Scientific Co. were used. These crucibles have unique airtight self-sealing lids. During the volatile run, the lid automatically rises and the released gases or moisture is expelled as the sample is heated. Then the lid sinks back to restore the seal when the sample is cooled. This self-sealing action prevents sample from being exposed the moisture of the environment, thus eliminate inaccurate weighing caused by the moisture uptake.

This procedure is performed in two steps. In the first step, empty crucible with lid is weighed and its weight is recorded. Then, about 1 gram of spent catalyst is placed into the crucible and the weight of crucible with sample is measured and recorded. The difference between these two weights gives the amount of spent catalyst whose coke content will be determined. The crucible containing spent catalyst is placed into a muffle furnace. The temperature of muffle

furnace is increased to 160 °C and kept constant at this temperature for at least 6 hours. During this heating process, the moisture on the spent catalyst is removed. After the furnace is allowed to cool down to room temperature, the moisture-free spent catalyst is weighed. This allows us to determine moisture-free weight of the sample. In the second step, the crucible with the spent catalyst sample is placed inside the same muffle furnace. The temperature is raised to 560 °C and kept at this temperature for 16 hours. Then the furnace is allowed to cool down to room temperature again. This process removes the coke on the catalyst and makes the calcined catalyst moisture free. The weight of crucible with calcined moisture-free catalyst is measured. The dry-weight difference between the spent and calcined catalysts gives the amount of coke removed from the catalyst.

3.1.3 Surface Area Measurements

Surface area measurements were performed by Dr. Edwin L. Kugler using continuous flow adsorption method. A Coulter Omnisorp 360 was used to obtain the nitrogen adsorption and desorption isotherms of standard Round Robin catalysts, RR3 and RR6 and commercial equilibrium FCC catalysts before and after cracking reactions. The BET and T-Plot surface areas were determined from the nitrogen adsorption isotherms. Pore volumes were calculated from desorption isotherms.

3.2 Catalyst Pretreatment

Commercial equilibrium FCC catalysts with three different metal contaminant levels, namely, ECat-LOW, ECat-INT, and ECat-HIGH were used. These catalysts are either calcined or pretreated before they are used in catalytic cracking reaction. Calcination was performed at 550

°C for 6 hours to make sure no coke deposits exist before cracking reactions. Two types of pretreatment using hydrogen and methane are performed in this study. These pretreatments were performed at 700 ºC for approximately 6 hours by using 8% hydrogen in argon or 8% methane in helium with a quartz reactor in the microactivity test (MAT) unit. They are aimed to reduce the oxidation state of metal contaminants on the catalyst. These gas mixtures were obtained from Matheson and used as received.

3.3 Catalyst Evaluation

3.3.1 Feed, FCC catalysts

Two types of feed were used in the cracking experiments, SIHGO and n-hexadecane. Performances of the commercial equilibrium FCC catalysts were evaluated before and after catalysts were pretreated with hydrogen and methane (see section 3.2 for the details of catalyst pretreatment).

3.3.2 Cracking Experiments

Microactivity test measurements of catalyst activity were performed according to the procedures of ASTM D-3907 using both SIHGO and n-hexadecane feed. The MAT unit was manufactured by Industrial Automated Systems (Parlin, New Jersey). The microactivity test unit consists of a furnace for maintaining constant cracking temperature (500 °C), a syringe pump whose speed can be varied to inject the cracking feed, a liquid product receiver and a gas collection vessel (Figure 3.4). A flow meter is used to control the flow of nitrogen through the reactor. Nitrogen is used as a purge gas before a run and immediately after a run in order to

remove the lighter gases, which are dissolved in the liquid product. Liquid product was collected in a trap at 0 °C and vapor product was collected in a glass vessel by downward displacement of water to calculate the extent of conversion and the material balance for the experiment.

To achieve different conversions the reaction severity was varied by changing the catalyst-to-oil ratio (C/O) where C/O ratio is defined as the amount of catalyst divided by the total amount of feed. This ratio was changed by changing the amount of feed while keeping the catalyst amount constant at 5 grams. C/O ratios of 3, 5, and 8 were used in the cracking experiments. The procedure for MAT experiments was previously described in detail by Subramanian (1993).
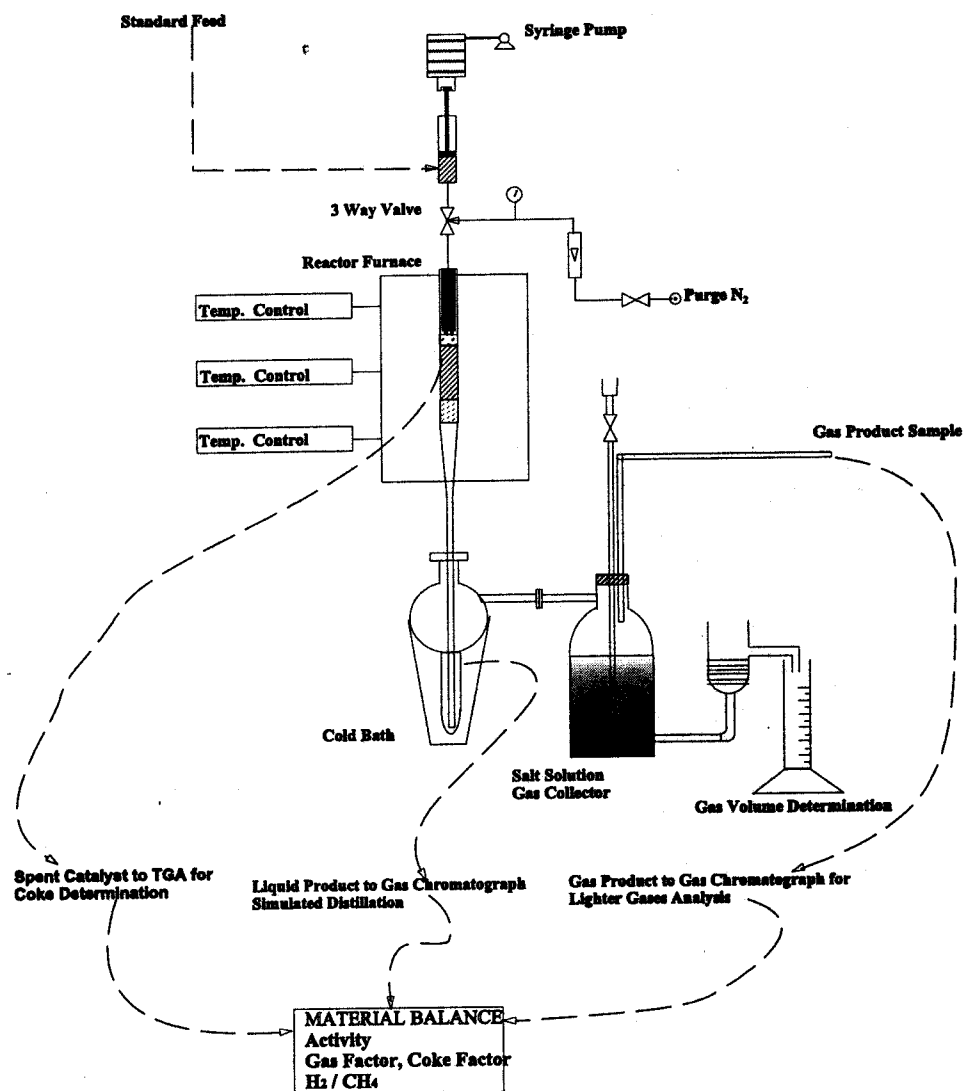
Figure 3.4 Laboratory Set-up for Microactivity Test (MAT) Unit

3.3.3 Analysis of products

The volume of the displaced brine (V_B), the gas temperature (T_R) and the atmospheric pressure are recorded for MAT runs. The gas sample is immediately analyzed using a VARIAN 3600 gas chromatograph. H_2, C_1, C_2, C_3, C_4, and C_5^+ lump are determined quantitatively (Appendix A). This GC has two types of detectors, an FID and a TCD. A porous-layer open-tubular (PLOT) GS-Alumina column and a HAYESEP-DIP 60/80 column are used to accomplish the separation. The PLOT alumina column identifies C_1 to C_5 's. The PLOT column is connected to the FID for direct quantification of hydrocarbon products. The HAYESEP column is used in series with a TCD to identify and measure hydrogen. This column uses a porous polymer for separation. Initially, a calibration standard of 1 % hydrogen and 0.98 % iso-butane in nitrogen is run. Since retention time and concentration of these two gases are known, quantitative analysis of the gas products obtained from MAT analysis is performed. This allows the determination of the amount (weight) of gaseous products obtained from each run, which is used to calculate the mass balance over the entire unit (detailed calculation is presented in Appendix B).

The liquid products, after weighing, are dissolved in CS_2 solvent and analyzed by GC simulated distillation (Appendix C). D2887 simulated distillation is used to determine the percentage of the liquid products boiling at certain temperature ranges (gasoline: IBP- 421 F, light cycle oil (LCO): 421 - 650 F, and heavy cycle oil (HCO): 650 F and above). A Supelco Petrocol B packed column installed in a VARIAN 3400 GC is used. Initially, a blank base line run is carried out and stored to nullify any effect of baseline drift due to temperature programming. Next, a calibration standard of n-alkanes is run. The verification of the gas chromatograph analysis is checked once every three runs by using a reference oil mixture. An auto-sampler is used to inject

the same amount of sample (0.3μL) for every run. A weight percent off versus temperature report is generated. Using this, the conversion as defined by ASTM 3907 can be calculated.

Coke on the spent catalyst is determined gravimetrically by burning it off in a muffle furnace. Carbon and hydrogen concentration on spent catalysts were also determined by measuring the carbon dioxide formation and oxygen consumption during the temperature-programmed oxidation (TPO) analysis. The details of TPO analysis and gravimetric measurements are given in section 3.1.2.

4.0 REDUCIBILTY OF CONTAMINANT METALS ON FCC CATALYSTS BY TEMPERATURE PROGRAMMED REDUCTION (TPR)

Temperature-programmed reduction (TPR) has been widely used to characterize different catalysts. Hurst et al. (1982) have written a detailed review about the method. TPR reveals information about the temperature range where reduction occurs, oxidation state of the metals, the presence of various surface phases, possible interactions between species, interaction with support and the factors that affect dispersion. TPR experiments are very useful in case of multi-metallic systems, for the evaluation of the role of the added compounds or doping agents (alloy formation or promotion effects). TPR has been applied to characterize nickel and vanadium on cracking catalysts (Tatterson et al., 1988; Cadet et al., 1991; Cheng et al., 1993; Doolin et al., 1991).

4.1 Reduction of Unsupported Metal Oxides (NiO, $NiAl_2O_4$, and V_2O_5)

Commercial cracking catalysts are contaminated with various metals from the feedstock. These contaminant metals are predominantly nickel and vanadium. Therefore, the individual TPR spectra of these unsupported metals become very important to evaluate their contributions to the TPR spectra of commercial, metal-contaminated, equilibrium FCC catalysts.

The TPR spectra for bulk NiO, $NiAl_2O_4$, and V_2O_5 are compared in Figure 4.1a, b and c. TPR profile for unsupported NiO (Figure 4.1a) shows a sharp peak at around 380 °C whereas for $NiAl_2O_4$ (Figure 4.1b) a peak is observed near 780 °C. These results are in agreement with published results (Cadet et al., 1991; Li et al., 1995). These TPR spectra show that $NiAl_2O_4$ type compounds are more difficult to reduce compared to NiO.
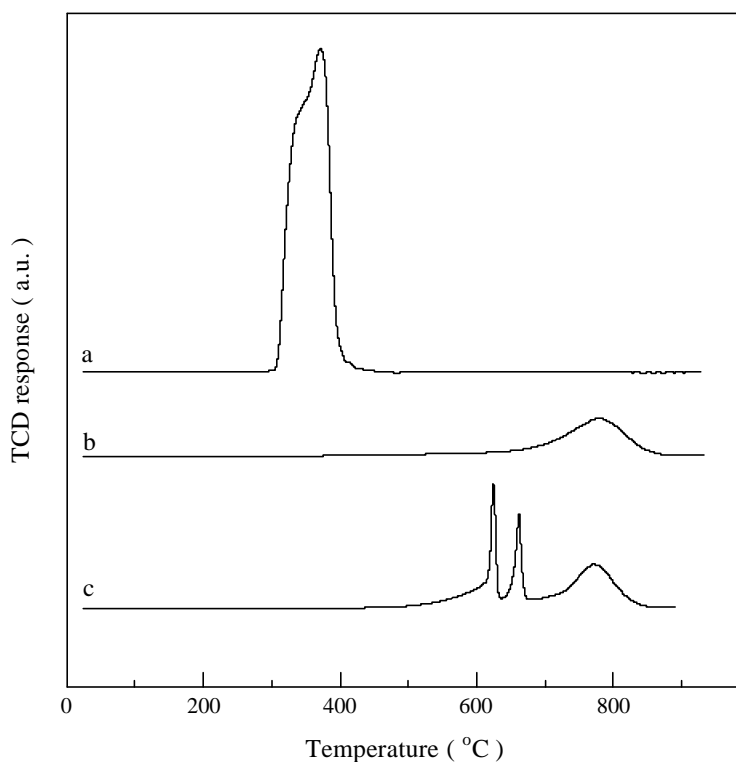
Figure 4.1 TPR Spectra for Unsupported Metal Oxides: (a) NiO; (b) NiAl$_2$O$_4$; (c) V$_2$O$_5$

In the case of unsupported V$_2$O$_5$ reduction given in Figure 4.1c, the TPR spectrum shows three peaks at around 624, 662 and 780 °C. Other groups (Koranne et al., 1994; Jouguet et al., 1995) have also observed similar reduction profiles for bulk V$_2$O$_5$. Jouguet et al (1995) have observed that reduction with pure hydrogen at atmospheric pressures results in formation of V$_2$O$_3$. At lower hydrogen partial pressures the reduction was found to be incomplete.

Jouguet et al. (1995) have concluded that the first peak occurs on reduction to V_6O_{13}, while the second peak results from reduction to VO_2. Reduction to V_2O_3 produces the final peak at a temperature above 800 °C. Jouguet et al. (1995) have confirmed their results by determining the chemical compositions of remaining solids at every step of their TPR spectrum with x-ray analysis.

4.2 Reduction of Supported Metal Oxides

The TPR spectra of calcined commercial equilibrium FCC catalysts are shown in Figure 4.2a, b and c. In general two broad peaks are observed in these profiles, a low temperature peak at around 525 °C and a high temperature peak at around 820 °C. The profiles show sharper peaks with increasing metal levels on the equilibrium FCC catalyst. It becomes difficult to understand the individual contribution of contaminant metals (nickel and vanadium) into the spectra in Figure 4.2. In order to resolve these two broad peaks, nickel and vanadium have been impregnated on different FCC catalysts by the incipient-wetness impregnation method. Figure 4.3a shows the TPR spectra of nickel-impregnated Octacat FCC catalyst. The catalyst was then oxidized and reduced seven times. After each TPR experiment, the system was allowed to cool down to room temperature. Then air was passed through the catalyst sample while the temperature was ramped to 865 °C at a rate of 10 °C/min. It can be seen that after seven repetitive reduction/oxidation steps, the low temperature peak at 450 °C corresponding to the NiO reduction becomes smaller while a distinct high temperature peak appears around 800 °C (see Figure 4.3b). This high temperature peak can be attributed to the formation of nickel aluminate and/or nickel silicate type compounds. These types of observations have been made by others (Cadet et al., 1988; Cheng et al., 1993; Afzal et al., 1993). If we compare these results with the reduction of bulk NiO and $NiAl_2O_4$, we

can see that reduction temperature for supported NiO (450 °C) is higher than that of bulk NiO (380

°C). The fact that unsupported oxides are more easily reduced than supported ones was observed

by Hurst et al. (1982) and explained in detail. The reduction temperatures of bulk $NiAl_2O_4$ and

$NiAl_2O_4$ formed on FCC catalyst are almost the same (780 ℃). This high temperature is not

surprising since $NiAl_2O_4$ is a quite stable compound.
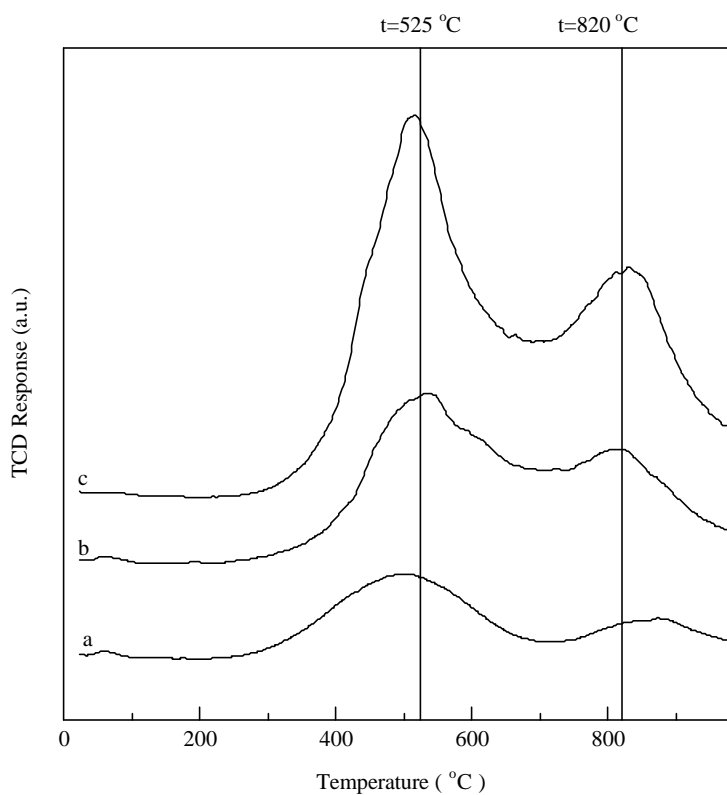
Figure 4.2 TPR Spectra for Commercial Equilibrium FCC Catalysts:(a) ECat-LOW; (b) ECat-INT; (c) ECat-HIGH

61
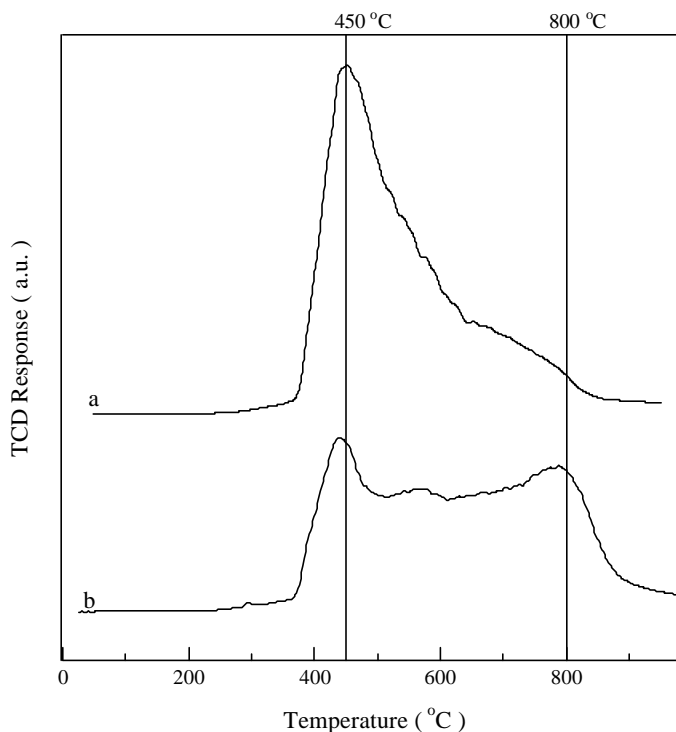
Figure 4.3 TPR Spectra for NiO Impregnated on FCC Catalyst: (a) TPR of Supported NiO after Impregnation; (b) TPR of Supported NiO after Seven Reduction/Oxidation Cycles.

When vanadium was similarly impregnated on commercial equilibrium FCC catalyst (ECat-LOW), as seen from Figure 4.4, the reduction temperature for supported vanadium becomes lower than that of bulk V_2O_5 (see Figure 4.1). Only one significant peak is observed in this spectrum at around 500 °C. The reduction of bulk V_2O_5 (see Figure 4.1) resulted in three peaks in the temperature range from 600 to 800 °C. However, Koh et al. (1992) have reported that a low concentration of V_2O_5 on many different supports resulted in only one significant reduction peak located at a temperature between 450 and 600 °C. This decrease in reduction temperature of supported V_2O_5 compared to bulk V_2O_5 has been attributed to the formation of a highly dispersed

monolayer phase on the support and the weakening of the vanadium-oxygen bond due to the interactions with the support (Cheng et al., 1993; Stobbe et al., 1995). Figures 4.5 and 4.6 can be obtained after deconvoluting the TPR profiles in Figure 4.4a-b for ECat-LOW before and after vanadium impregnation, respectively. In Figure 4.6, areas for peaks X, Y and Z are forced to same as those in Figure 4.5. As seen from this figure, a reasonable curve fitting can be satisfied with an additional peak W at 508 °C. The peak W can be attributed to the reduction of impregnated vanadium on the catalyst.
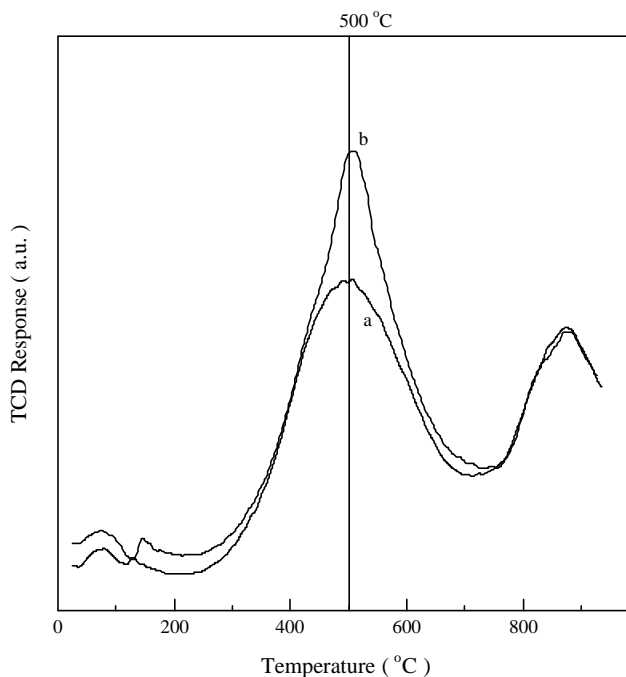
Figure 4.4 TPR Spectra of ECat-LOW: (a) before Vanadium Impregnation; (b) after Vanadium Impregnation
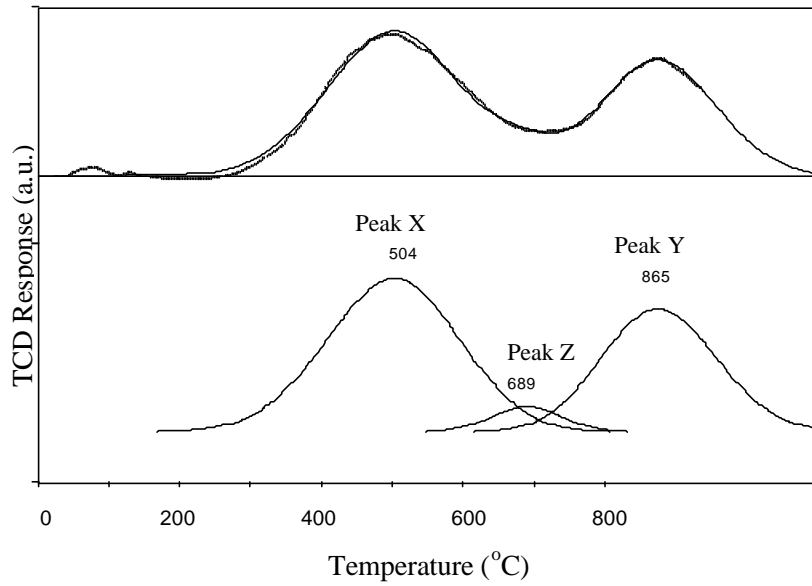
Figure 4.5 Analysis of TPR Spectrum for FCC Catalyst (ECat-LOW) before Vanadium Impregnation
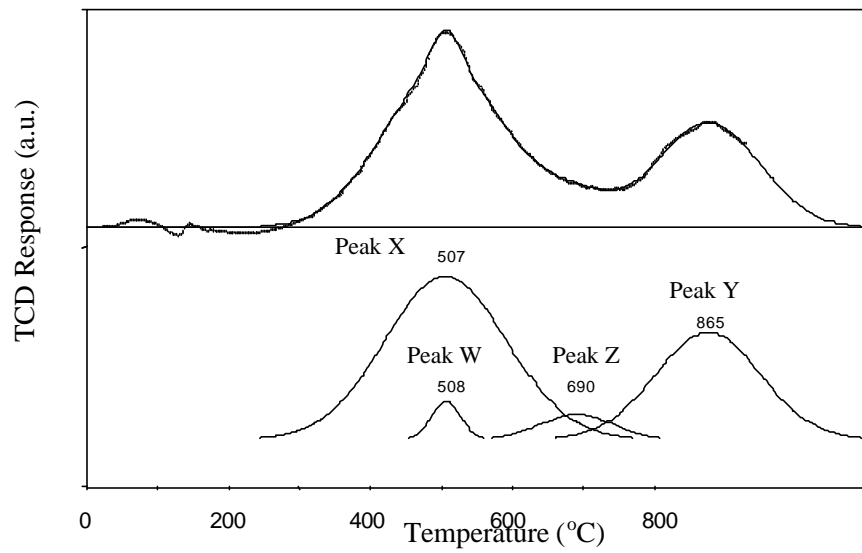
Figure 4.6 Analysis of TPR Spectrum for FCC Catalyst (ECat-LOW) after Vanadium Impregnation

TPR profiles for ECat-INT and ECat-HIGH (Figure 4.2b-c) were also deconvoluted into three peaks, which gave us Figures 4.7 and 4.8. The reason for observing a much smaller peak Z for ECat-LOW (Figure 4.5) compared to both ECat-INT (Figure 4.7) and ECat-HIGH (Figure 4.8) is due to the lower concentration of vanadium on ECat-LOW. The low temperature peak X is the result of reduction of both vanadium and NiO on the equilibrium catalyst. When the vanadium level on the catalyst increases as in the cases of ECat-INT and ECat-HIGH, reduction of vanadium becomes more difficult. Therefore, Peak Z starts to become significant in the TPR profiles with increasing vanadium level (Figures 8 and 9). Peak Y in all TPR spectra can be attributed to the reduction of $NiAl_2O_4$ on the equilibrium catalysts. The area for peak Y that is proportional to the $NiAl_2O_4$ concentration on the catalyst increases with the catalyst age. The more the catalyst is exposed to the cyclic reduction and oxidation processes, the more $NiAl_2O_4$ forms on the catalyst.

In short, we can conclude that the low temperature peak corresponds to the reduction of NiO and V_2O_5 whereas the high temperature peak corresponds to the reduction of nickel aluminate and silicate type compounds. Several researchers (Cheng et al., 1993, Haas et al., 1992) have drawn similar conclusions.
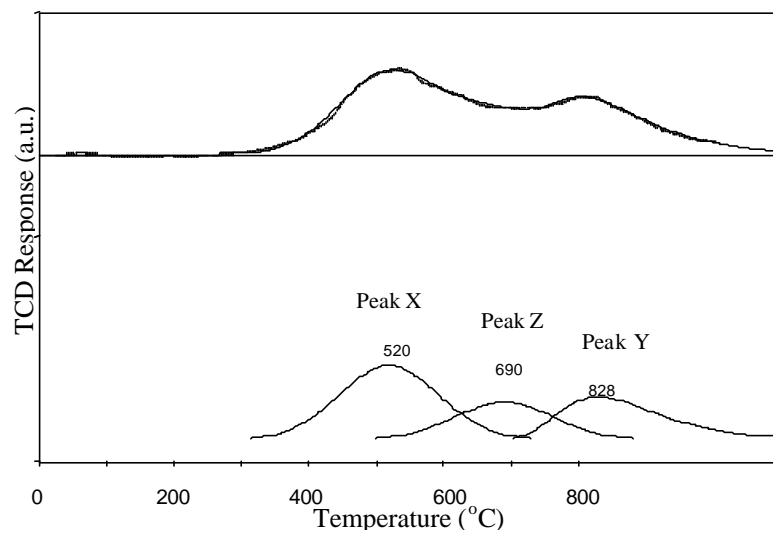
Figure 4.7 Analysis of TPR Spectrum for Commercial Equilibrium FCC Catalyst (ECat-INT)
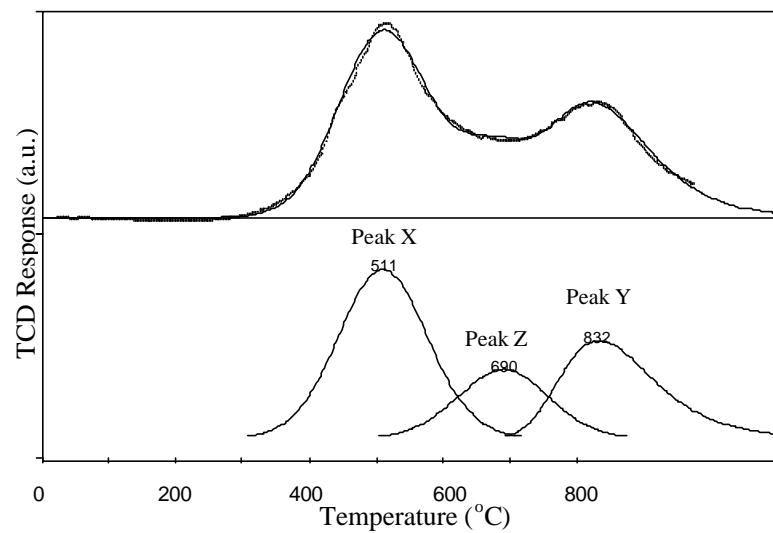
Figure 4.8 Analysis of TPR Spectrum for Commercial Equilibrium FCC Catalyst (ECat-HIGH)

66

TPR profiles using thermal conductivity (TCD) and flame ionization detector (FID) are given in Figure 4.9. In these experiments, catalyst samples are used as received from the refinery (Figure 4.9a,c) and after being calcined (Figure 4.9b,d). The only difference between these catalysts is that the catalyst received from the refinery contains a small amount of carbon on it. If we have a close look at the profile (Figure 4.9a) for the catalyst as received from the refinery, we observe a small negative peak at around 860 °C. Corresponding FID signal for the same experiment also shows a little response at around the same temperature. This must be due to gas formation during the experiment. The possibility of being methane is quite low since FID is very sensitive to methane and creates very significant response to this gas. However, FID will produce very little signal because of carbon monoxide formation. This negative signal can be attributed to the carbon monoxide desorption from the decomposition of oxidized carbon. Similar observations have been made by several researchers (Feng et al., 2000; Querini et al., 1997; Kelemen et al., 1986; Otake et al., 1993; Dandekar et al., 1998). Querini et al. (1997) has shown that the carbon oxides production during the gasification of coke on an Al_2O_3 support under an inert gas was result of a direct reaction of the coke deposits with hydroxyl groups on the surface of Al_2O_3. It was also found that the maximum amount of coke that can be gasified is limited to the amount of hydroxyl groups on the alumina surface (Querini et al., 1997).
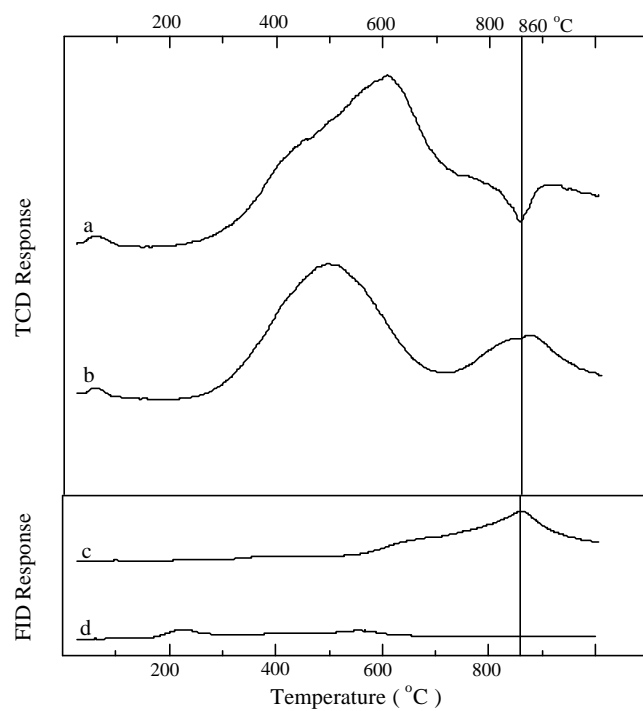
Figure 4.9 TPR Spectra for Commercial Equilibrium Catalyst (ECat-LOW): (a) and (c) are TCD and FID Responses, respectively, for ECat-LOW as received; (b) and (d) are TCD and FID Responses respectively for Calcined ECat-LOW

4.3 Conclusions

Temperature-programmed reduction was used to determine the reducibility of nickel and vanadium on commercial equilibrium FCC catalysts. TPR spectra of commercial equilibrium catalysts were deconvoluted into three peaks, in order to determine the individual contribution of the metal oxides to the profile. The sizes of the peaks increase with increasing metal levels on the equilibrium catalyst. In the TPR spectrum, the peak that appears at low temperature (500-525 °C) was assigned to the reduction of NiO and V_2O_5. The peak at around 690 °C was assigned to continuation of vanadium pentoxide reduction at relatively high vanadium concentration on the catalyst. The high temperature peak above 800 °C was assigned to the reduction of nickel aluminate and silicate type compounds. This information from TPR profiles of equilibrium catalysts before and after pretreatment with hydrogen (i.e., reduction in the oxidation states of nickel and vanadium) helped us to interpret the results from the cracking experiments.

5.0 CHARACTERIZATION OF COKE ON FCC CATALYSTS BY TEMPERATURE PROGRAMMED OXIDATION (TPO)

Formation of coke that consists of the carbonaceous compounds (polyaromatic or non-polyaromatic) during catalytic cracking reactions causes FCC catalyst to deactivate. The properties of coke such as amount, nature and location are affected by feed composition, catalyst type and reaction conditions. These properties give some idea about the FCC catalyst performance and also play important roles in combustion kinetics during the regeneration process. Therefore, an extensive understanding of coke properties is essential in the development of new FCC catalysts and improvement of present commercial FCC operations.

Although many advanced analytical techniques are available, coke characterization continues to be a challenging task of the new millennium. It is very difficult to determine the composition of coke because it is difficult to separate coke from the zeolite portion of the catalyst by conventional extraction methods. This explains why recently in-situ methods for coke characterization became very important (Querini et al., 1997). In some cases coke concentration on the catalyst can be less than 1%. The low levels of coke content on the catalyst makes it necessary to use a very sensitive analytical technique for reproducible and accurate results. Since FCC coke is very complex, usually multiple analytical techniques have to be applied for the determination of coke composition and structure.

Characterization of coke on spent catalysts is an area where temperature-programmed techniques have found many applications. Other analytical methods such as FTIR, TEM, laser Raman spectroscopy, EELS, ^{13}C-NMR, Auger electron spectroscopy, secondary ion mass spectrometry, and small-angle neutron scattering are very useful to determine coke composition, structure and location. However these techniques do not provide any information on the reactivity

and behavior of coke under thermal treatments to which catalysts are frequently exposed (Querini et al., 1997).

With temperature-programmed techniques, coke on several catalyst systems has been characterized with respect to its reactivity towards hydrogen (temperature-programmed hydrogenation, TPH) (McCarty et al., 1979; Figueiredo et al., 1986; Teixeira et al., 1994; Wrammerfors et al., 1994) and oxygen (temperature-programmed oxidation, TPO) (Van Doorn et al., 1992; Duprez et al., 1997; Goula et al., 1996; Baker et al., 1995; Oh et al., 1997; Larsson et al., 1998; Grau et al., 1991; Barbier et al., 1990). Temperature programmed gasification with carbon dioxide has also been tried to characterize the carbon deposits on spent catalysts (Van Doorn et al., 1986). The location and nature of coke on spent catalyst affect the coke oxidation kinetics that is a very crucial factor in optimizing catalyst regeneration processes. Temperature-programmed oxidation (TPO) becomes a very important tool to study coke combustion on spent catalysts.

TPO determines the total amount of coke, the hydrogen-to-carbon ratio in the coke and location of coke deposited on the spent catalyst. The information about the coke properties is inferred from TPO profiles through the shape, area and position of each peak. The aromaticity of coke is usually judged by the atomic H/C ratio. This ratio can be easily determined stochiometrically by measuring the oxygen consumption and carbon dioxide production during the TPO experiment. The decrease in atomic H/C ratio (<1) is accepted as the indication of increasing polyaromatic content of the coke. The H/C ratio of 0.41 was found to be a typical value for spent FCC catalyst from the industrial cracking reactor (Li et al., 1999).

Several groups have used the TPO method to characterize the coke on FCC catalysts (Doolin et al., 1991; Dimitriadis et al., 1998; Li et al., 1999; Minh et al., 1997; Li et al., 1998).

71

The effect of metal contaminants (e.g., vanadium and nickel) on regeneration of spent FCC catalysts has been observed by some of these groups (Doolin et al., 1991; Dimitriadis et al., 1998; Minh et al., 1997). Similar types of observations were made for the regeneration of other coke-deactivated catalyst systems (Yoshinura et al., 1986; Zeuthen et al., 1995; Bartholdy et al., 1995).

In this work, an existing TPR apparatus was modified into a TPO apparatus. This combined TPR/TPO apparatus was used to demonstrate the coking properties of commercial equilibrium FCC catalysts with or without pretreatments. Coked cracking catalysts were examined by TPO in order to find out the differences in the amount and nature of the coke. The quantitative results obtained from TPO are compared with those from thermogravimetric analysis (TGA). The effects of metal contaminants, cracking feed type and pretreatments on the TPO spectra of commercial equilibrium FCC catalysts were investigated.

5.1 Determination of Coke Content

Figures 5.1 and 5.2 show the thermogravimetric profiles and derivative curves for spent standard catalysts, RR6 and RR3, respectively. RR6 and RR3 were round robin standard FCC catalysts obtained from the National Institute for Standards and Technology. In these figures, S1 and S2 represent the spent catalyst samples of RR6 from two different cracking experiments. Similarly S3 and S4 represent the spent catalyst samples of RR3 from two different cracking experiments. As seen in both Figures 5.1 and 5.2, the first negative peaks that appear at low temperatures (100-125 °C) in derivative curves indicated the weight loss as a result of the moisture removal from the spent catalyst. The second negative peaks at relatively high temperatures (around 565 °C) in the derivative curves represent the weight lost due to the coke removal by oxidation. From the difference in weight measurements corresponding to the second

negative peak we can determine the amount of coke per gram of spent catalyst. The coke contents of these spent standard catalysts from TGA analysis are given in Table 5.1. The coke contents of the same spent catalysts labeled S1, S2, S3, and S4 were also determined by weight measurements after calcination in the muffle furnace.

As seen in Table 5.1, the results obtained from both TGA and calcination in a muffle furnace were found to be in excellent agreement. This confirmed that weight measurements using quartz crucibles before and after calcination are quite reliable for determination of coke amounts on the spent catalysts. The inaccurate weight measurements caused by the moisture uptake from environment were eliminated (see section 3.1.2.2). The only disadvantage of calcination in a muffle furnace is that it is a lengthy procedure. The determination of coke amount by calcination was also performed without using self-sealing quartz crucibles. Those results were found to be inconsistent and not reproducible. The main reason was the changes in the humidity of the room environment.

The results of coke determination by three different sources, including TPO analysis, weight measurements, and combustion analysis from a commercial laboratory were summarized and compared in Table 5.1. As seen from this table, agreement between these techniques is quite satisfactory, indicating that any of these methods can be used equally well for determination of coke amount on the spent catalysts. Among them, TPO was found to be very useful since it provides information about the hydrogen to carbon ratio and oxidation profile as well.
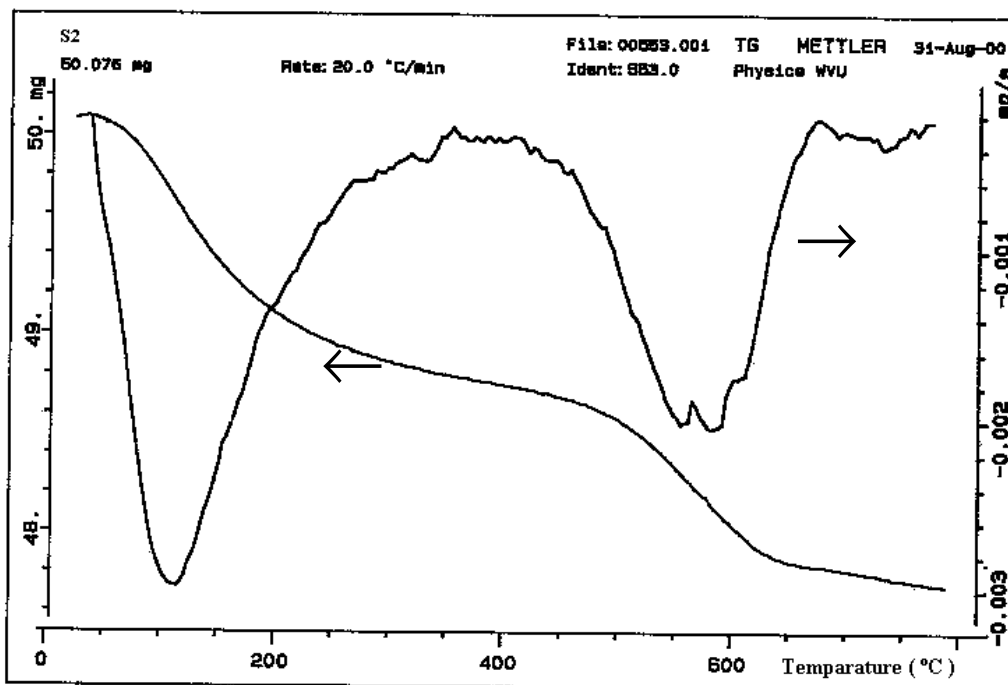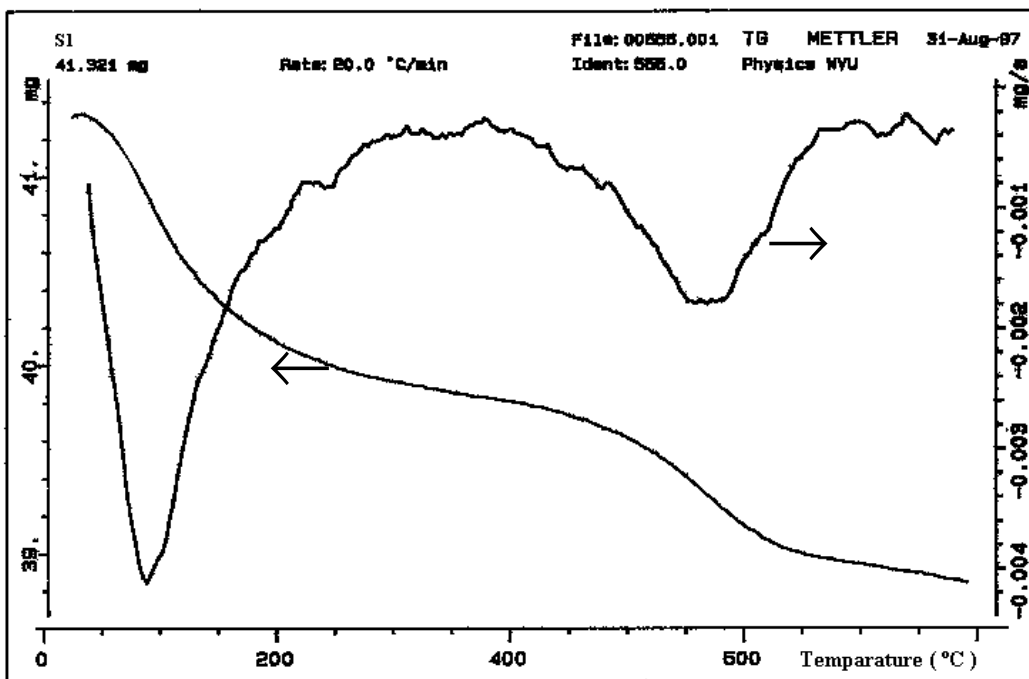
Figure 5.1 Thermogravimetric Profiles (Left-hand Scale) and Derivative Curves (Right-hand Scale) for Spent Standard ASTM Catalysts S1) RR6; S2) RR6
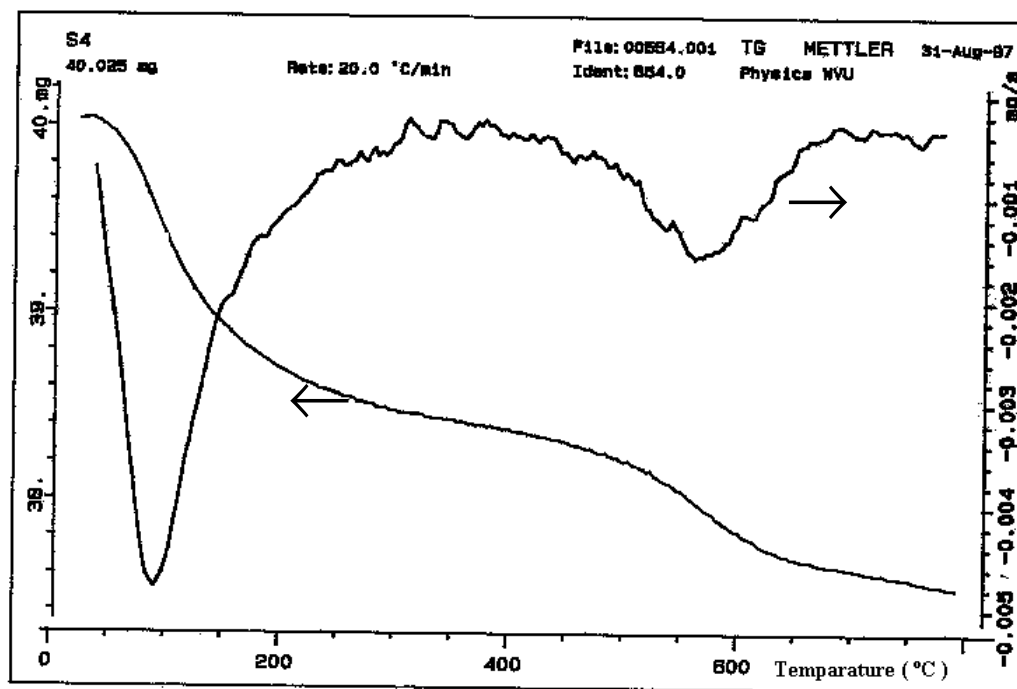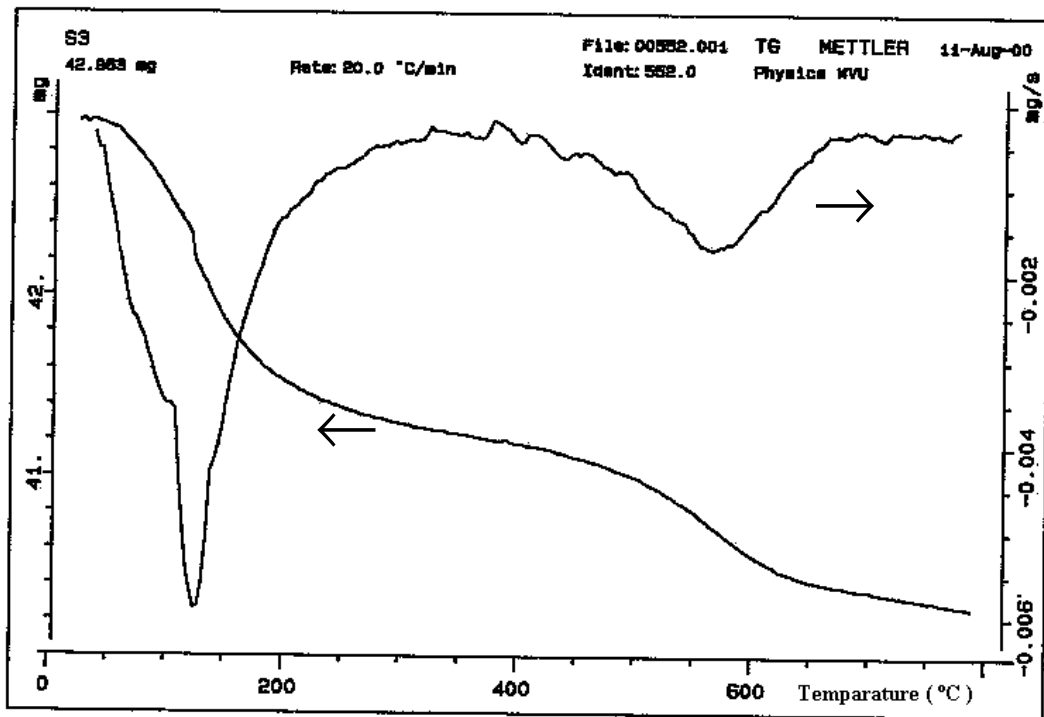
Figure 5.2 Thermogravimetric Profiles (Left-hand Scale) and Derivative Curves (Right-hand Scale) for Spent standard ASTM Catalysts S3) RR3; S4) RR3

The more detailed results from weight measurements and TPO analysis for the different spent catalysts are tabulated and compared in Table 5.2. The spent catalysts in this table are either calcined or pretreated prior to the cracking reactions. Therefore some of these results reflect the changes in H/C ratio and coke amount as a result of the type of pretreatments applied. H/C ratio was obtained by measuring the oxygen consumption and carbon dioxide production during the TPO experiment. From the coke combustion reaction, the H/C ratio can be calculated as follows:

$$CH_x + (1+\frac{x}{4})O_2 \rightarrow CO_2 + \frac{x}{2}H_2O$$

$$\frac{H}{C} = x = 4 \times \left(\frac{O_2 consumed}{CO_2 produced} - 1 \right)$$
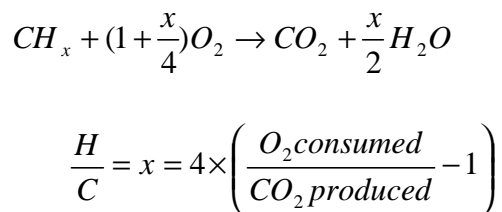
Table 5.1 Comparisons of Techniques for Coke Determination on Spent FCC Catalysts

Sample	Commercial Laboratory Results (by combustion)		TPO Results			Weight Measurements
	Carbon%	Hydrogen%	Carbon%	Hydrogen%	H/C (molar)	Coke%
FCC-01	0.83	<0.5	0.79	0.05	0.80	0.95
FCC-02	1.18	<0.5	1.21	0.08	0.84	1.29
FCC-03	1.09	<0.5	1.07	0.09	0.96	1.16
FCC-04	1.33	<0.5	1.42	0.09	0.76	1.50

	TGA Results	Weight Measurements
	Coke%	Coke%
S1 (RR6)	1.98	1.87
S2 (RR6)	1.94	1.96
S3 (RR3)	1.86	1.81
S4 (RR3)	1.50	1.58

Figure 5.3 shows the changes of overall H/C ratios with respect to coke contents of the spent equilibrium catalysts. If we look at the H/C ratios of calcined equilibrium catalysts at a constant carbon amount on the catalyst, the lowest H/C ratios were observed for ECat-LOW. The H/C ratios for ECat-INT and ECat-HIGH were found to be close to each other and higher than those for ECat-LOW. This indicates that the coke formed on the catalysts with high metal concentration is less aromatic than the catalyst with relatively low metal concentration for a given coke content. This difference in the nature of the coke can be explained by the way coke is formed. For example, coke formed by hydrogenolysis on the metal portion of the catalyst was found to be richer in hydrogen compared to the coke formed by carbenium ion reactions on the acid sites of the catalyst (Menon, 1990; Pieck et al., 1992). The overall H/C ratio becomes greater when the majority of the coke is formed on the metal surface.

Usually pretreatments are performed to minimize the coke formed by hydrogenolysis on the metal surface. In our case, catalysts pretreated with hydrogen or methane demonstrated lower H/C ratios compared to calcined catalysts, indicating that less coke is formed on the metals after pretreatment. The effect of pretreatment was found to be more significant for ECat-HIGH and ECat-INT compared to ECat-LOW. When the metal concentration on the catalyst is high enough, the effect of pretreatment on the nature of coke becomes more pronounced.

Table 5.2 Comparisons of Results from TPO and Weight Measurements Analyses

Catalyst	Pretreatment	TPO Results			Weight Measurement	%Error in coke% (between TPO and weight measurement results)
		Carbon%	H/C	Hydrogen%	Coke%	
ECat-LOW	Calcined	1.74	0.45	0.07	1.89	-4.42
		1.55	0.49	0.06	1.69	-4.97
		1.41	0.57	0.07	1.42	4.05
		1.70	0.53	0.08	1.85	-3.93
		1.33	0.60	0.07	1.41	-0.71
	H$_2$ Pretreated	1.61	0.47	0.06	1.71	-2.40
		1.38	0.60	0.07	1.43	1.38
		1.52	0.52	0.07	1.67	-5.03
	CH$_4$ Pretreated	1.53	0.55	0.07	1.64	-2.50
ECat-INT	Calcined	1.36	0.79	0.09	1.56	-7.59
		1.42	0.76	0.09	1.41	6.62
		1.21	0.84	0.08	1.38	-6.98
	H$_2$ Pretreated	1.16	0.82	0.08	1.28	-3.23
ECat-HIGH	Calcined	1.65	0.61	0.08	1.78	-2.89
		1.55	0.65	0.08	1.66	-1.84
		1.52	0.69	0.09	1.51	6.21
		1.39	0.80	0.09	1.48	0.00
		1.53	0.68	0.09	1.69	-4.32
		1.47	0.71	0.09	1.69	-8.33
		1.07	0.96	0.09	1.25	-7.76
	H$_2$ Pretreated	1.33	0.69	0.08	1.36	3.55
		1.13	0.86	0.08	1.29	-6.61
		1.65	0.54	0.07	1.82	-5.81
	CH$_4$ Pretreated	1.41	0.65	0.08	1.42	4.70
		1.21	0.76	0.08	1.37	-6.20
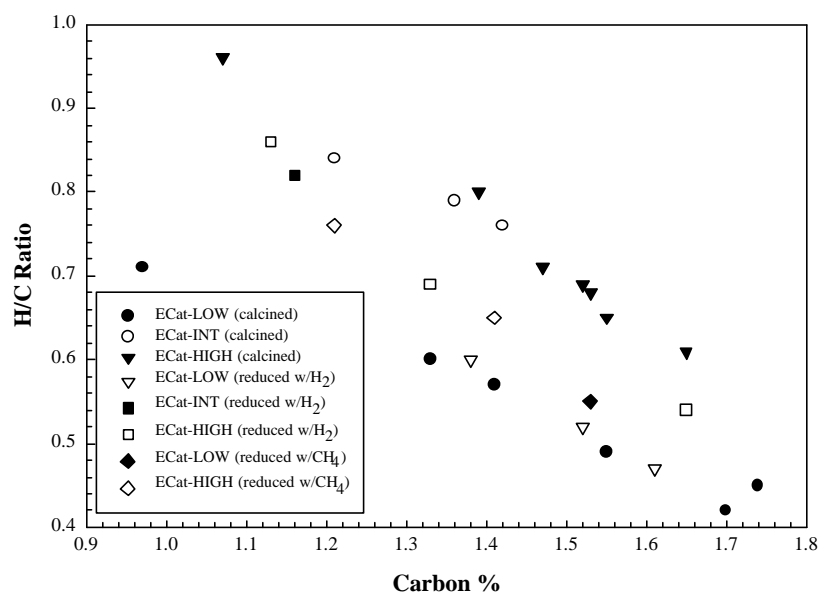
Figure 5.3 H/C Ratios of the Coke on Spent Equilibrium FCC Catalysts before and after Pretreatment

As seen from Figure 5.3, H/C ratios decrease with increasing carbon contents for all the catalysts. Regardless of the zeolite types such as USHY, HZSM5, and HERI, H/C ratio was always found to decrease with increasing coke content (Guisnet et al., 1989). This is consistent with our findings. Today, it is accepted that the coke deposited on the zeolite catalysts is a mixture of highly unsaturated hydrocarbons with an average H/C ratio varying from 0.3 to 1 (Oudar et al., 1985). This is in good agreement with our finding that total H/C ratios varying in a range between 0.4 to 1.0, indicating the majority of the coke must consist of polyaromatic species.

Generally the coke is classified as soluble and insoluble coke. Soluble coke molecules are usually too volatile and too weakly basic to be located on the outer surface, therefore must be located in the pores. The insoluble portion of the coke can be distinguished by its dark black color

and its low solubility in methylene chloride. The components of insoluble coke were found to be polyaromatic with an atomic H/C ratio of 0.4-0.5 for USHY type zeolite (Guisnet et al., 1989). It has been confirmed that insoluble coke is formed as a result of the growth of soluble coke molecules trapped in the pores (Guisnet et al., 1989). Based on this fact, at least part of insoluble coke molecules should be located in the micropores of the zeolite. This hypothesis has been confirmed by our BET surface area measurements given in detail earlier.

The shape of TPO profiles is affected by the combustion mechanism, which is determined by the properties of coke and the catalyst. Some researchers (Li et al., 1999; Moljord et al., 1994; Henriques et al., 1997) reported that coke oxidation rate was practically independent of the coke content and composition. The effect of H/C on oxidation rate is generally considered insignificant, although a high H/C ratio can be an indicator of reactive carbons (Li et al., 1999). The catalytic coke formed on the catalyst can be bonded to the acid sites and contaminant metals as well as other carbon species. Despite different bonding energies of coke species, the acidity of the catalyst and the combustion promoting effect of the contaminant metal are the most effective parameters which affect combustion mechanisms. Assuming that pretreatment does not change the acidity of the equilibrium catalyst, the changes in the shape of TPO profile after pretreatment can only be explained by the formation of relatively less coke on the contaminant metals.

5.2 Coke Characterization

5.2.1 Characterization of the Coke by Temperature-Programmed Methods

Figure 5.4 shows the TPH spectra of spent equilibrium catalysts. A flame ionization detector (FID), which is very sensitive to hydrocarbons, detects the methane formation. Carbon on

the FCC catalyst can be characterized according to its reactivity with hydrogen to form methane. The chemical identification of the various carbon states has been made by McCarty et al. (1979). However, the gasification of carbon with hydrogen requires high temperatures especially for the less reactive forms of carbon like graphitic carbon. For this reason, it may not be very easy to observe all types of carbons using temperature-programmed hydrogenation within a reasonable temperature range. On the other hand, reactivity of oxygen and carbon at relatively low temperatures makes TPO a very powerful and attractive technique for coke characterization. In this work, we have studied both TPH and TPO for the characterization of coke.

When we look at the temperature programmed-hydrogenation (TPH) of spent FCC catalysts in Figure 5.4, we can see that the calcined FCC catalyst does not create a very significant signal in flame ionization detector (FID) (see Figure 5.4c). The signal from the FID comes mostly from methane formed during hydrogenation of coke. Figure 5.4a shows the profile for spent catalyst obtained from the cracking reaction of sour imported heavy gas oil (SIHGO) on the equilibrium catalyst with intermediate metals level. Without any deconvolution, at least four peaks can be detected from Figure 5.4a. Most of the coke reacts with hydrogen at around 500 °C with a little shoulder at around 300 °C. Another peak starts to appear at relatively elevated temperature (850 °C) with a front shoulder around 750 °C. The last peak in this spectrum represents the less reactive coke and requires high temperatures for gasification with hydrogen. When we check the profile in Figure 5.4b for the same catalyst used for n-hexadecane cracking, three smaller, but nicely separated peaks are observed at around the same temperature ranges as in Figure 5.4a. This is a good indication for the formation of different types of coke on the catalyst from only one reactant.
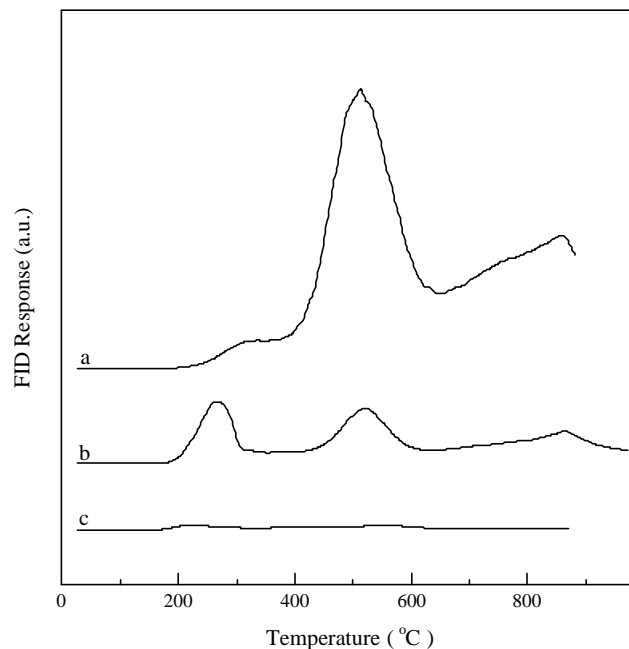
Figure 5.4 TPH Spectra for Spent Commercial Equilibrium FCC Catalyst (ECat-INT): (a) SIHGO Feed; (b) n-Hexadecane Feed; (c) Calcined Equilibrium Catalyst

5.2.2 TPO of Coke Deactivated Commercial Metal Contaminated Equilibrium FCC Catalysts

TPO spectra for spent commercial equilibrium catalysts obtained from SIHGO, ASTM feed, and n-hexadecane cracking are shown in Figures 5.5, 5.6, and 5.7 respectively. Each figure shows results for catalysts with three different contaminant metal levels. It is clear that when the metal level on the equilibrium catalysts increases, the temperature for maximum oxygen consumption decreases. This could be attributed to the catalytic effect of vanadium and nickel on the oxidation reaction. Similar decreases in temperature corresponding to the maximum oxygen consumption during the regeneration of FCC (Doolin et al., 1991; Dimitriadis et al., 1998; Minh et al., 1997) and other catalysts with metal contaminants have been observed previously (Yoshinura et al., 1986; Zeuthen et al., 1995; Bartholdy et al., 1995).

Figure 5.8 shows the TPO spectra for spent ASTM FCC catalysts (RR3 and RR6) obtained from the cracking reaction with ASTM standard feed. As seen from this figure, TPO profiles of each standard catalyst are almost the same and the temperature at which maximum oxygen consumption occurs is around 550 °C. Since these catalysts are not equilibrium catalysts, they are not expected to carry significant amounts of metal contaminants on them. Therefore, it is not very surprising to have quite similar profiles for these catalysts.
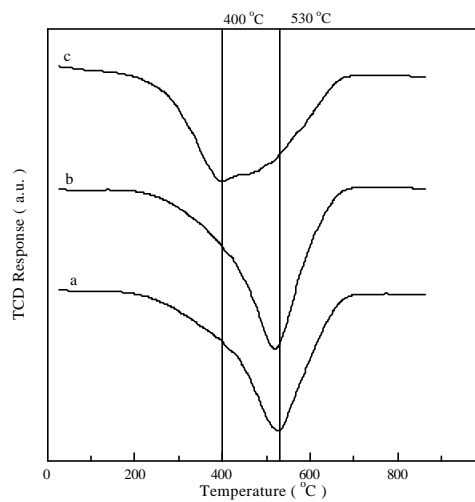
Figure 5.5 TPO Spectra for Spent Commercial Equilibrium Catalysts. SIHGO was used as Cracking Feed. (a) ECat-LOW; (b) ECat-INT; (c) ECat-HIGH
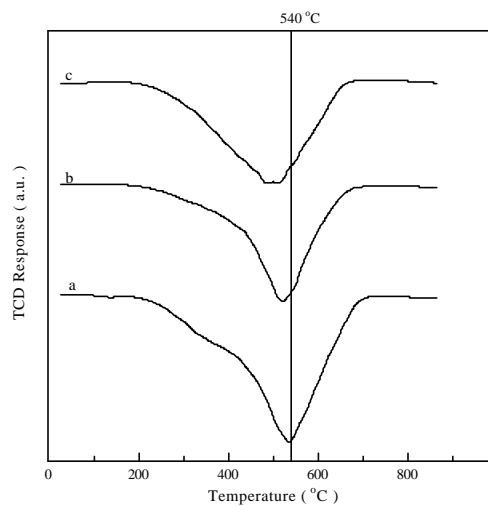
Figure 5.6 TPO Spectra for Spent Commercial Equilibrium Catalysts. Standard ASTM Feed was used in Cracking Reactions. (a) ECat-LOW; (b) ECat-INT; (c) ECat-HIGH
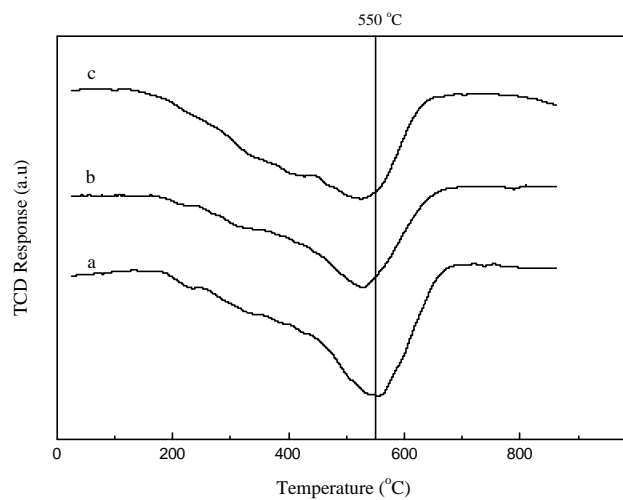
Figure 5.7 TPO Spectra for Spent Commercial Equilibrium Catalysts. n-hexadecane was used in Cracking Reactions. (a) ECat-LOW; (b) ECat-INT; (c) ECat-HIGH
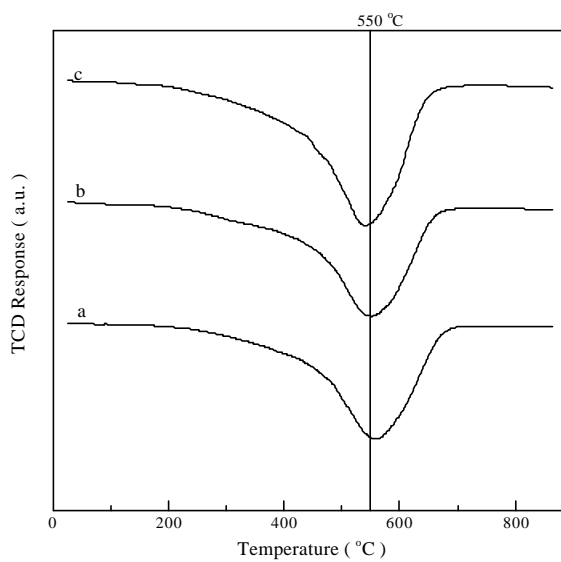
Figure 5.8 TPO Spectra for Spent Standard Catalysts. Standard ASTM Feed was used   in Cracking Reaction. (a) and (b) RR3; (c) RR6

These TPO profiles can be analyzed by deconvoluting them. Since only positive peaks can be fitted, original negative TPO profiles in Figures 5.5, 5.6, and 5.7 were inverted to obtain positive peaks. These positive peaks have been fitted with Gaussian-type functions. Deconvolution results of TPO spectra shown in Figures 5.5, 5.6 and 5.7 are presented in Figures 5.9-5.11, 5.13-5.15, and 5.17-5.19, respectively. The lowest temperature peak has been designated K and the following peaks at increasing temperature have been labeled L, M and N. Quantitative analysis results for spent catalysts with three different metal levels which were obtained from the cracking of three different types of feed, are tabulated in Table 5.3. In this table, the measured area for each peak has been divided by kinetic conversion (second-order rate constant, where K = % Conversion/(100-% Conversion)) to obtain specific peak area. The percentage area for each peak is shown in parenthesis.

Deconvolution of TPO spectra for spent equilibrium catalysts obtained from the cracking of SIHGO (see Figures 5.9-5.11) resulted in four positive peaks. A close examination of deconvoluted peaks shows that the location of peaks in Figures 5.9-5.11 shifts to lower temperatures with increasing metal levels on the equilibrium catalysts. As seen from Figure 5.12b, a good relation exists between amount of metal (nickel + vanadium) on the catalyst and temperature of coke burn-off for each peak. The contribution of Peak L to the total area increases with increasing metals level on the catalyst (see Figure 5.12a) whereas the contribution of Peak N to the total area remains almost constant. With ASTM standard feed deconvoluted TPO spectra also show four positive peaks (see Figures 5.13-5.15). As seen from Figure 5.16b, the location of each peak shifts to lower temperatures with increasing concentration of contaminant metals.

86
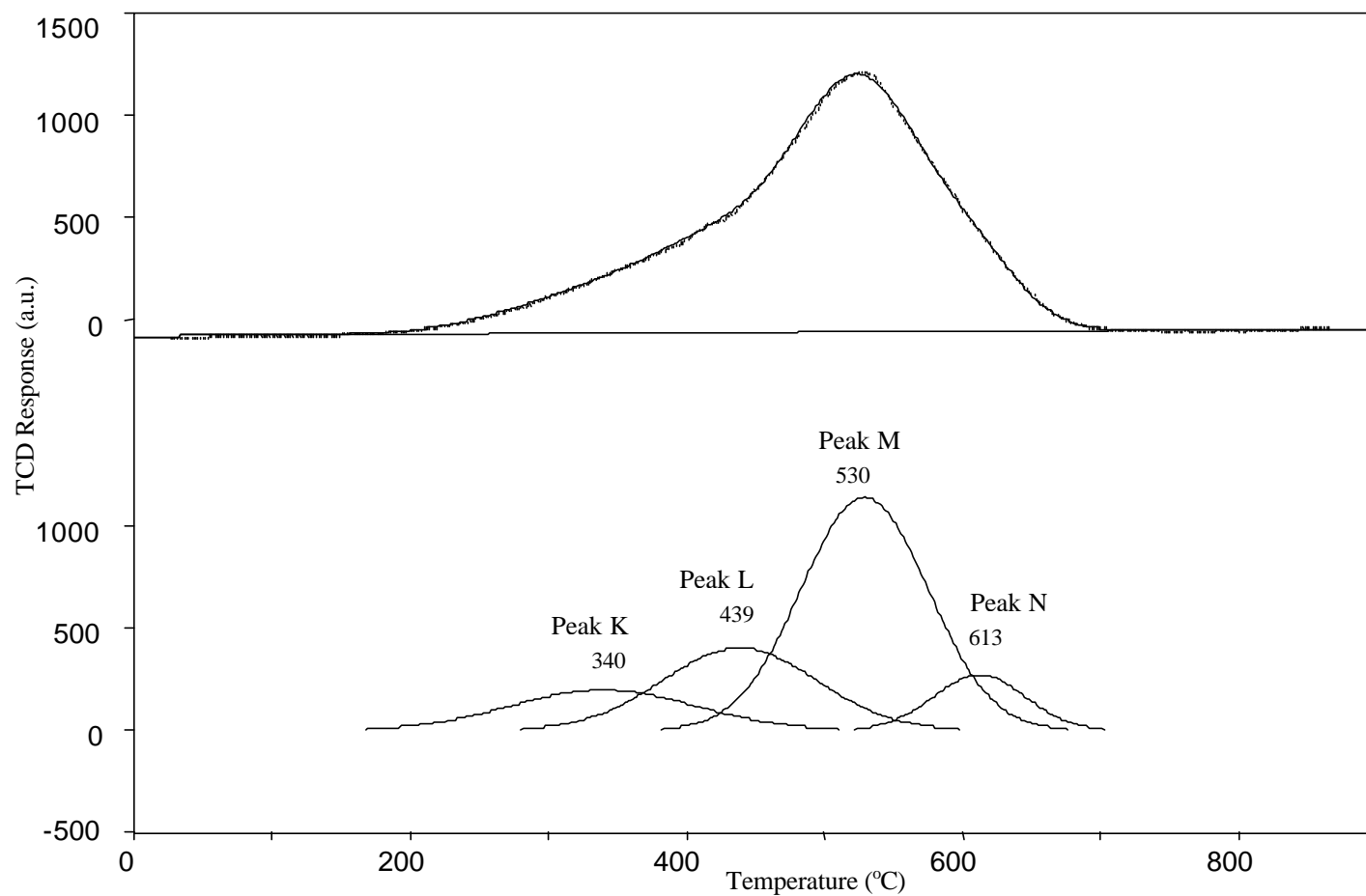
Figure 5.9 Analysis of TPO Spectrum for Spent Equilibrium FCC Catalyst (ECat-LOW). SIHGO was used as Cracking Feed. (Top) Experimental Curve and Composite Curve from Analysis. (Bottom) Individual Peaks from Analysis
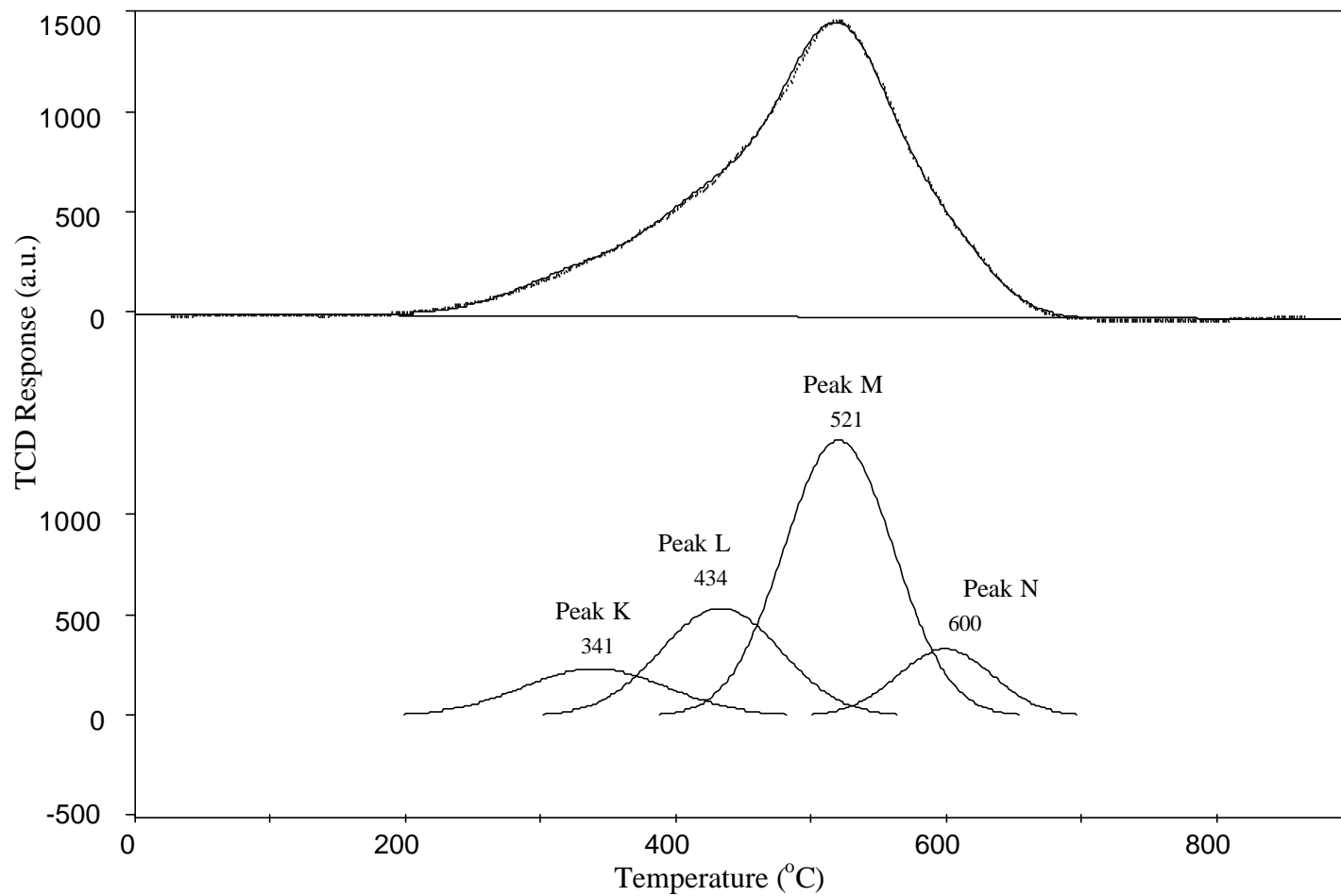
Figure 5.10 Analysis of TPO Spectrum for Spent Equilibrium FCC Catalyst (ECat-INT). SIHGO was used as Cracking Feed. (Top) Experimental Curve and Composite Curve from Analysis. (Bottom) Individual Peaks from Analysis.
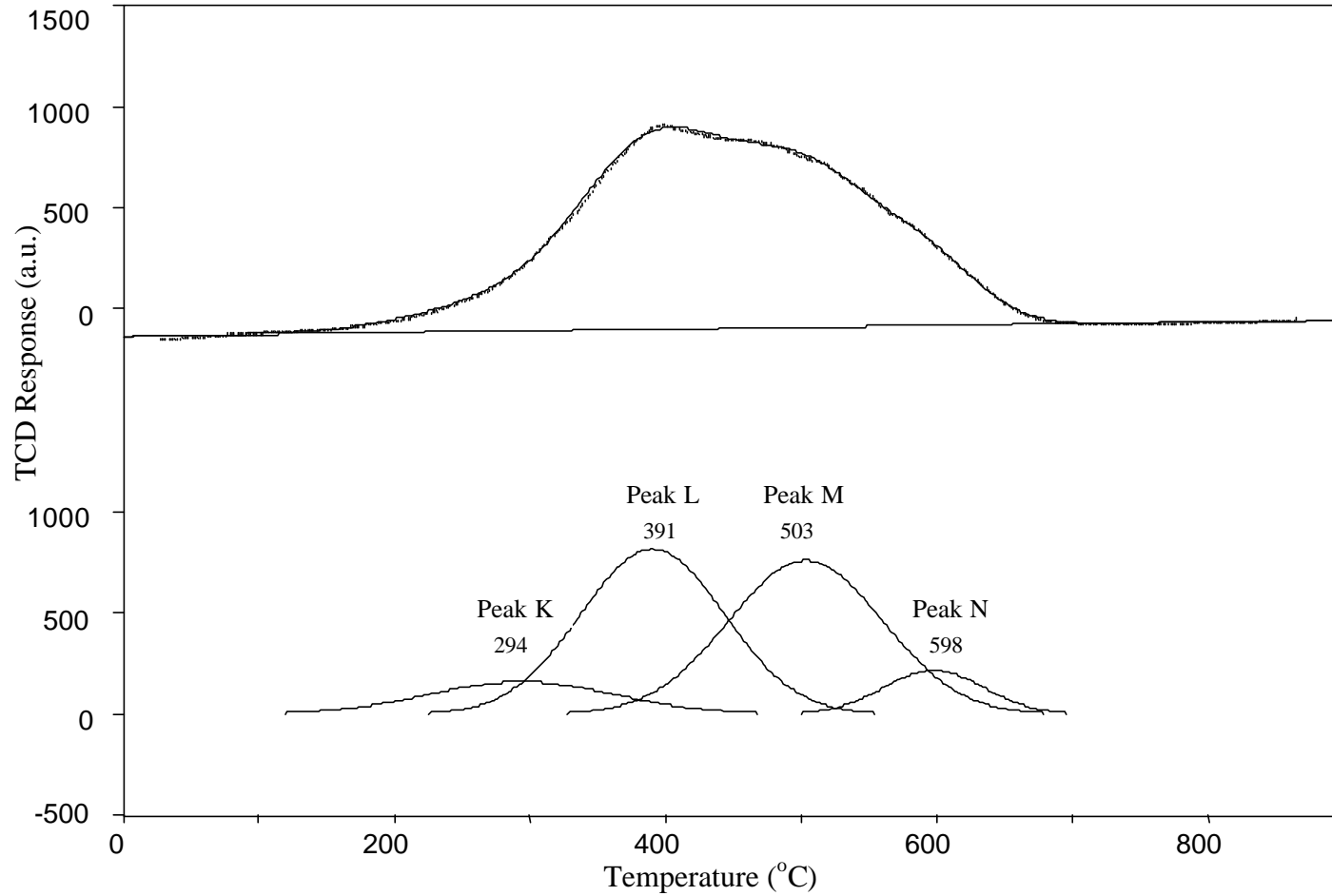
Figure 5.11 Analysis of TPO Spectrum for Spent Equilibrium FCC Catalyst (ECat-HIGH). SIHGO was used as Cracking Feed. (Top) Experimental Curve and Composite Curve from Analysis. (Bottom) Individual Peaks from Analysis.
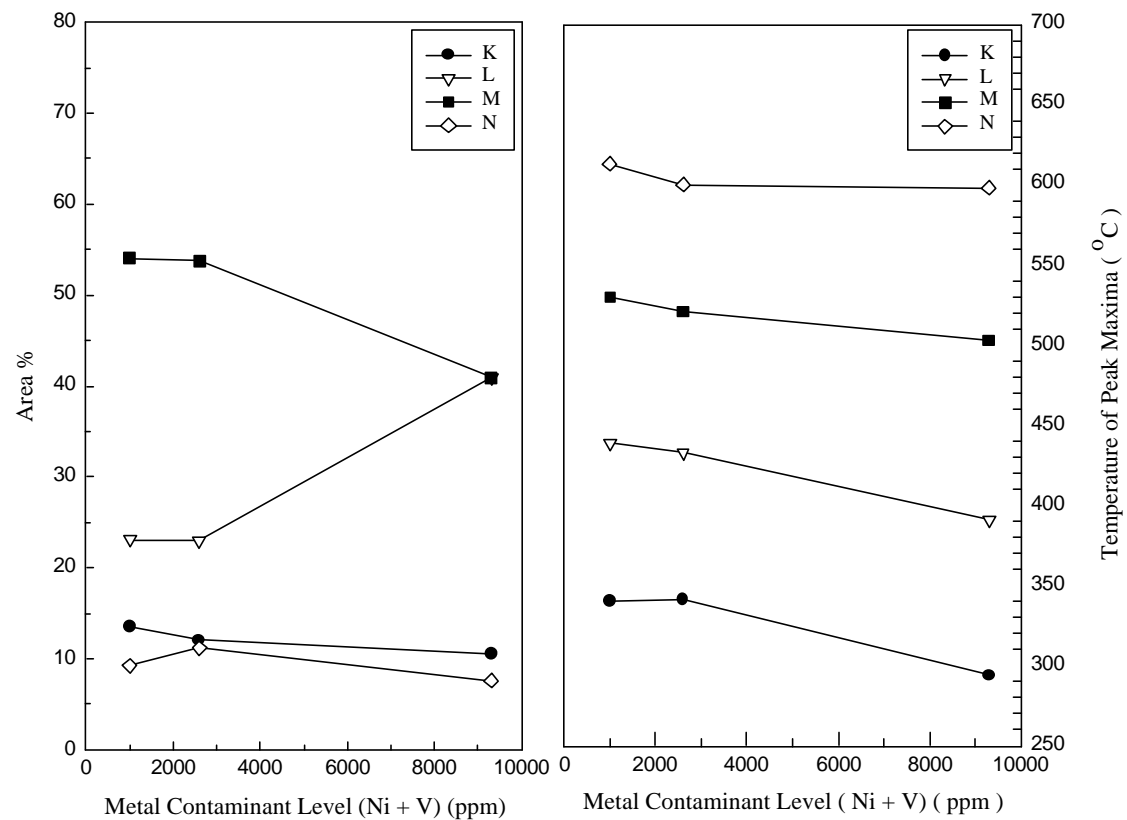
Figure 5.12 Quantitative Results from TPO Spectra with SIHGO Feed Shown in Figures 7-9: (a) Relative Areas; (b) Peak Positions
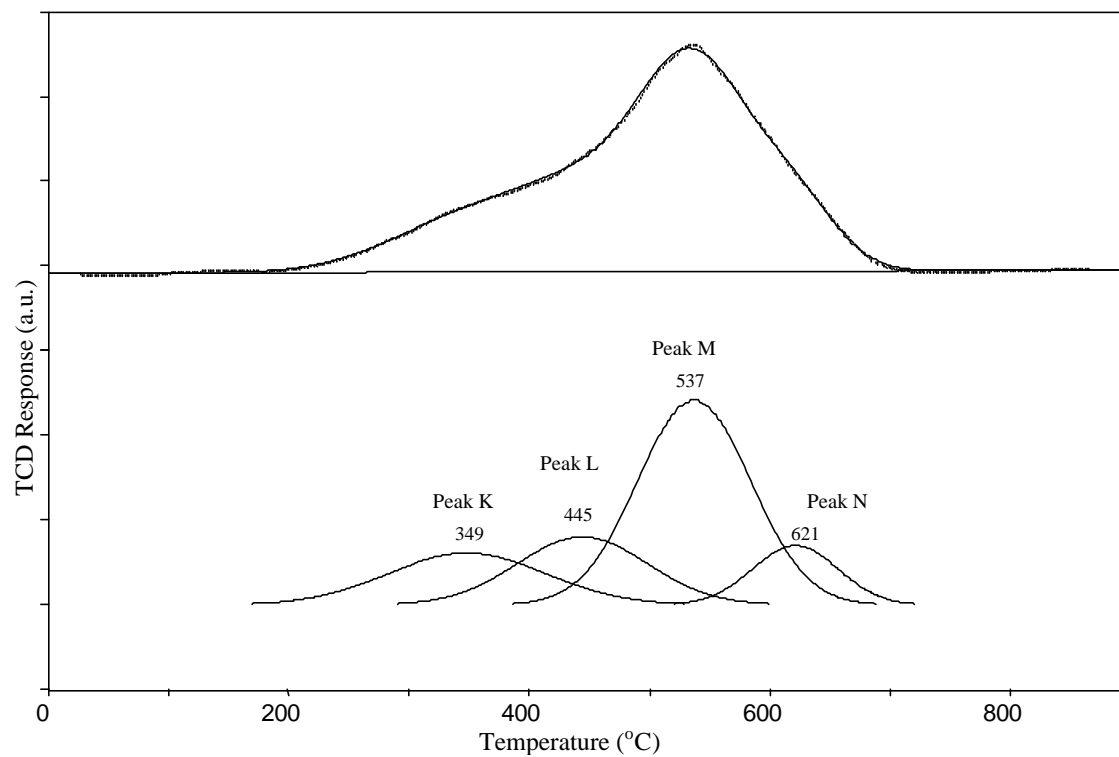
Figure 5.13 Analysis of TPO Spectrum for Spent Equilibrium FCC Catalyst (ECat-LOW). Standard ASTM Feed was used in Cracking Reactions. (Top) Experimental Curve and Composite Curve from Analysis. (Bottom) Individual Peaks from Analysis
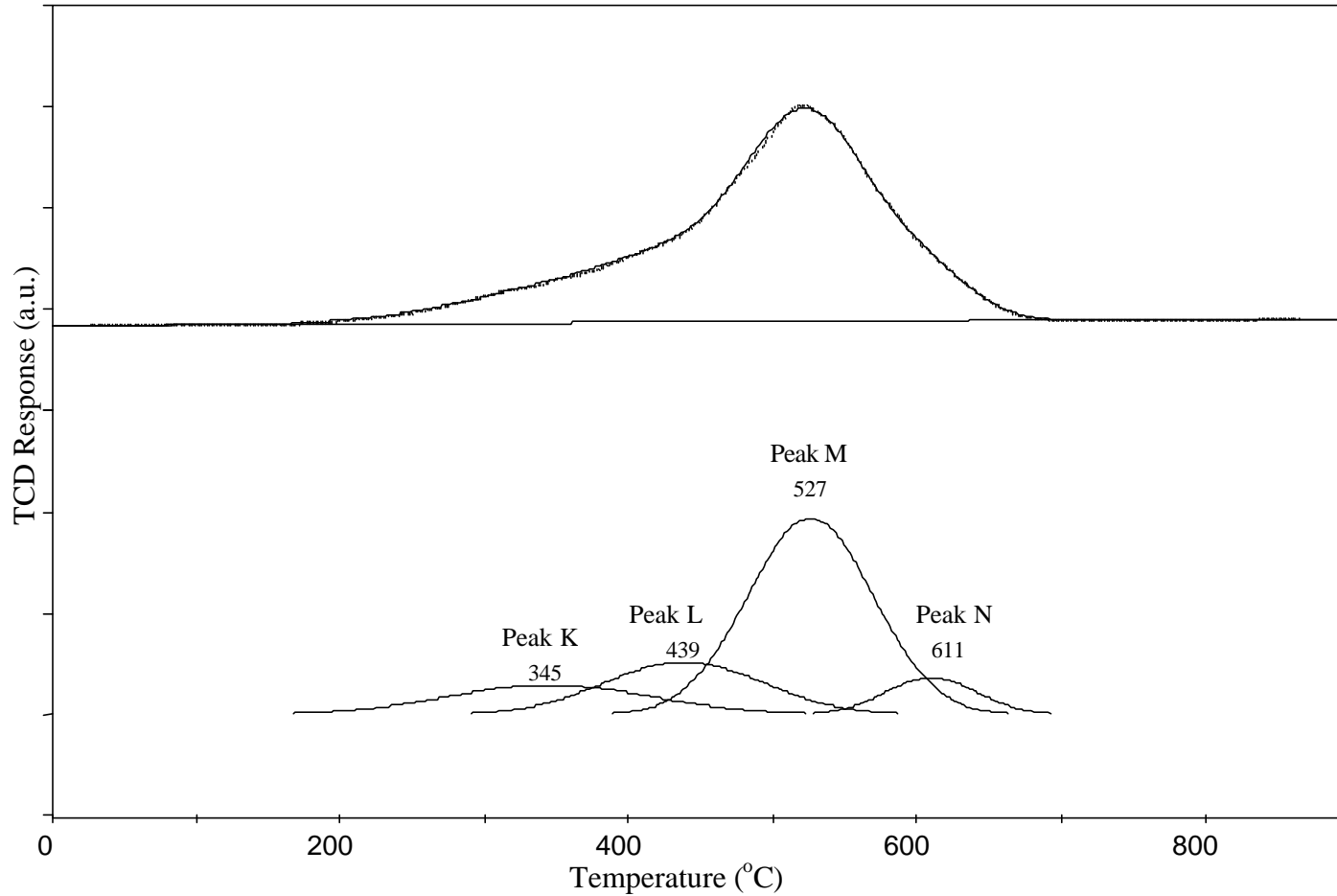
Figure 5.14 Analysis of TPO Spectrum for Spent Equilibrium FCC Catalyst (ECat-INT). Standard ASTM Feed was used in Cracking Reactions. (Top) Experimental Curve and Composite Curve from Analysis. (Bottom) Individual Peaks from Analysis.
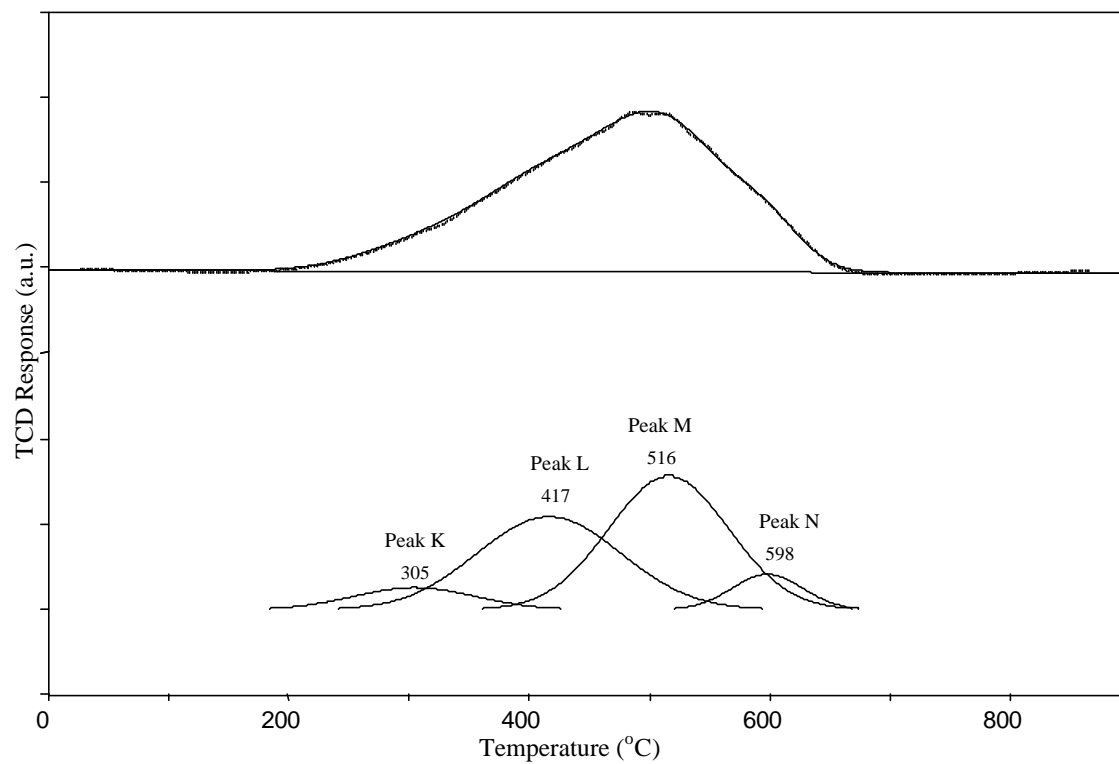
Figure 5.15 Analysis of TPO Spectrum for Spent Equilibrium FCC Catalyst (ECat-HIGH). Standard ASTM Feed was used in Cracking Reactions. (Top) Experimental Curve and Composite Curve from Analysis. (Bottom) Individual Peaks from Analysis.
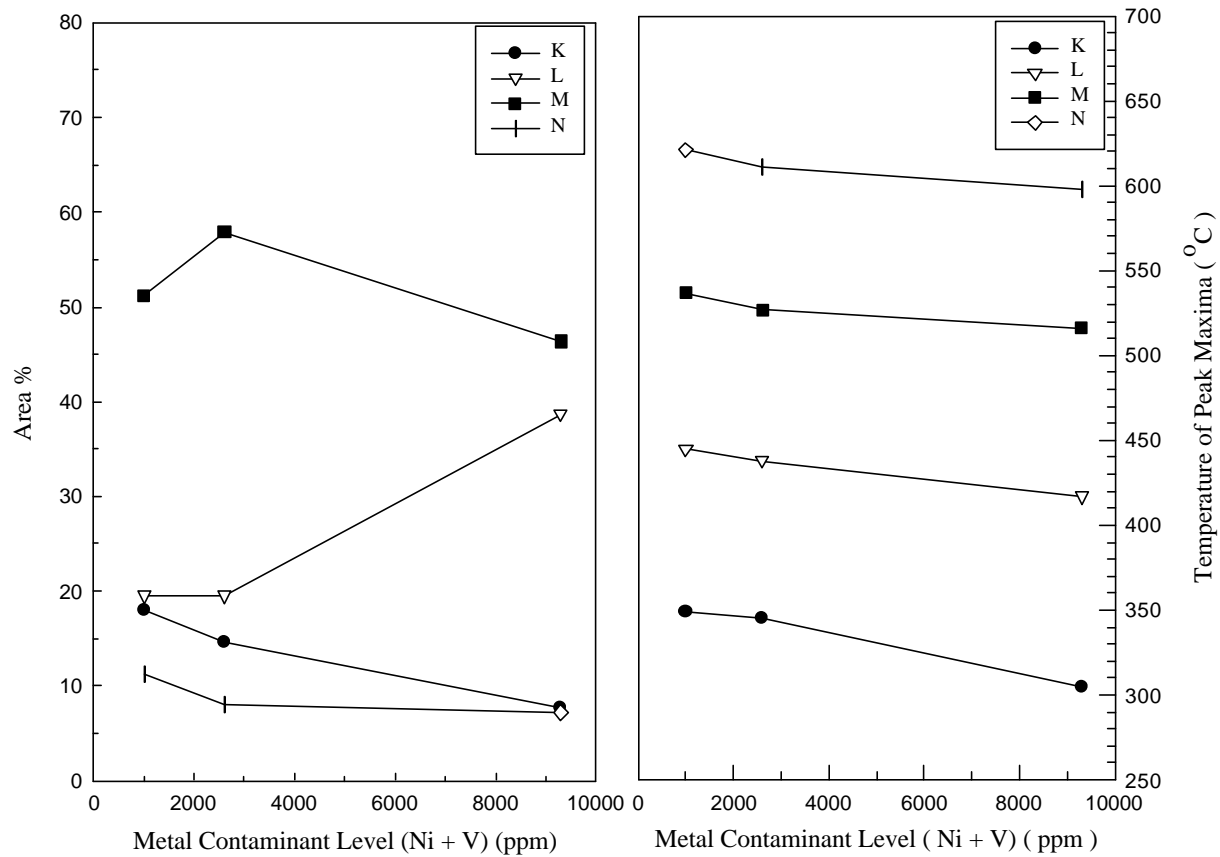
Figure 5.16 Quantitative Results from TPO Spectra with ASTM Feed Shown in Figures 11-13: (a) Relative Areas; (b) Peak Positions
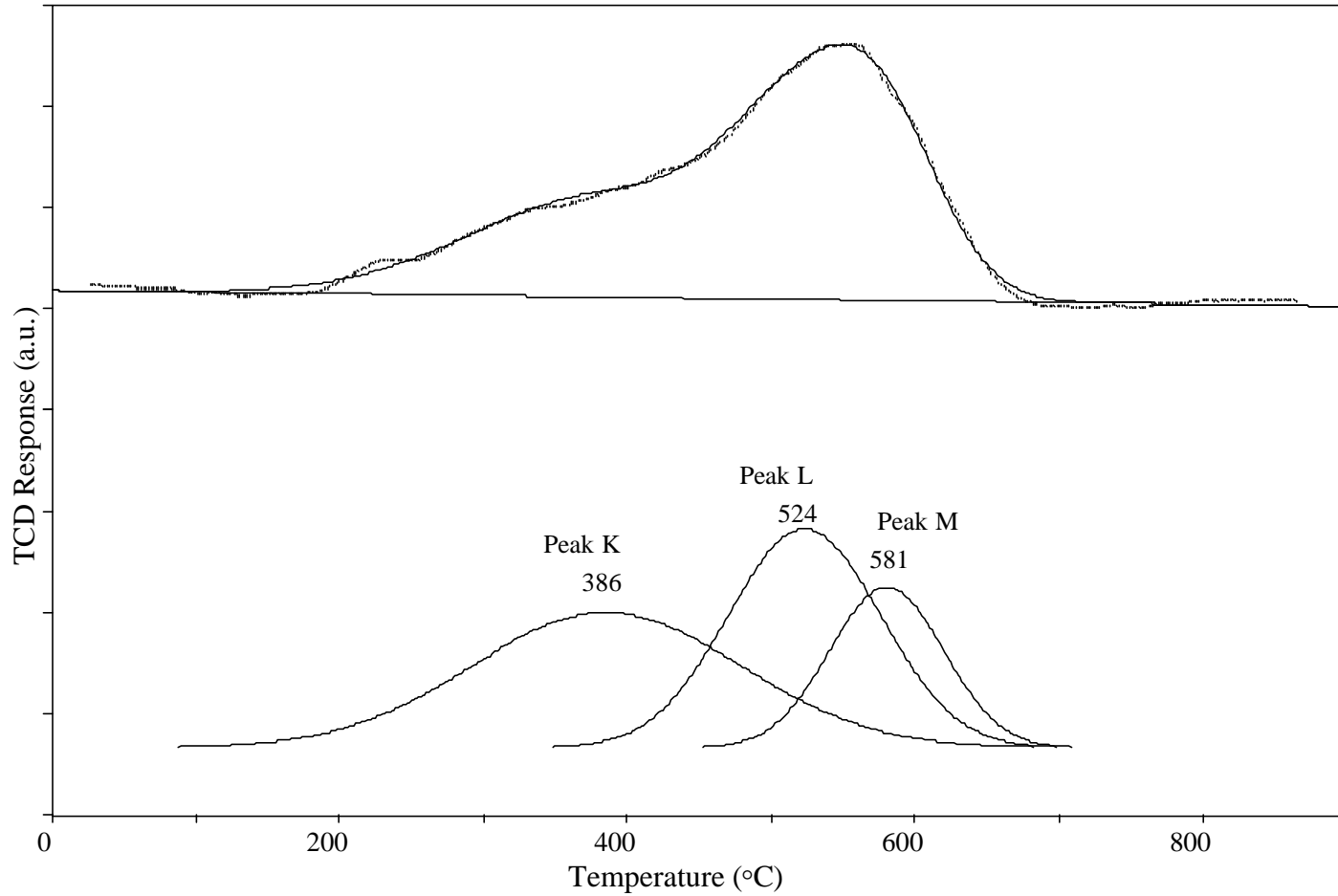
Figure 5.17 Analysis of TPO Spectrum for Spent Equilibrium FCC Catalyst (ECat-LOW). n-hexadecane was used as Cracking Feed. (Top) Experimental Curve and Composite Curve from Analysis. (Bottom) Individual Peaks from Analysis.

Figure 5.18 Analysis of TPO Spectrum for Spent Equilibrium FCC Catalyst (ECat-INT). n-hexadecane was used as Cracking Feed. (Top) Experimental Curve and Composite Curve from Analysis. (Bottom) Individual Peaks from Analysis.

Figure 5.19 Analysis of TPO Spectrum for Spent Equilibrium FCC Catalyst (ECat-HIGH). n-hexadecane was used as Cracking Feed. (Top) Experimental Curve and Composite Curve from Analysis. (Bottom) Individual Peaks from Analysis.

Table 5.3 Quantitative Results from TPO Spectra Shown in Figures 5.9-5.11; 5.13-5.15; 5.17-5.19. The Number in Parenthesis is the Area % for Each Peak.

| Catalyst | Feed | K^c | Peak Area/K^c (x 10^{-4}) (Area %) | | | | LT^a / HT^b | Total Area/K^c (x 10^{-4}) |
			Peak K	Peak L	Peak M	Peak N		
ECat-LOW	SIHGO	1.38	2.36 (13.53)	4.03 (23.11)	9.43 (54.02)	1.62 (9.29)	0.58	17.44
	ASTM	3.00	1.66 (18.08)	1.79 (19.50)	4.70 (51.20)	1.03 (11.22)	0.60	9.18
	n-$C_{16}H_{34}$	1.34	1.76 (41.41)	1.61 (37.88)	0.88 (20.71)	---	---	4.25
ECat-INT	SIHGO	1.33	2.34 (12.03)	4.47 (22.98)	10.46 (53.78)	2.18 (11.21)	0.54	19.45
	ASTM	2.23	1.20 (14.62)	1.60 (19.49)	4.75 (57.86)	0.66 (8.04)	0.52	8.21
	n-$C_{16}H_{34}$	1.25	1.47 (32.24)	2.04 (44.74)	1.05 (23.02)	---	---	4.56
ECat-HIGH	SIHGO	0.96	2.91 (10.55)	11.28 (40.91)	11.28 (40.91)	2.10 (7.62)	1.06	27.57
	ASTM	1.64	0.99 (7.70)	4.97 (38.68)	5.96 (46.38)	0.93 (7.24)	0.87	12.85
	n-$C_{16}H_{34}$	1.25	1.34 (19.94)	3.34 (49.70)	2.04 (30.36)	---	---	6.72
	Before MeCl (SIHGO)	0.89	2.22 (7.13)	12.87 (41.28)	10.22 (32.78)	5.86 (18.81)	0.94	31.17
	After MeCl (SIHGO)	0.89	2.91 (9.02)	10.89 (33.77)	12.09 (37.49)	6.36 (19.72)	0.75	32.25

---

a   LT; the total area under low temperature oxidation peaks K and L
b   HT; the total area under high temperature oxidation peaks M and N
c   Kinetic Conversion, K = Conversion/(100-Conversion)

Figure 5.16a shows that the contribution of Peak L again increases while contribution of Peak N remains constant with increasing metal level. For both cases with SIHGO and ASTM feed the ratio of areas under low temperature peaks (Peaks K and L) to areas under high temperature peaks (Peaks M and N) increases with increasing metal level. As seen in Table 5.3, for spent catalysts obtained from SIHGO cracking, this ratio increases from 0.58 to 1.06 with increasing metals level. Similarly, in the case of ASTM feed, this ratio increases from 0.60 to 0.87. This shows that coke oxidation by these contaminant metals on the catalyst is presented in the lower temperature peaks. In fact, increasing intensity of Peak L with metals level makes it a good candidate for the coke burn-off catalyzed by contaminant metals on the catalyst. In the case of spent catalysts from the cracking of n-hexadecane, deconvolution of TPO spectra results in three peaks (see Figures 5.17-5.19). Again as seen from Figure 5.20, temperature shifts to lower values and the contribution from peak L increases with increasing metal level.

The same effect is seen with all three cracking feeds. As the concentration of contaminant metals increase, the temperature of peak maxima shift to lower temperatures and the magnitude of peak L increases, being the largest percentage of total area of the ECat-HIGH samples. Heavy secondary products referred to as coke typically consist of polyaromatic, condensed-ring structures which may approach the character of graphite.

The feed composition has been found to be the most important variable that affects commercial FCC-unit operation (Harding et al., 1996). The cracking of paraffinic compounds gives lower coke yields than that of aromatic compounds, and both the rate of cracking and the rate of coke formation increase as the molecular weight of the paraffinic reactant increases (Gates et al., 1979). Aromatics without side chains do not crack very much, because of the high stability of

the benzene rings, and if they do, their principal product is undesirable coke. Polar aromatic compounds are very difficult to crack and make high yields of coke (Stratiev et al., 1997).

Our TPO results have shown that the highest coke yields were caused by SIHGO and ASTM feed cracking. However, n-hexadecane cracking did not make much coke (see total area in Table 5.3). This clearly shows the significant effect of aromatic and polar constituents of SIHGO and ASTM feed on coke making. Another interesting observation is that TPO spectra from ASTM feed and SIHGO were fitted into four peaks, while the TPO spectra from n-hexadecane cracking were reasonably fitted into three peaks. The last peak designated as Peak N in the deconvolution analyses of TPO spectra from SIHGO and ASTM feed does not appear in the deconvulation analyses of TPO spectra from n-hexadecane. The TPO spectra obtained from actual petroleum feeds are nearly symmetric in shape with the presence of a significant front and back shoulder. On the other hand, TPO spectra from n-hexadecane have a significant front shoulder and a relatively sharper back edge, which causes Peak N to disappear in the deconvolution analyses shown in Figures 5.17-5.19.
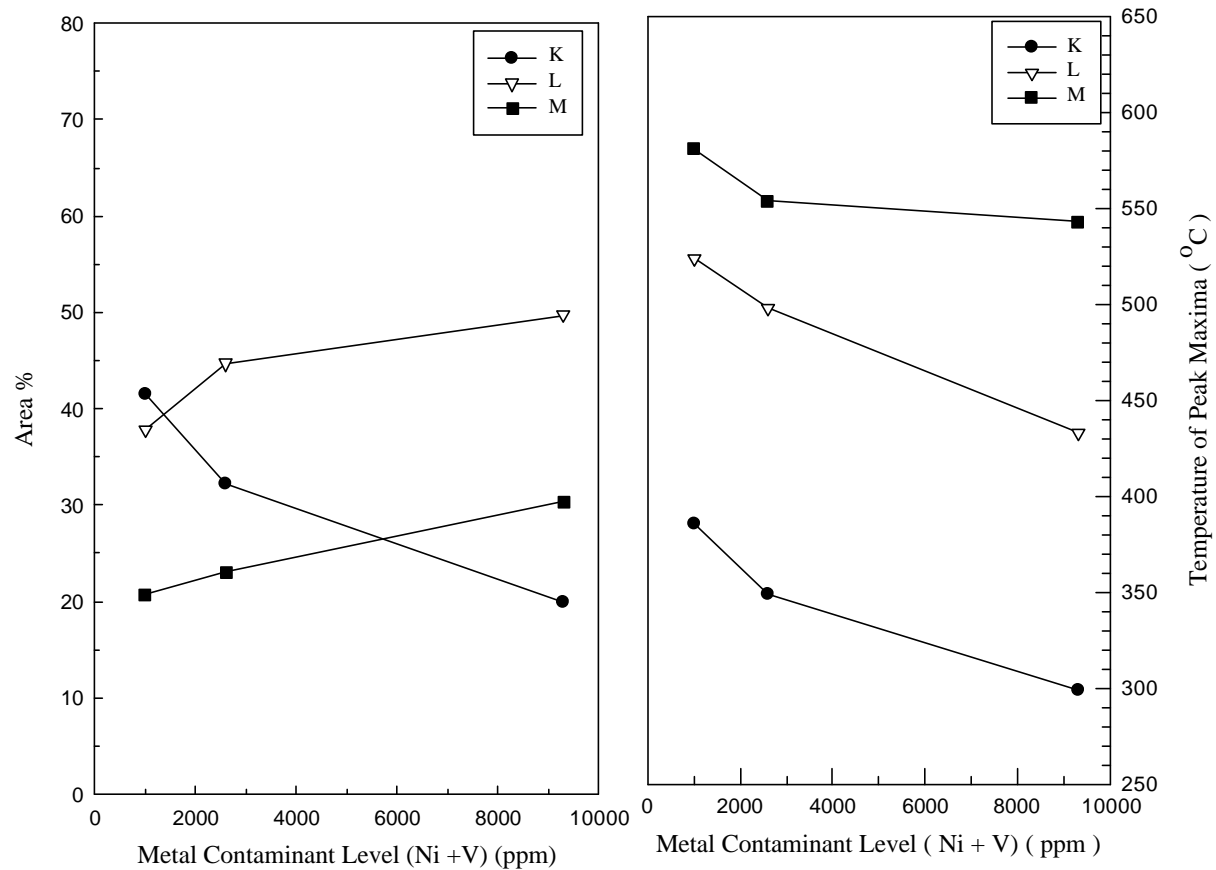
Figure 5.20 Quantitative Results from TPO Spectra with n-hexadecane Feed Shown in Figures 15-17: (a) Relative Areas; (b) Peak Positions

We believe that Peak N represents more refractory coke or carbon formed by the aromatic and polar constituents of the feed. It is well known that aromatics and polar constituents in petroleum feeds contribute significantly to coke making. In n-hexadecane cracking, although there is a formation of aromatics, this may not be an efficient way of forming this type of carbon on the catalyst.

The oxygen consumption in TPO spectra can be assumed to be mainly a result of carbon burn-off. The area of each peak correlates with the amount of coke, the position of each peak correlates with its nature and its location. In all cases with SIHGO and ASTM feed cracking the relative contribution of Peak N remains almost constant. The shift to lower temperatures for Peak N can be due to the stronger catalytic effect of metal contaminants having an increased surface coverage at high metal concentrations on the equilibrium catalysts. The significant increase in the contribution of Peak L into the total area with increasing contaminant metal levels on the equilibrium catalyst can be considered as an indication of the "contaminant" coke formed by these metals.

The TPO spectra before and after Soxhlet extracting spent catalyst with methylene chloride for 16 hours are given in Figures 5.21 and 5.22, respectively. Peak L, which results from the front shoulder in the profile, becomes significantly smaller after Soxhlet extraction. The difference in TPO areas before and after methylene chloride extraction is very small (see Table 5.3). This shows that extraction did not remove very much coke from the catalyst, but did redistribute it. Nitrogen adsorption measurements showed that Soxhlet extraction with methylene chloride increased the micropore surface area.
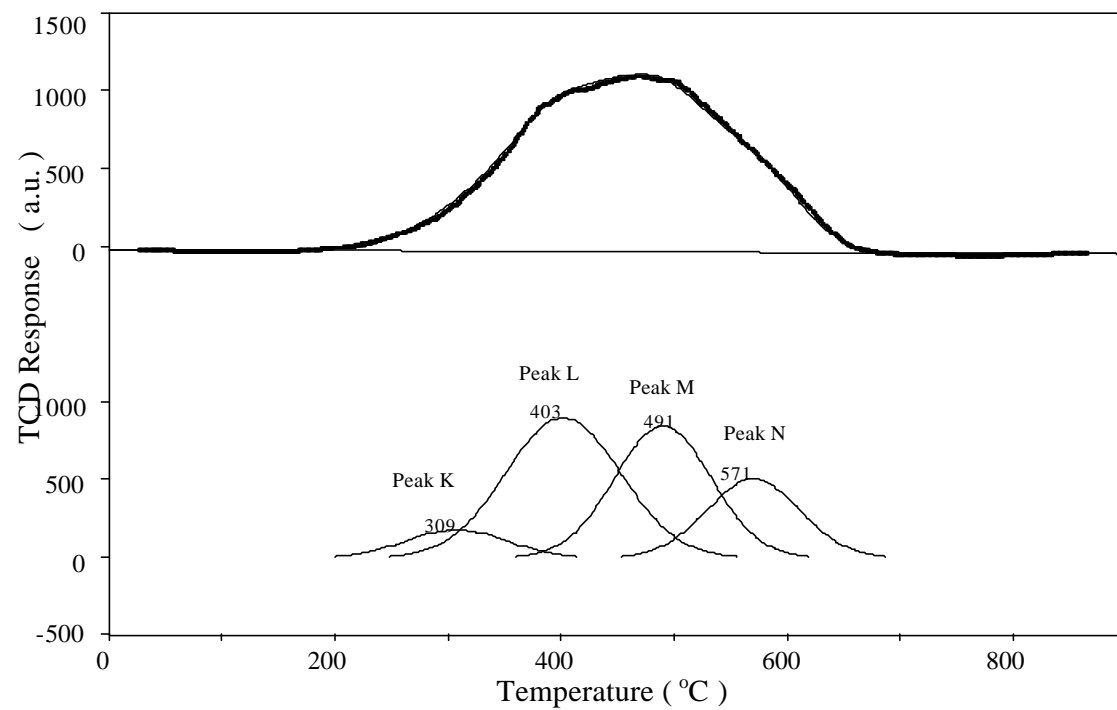
Figure 5.21 Analysis of TPO Spectrum for Spent Equilibrium FCC Catalyst (ECat-HIGH) before Methylene Chloride Extraction. SIHGO was used as Cracking Feed. (Top) Experimental Curve and Composite Curve from Analysis. (Bottom) Individual Peaks from Analysis.

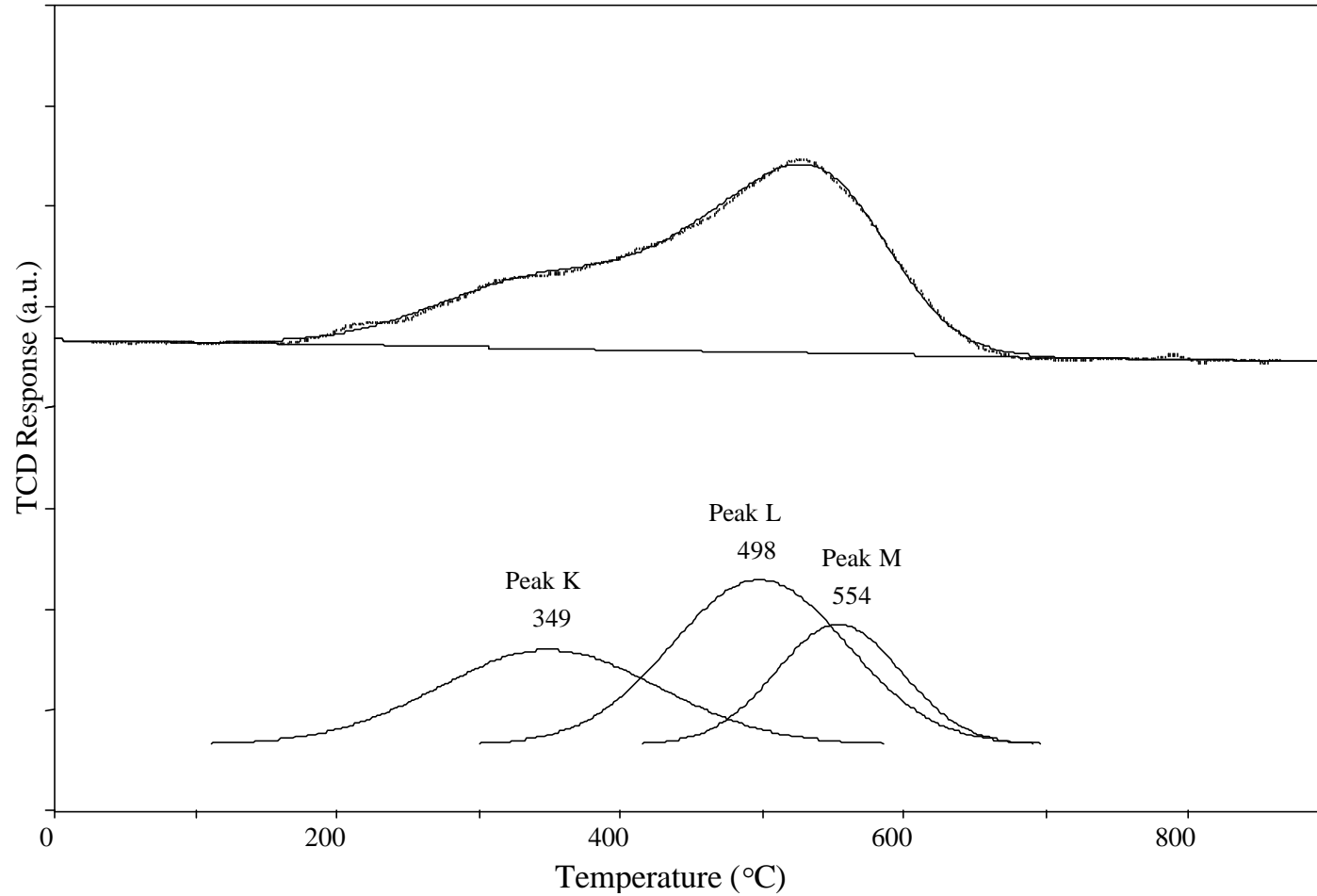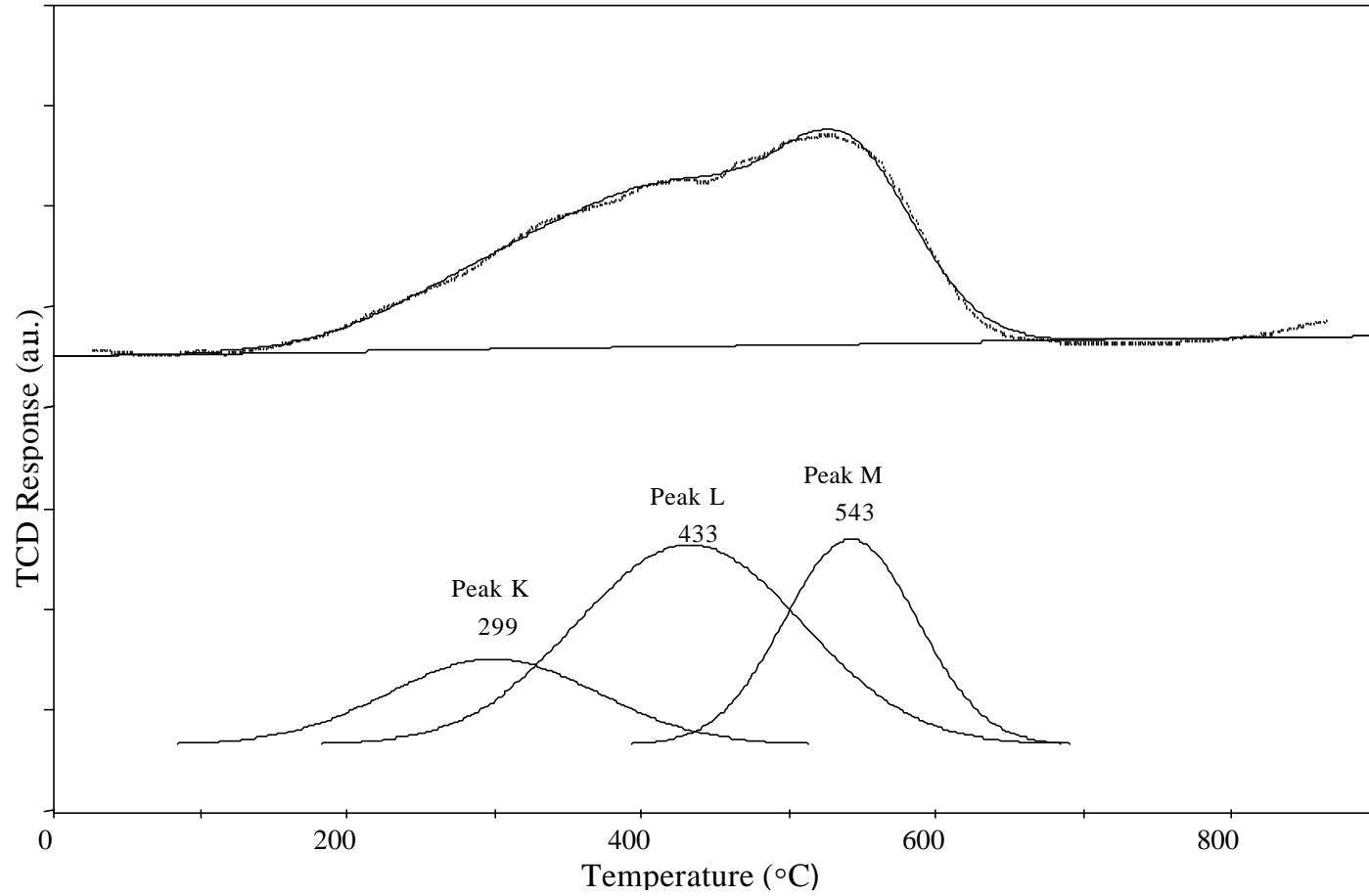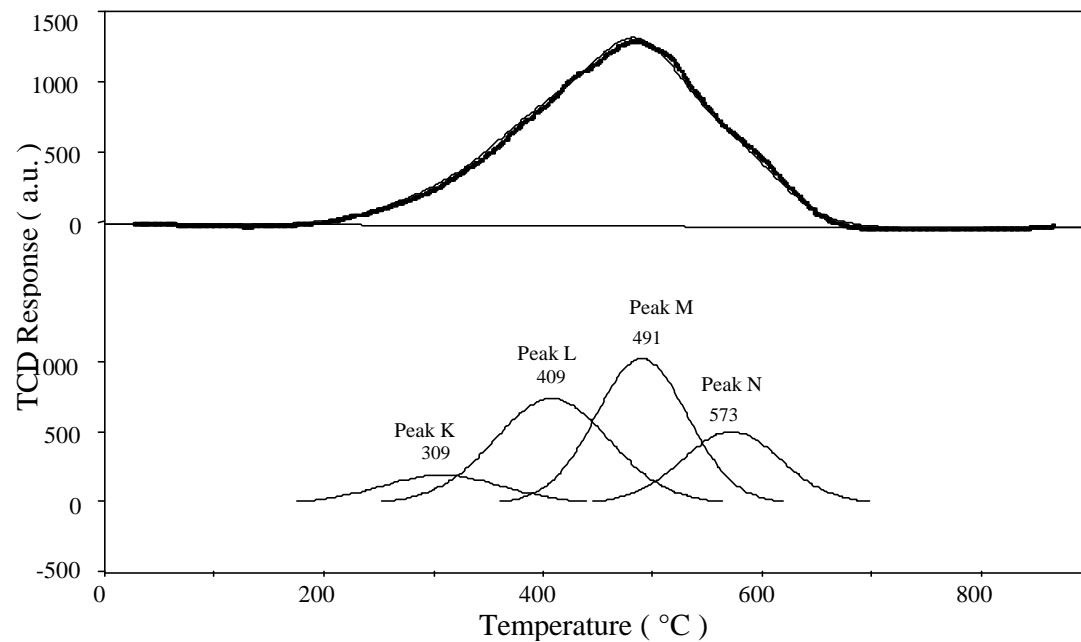**Figure 5.22 Analysis of TPO Spectrum for Spent Equilibrium FCC Catalyst (ECat-HIGH) after 16 hours Methylene Chloride Extraction. (Top) Experimental Curve and Composite Curve from Analysis. SIHGO was used as Cracking Feed. (Bottom) Individual Peaks from Analysis.**

This suggests that the carbon residues block part of the zeolite surface area. After the extraction and some of this carbon residue is removed, smaller pores can be accessed. Yanik et al. (1997) found that average pore diameter in FCC catalyst increases instead of becoming smaller after the reaction. They concluded that this would occur if the smaller pores were preferentially filled with coke or if the accessibility of these smaller pores were blocked by pore-mouth closure.

Since Peak L becomes smaller after extraction, this peak must be representing the coke located at the micropores of the catalyst. This is also confirmed with the decrease in ratio of areas under low-temperature peaks (Peak K and L) to high-temperature peaks (Peak M and N) after extraction (see Table 5.3). This ratio decreases from 0.94 to 0.75. Since we know that the size of Peak L changes significantly with increasing metal level, the carbon represented by Peak L should be located in the vicinity of metal contaminants and catalyzed by these metals during oxidation. We also know from surface area measurements that Peak L represents the carbon in the micropores of the zeolite, therefore we can conclude that some of these metals must be located in the pores of the zeolite. This is consistent with SIMS results showing vanadium in zeolite particles (Kugler et al., 1988).

Figure 5.23 presents data on coke oxidation as a function of catalyst. The measured area for each peak has been divided by the kinetic conversion as was shown in Table 5.3. The areas of each deconvoluted peak are shown on the y-axis while the total area for a given experiment is shown on the x- axis. Total area plotted on the x-axis is expected to be directly proportional to the amount of coke on the spent catalyst regardless of the feed type used. From this figure one can see that area under Peak M is a strong function of the amount of coke on the catalyst given in terms of total area.
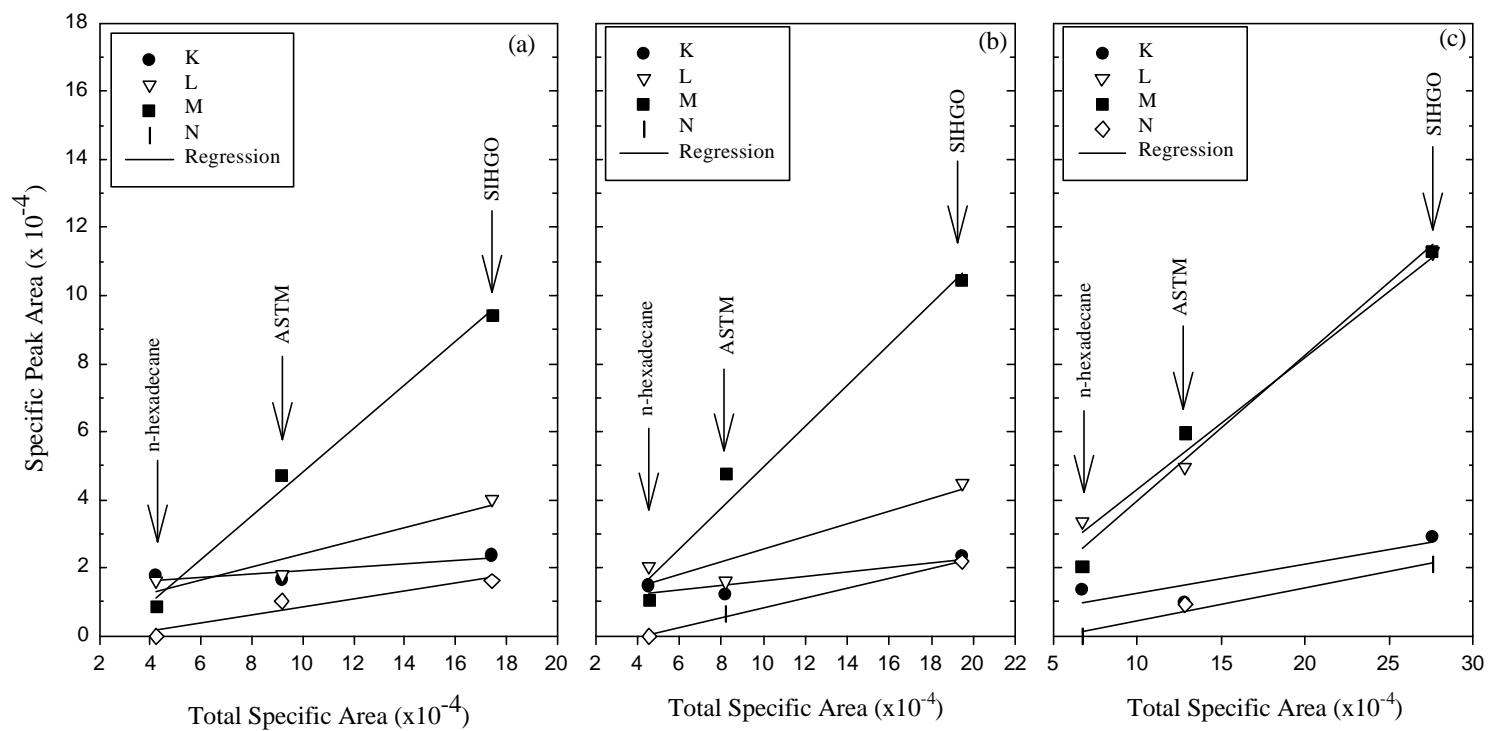
Figure 5.23 Quantitative Results from TPO Spectra Tabulated in Table 1: (a) ECat-LOW; (b) ECat-INT; (c) ECat-HIGH

This allows us to assign Peak M to the "catalytic" coke, which is formed during the acid-catalyzed cracking reactions.

In Figure 5.23a and 5.23b, the main source of coke is the "catalytic" coke (Peak M) formed by the catalytic cracking reactions. The effect of "contaminant" coke (Peak L) is not significant since metal levels on these spent catalysts are relatively low. Figure 5.23c shows that with high metals level the coke formed by acid-catalyzed cracking reactions (Peak M) and the coke formed by contaminant metals (Peak L) become comparable.

The location and the nature of coke responsible for Peak K have not been identified. Since the oxidation of coke represented by Peak K takes place at low temperatures, this peak should be a result of the oxidation of more reactive coke with high hydrogen content or the oxidation of coke located on the outer surface of the catalyst, which is easily accessible by oxygen molecules.

5.3 Effects of Pretreatment on TPO Spectra

Deconvolution analysis of TPO profiles for spent ECat-HIGH equilibrium catalysts with the highest metal concentration (9300ppm Ni and V) from the cracking of SIHGO at catalyst-to-oil ratios of 3 and 5 are shown in Figures 5.24-5.26 and Figures 5.28-5.30 respectively. Deconvolution of each TPO spectra resulted in four positive peaks. The lowest temperature peak has been designated K and the following peaks at increasing temperature have been labeled L, M and N.

Figure 5.24 Analysis of TPO Spectrum for Spent Equilibrium FCC Catalyst (ECat-HIGH-160). Pretreatment: Calcined at 550 °C, Feed: SIHGO, C/O=3. (Top) Experimental Curve and Composite Curve from Analysis. (Bottom) Individual Peaks from Analysis.

Figure 5.25 Analysis of TPO spectrum for Spent Equilibrium FCC Catalyst (ECat-HIGH-163). Pretreatment: Reduced with 8% Hydrogen in Argon at 700 °C, Feed: SIHGO, C/O=3. (Top) Experimental Curve and Composite Curve from Analysis. (Bottom) Individual Peaks from Analysis.

Figure 5.26 Analysis of TPO Spectrum for Spent Equilibrium FCC Catalyst (ECat-HIGH-165). Pretreatment: Reduced with 8% Methane in Helium at 700 °C, Feed: SIGHO, C/O=3. (Top) Experimental Curve and Composite Curve from Analysis. (Bottom) Individual Peaks from Analysis.

Figure 5.24 shows the TPO spectrum of spent ECat-HIGH equilibrium catalyst, which was calcined at 550 °C before cracking reactions. Figure 5.25 and 5.26 show the TPO spectra of spent ECat-HIGH after being reduced with 8% hydrogen in argon and 8% methane in helium at 700 °C prior to cracking reactions respectively. All of these TPO profiles given in Figures 5.24 to 5.26 were obtained from the cracking of SIHGO at a catalyst-to-oil ratio of 3. It is clear from these figures that both hydrogen and methane pretreatment has a significant effect on the TPO profiles. This is a good indication that changes occurred in the relative amounts of the certain types of coke represented by deconvoluted peaks in the TPO spectrum.

Quantitative analysis results for the TPO spectra for all three spent equilibrium catalysts are tabulated in Table 5.4. In this table the measured area for each peak has been divided by kinetic conversion (second-order rate constant, where K = % Conversion/(100-% Conversion)) to obtain specific peak area. The percentage area for each peak is shown in parenthesis.

Figures 5.27 shows the comparisons of the relative area of each peak for ECat-HIGH spent catalysts, which were either pretreated with hydrogen and methane or calcined only prior to the catalytic cracking reactions at a catalyst-to-oil ratio of 3. This figure shows that Peak L, which represents contaminant coke, decreases significantly with pretreatment. This can be attributed to the decrease in the activities of contaminant metals in their metallic states to produce coke.

Table 5.4 Quantitative Results from TPO Spectra Shown in Figures 5.24-5.30; the Number in Parenthesis is the Area % for Each Peak.

Catalyst	ID	Pretreatment	K	Peak Area/K (x10^{-3})				LT/HT	Total/K (x10^{-3})
				Peak K	Peak L	Peak M	Peak N		
ECat-LOW	153	C, C/O=3.0	1.4700	14.537 (8.98)	32.776 (19.00)	77.619 (49.17)	37.000 (22.85)	0.41	161.932
	154	C, C/O=5.0	2.1736	8.852 (8.74)	20.657 (20.40)	49.089 (48.49)	22.644 (22.37)	0.41	101.242
	155	C, C/O=8.0	2.8300	5.420 (8.32)	12.943 (19.86)	32.693 (50.17)	14.106 (21.65)	0.39	65.163
	156	R-H$_2$, C/O=3.0	1.3015	15.175 (8.91)	36.320 (21.32)	79.139 (46.45)	39.754 (23.33)	0.43	170.388
	157	R-H$_2$, C/O=5.0	1.9709	8.823 (8.38)	21.178 (20.12)	49.754 (47.27)	25.501 (24.23)	0.40	105.256
	159	R-CH$_4$, C/O=5.0	1.9438	9.394 (8.45)	22.461 (20.19)	51.198 (46.03)	28.172 (25.33)	0.40	111.225
ECat-INT	51	C, C/O=3.0	1.3810	14.649 (8.43)	33.925 (20.00)	91.745 (52.28)	33.548 (19.30)	0.39	173.867
	49	R-H$_2$, C/O=3.0	1.1739	14.260 (8.09)	34.330 (20.00)	100.946 (52.79)	26.629 (19.12)	0.38	176.165
ECat-HIGH	53	C, C/O=3.0	0.8868	22.948 (7.27)	107.815 (34.18)	118.967 (37.71)	65.742 (20.84)	0.71	315.471
	53-a	C, C/O=3.0	0.8868	21.132 (7.30)	96.087 (33.19)	109.878 (37.95)	62.404 (21.56)	0.68	289.502
	160	C, C/O=3.0	0.8536	22.259 (7.85)	96.720 (34.10)	105.658 (37.25)	58.973 (20.79)	0.72	283.610
	161	C, C/O=5.0	1.2671	14.198 (7.92)	57.59 (33.77)	69.576 (37.17)	37.882 (21.13)	0.67	179.253
	162	C, C/O=8.0	2.0525	8.775 (7.50)	36.054 (30.81)	48.940 (41.83)	23.240 (19.88)	0.62	117.009
	163	R-H$_2$, C/O=3.0	0.8132	23.278 (9.14)	61.485 (24.15)	108.337 (42.55)	61.485 (24.15)	0.50	254.919
	164	R-H$_2$, C/O=5.0	1.1556	12.002 (7.72)	34.943 (22.48)	73.520 (47.30)	34.978 (22.50)	0.43	155.443
	165	R-CH$_4$, C/O=3.0	0.8000	23.975 (8.31)	74.113 (25.70)	124.875 (43.30)	65.425 (22.69)	0.52	288.388
	166	R-CH$_4$, C/O=5.0	1.0721	14.542 (8.90)	37.245 (22.78)	71.197 (43.55)	40.481 (24.76)	0.46	163.465

C: calcined; R-H$_2$: reduced with H$_2$; R-CH$_4$: reduced with CH$_4$
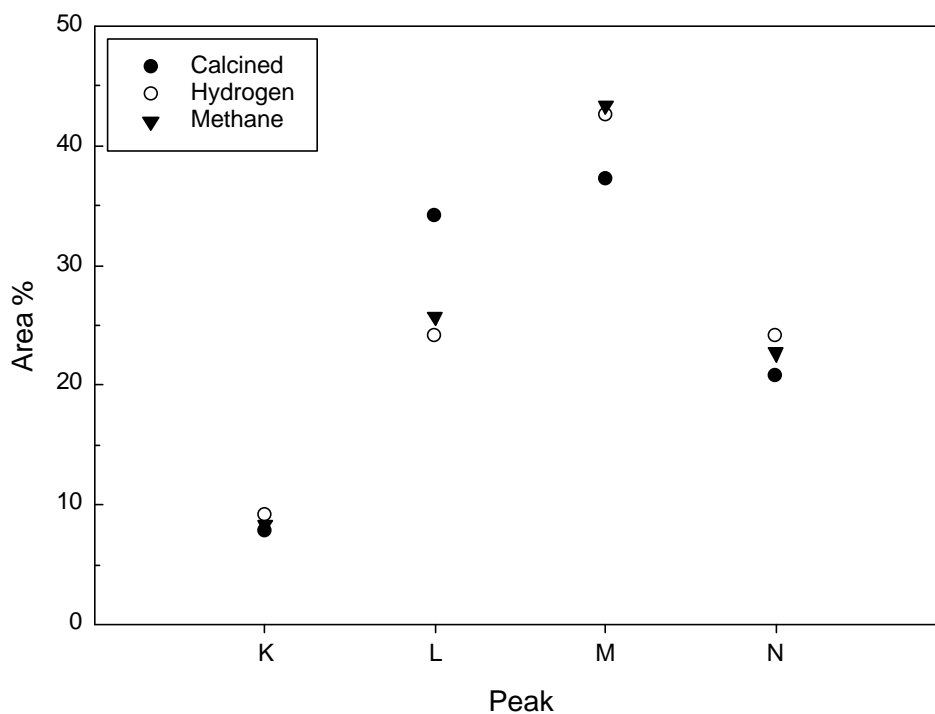
Figure 5.27 Changes of Relative Peak Areas for ECat-HIGH before and after Pretreatment at C/O = 3.0

Similarly, Figure 5.28 shows the TPO spectrum of spent ECat-HIGH equilibrium catalyst, which was calcined at 550 °C before cracking reactions. Figure 5.29 and 5.30 show the TPO spectra of spent ECat-HIGH after being reduced with 8% hydrogen in argon and 8% methane in helium at 700 °C prior to cracking reactions. All of these TPO spectra presented in Figures 5.28 to 5.30 were obtained from the cracking of SIHGO at a catalyst-to-oil ratio of 5.
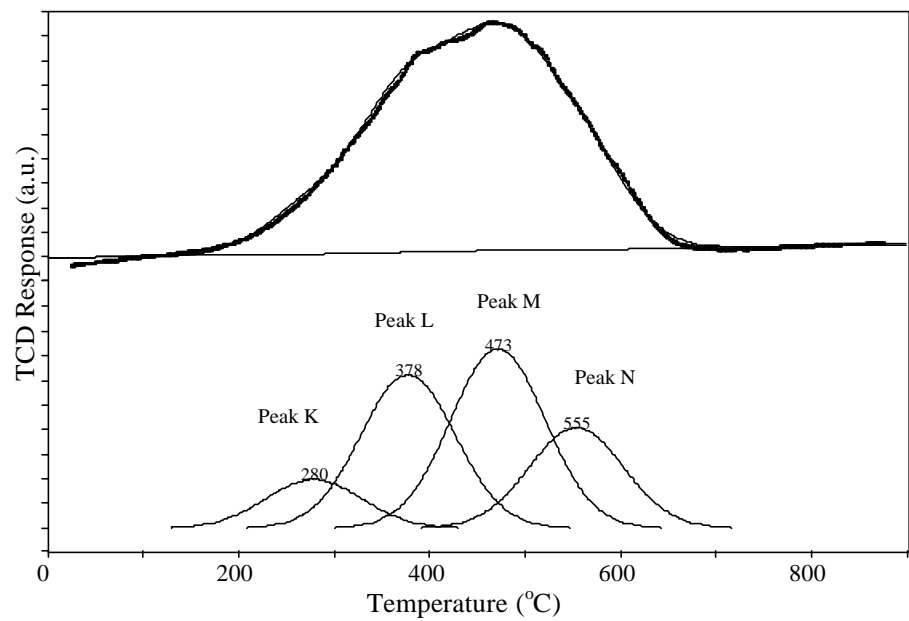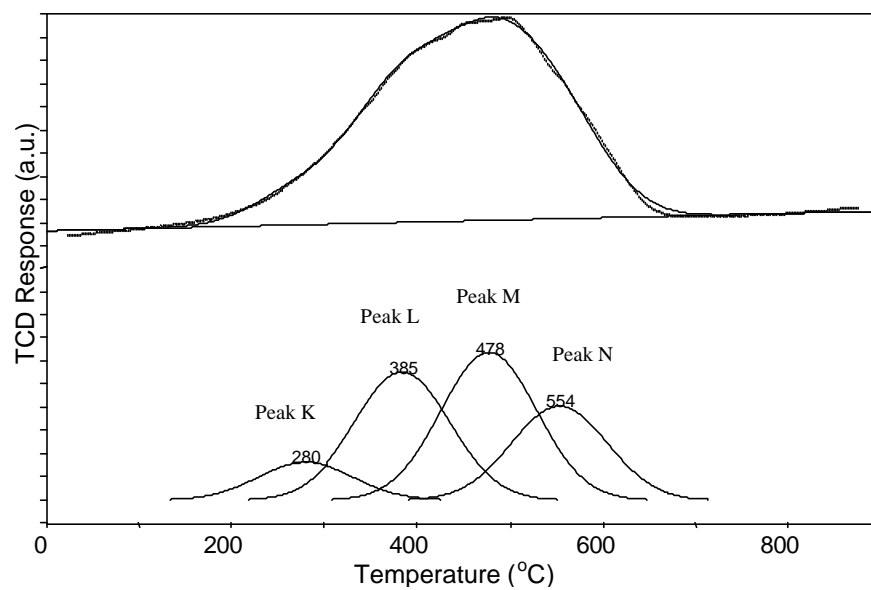
Figure 5.28 Analysis of TPO Spectrum for Spent Equilibrium FCC Catalyst (ECat-HIGH-161). Pretreatment: Calcined at 550 °C, Feed: SIHGO, C/O=5. (Top) Experimental Curve and Composite Curve from Analysis. (Bottom) Individual Peaks from Analysis.
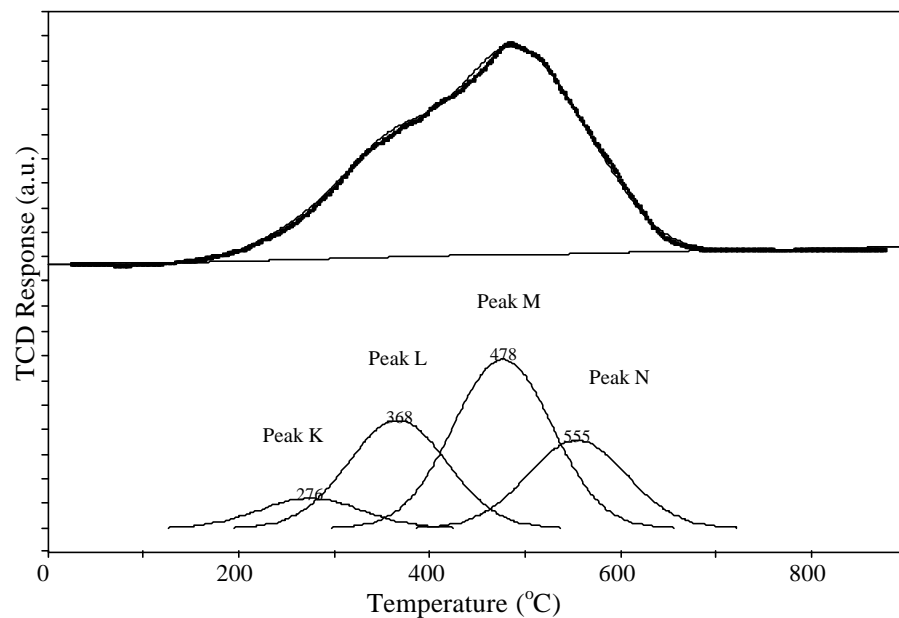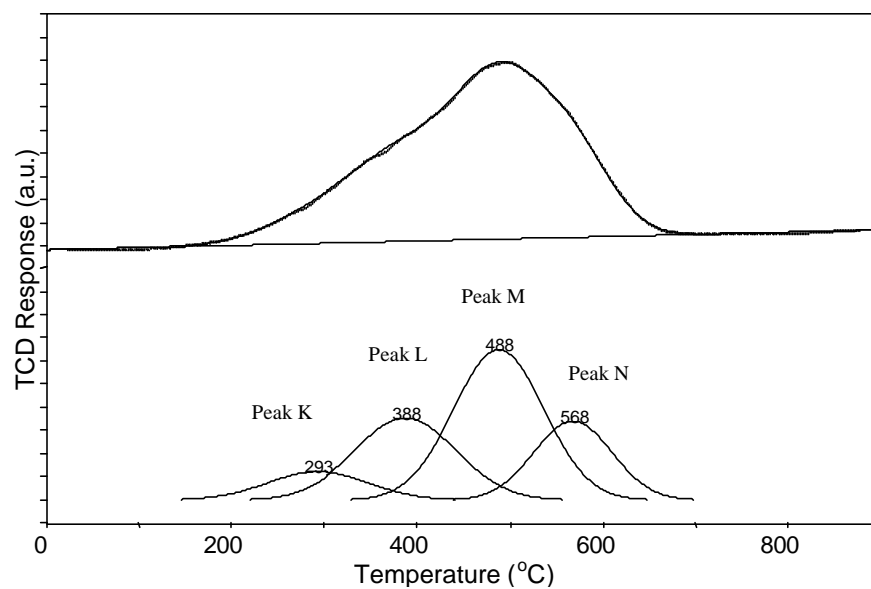
Figure 5.29 . Analysis of TPO Spectrum for Spent Equilibrium FCC Catalyst (ECat-HIGH-164). Pretreatment: Reduced with 8% Hydrogen in Argon at 700 °C, Feed: SIHGO, C/O=5. (Top) Experimental Curve and Composite Curve from Analysis. (Bottom) Individual Peaks from Analysis.
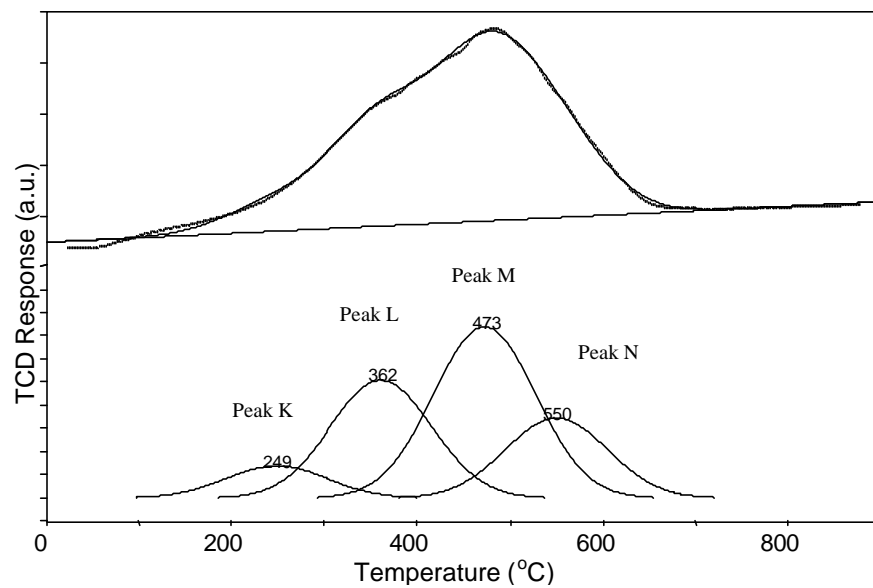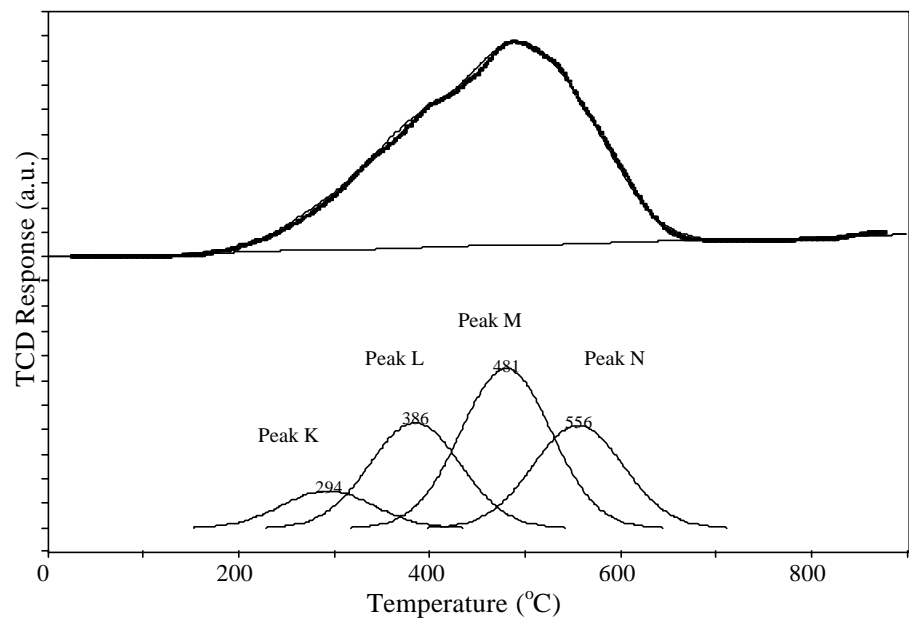
Figure 5.30 Analysis of TPO Spectrum for Spent Equilibrium FCC Catalyst (ECat-HIGH-166). Pretreatment: Reduced with 8% Methane in Helium at 700 °C, Feed: SIHGO, C/O=5. (Top) Experimental Curve and Composite Curve from Analysis. (Bottom) Individual Peaks from Analysis.

Figures 5.31 shows the comparisons of the relative area of each peak for ECat-HIGH spent catalysts, which were either pretreated with hydrogen and methane or calcined only prior to the catalytic cracking reactions at a catalyst-to-oil ratio of 5. Again, this figure shows that Peak L, which represents contaminant coke, decreases significantly with pretreatment. It seems that there is no significant effect of catalyst-to-oil ratio on the shape of TPO profiles.
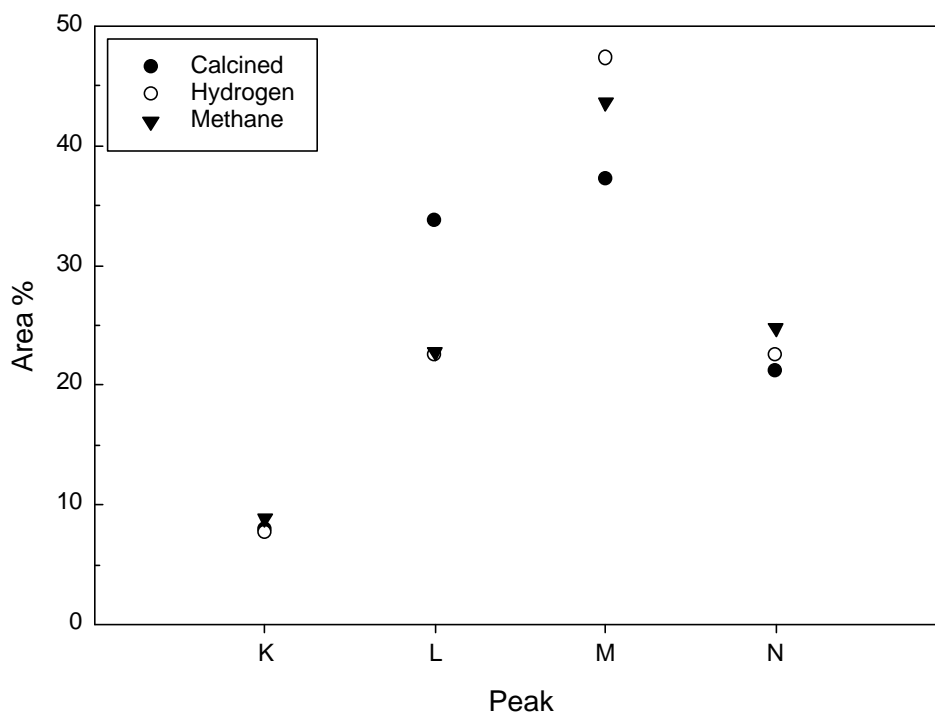
Figures 5.31 Changes of Relative Peak Areas for ECat-HIGH before and after Pretreatment at C/O = 5.0

As seen from Table 5.4, the changes with pretreatment are minor with ECat-LOW and ECat-INT spent catalyst samples. This must be due to the relatively low metal concentrations on these equilibrium catalysts compared to ECat-HIGH.

This well explains why we observed higher gasoline and lower coke yields using pretreated ECat-HIGH equilibrium catalyst with the highest metal concentration, ECat-HIGH for cracking reactions compared to calcined ECat-HIGH equilibrium catalyst. Our MAT results also showed that there were no significant changes in the catalyst performances before and after pretreatment for ECat-LOW and ECat-INT. The results from MAT units will be explained in section 6.0.

5.4 Conclusions

Temperature-programmed oxidation analysis was used to determine the nature and location of coke on spent equilibrium FCC catalysts. TPO profiles revealed useful information about the coke combustion kinetics in the presence of contaminant metals on the catalyst.

The carbon and hydrogen contents of spent FCC catalysts have been determined quantitatively. In TPO spectra peak maxima shifted to lower temperatures with increasing metal levels. This was attributed to the catalytic effect of metal contaminants on carbon combustion kinetics. Besides being a good quantitative analytical tool for measuring the total amount of coke on spent catalysts, the TPO analysis results together with results from surface area measurements and Soxhlet extraction with methylene chloride allowed us to identify the types and locations of coke on the spent catalyst. These results have shown that Peak L in TPO spectra represents the oxidation of "contaminant" coke in the vicinity of metals located in the pores of the zeolite. Peak N represents the "Conradson" coke, which is specific to the type of cracking feed. Peak M was

118

assigned to the "catalytic" coke formed during the acid-catalyzed cracking reactions. Peak K was attributed to the more reactive coke with high hydrogen content or the coke located on the outer surface of the catalyst, which is easily accessed by oxygen molecules during the oxidation reaction.

The capability of identifying the location and the nature of coke is important for understanding a catalyst deactivation process. Certain coke types at certain locations might have more significant effects on catalyst deactivation than other types at different locations on the spent catalyst. Therefore, the models for catalyst deactivation by coke should consider the type and the location of coke and the parameters affecting the coke type and location. The qualitative and quantitative information about coke on spent catalysts can be determined using TPO analysis results and this information can be used in catalyst deactivation and regeneration studies.

6.0 EFFECTS OF PRETREATMENT WITH HYDROGEN AND METHANE ON THE ACTIVITY OF EQUILIBRIUM FCC CATALYST

In this section, the effects of hydrogen and methane pretreatments on catalytic cracking performance of commercial equilibrium catalysts, contaminated with different levels of metals, will be investigated. SIHGO and n-hexadecane are used during the cracking experiments. N-hexadecane is chosen as a model compound representing long-chain alkanes present in a standard FCC feedstock. The results from SIGHO and n-hexadecane cracking allow us to evaluate the effects of pretreatment with hydrogen or methane on the performance of equilibrium FCC catalysts in the presence of contaminant metals (e.g., Ni and V). The properties of equilibrium FCC catalysts are given in Table 3.1. First the results from SIHGO cracking will be discussed. Then the results from n-hexadecane cracking will be presented.

6.1 Sour Imported Heavy Gas Oil (SIHGO) Cracking

6.1.1 Calcined Catalysts

Figure 6.1 shows the changes in MAT conversions of calcined equilibrium catalysts with contaminant metals level. These cracking reactions were performed using SIHGO at three different catalyst-to-oil ratios (3,5, and 8) and ASTM standard feed at a catalyst-to-oil (C/O) ratio of 3. MAT conversion decreases with increasing metals on the catalyst for a given feed and catalyst-to-oil ratio. The MAT conversions for ASTM cracking at a C/O of 3 were found to be higher than those for SIGHO cracking at a C/O of 3. The higher MAT conversions for ASTM feed were observed since this feed contains more paraffins, which are relatively easy to crack, compared to SIHGO. The relationship between conversion and the metal concentration is approximately linear

as also observed earlier by Larocca (1990). The data in Figure 6.1 is replotted in Figure 6.2. This time kinetic conversions (conversion%/(100-conversion%) are used instead of MAT conversions.

In Figure 6.3 MAT conversions for ECat-LOW and ECat-HIGH are plotted with respect to C/O ratios of 3, 5, and 8. Conversion increases with increasing C/O ratio for both ECat-LOW and ECat-HIGH. Again the conversion observed for ECat-LOW is higher than that of ECat-HIGH. The low conversions for ECat-HIGH compared to ECat-LOW are due to the negative impact of high metal concentration on MAT conversion. The aging of these two catalysts are also different. The lower surface area of ECat-HIGH is consistent with it being older than ECat-LOW (Table 3.1). The higher the metal contaminant level, especially nickel, the older the equilibrium catalyst. Because of the nature of FCC unit operation a part of the catalyst inventory is replaced with fresh catalyst periodically (normally once a day). This action causes a distribution of properties reflecting the age distribution in any equilibrium sample. If the feeds are the same and the catalysts are the same, a younger catalyst will have a higher surface area and contain less nickel.

Deactivation by aging is a combination of four separate, but interrelated, mechanisms: zeolite dealumination, zeolite decomposition, matrix surface collapse, and contaminant effects. Matrix can crack large molecules, which cannot diffuse into zeolite pores. After matrix cracking, the fragments are small enough to enter zeolite pores. Matrix can play an important role in upgrading bottoms. The amount and strength of acid sites on a silica-alumina matrix, which are responsible for its cracking activity, are associated with its alumina content. The matrix surface area and alumina content of those commercial catalysts generally vary in the same direction. Our surface area measurements show that matrix surface areas are 63, 63, and 45 m^2/g for ECat-LOW, ECat-INT and ECat-HIGH, respectively. This indicates that ECat-HIGH has low alumina content. Matrix surface area is effective in reducing bottoms yield and increasing LCO. In our case,

although ECat-HIGH has a relatively lower matrix surface area compared to ECat-LOW, this difference in matrix area did not affect the LCO and HCO yields very much. This shows that matrix cracking is not very effective. Matrix cracking improves gasoline octane because hydrogen transfer reactions are reduced compared to zeolitic cracking. Because hydrogen transfer reactions are bimolecular, their rate is enhanced by a high concentration of reactants in zeolite pores and by acid sites in close proximity to one another.
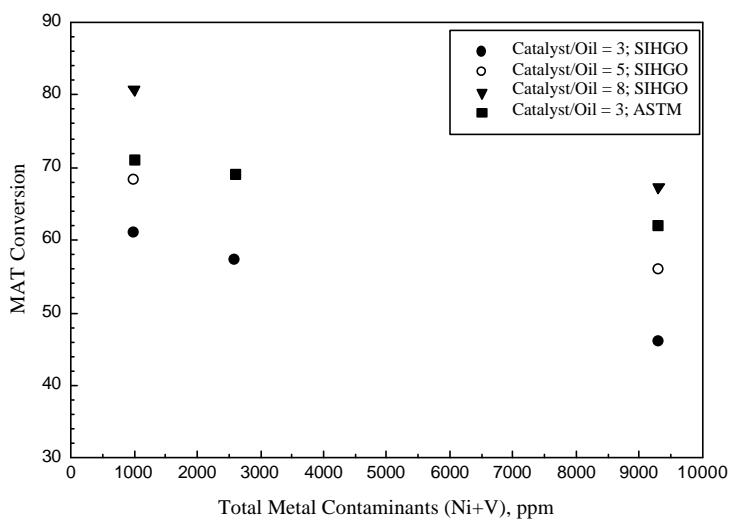
Figure 6.1 Effect of Metal Contaminant Level on MAT Conversion at Different Catalyst-to-Oil Ratios for SIHGO Cracking; Pretreatment: Calcined at 550 $^{\circ}$C in Air
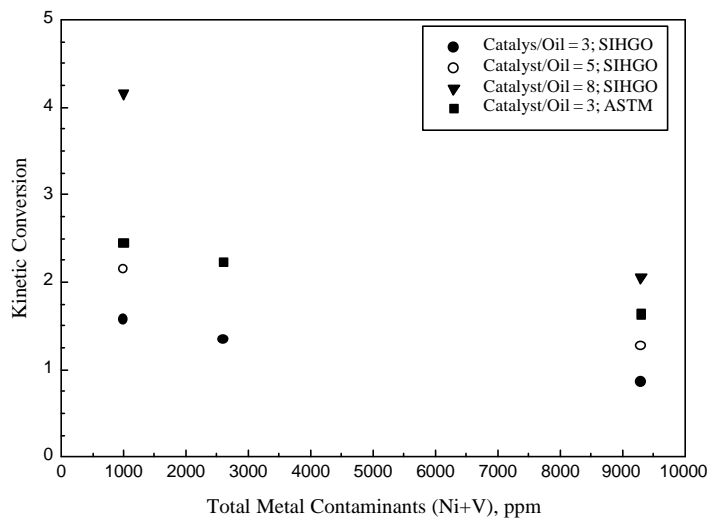
Figure 6.2 Effect of Metal Contaminant Level on MAT Kinetic Conversion at Different Catalyst-to-Oil ratios for SIHGO Cracking; Pretreatment: Calcined at 550 ^{o}C in Air
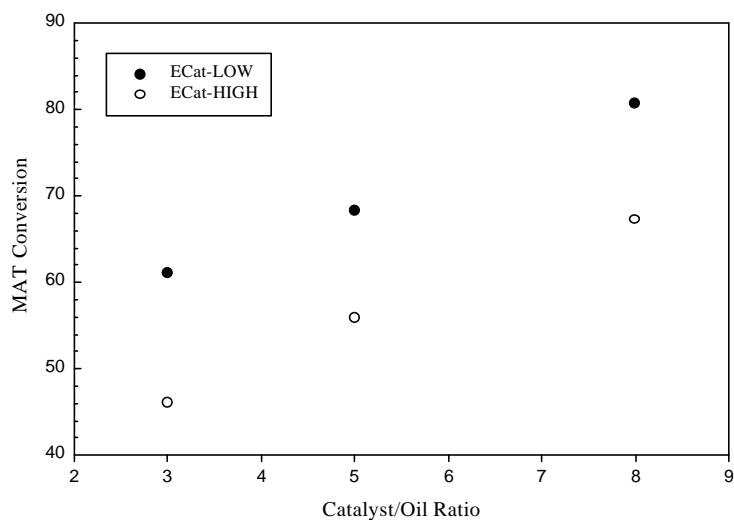
Figure 6.3 Effect of Catalyst-to-Oil Ratio on MAT Conversion. Feed: SIHGO; Catalyst: ECat-LOW and ECat-HIGH; Pretreatment: Calcined at 550 ^{o}C in Air

Figure 6.4 shows the changes of gas, gasoline and coke yields with respect to MAT conversion for calcined ECat-LOW. Yields for gas, gasoline and coke increase with increasing MAT conversion. Performing cracking reactions at different catalyst-to-oil ratios allowed us to change the conversions. The catalyst-to-oil ratios of 3, 5, and 8 were obtained by injecting different amounts of cracking feed while keeping the catalyst- amount constant at 5 grams. It is quite difficult to obtain exactly the desired catalyst to-oil-ratios and conversion values. Therefore we have used gas, gasoline, and coke yields for each corresponding conversion value regardless of the catalyst-to-oil ratio. The point where gas yield becomes higher than gasoline yield corresponds to MAT conversion of 74%. This can be attributed to the overcracking of gasoline at relatively high conversions. Figure 6.5 shows the yields of LCO and HCO for calcined ECat-LOW. Both LCO and HCO yield decrease with MAT conversion.
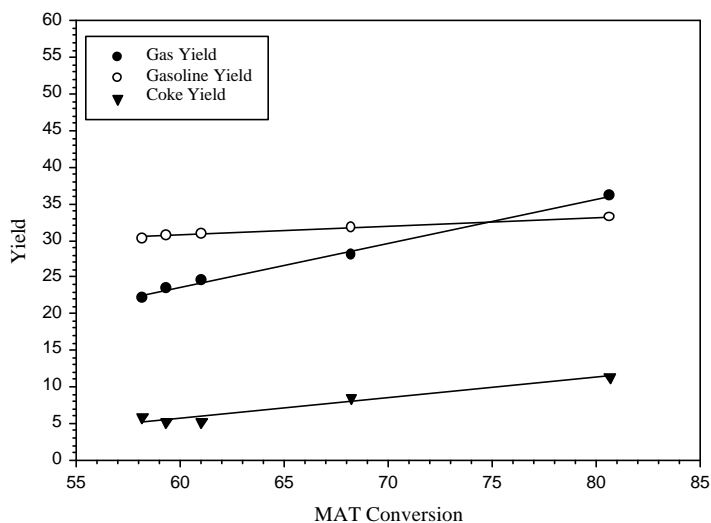
Figure 6.4 Yields of Gas, Gasoline and Coke as a Function of MAT Conversion; Feed: SIHGO, Catalyst: ECat-LOW; Pretreatment: Calcined at 550 °C in Air
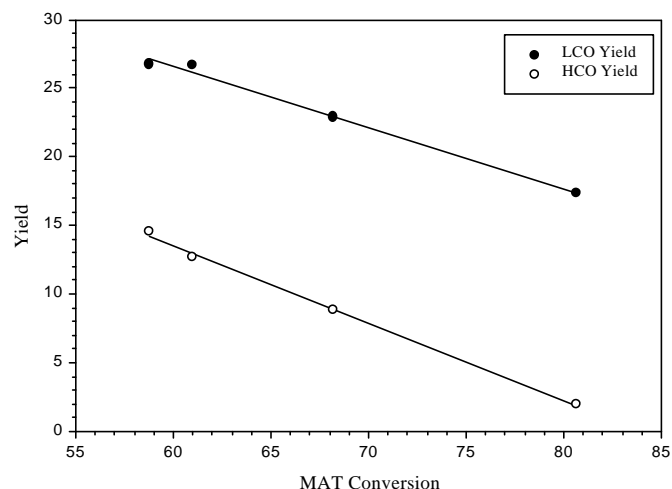
Figure 6.5 Yields of LCO and HCO as a Function of MAT Conversion; Feed: SIHGO, Catalyst: ECat-LOW; Pretreatment: Calcined at 550 °C in Air

Figure 6.6 shows the changes in yields of gas, gasoline, and coke with MAT conversion for ECat-HIGH. Again, as expected, yields of all components increase with conversion. The crossing point between gas and gasoline yield lines occurs at a MAT conversion of 60%. We can conclude that for highly contaminated catalyst, ECat-HIGH overcracking happens at lower conversion compared to less contaminated catalyst, ECat-LOW. Habib and coworkers (1977) observed that the conversion at which recracking begins to predominate over gas oil cracking shifts toward lower conversion with metals poisoning. The hydrogen transfer reactions are expected to be less significant for ECat-HIGH compared to ECat-LOW. This poor hydrogen transfer for ECat-HIGH leads to overcracking of primary products to secondary products of smaller molecular weight and causes carbon formation. Decreased site density is the controlling factor for Y zeolite (the higher the dealumination the lower the site density) causing bimolecular hydrogen transfer reactions to decline. When hydrogen transfer reactions increase, the MAT conversion increases. This role of hydrogen transfer reactions will be explained in the next sections.

Figure 6.6 Yields of Gas, Gasoline and Coke as a Function of MAT Conversion; Feed: SIHGO, Catalyst: ECat-HIGH; Pretreatment: Calcined at 550 °C.

Figure 6.7 shows the yields of LCO and HCO for ECat-HIGH. Both LCO and HCO yields decrease with increasing MAT conversions.

Using the yield data given in all the figures above, Figure 6.8 compares the yields of gas, gasoline, coke, LCO and HCO between ECat-LOW and ECat-HIGH at a constant MAT conversion of 60%. As seen from this figure, gas and coke yield increase while gasoline yield decreases with increasing metals level. LCO and HCO yields do not change significantly.

Figure 6.7 Yields of LCO and HCO as a Function of MAT Conversion; Feed: SIHGO, Catalyst: ECat-HIGH; Pretreatment: Calcined at 550 °C in Air
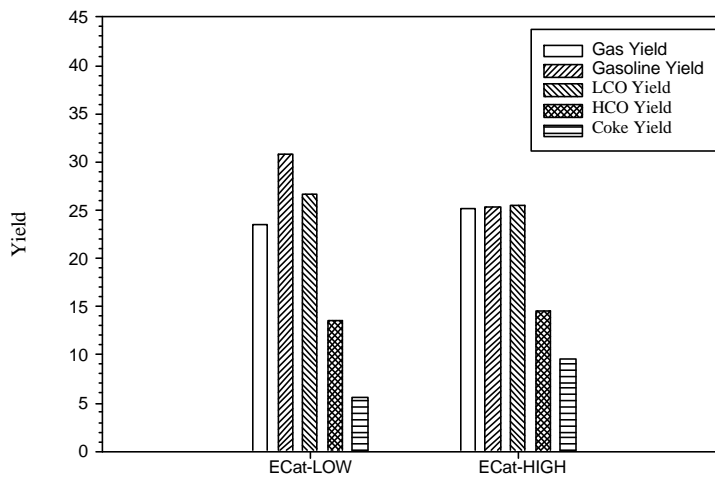
Figure 6.8 Comparison of Yields between Calcined ECat-LOW and ECat-HIGH at 60% Conversion. Feed: SIHGO; Pretreatment: Calcined at 550 °C in Air

6.1.2 Pretreatment with Hydrogen or Methane

The negative effects of contaminant metals on the performance of equilibrium FCC catalysts have been shown in the preceding section. In this section, results obtained from similar experiments for either hydrogen- or methane-pretreated equilibrium catalysts will be discussed. Our surface area measurements have shown that hydrogen and methane pretreatments do not change BET surface areas significantly. For example, BET surface area of ECat-INT pretreated with hydrogen and methane was found to be 157 m^2/g whereas BET surface area of calcined ECat-INT was measured as 160 m^2/g. This indicates that the pretreatment conditions applied do not affect performance due to any changes in catalyst surface areas.

Figure 6.9 shows the effect of conversion on the yields of gas, gasoline and coke for ECat-LOW pretreated with hydrogen. The cracking was performed at two different C/O ratios (3 and 5). The cracking experiments at C/O ratios of 8 were not performed with pretreated catalyst. As mentioned earlier in section 3.3.2, this ratio was changed by changing the amount of feed while keeping the catalyst amount constant at 5 grams. In order to obtain C/O ratio of 8, 0.625 gram feed has to be cracked. Since the amount of liquid and gas products from the cracking of 0.625 gram feed is very small, the errors resulting from the weight measurements of liquid products increase. After knowing this limitation during the cracking experiments with non-pretreated calcined catalysts we preferred performing cracking experiments at C/O ratios of 3 and 5. Hydrogen pretreatment causes the MAT conversion at the same C/O ratios to shift slightly lower compared to the conversions for calcined ECat-LOW (shown in Figure 6.4). Figure 6.10 shows the yields of LCO and HCO with respect to MAT conversion. Both LCO and HCO decrease with increasing MAT conversions.

Similarly, Figures 6.11 and Figure 6.12 show the yields of gas, gasoline, coke, LCO and HCO with increasing MAT conversions for hydrogen pretreated ECat-HIGH. Similar MAT conversions were observed after pretreating the ECat-HIGH catalyst with hydrogen compared to calcined ECat-HIGH. However, the crossing point between gas and gasoline yield was not observed at 60 % MAT conversion. It looks like they do not cross each other at all. This may be the effect of hydrogen pretreatment preventing overcracking of gasoline.
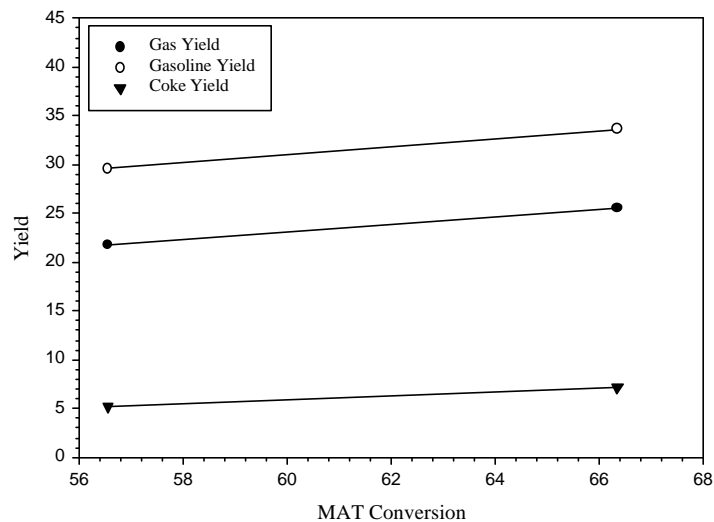
Figure 6.9. Yields of Gas, Gasoline and Coke as a Function of MAT Conversion; Feed: SIHGO, Catalyst: ECat-LOW; Pretreatment: 8% H$_2$/Ar at 700 °C for ~6 Hours
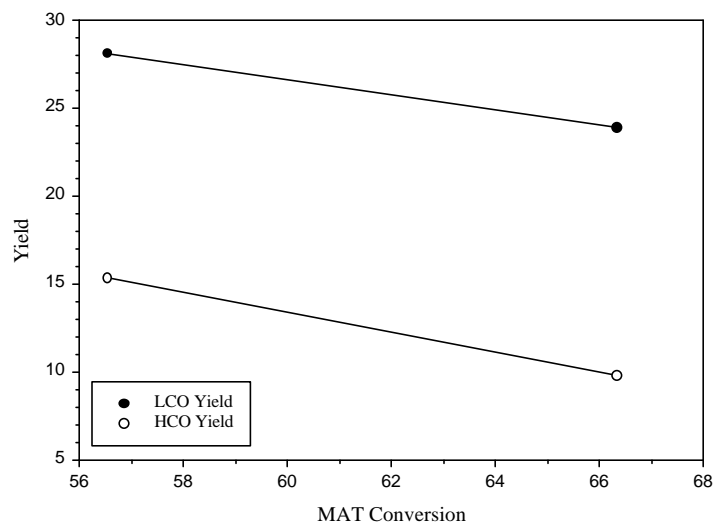
Figure 6.10. Yields of LCO and HCO as a function of MAT conversion; Feed: SIHGO, Catalyst: ECat-LOW; Pretreatment: 8% H$_2$/Ar at 700 °C for ~6 Hours.
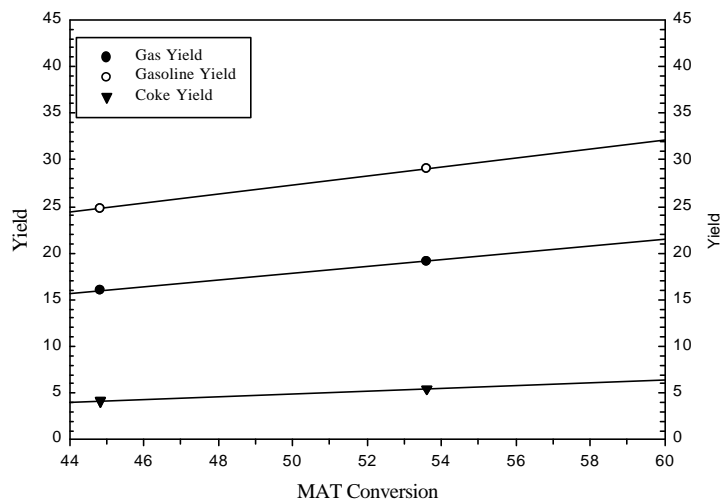
Figure 6.11. Yields of Gas, Gasoline and Coke as a Function of MAT Conversion; Feed: SIHGO, Catalyst: ECat-HIGH; Pretreatment: 8% H$_2$/Ar at 700 °C for ~6 Hours (Regression Lines are Extrapolated to Obtain the Yield Values at 60% Conversion)
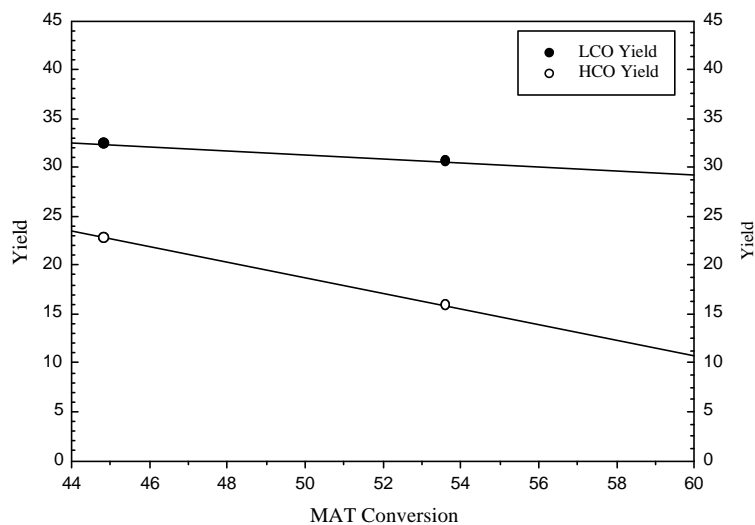
Figure 6.12. Yields of LCO and HCO as a Function of MAT Conversion; Feed: SIHGO, Catalyst: ECat-HIGH; Pretreatment: 8% H$_2$/Ar at 700 °C for ~6 Hours (Regression Lines are Extrapolated to Obtain the Yield Values at 60% Conversion)

131

The yields of gas, gasoline, coke, LCO and HCO for methane-pretreated ECat-LOW and ECat-HIGH are presented in Figures 6.13 to 6.16.
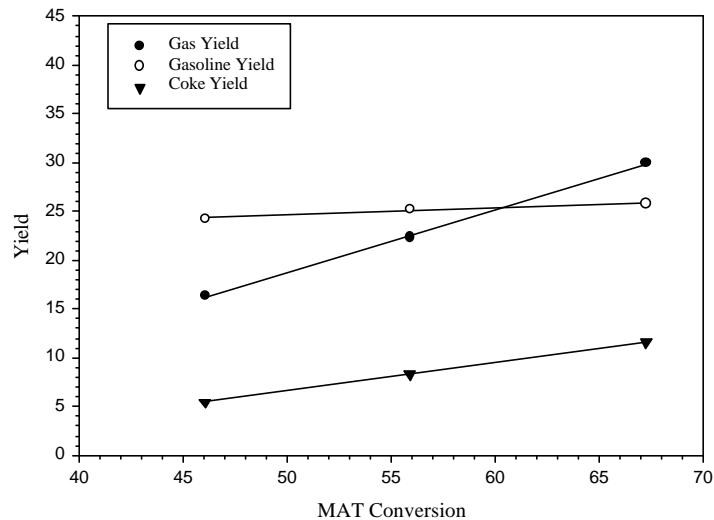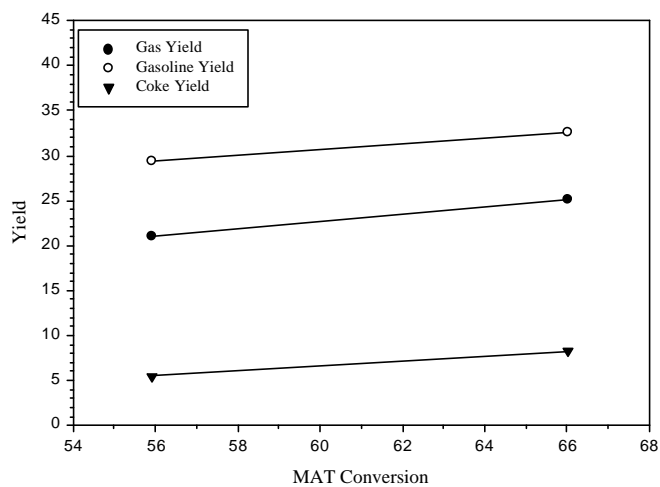

Figure 6.13 Yields of gas, gasoline and coke as a function of MAT conversion; Feed: SIHGO, Catalyst: ECat-LOW; Pretreatment: 8% CH$_4$/He at 700 °C for ~6hours.
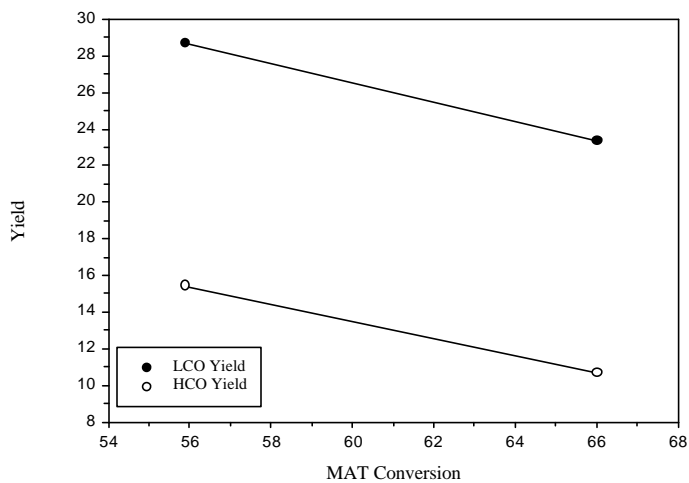
Figure 6.14. Yields of LCO and HCO as a Function of MAT Conversion; Feed: SIHGO, Catalyst: ECat-LOW; Pretreatment: 8% CH$_4$/He at 700 °C for ~6 Hours.
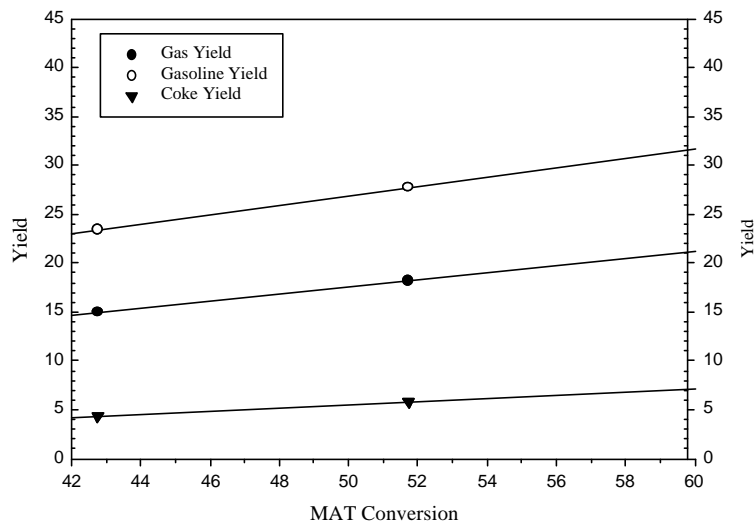
Figure 6.15. Yields of Gas, Gasoline and Coke as a Function of MAT Conversion; Feed: SIHGO, Catalyst: ECat-HIGH; Pretreatment: 8% CH$_4$/He at 700 °C for ~6 Hours (Regression Lines are Extrapolated to Obtain the Yield Values at 60% Conversion)
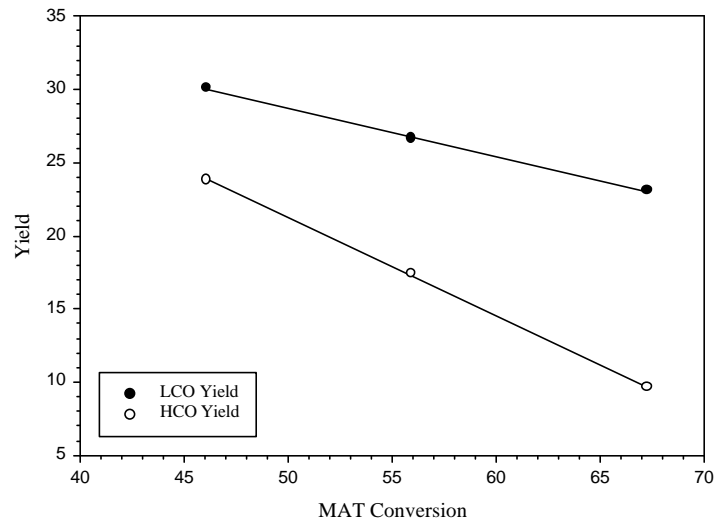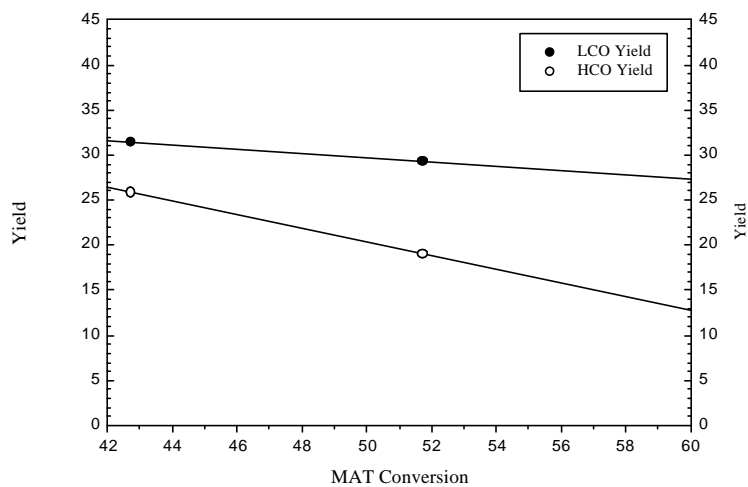

**Figure 6.16. Yields of LCO and HCO as a Function of MAT Conversion; Feed: SIHGO, Catalyst: ECat-HIGH; Pretreatment: 8% CH$_4$/He at 700 °C for ~6 Hours (Regression Lines are Extrapolated to Obtain the Yield Values at 60% Conversion)**

133

Figure 6.17 compares the yields of gas, gasoline, coke, LCO, and HCO before and after hydrogen or methane pretreatment of ECat-LOW at a constant MAT conversion of 60% using SIHGO feed. This figure shows no significant effect of pretreatments on the yields of gas, gasoline and coke for ECat-LOW. This is not surprising since there is not much contaminant metals on ECat-LOW.

Figure 6.18 shows the effects of pretreatments on the yields of gas, gasoline and coke for ECat-HIGH at a constant MAT conversion of 60% using SIHGO feed. As seen from Figure 6.18, with both hydrogen and methane pretreatment the gasoline and LCO yields increased while the gas, coke and HCO yields decreased compared to the calcined ECat-HIGH.
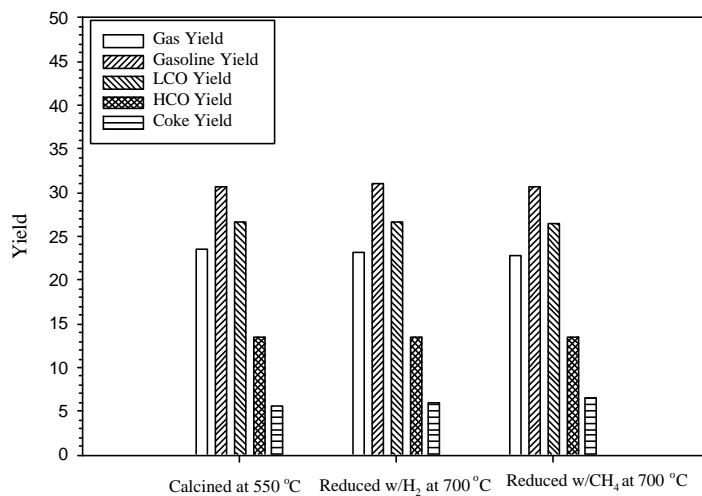
Figure 6.17 Comparison of Yields before and after H$_2$ and CH$_4$ Pretreatment for ECat-LOW at 60% Conversion; Feed: SIHGO
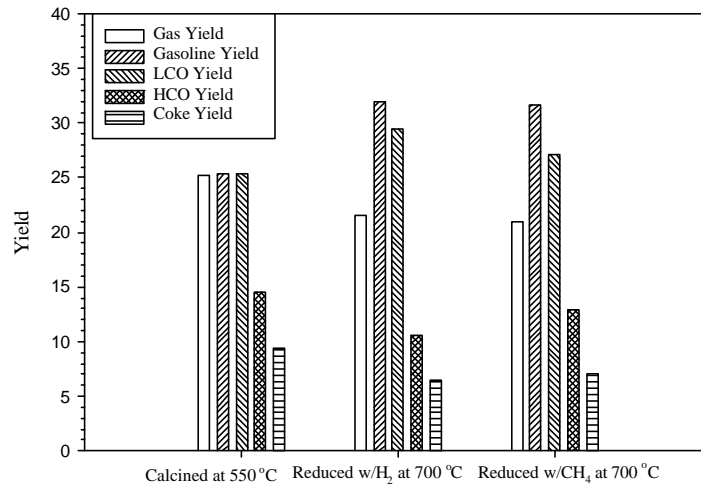
Figure 6.18 Comparison of Yields before and after H_2 and CH_4 Pretreatment for ECat-HIGH at 60% Conversion of SIHGO Feed.

Figure 6.19 shows the changes in coke yields with kinetic conversion before and after pretreating ECat-LOW and ECat-HIGH with hydrogen. For ECat-LOW the coke yield does not change significantly with pretreatment. The coke yield for ECat-HIGH decreases significantly after pretreatment.
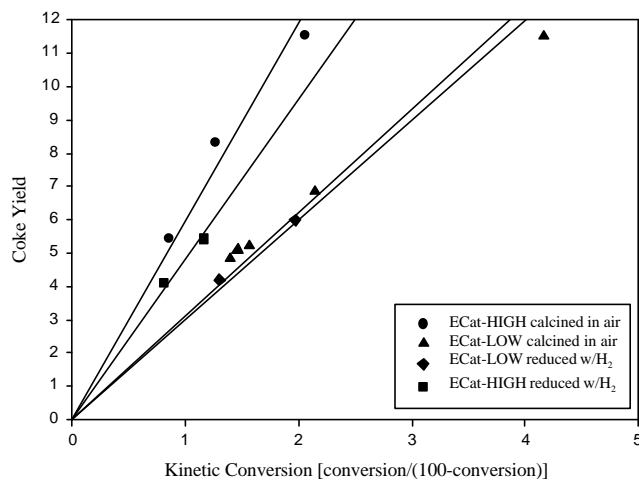
Figure 6.19 Changes in Coke Yield with Kinetic Conversion as a Function of Pretreatment

6.1.3 Hydrogen Production in the Presence of Contaminant Metals

H_2 yields from MAT experiments have usually been reported by using H_2/CH_4 molar ratio. Hydrogen production was found to be very sensitive to catalyst metal contamination. At low catalyst metals level (< 1000 ppm Ni+V) H_2/CH_4 ratios of less than 1.0 were found to be typical (Venuto et al., 1979). At metals level of 1000-1500 ppm, which is the normal level for many FCC units, H_2/CH_4 ratios of 1-2 were found to be typical (Venuto et al., 1979). For the case of severe metals contamination when Ni+V levels have risen above 5000 ppm, H_2/CH_4 ratios of 10 or higher would be typical (Venuto et al., 1979). As seen from Figure 6.20, H_2/CH_4 molar ratio is very sensitive to catalyst metal contamination. When the metals on the catalyst increase, this ratio also increases. This ratio increases with increasing MAT conversions for all the equilibrium catalysts as seen from Figure 6.20.
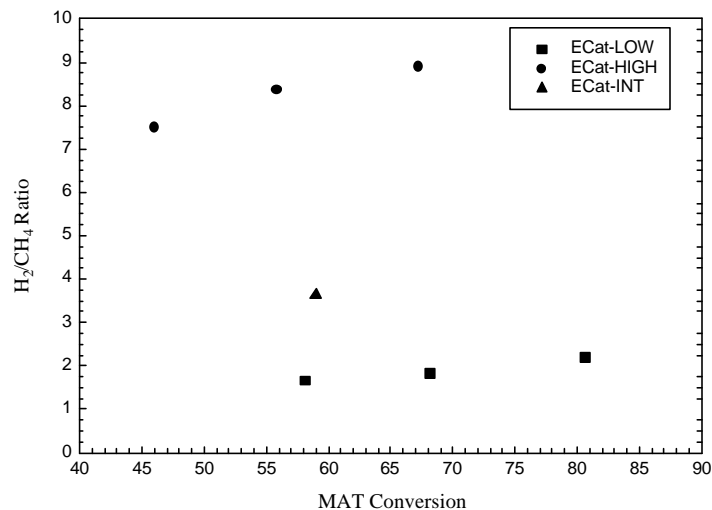
Figure 6.20 Comparison of Hydrogen-to-Methane Ratios for Three Different Calcined Catalysts at Different MAT Conversions

In our case, the H_2/CH_4 molar ratios were found to be 1.6, 3.5 and 8.5 for ECat-LOW (1000 ppm), ECat-INT (2600ppm) and ECat-HIGH (9300ppm), respectively, at a constant MAT conversion of 60% using SIHGO feed.

Figure 6.21 shows the hydrogen yield with respect to MAT conversion for ECat-LOW before and after pretreatment. Hydrogen production was measured to complete the picture of catalytic effects of contaminant metals. This figure shows that hydrogen yield increases with increasing conversion. Pretreatment did not have any significant effect on hydrogen yield. Hydrogen yield slightly decreased with both hydrogen and methane pretreatment.

Figure 6.22 shows the changes in hydrogen-to-methane ratio with hydrogen or methane pretreatments for ECat-LOW. Clearly, both pretreatments did not affect this ratio very much. This ratio increases with increasing conversion.
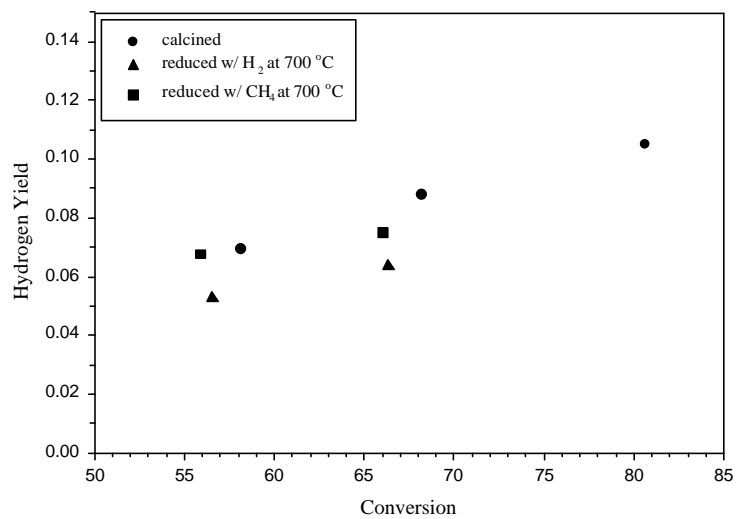
Figure 6.21 Hydrogen Yield with Respect to Conversion for ECat-LOW
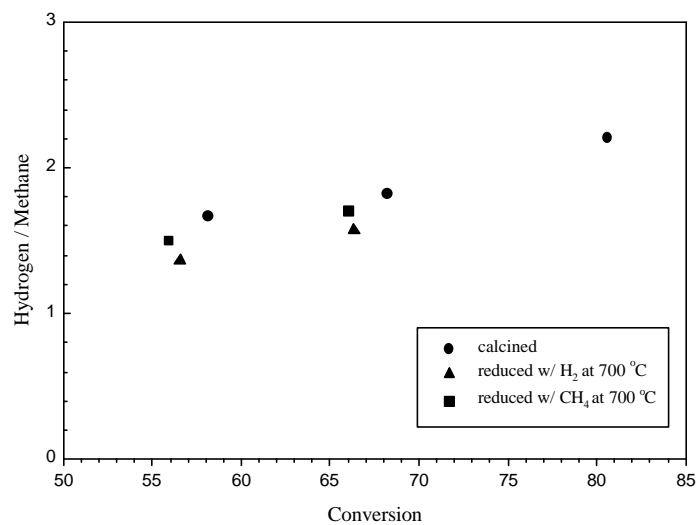
Figure 6.22 Hydrogen-to Methane Ratio with Respect to Conversion for ECat-LOW

138

Similarly, changes in hydrogen yield with MAT conversion for ECat-HIGH before and after pretreatment are given in Figure 6.23. As seen from this figure, pretreatment significantly decreases the hydrogen yield for ECat-HIGH. This is also reflected in hydrogen-to-methane ratio shown in Figure 6.24. This ratio decreases with both pretreatments. This indicates that metals on the catalyst lose their activities to produce hydrogen by dehydrogenation reactions. We see this net effect in ECat-HIGH, since this is the catalyst with highest metal concentration.
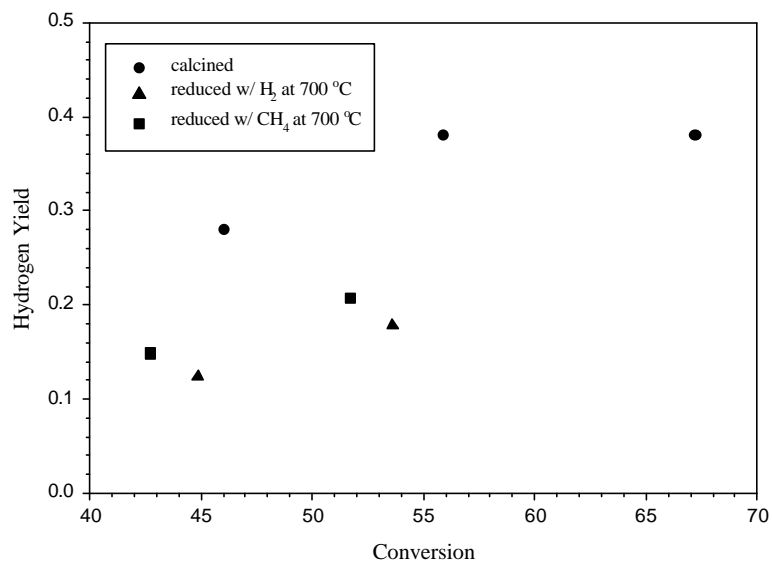
Figure 6.23 Hydrogen Yield with Respect to Conversion for ECat-HIGH
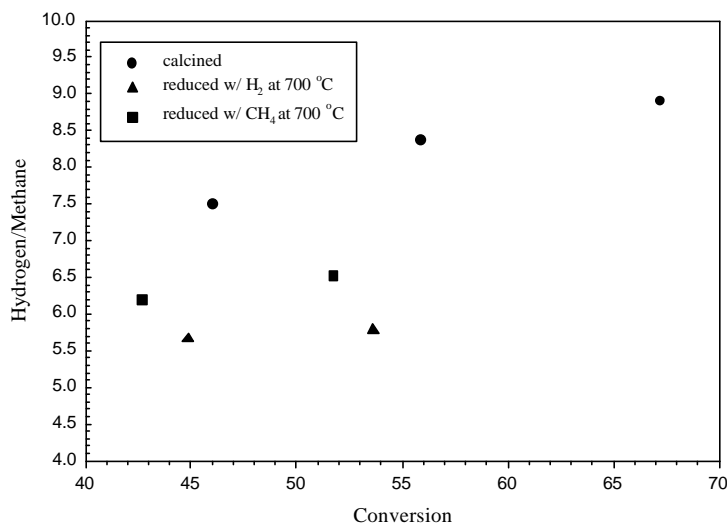
Figure 6.24. Hydrogen-to-Methane Ratio with Respect to Conversion for ECat-HIGH

6.1.4 Hydrogen Transfer Reactions

C_4 paraffin-to-C_4 olefin ratio is usually used as an indication of the hydrogen transfer reactions. If this ratio is high, it means hydrogen transfer reactions play an important role. Figure 6.25 compares the C_4 paraffin-to-C_4 olefin ratio between calcined ECat-LOW and calcined ECat-HIGH to determine the effect of metals level on hydrogen transfer reactions. As seen from this figure, this ratio, indicating hydrogen transfer reactions, increases with increasing conversions for both catalysts. However, this ratio for ECat-HIGH was always found to be less than that observed for ECat-LOW. This indicates that the hydrogen transfer reactions are reduced in the presence of metal contaminants. Therefore, more olefins are produced in the case of ECat-HIGH compared to ECat-LOW.

140
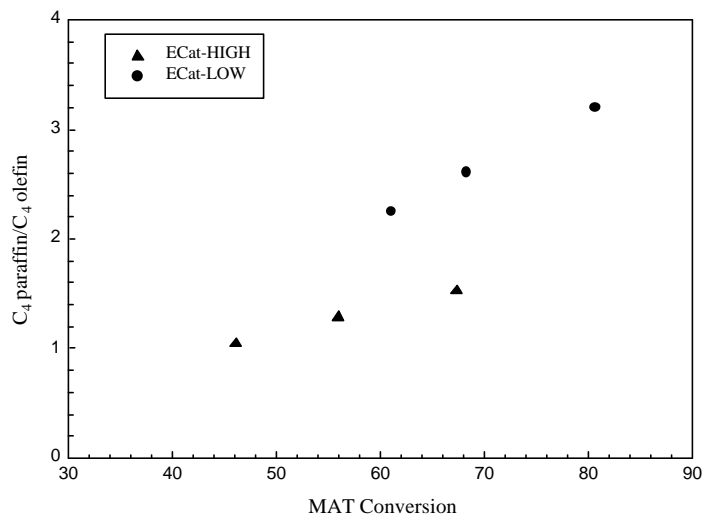
Figure 6.25 Comparisons of C$_4$ Paraffin-to-C$_4$ Olefin Ratios with Respect to MAT Conversions for Calcined ECat-LOW and ECat-HIGH

Figure 6.26 shows the C$_4$ paraffin-to-C$_4$ olefin ratios for calcined and pretreated ECat-LOW at different MAT conversions. As seen from this figure, this ratio increases with increasing conversions. However, pretreatments do not affect this ratio very much, indicating hydrogen transfer reactions are not affected by the pretreatment for ECat-LOW.

The situation was found to be completely different for ECat-HIGH. As seen from Figure 6.27, this ratio increased with both hydrogen and methane pretreatments. The effect of methane pretreatment was slightly more dominant than the hydrogen pretreatment. Clearly, the pretreatments increased the hydrogen transfer reactions for ECat-HIGH.
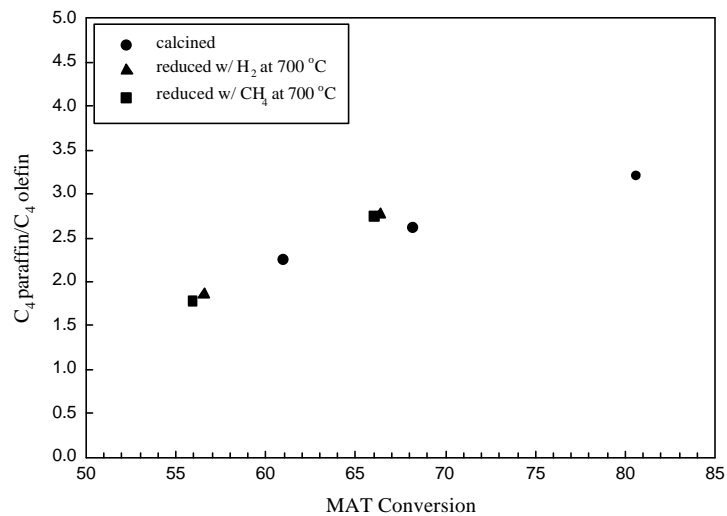
Figure 6.26. Comparison of C$_4$ paraffin-to-C$_4$ olefin ratios with respect to MAT conversions before and after pretreatment for ECat-LOW
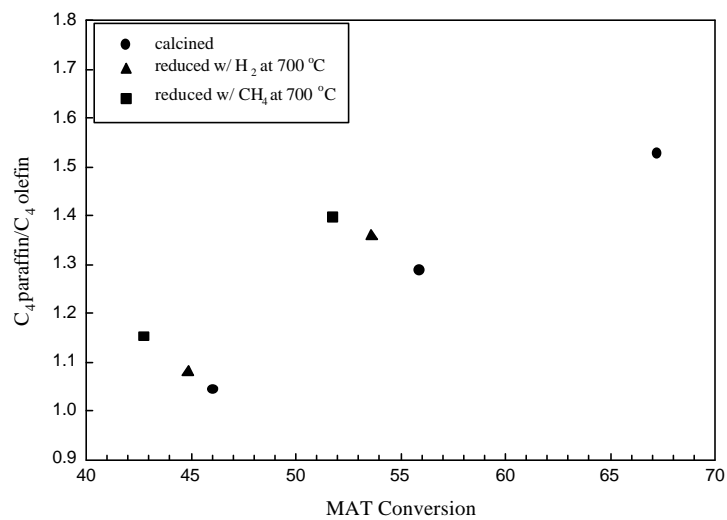
Figure 6.27 Comparison of C$_4$ Paraffin-to-C$_4$ Olefin Ratios with Respect to MAT Conversions before and after Pretreatment for ECat-HIGH

As reported in a previous study (Lee, 1989), cracking in the presence of hydrogen shifts products to higher molecular weights. The reason for this is not clearly understood. One speculation is that higher hydrogen partial pressure reduces the density of acid sites on the catalyst, which not only causes the products to shift to higher molecular weight but also causes a higher olefin-to-paraffin ratio as a result of less hydrogen transfer. Lee (1989) attributed this increase in olefin yield to the inhibition of hydrogen transfer reactions with higher hydrogen partial pressure. However, a mechanism supporting this idea was not given. It is also speculated that, in the presence of hydrogen during cracking reactions, some of the coke precursors could be hydrogenated and thus, the coke yield was significantly reduced compared to the base case. Coke precursors are thought to be hydrogen donors. Reduced coke precursors under hydrogen fluidization should reduce hydrogen transfer reactions, resulting again in higher olefin-to-paraffin ratios in the cracking products (Lee, 1989).

If we consider a mechanism for hydrogen transfer between an adsorbed carbenium ion and a donor molecule trapped in a zeolite pore, the donor molecule would be immobilized between the adsorbed carbenium ion and a second, neighboring acid site. If we consider hydrogen transfer to C_4 olefins, protonation of the linear C_4 olefins results in the formation of a secondary carbenium ion, while protonation of isobutene results in the formation of a more stable tertiary carbenium ion. The more stable tertiary carbenium ion is expected to have a longer lifetime than a secondary carbenium ion. Hydrogen transfer is a bimolecular reaction. Thus, the rate of hydrogen transfer is proportional to the lifetime of the carbenium ion times the probability that the carbenium ion will encounter a hydride donor during its lifetime. The latter is favored by a high acid site density or a high concentration of adsorbed olefins. This mechanism favors hydrogen transfer in catalysts with high zeolite concentration or in catalysts with zeolites containing many sites. It explains why lower

hydrogen transfer reactions are observed with highly contaminated equilibrium catalyst, since contaminated catalysts have very weak acid sites.

Hydrogen transfer reactions increase the gasoline range products by terminating carbocations and saturating olefins before they can undergo further cracking (Gates et al., 1979). The improved hydrogen transfer reactions with pretreatment for ECat-HIGH may cause the increase in gasoline yield and decrease in gas and coke yields.

6.2 N-hexadecane Cracking

N-hexadecane is widely used as an model compound in cracking reactions. This makes the analysis and interpretation of results relatively simple compared to results with a multi-component feed.

6.2.1 Calcined Catalysts

Figures 6.28 and 6.29 show the changes in overall and MAT conversions with contaminant metals on the catalyst at three different C/O ratios of 3, 5, and 8 from n-hexadecane cracking. As seen from these figures, overall and MAT conversions decrease almost linearly with increasing metals level for all C/O ratios.

We can see the effect of C/O ratio on MAT conversion obtained for ECat-LOW, ECat-INT, and ECat-HIGH in Figure 6.30. For all equilibrium catalysts MAT conversion linearly increases with increasing C/O ratio. While the MAT conversion for ECat-LOW and ECat-INT are very close to each other, very low MAT conversions are observed for ECat-HIGH. The difference in MAT conversion is reduced at a C/O of 8 for ECat-HIGH.
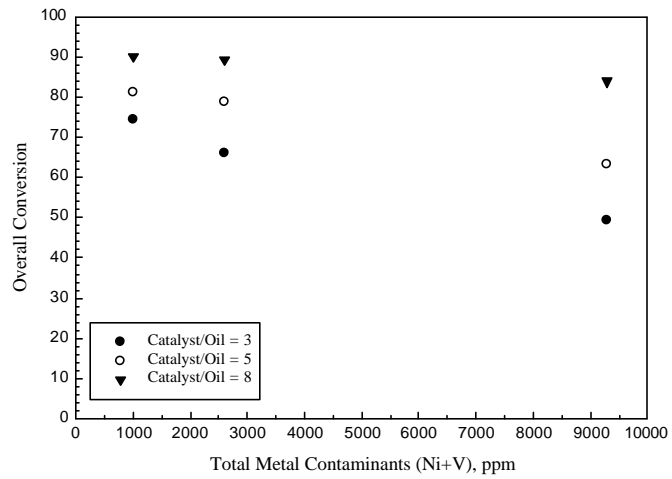
Figure 6.28. Effect of Metal Contaminant Level on Overall Conversion at Different Catalyst-to-Oil Ratios for n-hexadecane Cracking
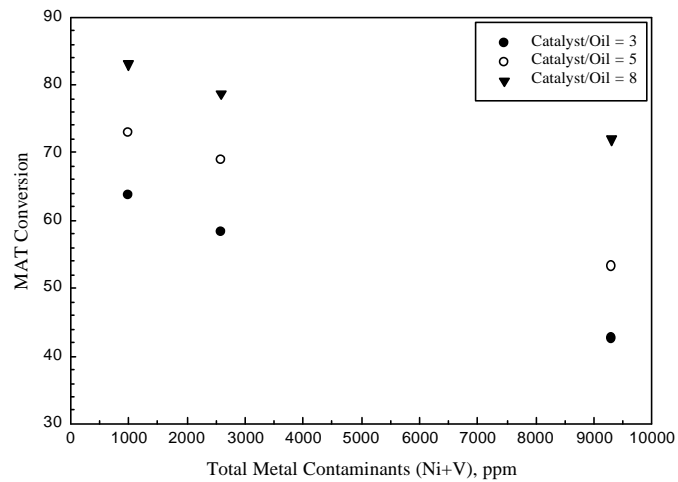
Figure 6.29 Effect of Metal Contaminant Level on MAT Conversion at Different Catalyst-to-Oil Ratios for n-hexadecane Cracking
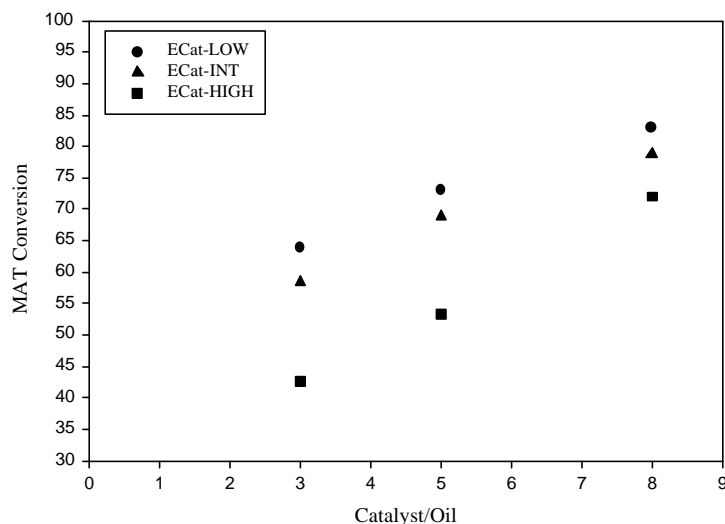
Figure 6.30 Effect of Catalyst-to-Oil Ratio on MAT Conversion. Feed: n-hexadecane; Catalyst: ECat-LOW, ECat-INT, and ECat-HIGH

Figure 6.31 shows the changes in yields of gas, gasoline and coke with MAT conversions for calcined ECat-LOW from n-hexadecane cracking. Compared to SIHGO cracking for the same catalyst, gas yields were always found to be the highest for n-hexadecane. There was no crossing between gas and gasoline yield lines. Relatively lower coke yields were observed for the same range of MAT conversion for n-hexadecane cracking. This can be explained by the less coke-making tendency of n-hexadecane compared to the gas oil feed containing aromatic and polar components.

Figure 6.32 shows the changes in the yields of C_{12}-C_{15} hydrocarbons and unreacted C_{16}. As seen from this figure, while the yield of C_{12}-C_{15} hydrocarbons decreases slightly but not much, the unreacted C_{16} yield decreases very significantly with increasing MAT conversion. This indicates that the increases in the yield of gas, gasoline and coke are coming from the cracking of n-hexadecane itself without changing C_{12}-C_{15} yield.

146

Figure 6.31 Yields of Gas, Gasoline and Coke as a Function of MAT Conversion; Feed: n-hexadecane, Catalyst: ECat-LOW; Pretreatment: Calcined at 550 °C.
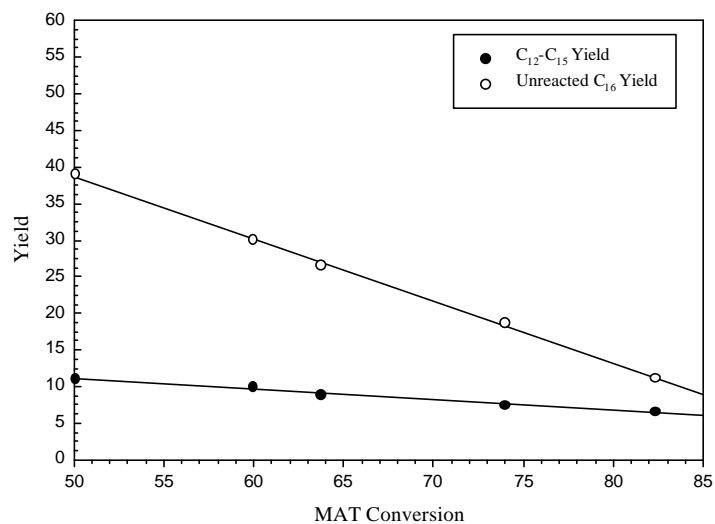
Figure 6.32 Yields of LCO and HCO with increasing MAT conversion; Feed: n-hexadecane, Catalyst: ECat-LOW; Pretreatment: calcined at 550 °C.

Similar trends are obtained in the case of ECat-INT as seen in Figures 6.33 and 6.34. This time the C_{12}-C_{15} yield increases slightly with conversion while the unreacted C_{16} yield decreases sharply.

Figure 6.35 shows the changes in the yields of gas, gasoline, and coke for ECat-HIGH. The changes in the yields of C_{12}-C_{15}, and unreacted C_{16} are shown in Figure 6.36. As we can see from Figure 6.35, for ECat-HIGH gasoline yield is very much lower compared to the less contaminated equilibrium catalysts, ECat-LOW and ECat-INT. The unreacted C_{16} yield decreases with high metals level while the C_{12}-C_{15} yield increases steadily as seen in Figure 6.36.

Figure 6.37 shows the comparisons of gas, gasoline and coke yields among calcined ECat-LOW, ECat-INT, and ECat-HIGH at 60% constant conversion of n-hexadecane feed. As seen from this figure, gas and coke yields increase with increasing metals level while the gasoline yields decrease.
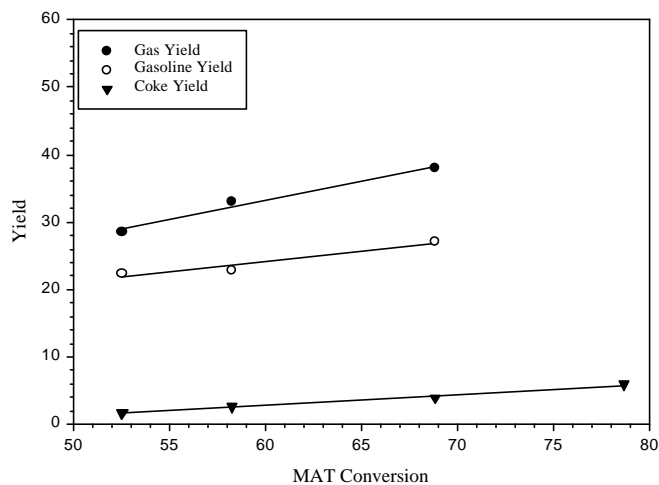
Figure 6.33 Yields of Gas, Gasoline and Coke as a Function of MAT Conversion; Feed: n-hexadecane, Catalyst: ECat-INT; Pretreatment: Calcined at 550 °C.
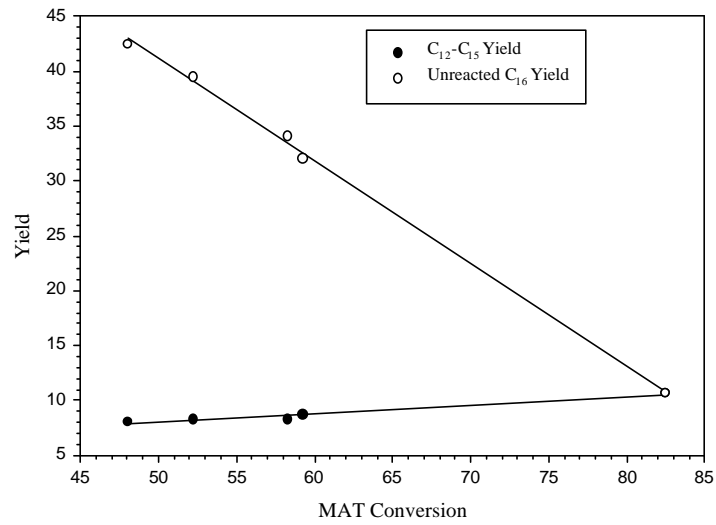
Figure 6.34 Yields of LCO and HCO as a Function of MAT Conversion; Feed: n-hexadecane, Catalyst: ECat-INT; Pretreatment: Calcined at 550 °C.
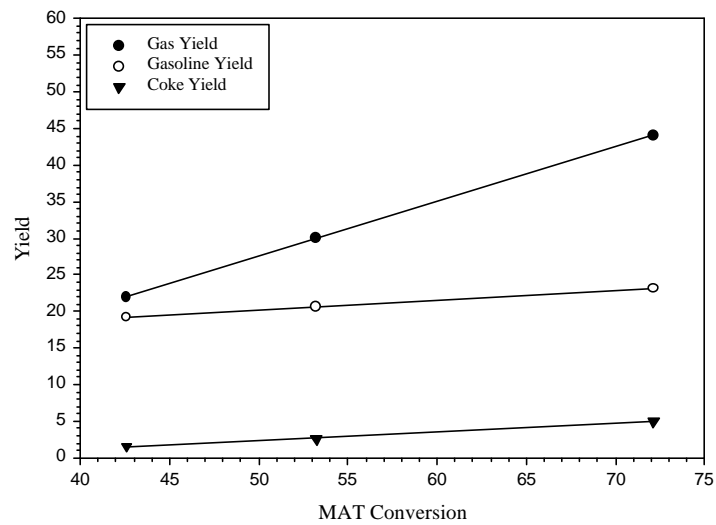
Figure 6.35 Yields of Gas, Gasoline and Coke as a Function of MAT Conversion; Feed: n-hexadecane, Catalyst: ECat-HIGH; Pretreatment: Calcined at 550 °C.

149
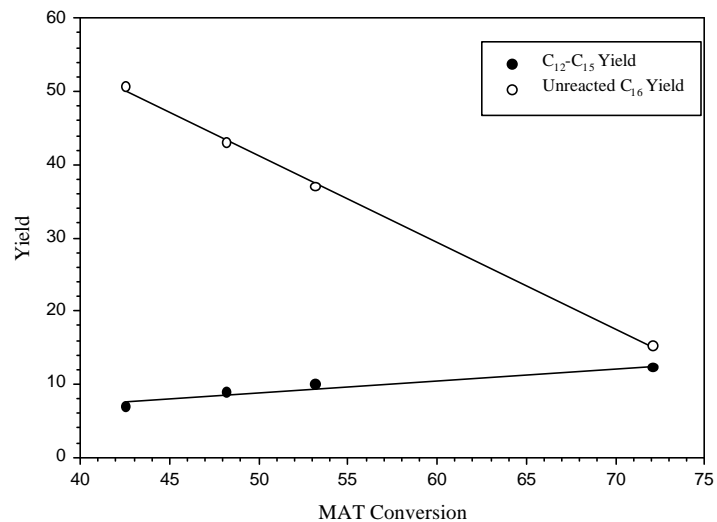
Figure 6.36 Yields of LCO and HCO as a function of MAT conversion; Feed: n-hexadecane, Catalyst: ECat-HIGH; Pretreatment: calcined at 550 °C.
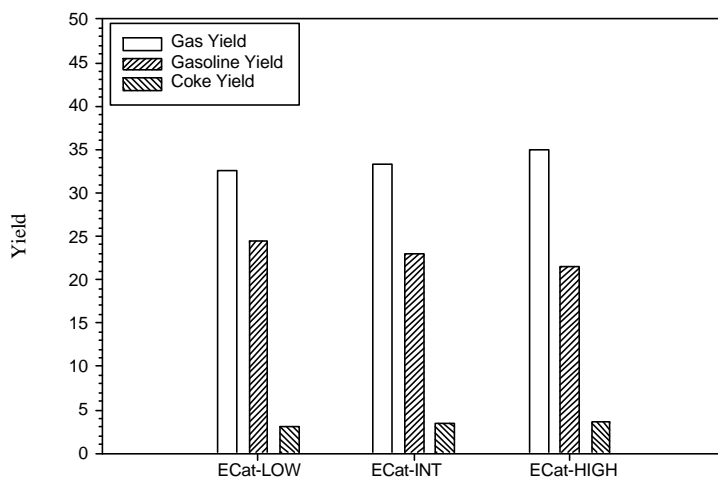
Figure 6.37 Comparison of Yields between Calcined ECat-LOW, ECat-INT, and ECat-HIGH at 60% Conversion of n-hexadecane

150

6.2.2 Pretreatment with Hydrogen or Methane

Figures 6.38 to 6.48 show the effects of pretreatment with hydrogen or methane on the yields of gas, gasoline, coke, C_{12}-C_{15} and unreacted C_{16} for ECat-LOW, ECat-INT and ECat-HIGH. The observations similar to ones made for calcined catalysts were made using pretreated catalysts.

Figure 6.49 compares the yields of gas, gasoline and coke before and after pretreating ECat-LOW at 60 % MAT conversion. We can see the increase in the gasoline yield and decreases in the coke and gas yield with pretreatment. We can see that methane pretreatment has a more pronounced effect on these yields compared to hydrogen pretreatment. These effects of pretreatments on gas, gasoline and coke yields were not observed for ECat-LOW catalysts with SIHGO cracking. Similarly, effects of pretreatment on the gasoline, gas and coke yields for ECat-INT and ECat-HIGH are compared at a constant MAT conversion of 60% in Figures 6.50 and 6.51, respectively. For ECat-INT, while the gasoline yield increased with both pretreatments, gas and coke yields decreased significantly. Effects of both pretreatments on the gasoline, gas and coke yields were quite dominant for ECat-HIGH. The effect of methane pretreatment was found to be more effective for ECat-HIGH compared to the hydrogen pretreatment. The slightly higher coke yield after methane pretreatment can be explained as the deposition of carbon on the metal surfaces contained by the equilibrium catalyst.
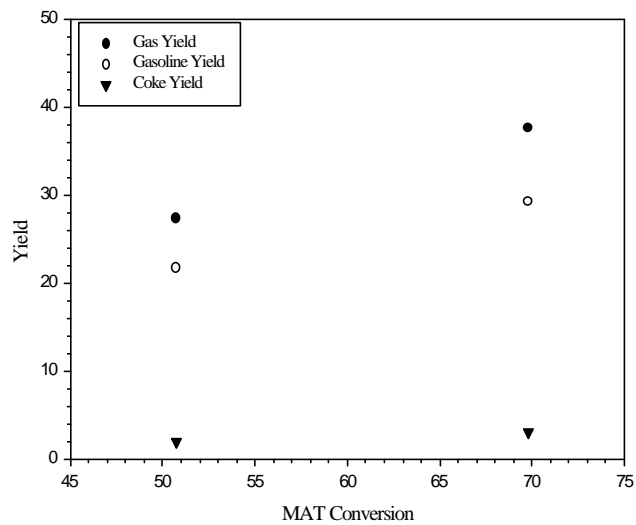
Figure 6.38 Yields of Gas, Gasoline and Coke as a Function of MAT Conversion; Feed: n-hexadecane, Catalyst: ECat-LOW; Pretreatment: 8% H_2/Ar at 700 °C for ~6 Hours.
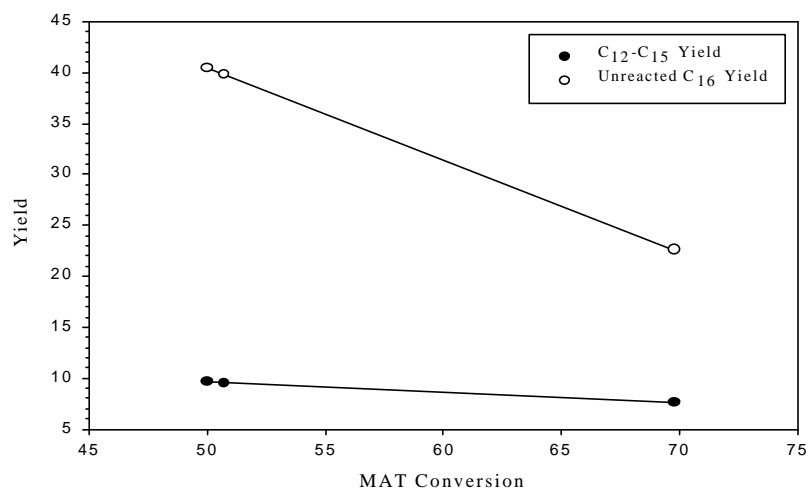
Figure 6.39 Yields of LCO and HCO as a function of MAT conversion; Feed: n-hexadecane, Catalyst: ECat-LOW; Pretreatment: 8% H_2/Ar at 700 °C for ~6 Hours.
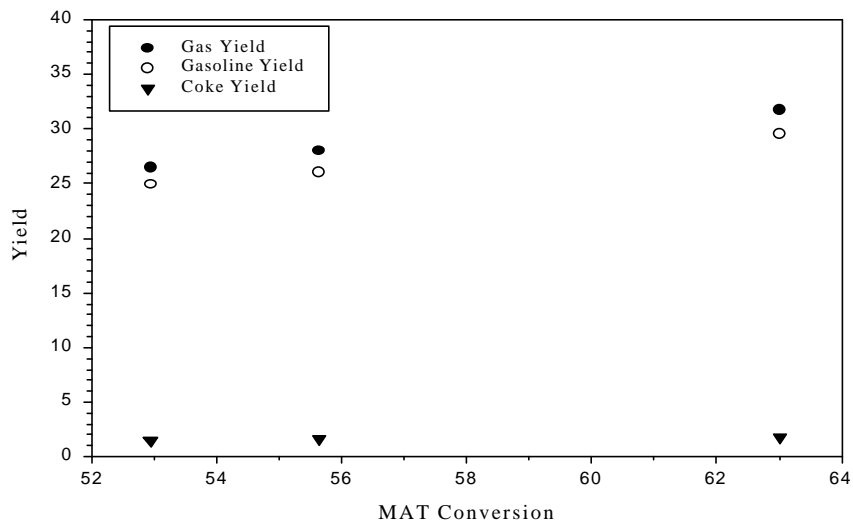
Figure 6.40 Yields of Gas, Gasoline and Coke as a Function of MAT Conversion; Feed: n-hexadecane, Catalyst: ECat-LOW; Pretreatment: 8% CH$_4$/He at 700 °C for ~6 Hours.
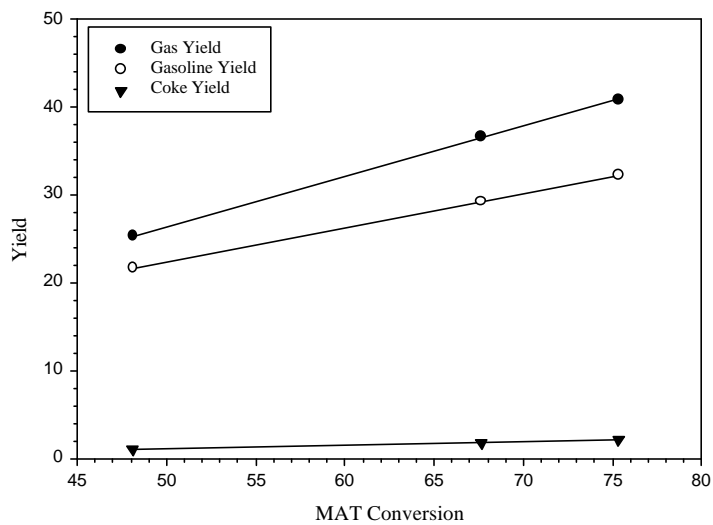
Figure 6.41 Yields of Gas, Gasoline and Coke as a Function of MAT Conversion; Feed: n-hexadecane, Catalyst: ECat-INT; Pretreatment: 8% H$_2$/Ar at 700 °C for ~6 Hours.
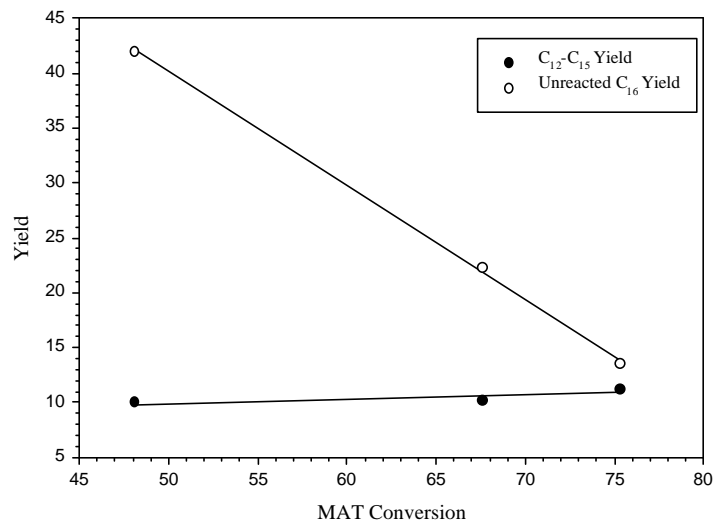
Figure 6.42 Yields of LCO and HCO as a Function of MAT Conversion; Feed: n-hexadecane, Catalyst: ECat-INT; Pretreatment: 8% H₂/Ar at 700 °C for ~6 Hours.
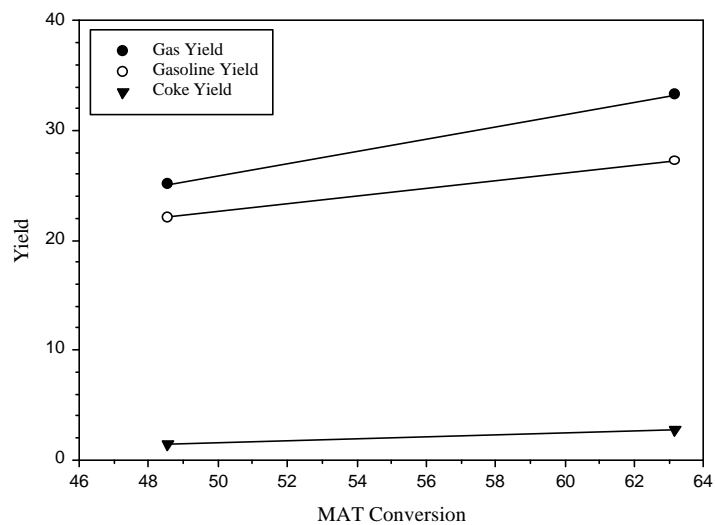
Figure 6.43 Yields of Gas, Gasoline and Coke as a Function of MAT Conversion; Feed: n-hexadecane, Catalyst: ECat-INT; Pretreatment: 8% CH₄/He at 700 °C for ~6 Hours.

154
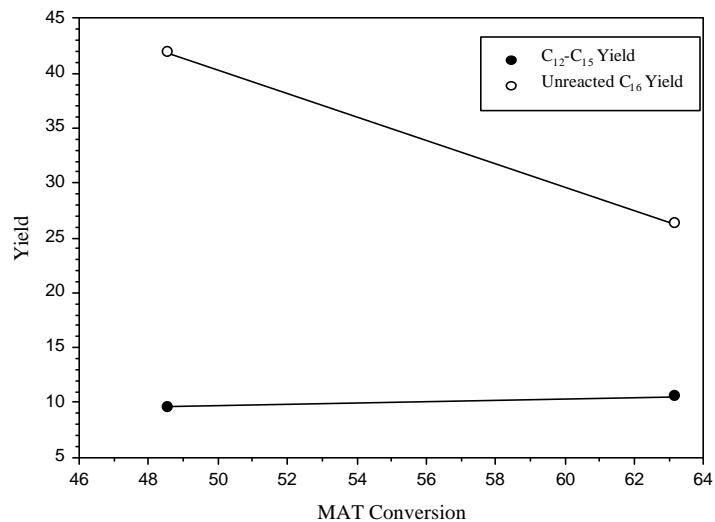
Figure 6.44 Yields of LCO and HCO as a function of MAT conversion; Feed: n-hexadecane, Catalyst: ECat-INT; Pretreatment: 8% CH₄/He at 700 °C for ~6 Hours.
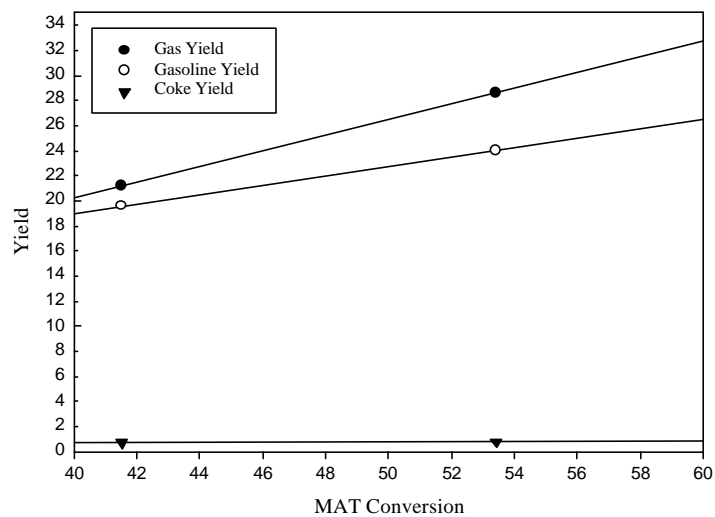
Figure 6.45 Yields of Gas, Gasoline and Coke as a Function of MAT Conversion; Feed: n-hexadecane, Catalyst: ECat-HIGH; Pretreatment: 8% H₂/Ar at 700 °C for ~6 Hours.
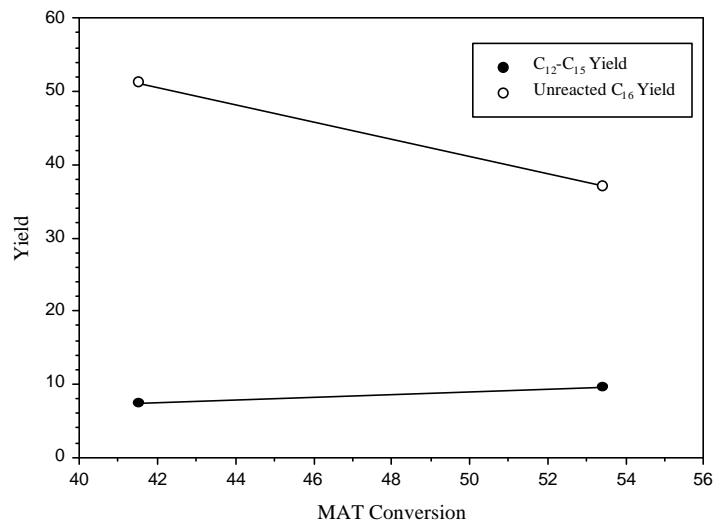
Figure 6.46 Yields of LCO and HCO as a function of MAT conversion; Feed: n-hexadecane, Catalyst: ECat-HIGH; Pretreatment: 8% H$_2$/Ar at 700 °C for ~6 Hours.
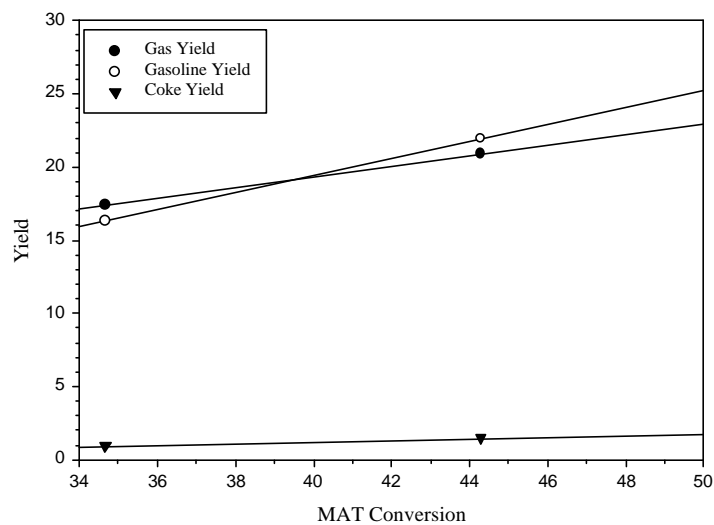
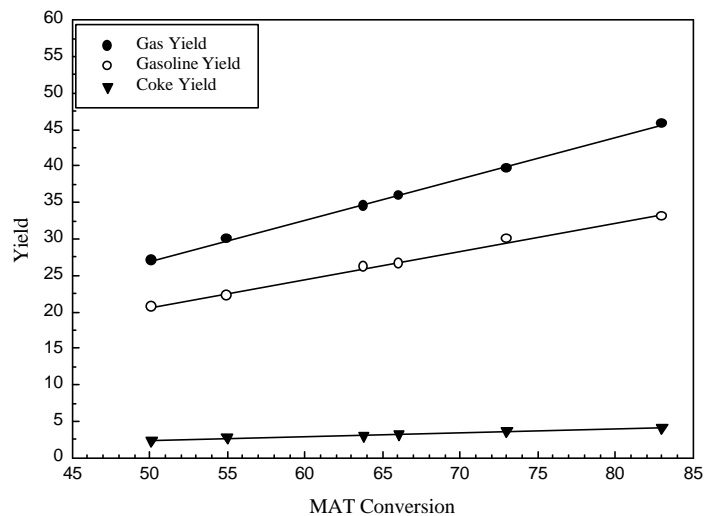**Figure 6.47 Yields of Gas, Gasoline and Coke as a Function of MAT Conversion; Feed: n-hexadecane, Catalyst: ECat-HIGH; Pretreatment: 8% CH$_4$/He at 700 °C for ~6 Hours.**
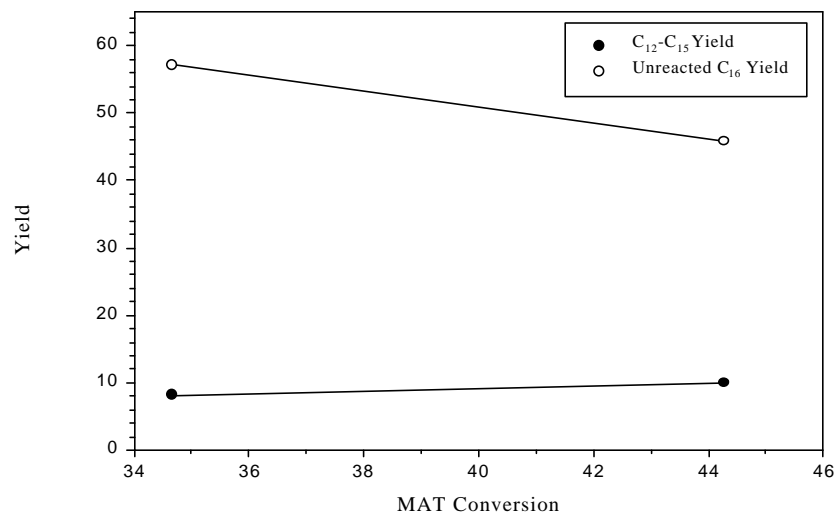
Figure 48 Yields of LCO and HCO as a function of MAT conversion; Feed: n-hexadecane, Catalyst: ECat-HIGH; Pretreatment: 8% CH$_4$/He at 700 °C for ~6 Hours.
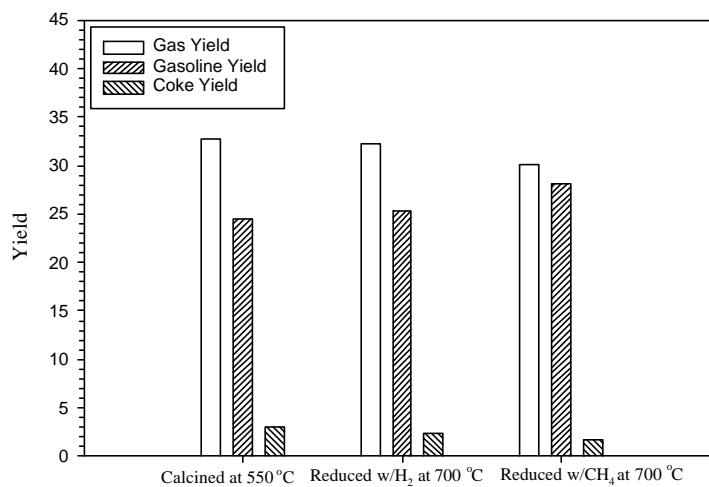
Figure 6.49 Comparison of Yields before and after H$_2$ and CH$_4$ Pretreatment for ECat-LOW at 60% Conversion using n-hexadecane Feed
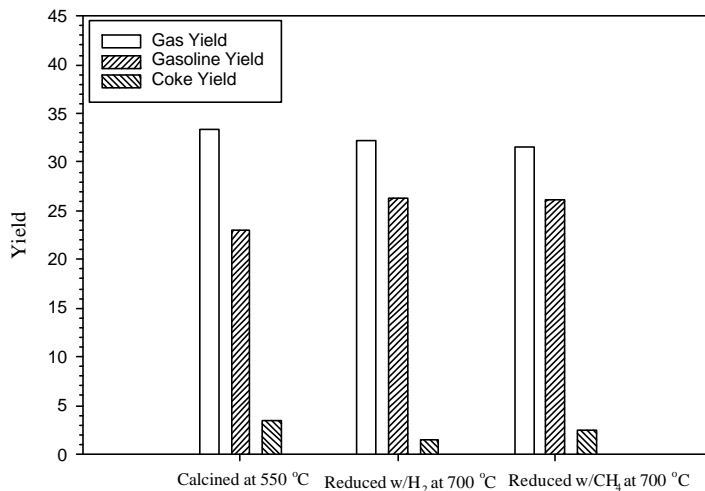
Figure 6.50 Comparison of Yields before and after H$_2$ and CH$_4$ Pretreatment for ECat-INT at 60% Conversion using n-hexadecane Feed
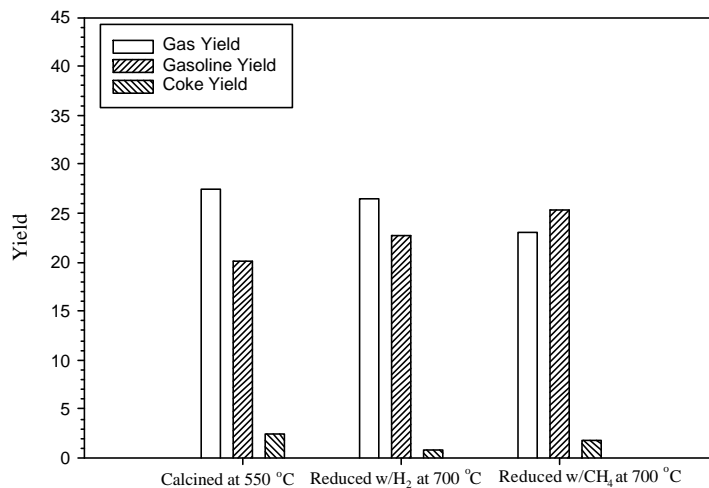
Figure 6.51 Comparison of Yields before and after H$_2$ and CH$_4$ Pretreatment for ECat-HIGH at 60% Conversion using n-hexadecane Feed

So far we have shown that pretreatment with either hydrogen or methane has significant effects on the performances of metal contaminated equilibrium FCC catalysts. These effects on the yields of gas, gasoline and coke have been shown clearly by the results obtained from both SIHGO and n-hexadecane cracking.

Lee and coworkers (1989) studied catalytic cracking in the presence of hydrogen. They found that the effects of hydrogen are quite feed dependent. In general, hydrogen presence during cracking reactions shifted products toward the heavier end, i.e., lower conversion; higher selectivities to gasoline, light cycle oil (LCO) and heavy cycle oil (HCO); and lower coke yield. Their results have shown that the light olefin-to-paraffin ratio significantly increases, while the light iso-paraffin to paraffin ratio slightly increases during the cracking reactions with hydrogen. The improvements in gasoline yield were found to be more significant with a relatively high-metal catalyst than those with a low-metal catalyst. Part of the improvements in performance of metal contaminated catalyst was attributed to metal reduction similar to hydrogen pretreatment.

The improvement of catalyst performance with hydrogen or methane pretreatments can be explained by the oxidation states of metals such as vanadium and nickel on these equilibrium catalysts. Under FCC conditions, nickel is present in either the +2 or zero valance state. It is known that nickel at zero valance state is more active for promoting dehydrogenation reactions causing coke and hydrogen production (Woltermann et al., 1996). In the zero oxidation state, nickel is mobile and agglomerates under reducing conditions found in FCC reactor. Agglomeration reduces the available surface and decreases the dehydrogenation activity of nickel. Nickel in +2 valance state is less likely to agglomerate into large particles and, on a surface like alumina, can embed itself in the alumina structure, forming nickel aluminate. In this case, nickel can stay highly dispersed during many redox cycles. Cadet et al. (1991) have shown that nickel aluminate can also

159

promote dehydrogenation reactions, although its dehydrogenation rate was found to be less than the rate for nickel metal.

Vanadium can also exist in several oxidation states between +3 and +5. However, vanadium does not exist at zero valance state under FCC conditions. It is now known that vanadium has a dehydrogenation activity and this dehydrogenation activity is closely related to its oxidation state (Woltermann et al., 1996; Cheng et al., 1993; Boock et al., 1996; Rudesill et al., 1998). Recently it was found that oxidized vanadium produces more coke and hydrogen compared to reduced vanadium, indicating its high dehydrogenation activity (Boock et al., 1995). In our equilibrium catalysts, vanadium exists at its +5 state in large quantities. Oxidized vanadium produces olefins from paraffins by dehydrogenation reactions while reducing itself into +4 and +3 oxidation states. This explains why we get higher olefins with highly contaminated equilibrium catalyst for both SIHGO and n-hexadecane cracking. This high olefin yield in our results is also reflected by the relatively low C_4 paraffin/C_4 olefin ratios for highly contaminated catalyst (ECat-HIGH) compared to less contaminated catalyst (ECat-LOW). This indicates that the presence of vanadium oxides increases olefin yields. Wallenstein et al. (2000) also reported higher olefin yields for the metallated catalysts. In their study, catalysts were impregnated with vanadium and nickel. Then they were exposed to 30 cycles of oxidizing and reducing atmosphere at 788 °C. The higher olefin yields for metallated catalysts compared to non-metallated catalyst was attributed to the dehydrogenation activity of vanadium and nickel.

As we know, both hydrogen and methane have the ability to reduce vanadium oxides present on the catalysts. Once the vanadium oxides are reduced during the catalyst pretreatment procedure, their catalytic activity to promote dehydrogenation reactions to form olefin from

paraffins decreases significantly. This is confirmed by the relatively high C_4 paraffin/C_4 olefin ratios after catalyst pretreatment with hydrogen or methane.

6.3 Temperature-Programmed Reduction (TPR) Analysis

The detailed information on the characterization of metal contaminated equilibrium catalysts by using TPR analysis is given in section 4.0. Here, only the TPR spectra of highly contaminated equilibrium catalyst, ECat-HIGH, before and after ex-situ hydrogen pre-treatment are presented to understand the effect of pretreatment on the observed catalyst activity.

Figure 6.52a-b shows the comparison of TPR spectra between calcined ECat-HIGH (Figure 6.52a) and ECat-HIGH after being pretreated with hydrogen at 500 °C (Figure 6.52b). As seen from these spectra, at 500 °C most of the metal oxides on the catalyst represented by the first peak around 520 °C are reduced. Our activity measurements have shown that there was no significant effect of pretreatment with hydrogen at 500 °C on the activity of ECat-HIGH.

Figure 6.53a-b compares the TPR spectra between calcined ECat-HIGH (Figure 6.53a) and ECat-HIGH after being pretreated with hydrogen at 700 °C (Figure 6.53b). In addition to the metal oxides represented by the first peak, metal oxides represented by the conjunction of the two peaks in the TPR spectrum are also reduced. Since the catalyst pretreated with hydrogen at 700 °C has shown improvement in its activity, the metal oxides reduced at this temperature must be the ones highly active for the dehydrogenation reactions. This also explains why the several U.S. patents suggest pretreatment temperatures above 650 °C, not 500 °C.
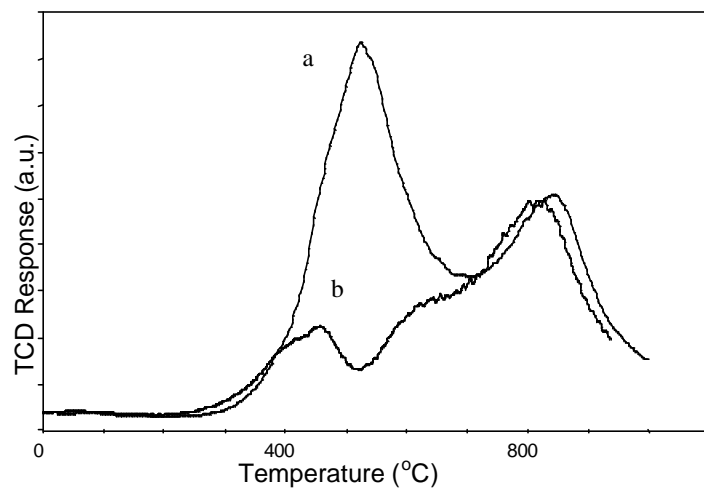
Figure 6.52 Comparison of TPR Spectra of ECat-HIGH: (a) Calcined; (b) Reduced with Hydrogen at 500 °C
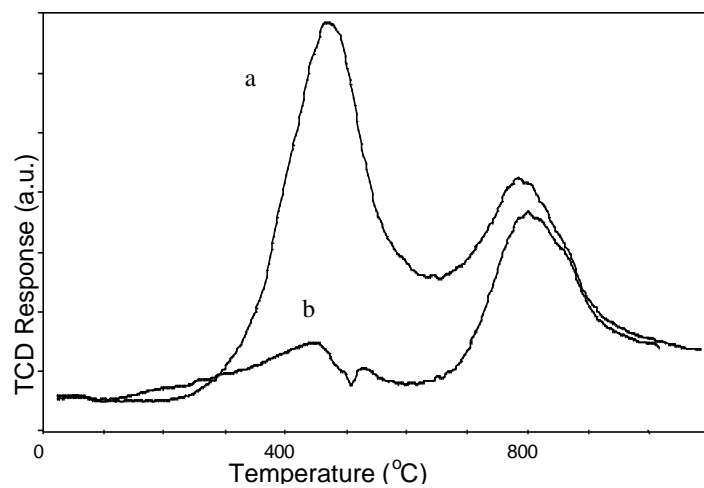
Figure 6.53 Comparison of TPR Spectra of ECat-HIGH: (a) Calcined; (b) Reduced with Hydrogen at 700 °C

6.4 Conclusions

The pretreatment with hydrogen or methane has significant effects on the performance of metal-contaminated equilibrium FCC catalysts. The yields of hydrogen and coke decrease after pretreatments while the gasoline yield increases. The improvement with pretreatment is found to be more significant with highly contaminated equilibrium catalyst. The C4-paraffin-to-C4-olefin ratio, which is a good indicator of hydrogen transfer reactions, decreases with increasing metal concentration on the catalyst. Pretreatment increases the hydrogen transfer reactions. Improved hydrogen transfer reactions cause gasoline range products to increase by terminating carbocations and saturating olefins before they can undergo further cracking. The decrease in hydrogen and coke yields with pretreatment explained by the reduction of the oxidation-state of the vanadium that is present at high levels on the equilibrium catalyst. Reduced vanadium produces less coke and hydrogen compared to oxidized vanadium, indicating a low dehydrogenation activity of reduced vanadium.

7.0 DETERMINATION OF THE COKE LOCATION ON FCC CATALYSTS BY SURFACE AREA MEASUREMENTS

The surface area of a solid catalyst includes the internal surface area associated with pores and the external surface area due to the outer boundary of the particles. The BET (after Brunauer, Emmett, and Teller) method is widely used for surface area determination of a catalyst. In this method, BET surface area is calculated from an adsorption isotherm (Brunauer et al., 1965). An adsorption isotherm is usually recorded as volume of gas adsorbed (cc/g at STP) versus relative pressure (i.e., sample pressure / saturation vapor pressure, P/P_o).

Lippens et al. (1965) determined that the multi-layer adsorption curve for nitrogen at different pressures and constant temperature is identical for a wide variety of adsorbents, providing no capillary condensation occurs. This curve is known as the universal multimolecular adsorption curve or t-curve. The experimental points of this t-curve were found to give good agreement with the isotherm equation of Harkins and Jura (Harkins et al., 1944).

$$t = \left[\frac{13.99}{\log(P_o / P) + 0.34} \right]^{\frac{1}{2}}$$

This equation is used in most applications for calculating t, the thickness of adsorbed gas as a function of nitrogen relative pressure. Lippens et al. (1965) proposed plotting the volumes of nitrogen adsorbed (V) at different P/P_o values as a function of t value from the above equation. For multi-layer adsorption, the experimental points should fall in a straight line and pass through the origin for a non-porous material. For a porous material, the line will have a positive intercept indicating micropores, or deviate from linearity suggesting filling of mesopores. For most materials, the linear portion of the curve between $t = 3.5$ to 6 Angstroms is used for determination

of *t*-plot surface area. Since the *t*-plot surface area does not include adsorption in micropores, the *t*-plot surface area measures the surface area of the FCC catalyst matrix.

The BET surface area is based on nitrogen gas adsorbed by the catalyst surface as well as that condensed in the zeolite pores. The BET surface area can be separated into two components. The *t*-plot surface area measures the surface area of the matrix portion of the catalyst. The zeolite area is obtained by subtracting the *t*-plot area from the BET surface area.

In this section we will present our surface area measurements on standard ASTM and commercial equilibrium catalysts before and after cracking reactions. We will explain how these surface area measurements help us to determine the location of coke on the catalysts

7.1 Surface Area Measurements before and after Cracking Reactions

Nitrogen adsorption was measured on both ASTM standard catalyst and equilibrium FCC catalysts both before and after cracking reactions, in order to understand coke deposition on the catalyst. Figure 7.1 shows a typical adsorption/desorption isotherm of calcined ASTM RR3 catalyst. As seen from Figures 7.1, the large uptake of nitrogen at low P/P_o indicates filling of micropores that are less than 20 A^o in diameter. The linear portion of the curve represents multilayer adsorption of nitrogen on the surface of the catalyst, and the concave upward portion of the curve represents filling of mesopores between 20 - 500 A^o and macropores larger than 500 A^o in diameter. The pore size distributions of the mesopores and macropores can be calculated by analysis of the desorption isotherm.

The BET and *t*-plot surface areas for spent and calcined standard catalysts (RR6 and RR3) are shown in Figures 7.2 and 7.3. The spent catalyst samples, S1, S2, S3, and S4, contain 1.98%, 1.94%, 1.86% and 1.50% coke on them respectively. As noted from the error bars, the values from

successive runs are quite in agreement. As seen from these figures, the total surface area decreases after coke deposits on the catalyst, while the matrix surface area remains almost constant. Therefore decrease in the total surface area can be attributed to the decrease of the zeolite surface area which is caused by the coke deposition in the zeolite pores.

Comparisons of pore volumes in the size range of 20-1000 A^o between calcined and spent standard catalysts are given in Tables 7.1.This size range covers all the mesopores (20-500 A^o) and part of the macropores (500-1000 A^o). As mentioned before, the nitrogen adsorption data for the macropores are not accurate enough to draw any conclusion. We focus only on the pore volume distributions in the mesopore range.
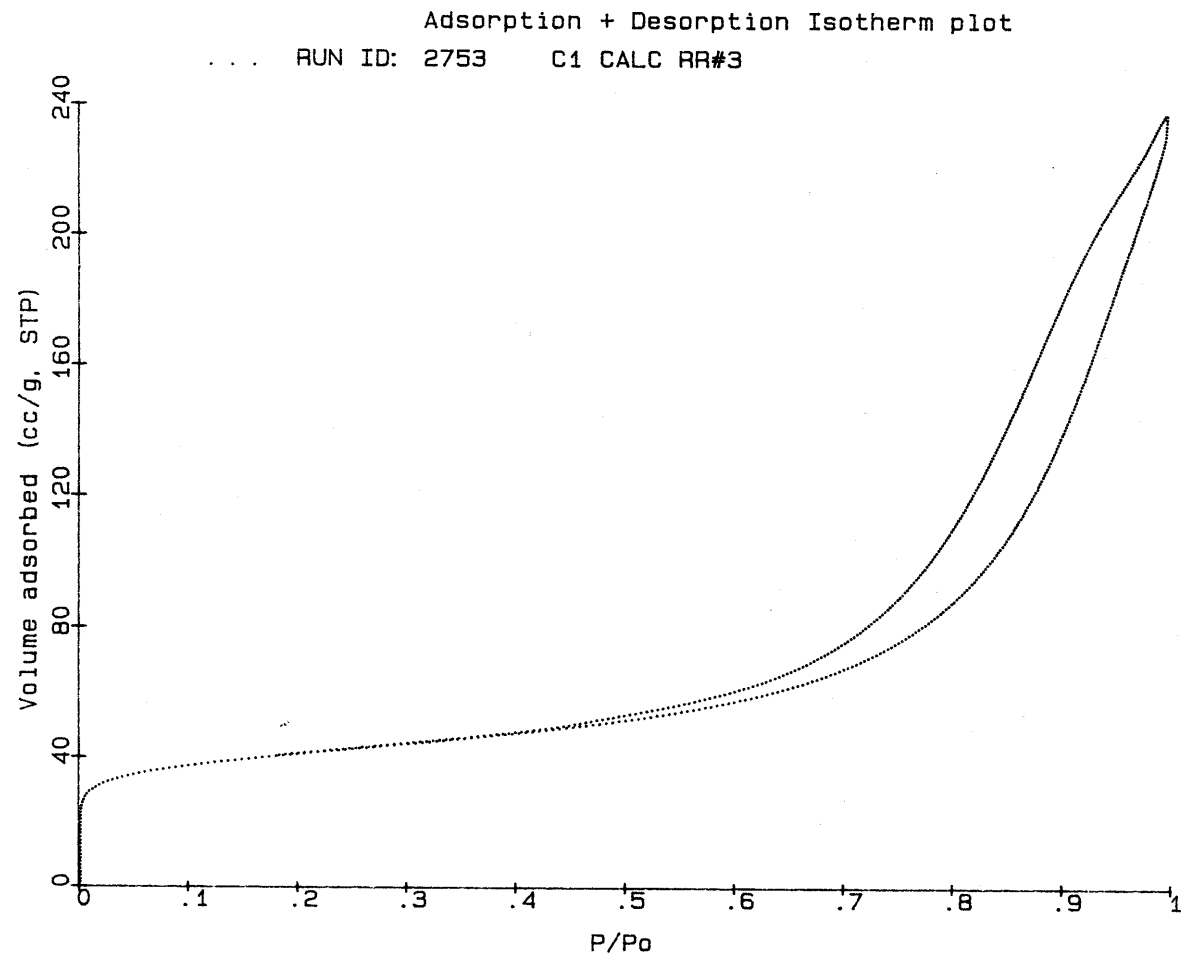
Figure 7.1 Adsorption/Desorption Isotherm of Calcined ASTM Standard RR3 Catalyst

167
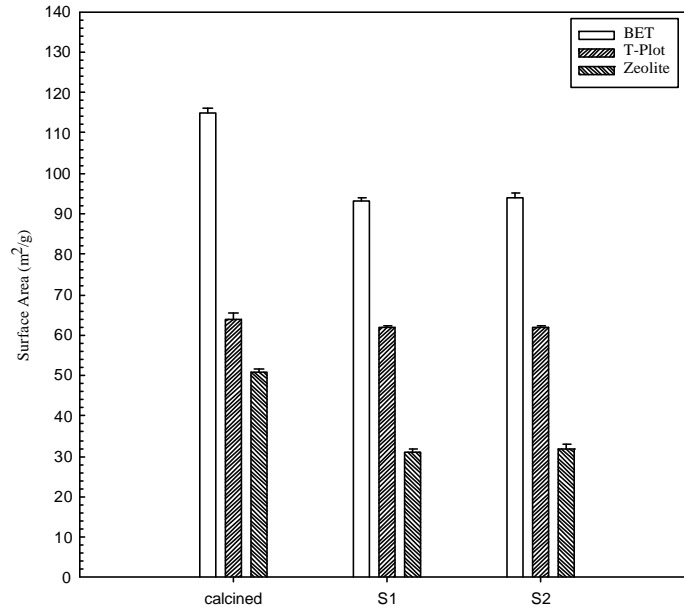
Figure 7.2 Comparisons of Surface Areas between Calcined and Spent (S1 and S2) ASTM Standard RR6 Catalysts
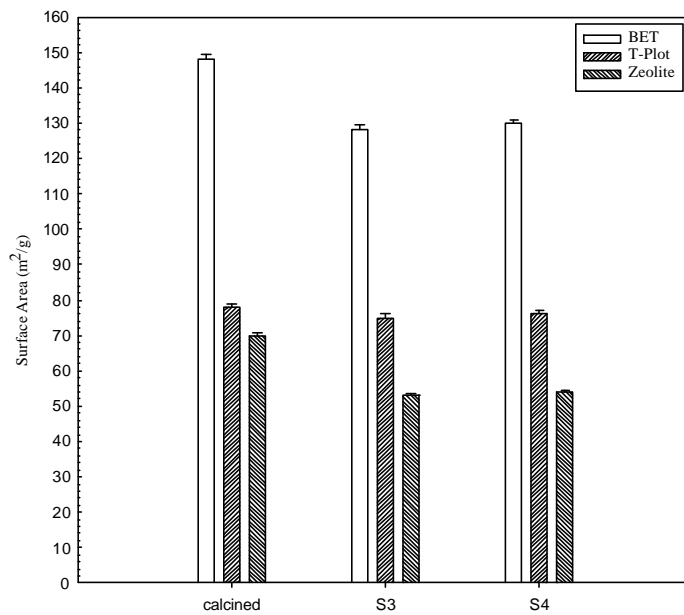
Figure 7.3 Comparisons of Surface Areas between Calcined and Spent (S3 and S4) ASTM Standard RR3 Catalysts

Table 7.1 Comparisons of Pore Volumes between Spent and Calcined ASTM Standard Catalysts (RR6 and RR3)

Sample I.D.		Pore Diameter (A^o)			
		20-100	100-300	300-600	600-1000
Sample 1 (RR6)	Spent	0.0747	0.1709	0.0237	0.0079
	Calcined	0.0806	0.1734	0.0255	0.0080
	V_s/V_c	0.93	0.99	0.93	0.99
Sample 2 (RR6)	Spent	0.0808	0.1674	0.0232	0.0089
	Calcined	0.0839	0.1750	0.0246	0.0087
	V_s/V_c	0.96	0.96	0.94	1.02
Sample 3 (RR6)	Spent	0.0859	0.1692	0.0238	0.0075
	Calcined	0.0888	0.1720	0.0241	0.0081
	V_s/V_c	0.97	0.98	0.99	0.93
Sample 4 (RR6)	Spent	0.0865	0.1647	0.0231	0.0075
	Calcined	0.0837	0.1763	0.0246	0.0098
	V_s/V_c	1.03	0.93	0.94	0.77
Sample 5 (RR3)	Spent	0.0880	0.1881	0.0324	0.0123
	Calcined	0.0914	0.1977	0.0351	0.0131
	V_s/V_c	0.96	0.95	0.92	0.94
Sample 6 (RR3)	Spent	0.0954	0.1880	0.0316	0.0112
	Calcined	0.1001	0.1959	0.0334	0.0103
	V_s/V_c	0.95	0.96	0.95	1.09

V_s/V_c: Ratio of pore volume of spent catalyst to that of calcined catalyst

In Table 7.1, pore volumes and the ratio of pore volumes (V_s/V_c) are tabulated for each set of experiments. The value of this ratio approaching 1 indicates that the mesopore volumes of spent and calcined catalysts are almost the same. From this we can conclude that coke does not form large deposits in mesopores of the catalyst during the cracking reactions. However, the consistently smaller pore volumes for the spent catalyst shown that same coke deposits in the catalyst mesopores. Data in Figures 7.2 and 7.3 show that zeolite surface area decreases with coke deposition while matrix surface area represented by *t*-plot remains constant. This indicates significant coke deposition in the micropores.

Table 7.2 shows the micropore volumes of calcined and spent ASTM standard catalysts obtained from *t*-plot analysis.

Table 7.2 Summary of Average Micropore Volumes and Coke Contents for Calcined and Spent ASTM Standard RR6 and RR3 Catalysts

Sample	Type	Coke%	Volume (avg)	V_R	V_A	$\theta = V_R/V_A$
S1 Spent	RR6	1.98	0.01352	8.25×10^{-3}	8.24×10^{-3}	1.001
S1 Calcined	RR6	0.00	0.02176			
S2 Spent	RR6	1.94	0.01380	8.08×10^{-3}	7.99×10^{-3}	1.011
S2 Calcined	RR6	0.00	0.02179			
S3 Spent	RR3	1.86	0.02306	7.75×10^{-3}	6.71×10^{-3}	1.154
S3 Calcined	RR3	0.00	0.02977			
S4 Spent	RR3	1.50	0.02293	6.25×10^{-3}	6.57×10^{-3}	0.951
S4 Calcined	RR3	0.00	0.02950			
RR6 #5 Spent	RR6	1.65	0.01166	6.88×10^{-3}	7.54×10^{-3}	0.912
RR6 #5 Calcined	RR6	0.00	0.01920			
RR6 #6 Spent	RR6	1.72	0.01133	7.17×10^{-3}	7.63×10^{-3}	0.940
RR6 #6 Calcined	RR6	0.00	0.01896			

V_R: real volume occupied by coke; V_A: volume made inaccessible to the nitrogen due to coke laydown

Each micropore volume given in Table 7.2 is the average of three data points calculated using *t*-plot analysis. The difference between the volumes for calcined and spent catalyst gives the value of V_A, the pore volume made inaccessible to the nitrogen due to coke laydown. V_R, the volume really occupied by coke is given by the ratio of mass of coke deposited per gram of catalyst to the density of coke. The density of coke is assumed to be 2.25 g/cm^3, the same as graphite. The comparison between V_A and V_R allows us to determine whether there is a blockage of pores by coke or not. If V_R/V_A is around 1, all of the coke is located in micropores without any pore blockage; if V_R/V_A is significantly less than 1, pores are blocked; If V_R/V_A is significantly greater than 1, coke is located in micropores and in larger pores also. As seen from Table 7.2 this value is around 1. Therefore we can conclude that nearly all of the coke is located in micropores without any blockage of pores.

Figure 7.4 shows the change of BET surface areas of equilibrium catalysts with respect to coke content. In this graph each trend line represents the data obtained for a catalyst with different metal level. We can see that BET surface areas of calcined equilibrium catalyst decrease with

increasing metals level. BET surface areas for calcined ECat-LOW, ECat-INT and ECat-HIGH were measured as 178, 160, and 115 m^2/g, respectively. This decrease in total surface area explains the low activities caused by the age and the high metals level of equilibrium catalysts. As seen in Figure 7.5, The BET surface areas of each equilibrium catalyst always decrease with increasing coke amounts.

Figures 7.5-7.7 show that the matrix surface area of each equilibrium catalyst does not change with increasing coke content on the catalyst. The decrease in total surface area with increasing coke content can only be explained by the decrease in zeolite surface area due to the coke deposition in the micropores of catalyst.

As seen from Figure 7.8, micropore volume decreases with increasing coke content due to the coke deposits in the micropores of catalyst. The V_R/V_A ratios given in Table 7.3 were found to be around 1. if the value of this ratio approaches 1 the pores are not blocked by coke deposits on the catalyst. Besides for the zeolite with three-dimensional micropore structures as in our case, pore blockage by coke is not as effective as in the case of zeolite with one-dimensional pore structures.
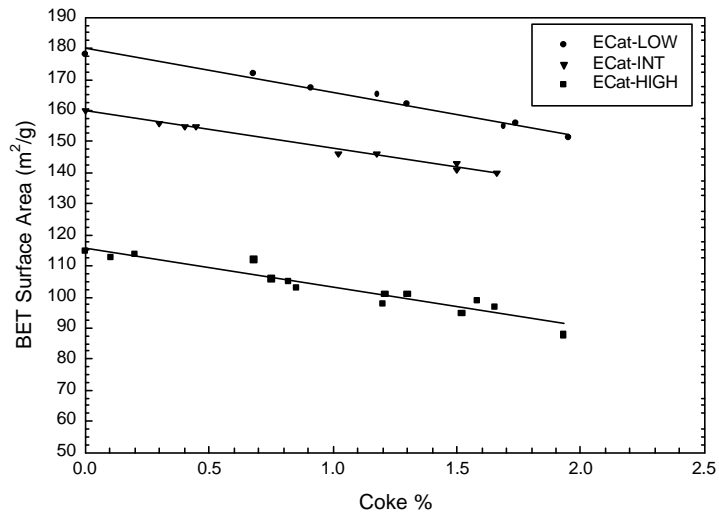
Figure 7.4 Changes in BET Surface Area with Coke Contents of Spent Equilibrium Catalysts
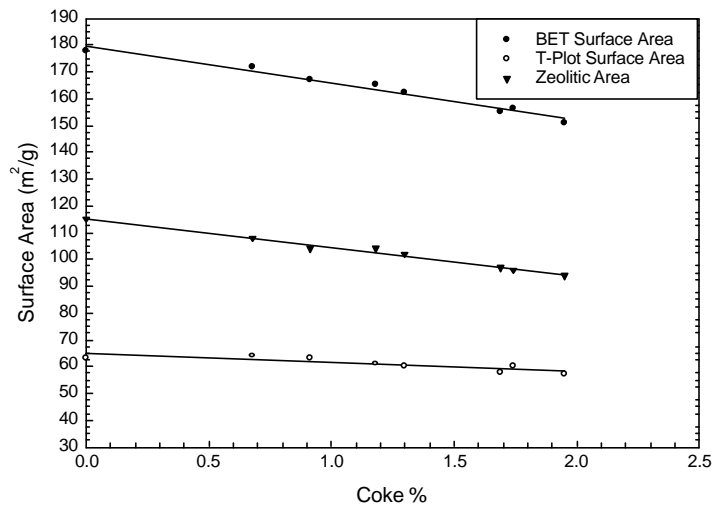
Figure 7.5 Changes in Surface Areas with Coke Contents of Spent Equilibrium catalyst (ECat-LOW)

172
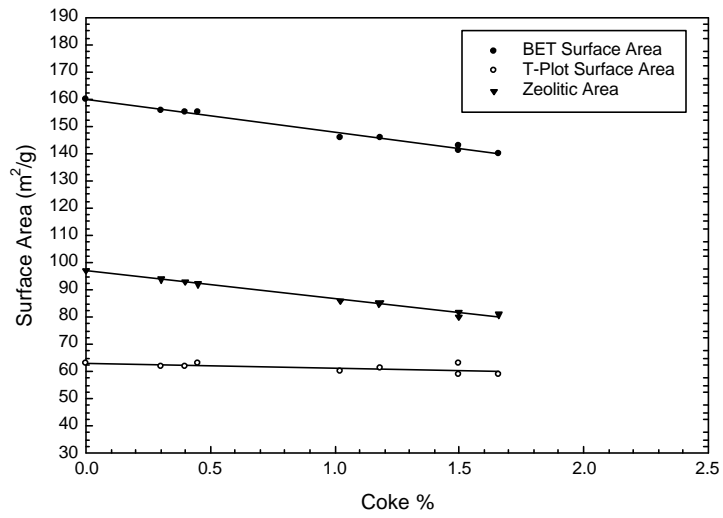
Figure 7.6 Changes in Surface Areas with Coke Contents of Spent Equilibrium Catalyst (ECat-INT)
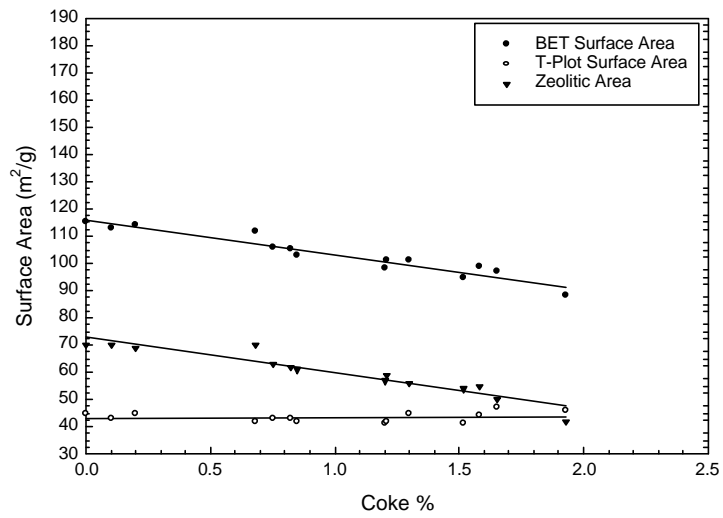
Figure 7.7 Changes in Surface Areas with Coke Contents of Spent Equilibrium Catalyst (ECat-HIGH)
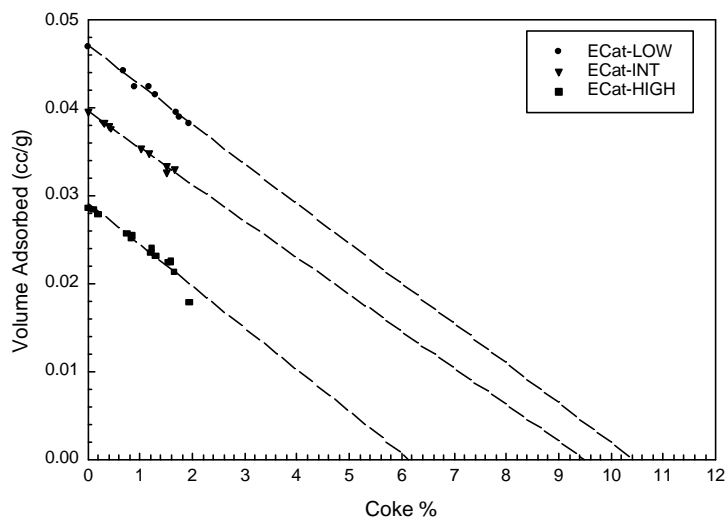
Figure 7.8 Changes in MicroporeVolumes with Coke Contents of Spent Equilibrium Catalysts

Table 7.3 Summary of Average Pore Volumes and Coke Contents for Calcined and Spent Equilibrium Catalysts

Type	Catalyst	Coke%	Volume (avg)	V_R	V_A	$\theta = V_R/V_A$
Spent	ECat-HIGH	1.30	0.02315	5.42×10^{-3}	5.54×10^{-3}	0.978
	ECat-HIGH	1.58	0.02254	6.58×10^{-3}	6.15×10^{-3}	1.070
	ECat-HIGH	1.65	0.02293	6.88×10^{-3}	7.29×10^{-3}	0.944
	ECat-HIGH	0.75	0.02573	3.13×10^{-3}	2.96×10^{-3}	1.055
	ECat-HIGH	1.20	0.02358	5.00×10^{-3}	5.11×10^{-3}	0.978
	ECat-HIGH	0.82	0.02525	3.42×10^{-3}	3.44×10^{-3}	0.994
Calcined	ECat-HIGH	0.00	0.02869	-----	-----	-----
Spent	ECat-INT	1.02	0.03538	4.25×10^{-3}	4.20×10^{-3}	1.012
	ECat-INT	1.66	0.03308	6.92×10^{-3}	6.50×10^{-3}	1.064
	ECat-INT	0.40	0.03795	1.67×10^{-3}	1.63×10^{-3}	1.022
	ECat-INT	0.30	0.03834	1.25×10^{-3}	1.24×10^{-3}	1.008
Calcined	ECat-INT	0.00	0.03958	-----	-----	-----
Spent	ECat-LOW	1.30	0.04158	5.42×10^{-3}	5.45×10^{-3}	0.994
	ECat-LOW	0.68	0.04418	2.84×10^{-3}	2.85×10^{-3}	0.996
	ECat-LOW	1.92	0.03893	8.00×10^{-3}	8.10×10^{-3}	0.988
Calcined	ECat-LOW	0.00	0.04703	-----	-----	-----

V_R: real volume occupied by coke; V_A: volume made inaccessible to the nitrogen due to coke laydown

174

If the coke filled all the micropores of the catalysts the maximum amount of coke would be 10.4, 9.5, and 6.1 % for ECatLOW, ECatINT, and ECat-HIGH respectively. These values were obtained by extrapolating the data in Figure 7.10 to zero pore volume. Previously Guisnet et al. (1989) made this type of plot in the literature. The corresponding calculated densities of coke in the pores of these catalysts would be 2.21, 2.40, and 2.13 g/cm^3. These values are in good agreement with the assumption of coke density to be 2.25 g/cm^3 used to establish Table 7.2 and 7.3.

Table 7.4 compares the pore volumes (20-1000 A^o size range) of calcined and spent equilibrium catalysts using V_s/V_c ratio. If the value of V_s/V_c ratio approaches 1 this means that mesopore volumes of spent and calcined catalysts are almost the same. As in the case of ASTM standard catalyst, the coke does not form large deposits in mesopores of equilibrium catalyst during the cracking reactions.

Table 7.4 Comparisons of Pore Volumes between Spent and Calcined Equilibrium Catalysts

Samples I.D.			Pore Diameter (A^o)			
			20-100	100-300	300-600	600-1000
Sample 1	ECat-LOW	Spent	0.0808	0.0399	0.0251	0.0128
		Calcined	0.0894	0.0395	0.0224	0.0096
		V_s/V_c	0.90	1.01	1.12	1.33
Sample 2	ECat-INT	Spent	0.0670	0.0741	0.0378	0.0139
		Calcined	0.0764	0.0776	0.0433	0.0258
		V_s/V_c	0.88	0.95	0.87	0.54
Sample 3	ECat-HIGH	Spent	0.0564	0.0542	0.0293	0.0122
		Calcined	0.0628	0.0559	0.0326	0.0133
		V_s/V_c	0.90	0.97	0.90	0.92
Sample 4	ECat-HIGH	Spent	0.0542	0.0503	0.0298	0.0178
		Calcined	0.0562	0.0508	0.0292	0.0181
		V_s/V_c	0.96	0.99	1.02	0.98
Sample 5	ECat-HIGH	Spent	0.0572	0.0542	0.0313	0.0150
		Calcined	0.0628	0.0559	0.0326	0.0133
		V_s/V_c	0.91	0.97	0.96	1.13
Sample 6	ECat-HIGH	Spent	0.0561	0.0553	0.0356	0.0201
		Calcined	0.0628	0.0559	0.0326	0.0133
		V_s/V_c	0.89	0.99	1.09	1.51
Sample 7	ECat-HIGH	Spent	0.0585	0.0559	0.0384	0.0210
		Calcined	0.0628	0.0559	0.0326	0.0133
		V_s/V_c	0.93	1.00	1.18	1.58

V_s/V_c: Ratio of pore volume of spent catalyst to that of calcined catalyst

7.2 Conclusions

The BET and *t*-plot surface area measurements before and after cracking reactions identified the location of coke on spent catalyst. Surface area measurements indicated that the coke formed during cracking reactions preferentially deposits in the micropores of the catalyst without blocking the larger pores of catalyst.

8.0 VISUALIZATION OF FCC CATALYST SURFACE BY ATOMIC FORCE MICROSCOPY (AFM)

A common problem in petroleum refining is catalyst deactivation due to deposition of metal contaminants (e.g., nickel, vanadium and iron) on the catalyst from the hydrocarbon feed. Catalyst activity decreases as the production of coke and hydrogen increase at the expense of gasoline.

Presence of metal contaminants on the FCC catalyst has been widely studied by using microscopic and elemental imaging techniques such as scanning electron microscopy (SEM) (Beyerlein et al., 1993), and secondary ion mass spectrometry (SIMS) (Kugler et al., 1988; Jaras, 1982). These results have shown that vanadium is mobile and accumulates throughout the catalyst particles with a preference for rare earth exchanged Y-zeolite. On the other hand, nickel and iron tend to remain fixed at the catalyst particle surface where they are deposited.

Significant effects on catalyst performance are often observed by slightly modifying catalyst composition and structure, especially on the surface. This finding is not surprising since the hydrocarbon feed for cracking reactions first contacts the catalyst surface before it diffuses into the catalyst pores. Assuming that cracking reactions take place mainly on the top 10 - 15 µm of FCC catalyst, techniques for characterizing surface chemical composition and pore structure become extremely important for understanding catalyst performance.

An example of the impact of new instrumental techniques is provided by atomic force microscopy (AFM), a powerful technique that can generate the images of surfaces with atomic resolution. Recently, several studies were conducted to observe the FCC catalyst surfaces using atomic force microscope (AFM) (Occelli et al., 1994; Occelli et al., 2000). In these studies both FCC catalysts artificially contaminated with vandyl naphthenenate and commercial equilibrium

FCC catalysts with metal contaminants have been used. Their AFM images revealed a surface architecture characterized by valleys, ridges, crevices, and slits (Occelli et al., 1994). The papers suggest that vanadium oxides decrease the surface roughness by filling valleys and cracks. In the case of equilibrium FCC catalysts, AFM images have shown that the catalyst surface contains debris. It has been speculated that this debris might be nickel and vanadium oxides (Occelli et al., 2000). However AFM could not bring an undisputable proof of the assignment of the observed debris as nickel and vanadium oxides.

In this work, actual surface images of equilibrium FCC catalyst samples with different metal contamination levels have been obtained to study the details of the surface topography. These images helped us to visualize the surface pores as well as the architecture that surrounds the pore's entrance.

The calcined equilibrium FCC catalysts were labeled ECat-LOW, ECat-INT, and ECat-HIGH having 1000ppm, 2600ppm and 9300 ppm total metal contaminants (nickel and vanadium) respectively.

Figures 8.1 to 8.3 show the surface characteristics for typical regions in the form of 2-D images for ECat-LOW, ECat-INT, and ECat-HIGH respectively. As seen in Figures 8.1 to 8.3, the area analyses of these surfaces were carried out to evaluate the r.m.s. and average roughness on the AFM scans of the surfaces. These results are shown below each corresponding figure. The histogram in these figures shows that the distribution of pixel heights over the surface. The bearing ratio indicates the percentage of all pixels on the image that have heights greater than a particular value chosen from the x-axis of bearing ratio graph (see Figure 8.1).
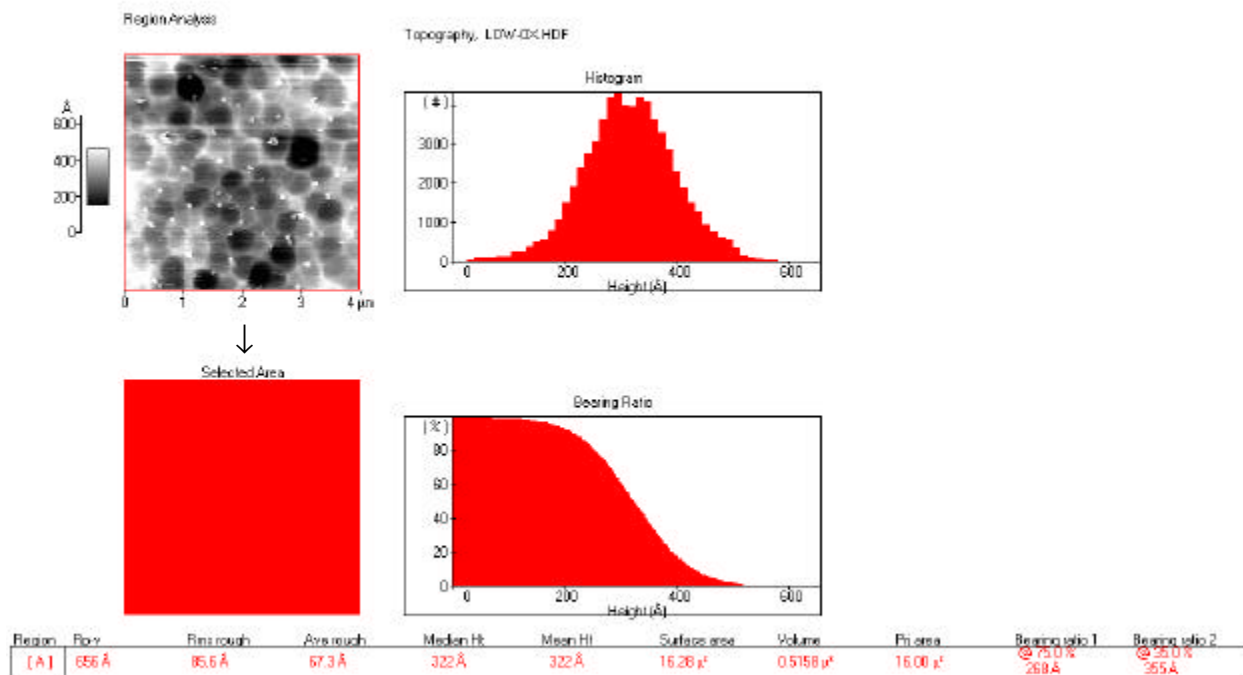
Figure 8.1 Topological Histogram of Calcined ECat-LOW
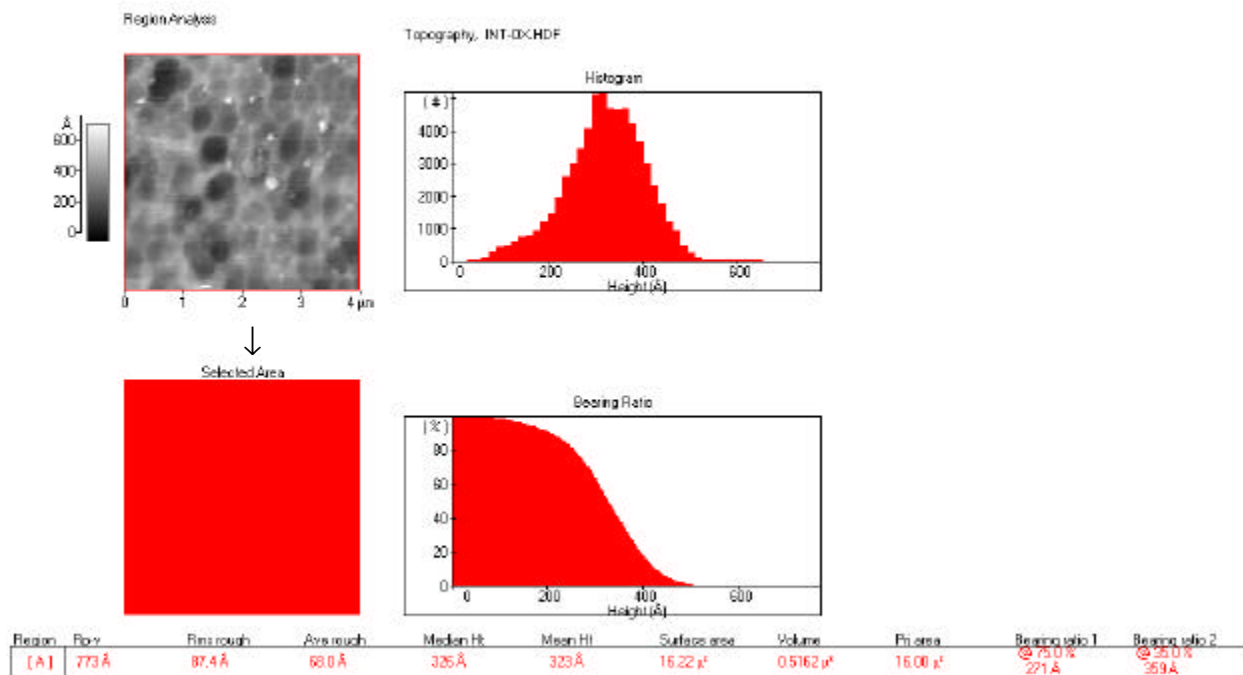
Figure 8.2 Topological Histogram of Calcined ECat-INT
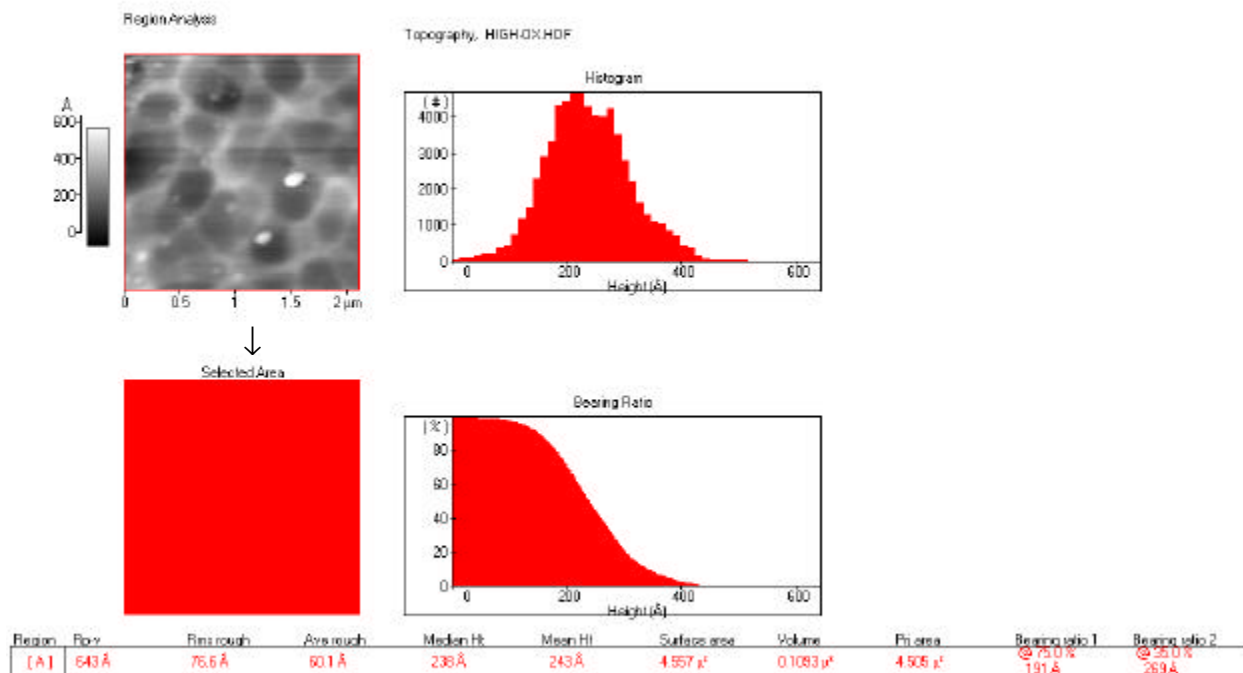
Figure 8.3 Topological Histogram of Calcined ECat-HIGH

The observed r.m.s. roughness values have shown that the catalysts surfaces are quite rough as expected. In all cases the histograms are seen to be very close to Gaussian about the mean heights of 300, 300, and 210 A° for ECat-LOW, ECat-INT, and ECat-HIGH respectively.

If we look at the 2-D surface images given in Figures 8.1-8.3, we can clearly see the surface pores and the features around these pores on the catalyst surface. Large pores can enhance the surface retention of gas oil during cracking and feed FCC interior where cracking takes place. In our case, pore mouth diameter slightly decreases with increasing metal levels, but it does not seem to be very significant. In all of these images, the catalyst surface contains debris that appears as a bright spot in the images. As mentioned earlier, others have also made similar observations.

Another interesting observation made was the number of this debris and their organization on the catalyst surface. For ECat-LOW, this debris seems to be very small in size (0.1 μm) and it is distributed almost homogeneously in a wide surface range. For ECat-INT and ECat-HIGH, the size of this debris is larger than that of ECat-LOW and it is randomly distributed on the catalyst surface. The metal concentration on the catalyst gives an idea about the age of catalyst. The higher the metal concentration the older the catalyst is. In this case metal concentration indicates that ECat-HIGH is the oldest of all. The increasing size of this debris shows that debris has a tendency to agglomerate randomly as catalyst ages. The number of this debris becomes smaller with increasing catalyst age.

Figures 8.4-8.6 show the 3-D AFM images for calcined ECat-LOW, ECat-INT, and ECat-HIGH respectively. From these images one can easily see the sizes of these debris and their locations. It seems that the debris is located around the pore entrances. In the case of ECat-HIGH, the surface cracks as seen from Figure 8.6 were observed. These cracks can be attributed to the age of catalyst. Occelli et al. (Occelli et al., 1994) have also observed similar type of cracks and reported the reduction of surface roughness as a result of filling these observed cracks with vanadium oxides.
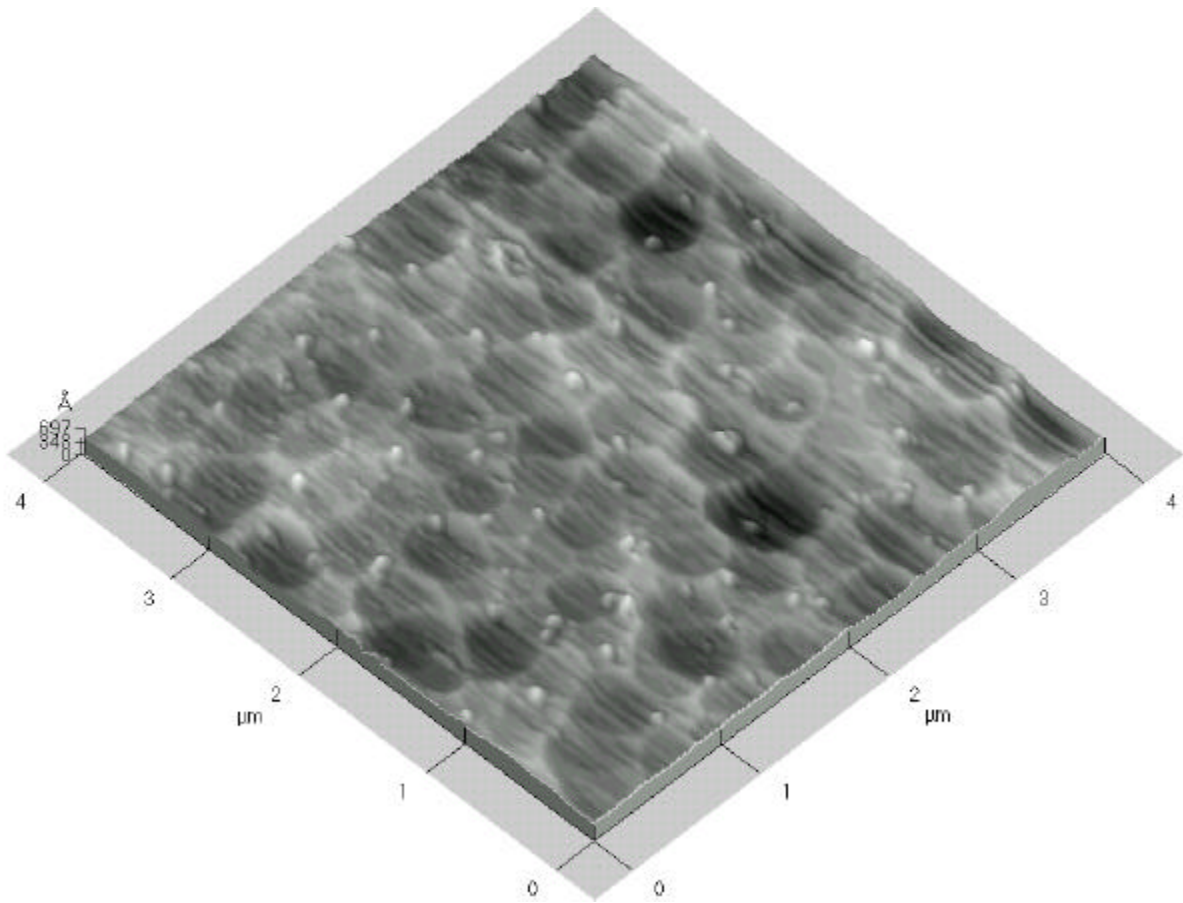
Figure 8.4 3-D AFM Image of the ECat-LOW FCC Catalyst Surface
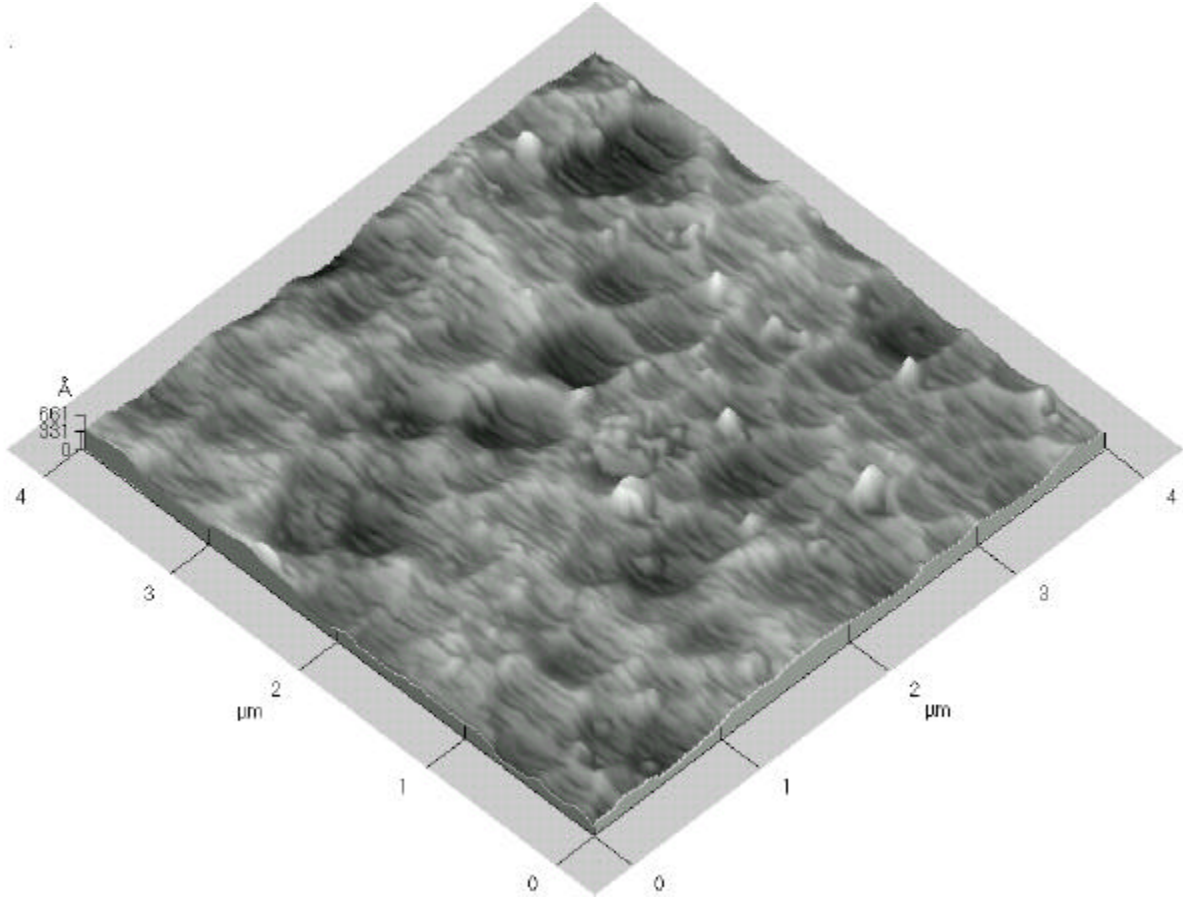
Figure 8.5 3-D AFM Image of the ECat-INT FCC Catalyst Surface
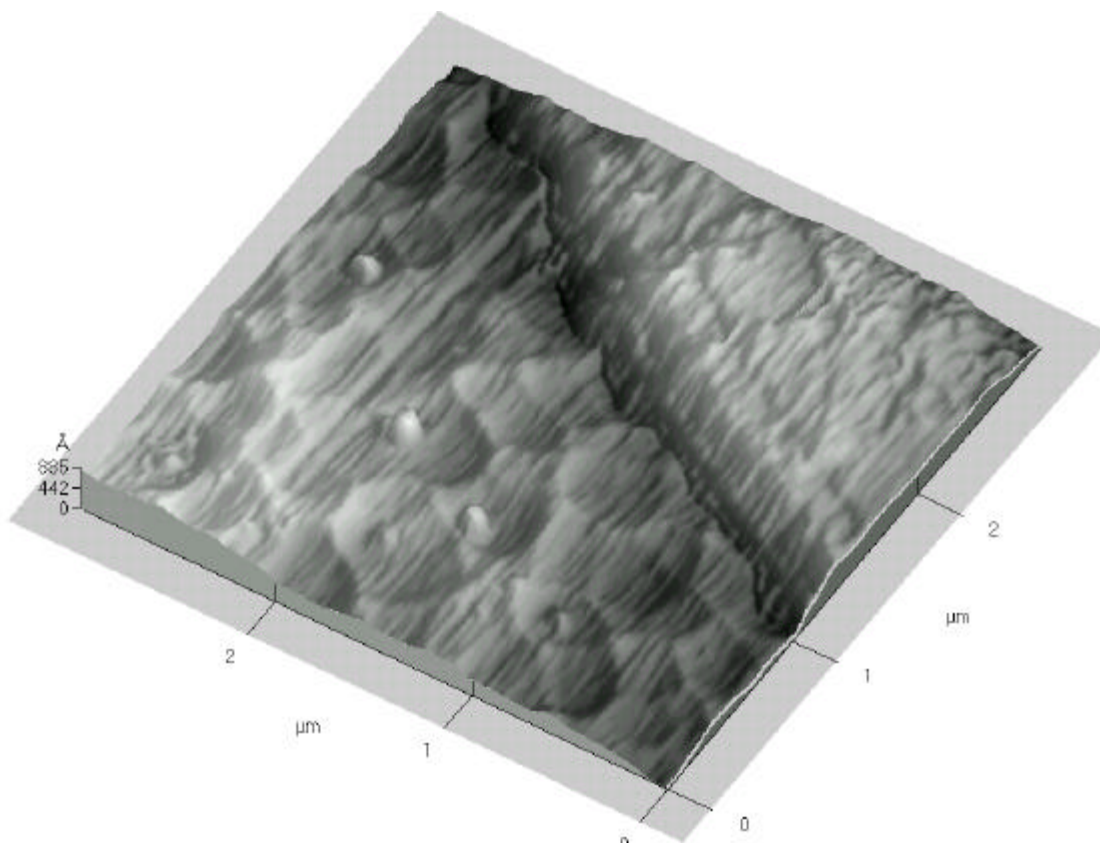
Figure 8.6 3-D AFM Image of the ECat-HIGH FCC Catalyst Surface

Table 8.1 gives information about the metal concentration, surface areas, r.m.s. roughness and microactivity test (MAT) conversions for the FCC catalysts used in this study. As seen from Table 8.1, there is a good correlation between MAT conversions and surface roughness. When metal concentration increases, surface roughness decreases along with MAT conversions. The *t*-plot surface area, which is accepted as the measure of matrix surface area, decreases with decreasing surface roughness. This opens a new perspective for AFM applications in the catalysis studies. The surface structures obtained by AFM can be related to the catalyst performance. These specific structures on the catalyst surface may play an important role for hydrocarbon adsorption and cracking. However, more detailed study by combining several techniques is needed to understand the effects of surface topography on the catalyst performance.

185

Table 8.1. Properties of Equilibrium FCC Catalysts

Catalyst	Metal Concentration (ppm)		Surface Area (m^2/g)		RMS Roughness (A°)	MAT Conversion
	Nickel	Vanadium	BET	t-Plot		
ECat-LOW	300	700	178	63	85.6	71
ECat-INT	900	1700	160	63	87.4	69
ECat-HIGH	2600	6700	115	45	76.6	62

Although AFM provides us with the actual images of the catalyst surfaces, unfortunately it does not give any information on surface chemical composition that may give information on the identity of the above-mentioned debris. To our knowledge, nobody in the literature has identified the nature of the debris observed on the surface of FCC catalyst.

In our case, the surface may contain vanadium, nickel, and iron, which are usually responsible for the deactivation of FCC catalyst. It is crucial to obtain spatially- resolved elemental images of the catalyst surface. This surface chemical composition information combined with AFM images allow us to better interpret the catalyst activity data obtained.

In order to identify elemental composition of this debris, SEM-EDS analysis was performed in the laboratory at National Institute for Occupational Safety and Health (NIOSH). Under the scanning electron microscope, more than 15 locations were marked on the surface of a single catalyst particle whose SEM image is shown in Figure 8.7. During the selection of these locations, bright spots representing higher surface structures on the SEM image were aimed. Then, these locations were analyzed for possible elements. As seen from the typical EDS spectrum in Figure 8.8 these results have shown the presence of Fe at some of these marked locations on the ECat-INT catalyst surface.
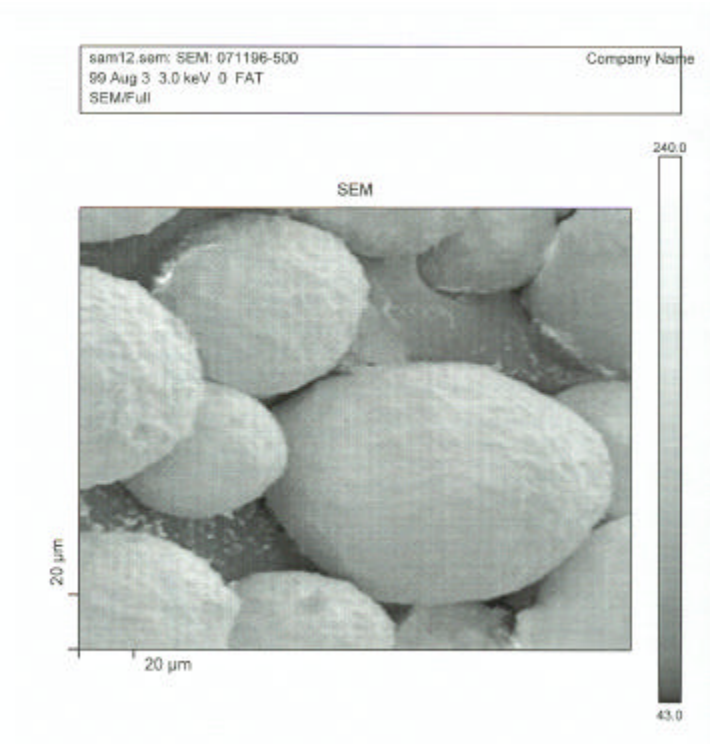
Figure 8.7 SEM Image of ECat-INT FCC Catalyst
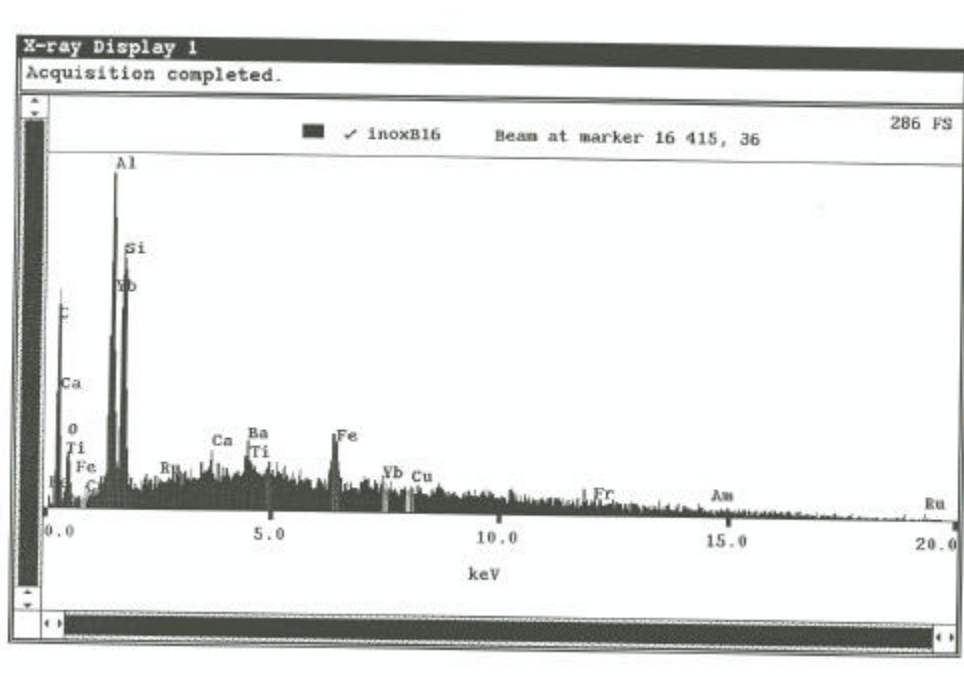
Figure 8.8 X-ray Spectrum at a Certain Marked Location on the Surface of ECat-INT Catalyst Particle

In order to confirm these results we have needed a more sensitive technique. We thought that this task could be achieved by using the Imaging Secondary Ion Spectrometry (SIMS) technique, which is the most sensitive of all the currently available surface analytical techniques. In Imaging SIMS (or Mapping SIMS) analysis the aim is to obtain sufficient signal to provide compositional analysis of the surface layer without actually removing a significant fraction of a monolayer, i.e., to be able to analyze less than 10^{14} atoms/molecules. The technique is then capable of providing compositional information about the topmost atomic layers of the surface. This makes it possible to determine the trace elemental compositions of the catalyst surface and to map the distribution of targeted elements as a function of surface position. The catalyst samples were sent to the Image and Chemical Analysis Laboratory (ICAL) at Montana State University for SIMS and SEM-EDS analyses. The SIMS analysis results have shown the presence of vanadium and iron concentrated at certain locations on the catalyst surface (Figures 8.9 and 8.10). In fact, these findings are consistent with previous investigations. Beyerlin et al. (1993) have also confirmed the presence of high concentrations of Ni and Fe at the periphery of the certain sections of FCC catalyst by using X-ray microscopy along with scanning electron microscopy. Their results have shown that iron, like nickel, also remains fixed at the catalyst particle surface.

Secondary electron image (Figure 8.11), backscatter electron image (Figure 8.12) and x-ray maps were collected from the surface of ECat-HIGH catalyst particle coated with a thin layer of carbon. SEM images were very similar to AFM images. Several spots that varied in composition from the bulk were observed using the backscatter detector, which can detect the variations in density (Figure 8.12). As seen from Figure 8.12, we have observed some particulate of much higher density that contained Sn and Fe. Figure 8.13 shows the X-ray map for Fe, we can see the presence of iron on this particulate (Figure 8.14).

We did not find any indications that small size ball shaped debris was of any different composition from the background, either from the backscattered images or the x-ray maps (see Figures 8.15 and 8.16). It is known that catalyst steaming promotes zeolite debris formation and causes Na repartitioning between the zeolite and matrix phases, increasing Na concentration in the matrix (Lampert et al., 1992; Fleisch et al., 1986). The Al removal from the zeolite lattice is accompanied by Al diffusion through the channel network to the zeolite particle surface. The diffusion of Al to the particle surface takes place only in the presence of steam and migrating species was speculated to be hydroxylated Al ion (Fleisch et al., 1986). This increases the possibility of the presence of alumina debris or clusters on the catalyst surface. However, additional work should be done to determine the elemental composition of the debris on the catalyst surface.

8.1 Conclusions

The surface characteristics (pores as well as the architecture that surrounds the pore's entrance) of equilibrium FCC catalyst samples with different metal contamination levels have been studied using AFM. The roughness of surface decreased with increasing metal concentrations on the catalyst. AFM images have revealed the presence of debris on the catalyst surface. The iron was detected in some these debris using SEM-EDS analysis.
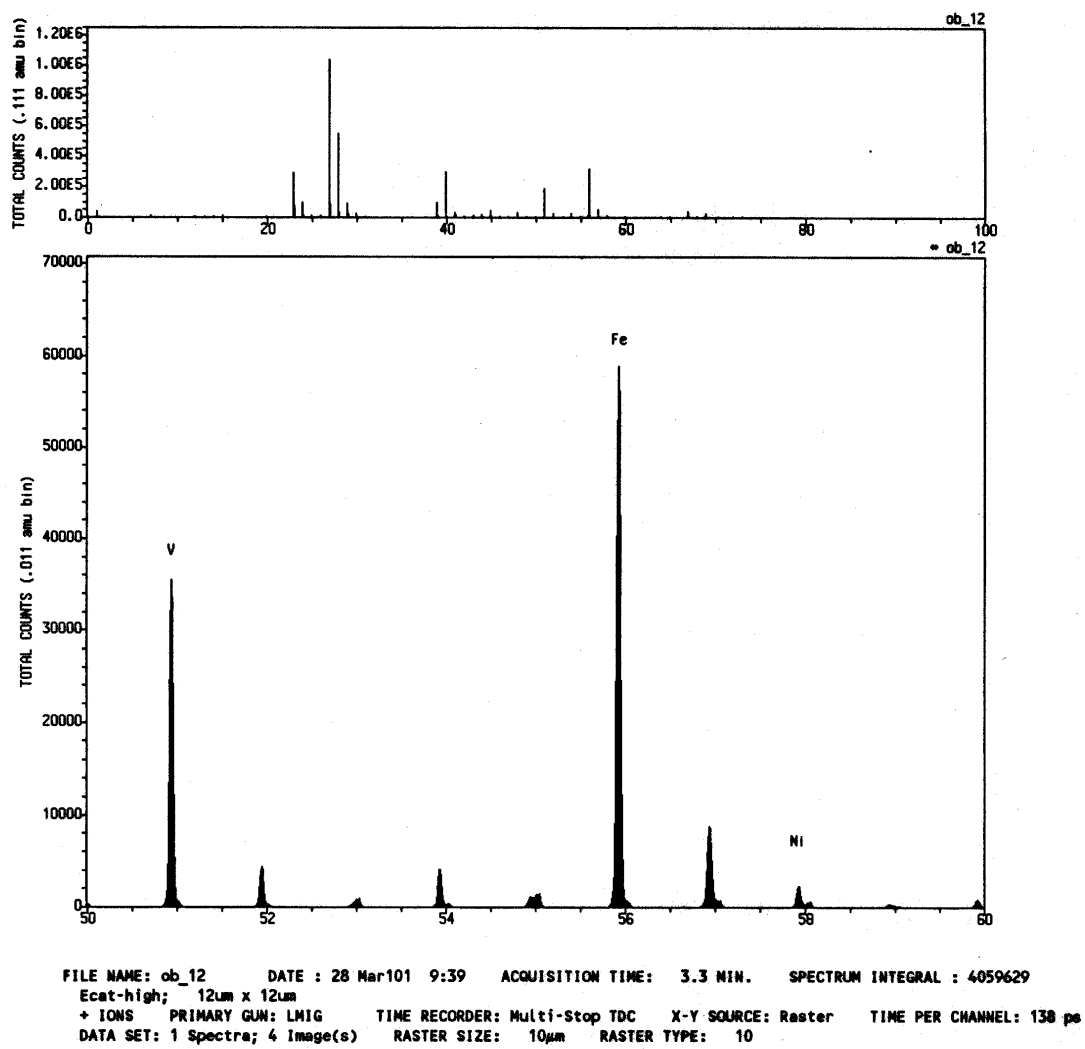
Figure 8.9 TOF-SIMS Spectrum on the Surface of ECat-HIGH Catalyst Particle

File Name:
ob_12t
Mass:
Lo: 0.0000
Hi: 1000.0000
Status:
Saved On Disk
Spectrum:
ob_12
Image Scale:

2 μm
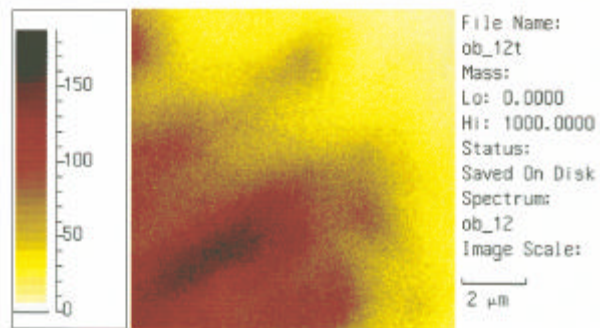
Comments: Total Ion Image, 12x12um

File Name:
ob_12v
Mass:
Lo: 50.8000
Hi: 51.0111
Status:
Saved On Disk
Spectrum:
ob_12
Image Scale:

2 μm
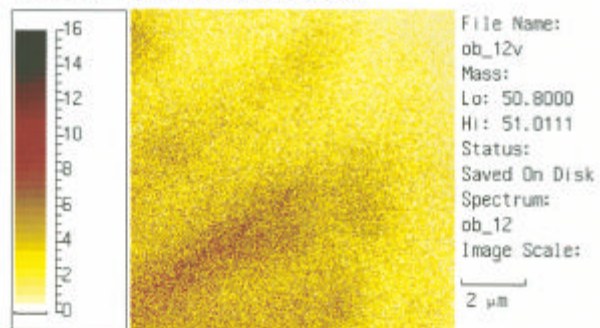
Comments: Vanadium Image, 12x12um

File Name:
ob_12fe
Mass:
Lo: 55.7667
Hi: 55.9778
Status:
Saved On Disk
Spectrum:
ob_12
Image Scale:

2 μm

Comments: Iron Image, 12x12um

Figure 8.10 SIMS Images on the Surface of ECat-HIGH Catalyst Particle
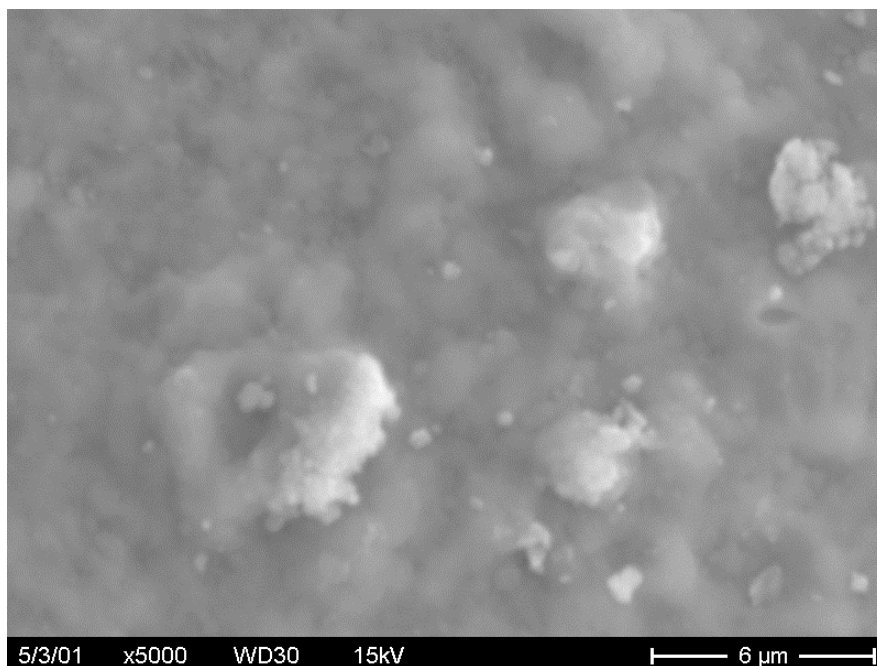
Figure 8.11 Secondary Electron Image on the Surface of ECat-HIGH Catalyst Particle
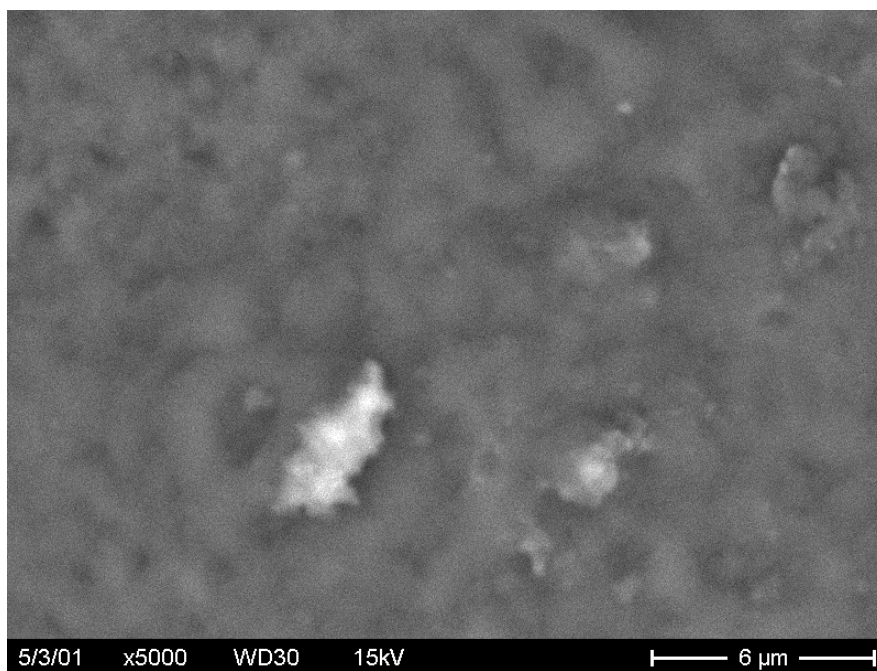
Figure 8.12 Backscattered Electron Image on the Surface of ECat-HIGH Catalyst Particle
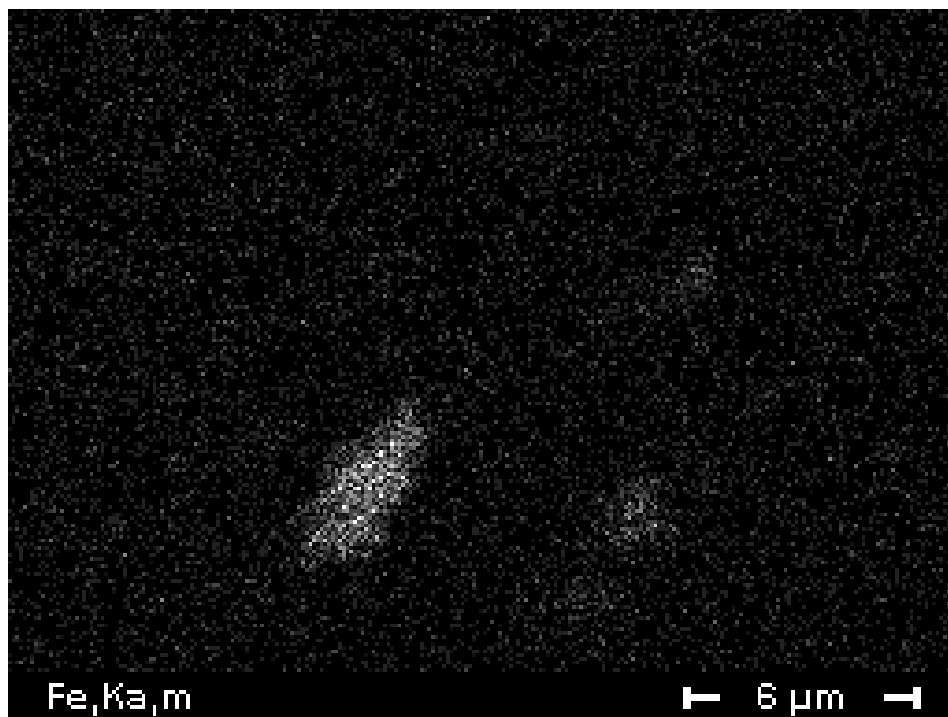
Figure 8.13 X-ray Mapping for Iron on the Surface of ECat-HIGH Catalyst Particle
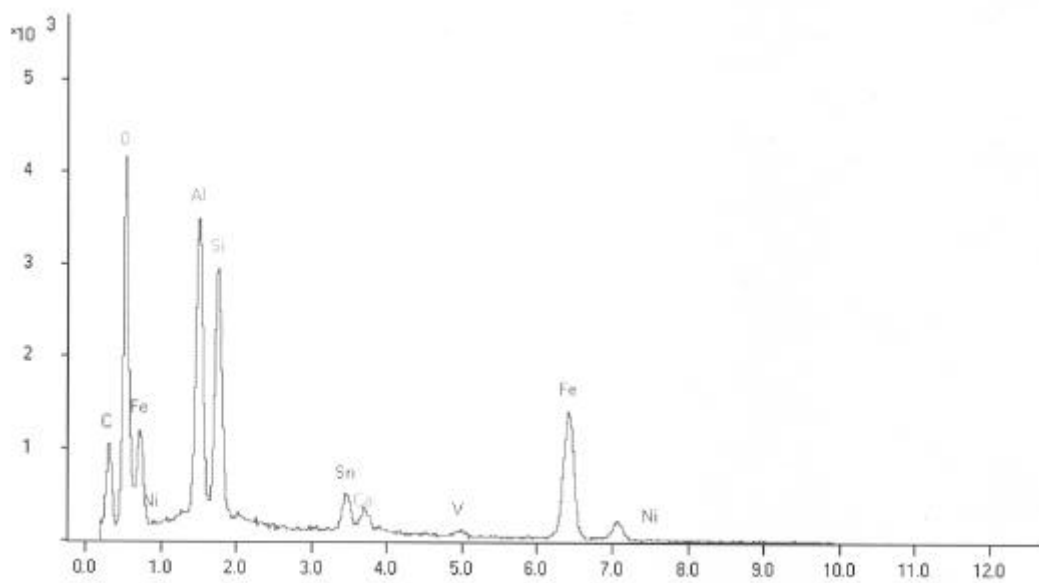
Figure 8.14 EDS Spectrum of the High Density Particulate on the Surface of ECat-HIGH Catalyst Particle
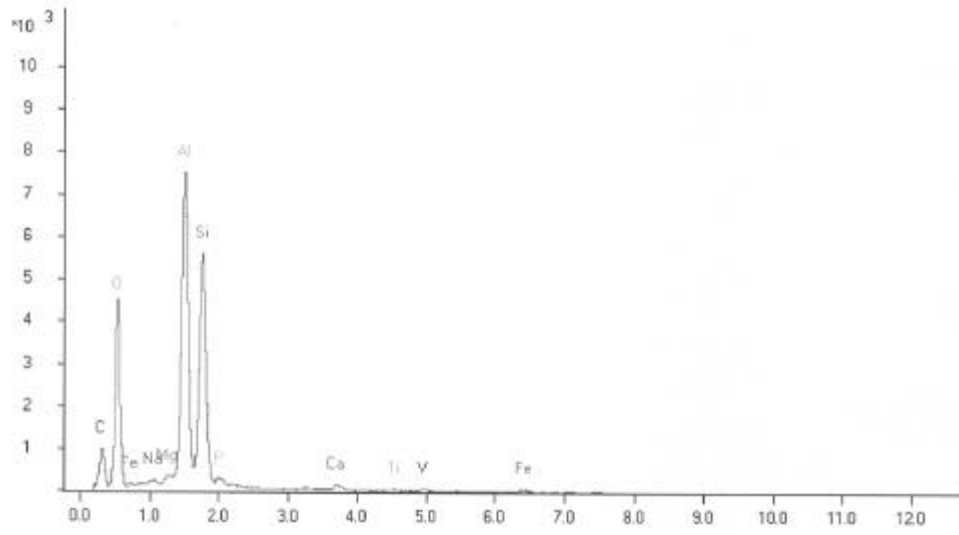
Figure 8.15 EDS Spectrum at the Ball-shaped Debris
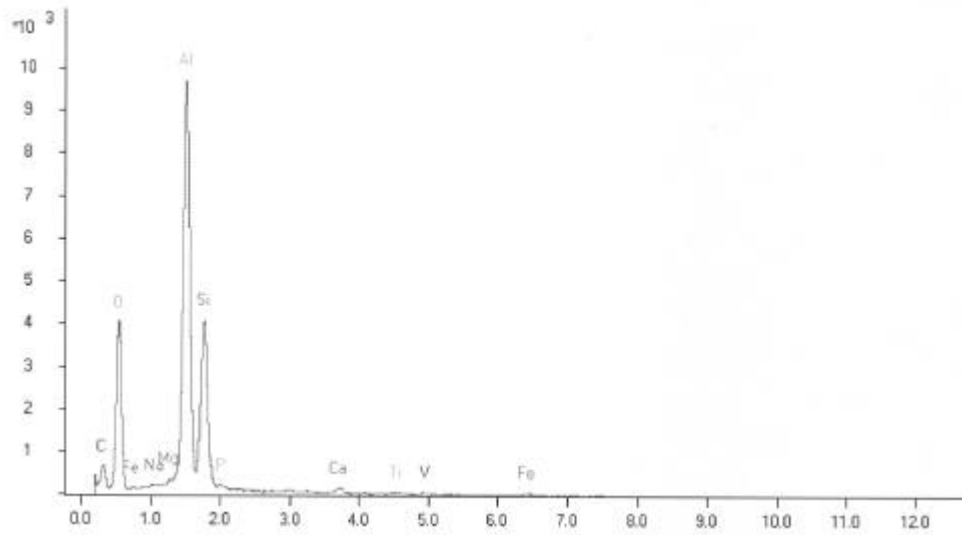
Figure 8.16 EDS Spectrum Adjacent to the Ball-shaped Debris

9.0 CONCLUSIONS

Temperature programmed techniques, TPR and TPO, were successfully applied to characterize metal-contaminated commercial FCC equilibrium catalysts. TPR spectra of commercial equilibrium catalysts were deconvoluted into three peaks. The peak that appears at low temperature (500-525 °C) was assigned to the reduction of NiO and V_2O_5. The peak at around 690 °C was assigned to continuation of vanadium pentoxide reduction at relatively high vanadium concentration on the catalyst. The high-temperature peak above 800 °C was assigned to the reduction of nickel aluminate and silicate type compounds.

TPO was used for the characterization of coke on spent equilibrium catalyst. The nature of coke and its hydrogen and carbon contents were determined in the presence of metal contaminants. The effects of these metals on carbon combustion kinetics were observed by TPO profiles. These metals cause oxidation temperature in TPO spectrum to shift to lower temperatures significantly by acting as an oxidation catalyst. TPO profiles of spent equilibrium catalysts from the cracking of both sour imported heavy gas oil (SIHGO) and ASTM standard feed were deconvoluted into four peaks (Peak K, L, M and N). The Peak K was attributed to the oxidation of more reactive coke rich in hydrogen content. Peak L in the TPO spectrum was assigned to the "contaminant" coke in the vicinity of metals. Peak M was assigned to the "catalytic" coke formed by cracking reactions. The Peak N was assigned to the more refractory type coke known as "Conradson" coke which is oxidized at high temperatures.

The effects of pretreatment of catalyst with hydrogen and methane on the TPO spectra (i.e., the nature and location of coke) were determined. The amount of coke does not have any significant effect on the shape of TPO spectra. However, pretreatment affects the shape of TPO profile in the presence of high metal concentration.

Pretreatment with both hydrogen and methane improved the performance of the FCC catalyst with high metal concentration by decreasing the yields of hydrogen and coke and increasing the gasoline yield. Hydrogen transfer reactions were evaluated by measuring C_4 paraffin-to-C_4 olefin ratios. Hydrogen transfer reactions decrease with metal concentration. Pretreatment with hydrogen and methane causes the hydrogen transfer reactions to increase. Reduction in the gasoline yield in the presence of metals was found to be due to mainly increase in the coke yields. Metals do not play a significant role in heavy bottoms conversion reactions. However, metals affected the secondary reactions in the cracking process. Enhancement of catalyst performance coincides with the disappearance of peak at around 690 °C in the TPR profile, after pretreatment with hydrogen at 700 °C. This suggests the vanadium oxides represented by this intermediate peak have high dehydrogenation activities during cracking reactions.

The surface area measurements before and after cracking reactions identified the location of coke on spent catalyst. Surface area measurements indicated that the coke formed during cracking reactions preferentially deposits in the micropores of the catalyst.

AFM images helped us to visualize the surface pores as well as the architecture that surrounds the pore's entrance of equilibrium FCC catalysts. Surface roughness decreases with increasing metal concentration and age of the catalyst. The debris was observed on the surface of all equilibrium catalysts. The presence of iron was detected in some of this debris using SEM-EDS analysis.

10.0 RECOMMENDATIONS
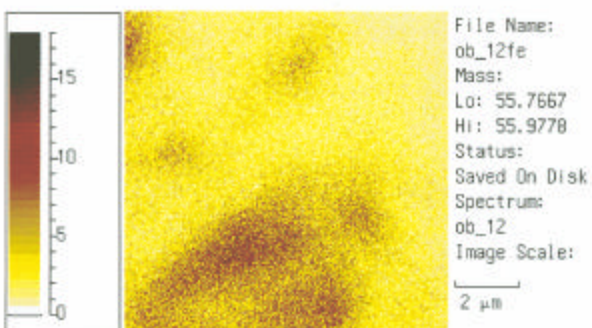
The temperature-programmed oxidation (TPO) apparatus developed during this study monitors the instantaneous O_2 consumption. During the TPO experiment CO_2 from the combustion reaction is condensed in a liquid nitrogen trap. At the end of the run the amount of CO_2 is measured to determine the carbon content of coke. By measuring the amount of CO_2 formed and O_2 consumed, the H/C ratio can be determined from the stochiometry of coke combustion reaction. At very low hydrogen and carbon content on the spent catalyst, the H/C ratio cannot be determined accurately. In order to increase the accuracy, it is recommended that the apparatus be modified to measure the amount of H_2O formed during TPO analysis. This task can be achieved with a simple modification to existing experimental set-up. A hygrometer can be added before the dry-ice/acetone trap to record the humidity downstream of the reactor. The hygrometer can be calibrated by decomposing known amounts of $Ca(OH)_2$. A similar modification has also been described by Li et al., 1998.

Since TPO analysis reveals very useful information about the nature and location of coke on the catalyst this experimental technique and the interpretation of TPO spectrum should be standardized like an ASTM method. This definitely will help the comparison of data obtained from different laboratories.

MAT results have shown that the contaminant metals on the equilibrium catalysts causes excess hydrogen and coke production due to the dehydrogenation reactions catalyzed by these metals. Cracking of a model compound with a tracer may help the interpretation of TPO results. Then, this information from TPO analysis and cracking experiments can be used to understand the effect of pretreatment with hydrogen and methane on the dehydrogenation activities of these metals.

It is also recommended to characterize the liquid products from cracking reactions. This can be done by PIONA analysis (Paraffin Isoparaffin Olefin Naphthene Aromatic) using GC or near-infrared spectroscopy. PIONA analysis may help to see the effect of metal contaminants on liquid product distribution.

BET and *t*-plot surface areas of calcined and coked catalyst samples were calculated from the nitrogen adsorption measurements. It was interesting to observe the significant changes in BET C values of calcined and coked catalyst samples. BET C value is a constant that is related to the heat of adsorption. This value is mainly influenced by the surface nature of pore walls in the sample, such as the polarity of the surface. Since the nitrogen molecules have a quadrupole, the interaction between the adsorbed nitrogen molecules and the surface increases with polarity. Hence, heat of adsorption increases. It is expected that the sample with a low BET C is more hydrophobic. Further systematic nitrogen adsorption analysis of calcined and coked catalyst samples is recommended to determine the possible relation between the BET C values and the surface nature of pore walls covered by coke molecules.

11.0 REFERENCES

Afzal, M., Theocharis, C. R., and Karim, S., Colloid. Polym. Sci. **271**, 1100 (1993).

Agrawal, B. B., and Gulati, I. B., Petroleum and Hydrocarbons **6**, 193 (1972).

Anderson, S. L. T., and Lundin, S. T., Appl. Catal. **9**, 317 (1984).

Arey, W. F., and Kronenberger, L., Oil Gas J. **66,** 131 (1969).

Armstrong, L. G., and Pratt, K. C., Fuel Process. Technol. **6**, 137 (1972).

Baker, R. T., and Metcalfe, I. S., Ind. Eng. Chem. Res. **34**, 1558 (1995).

Baker, R. W., Maher, P. K., and Blazek, J. J., Hydrocarbon Process. **17**, 125 (1968).

Barbi, N. C., Electron Probe Microanalysis using Energy Dispersive X-ray Spectroscopy, Princeton Gamma-Tech. Inc., Princeton, NJ, 1982.

Barbier, J., Churin, E., and Marecot, P., J. Catal. **126**, 228 (1990).

Bartholdy, J., Zeuthen, P., and Massoth, F. E., Appl. Catal. **129**, 33 (1995).

Bearden, R., and Stuntz, G. F., U.S Patent 4,409,093, Oct. 11 (1983a).

Bearden, R., and Stuntz, G. F., U.S Patent 4,372,840, Feb. 8 (1983b).

Bearden, R., and Stuntz, G. F., U.S Patent 4,280,896, July 28 (1981).

Beck, H.W., Carruthers, J. D., Cornelius, E. B., Hettinger, W. P., Kovach, S. M., Palmer, J. L., and Zandona, O. J., U.S. Patent 4,432,890, Feb. 21 (1984).

Bencosme, S., and Labady, M., Appl. Catal. **22**, 221 (1986).

Bernardo, C. A., and Trimm, D. L., Carbon **17**, 115 (1979).

Bertsch, C. F., U.S. Patent 4,522,704, June 11 (1985a).

Bertsch, C. F., U.S. Patent 4,504,381, March 12 (1985b).

Bertus, J. B., and McKay, D. L., U.S. Patent 4,377,494, March 22 (1983).

Beyerlein, R. A., Reagan, W. J., Zajac, G. W., Hall, J. B., Huggins, B. J., Choi-Feng, C., Jones, K. W., and Spanne Per., " 13th North American meeting of the catalysis society", Pittsburgh, PA, Paper B-12, (1993).

Beuther, H., and Flinn, R. A., Ind. Eng. Chem. Prod. Res. Dev. **2**, 53 (1963).

Blazek, J. J., Oil Gas J. **71**, 65 (1973b).

Blazek, J. J., Catalagram **42**, 3 (1973a).

Bohmer, R. W., McKay, D. L., and Knopp, D. L., Presented at the National Petroleum Refiners Association Annual Meeting, San Francisco, CA, paper AM-89-51 (1989).

Boock, L. T., Petti, T. F., Rudesill, J. A., ACS Symposium Series **634**, 171 (1996).

Boock, L. T., Petti, T. F., Rudesill, J. A., John, A., Proceedings of the 210th National Meeting of the American Chemical Society, Chicago, IL, 421 (1995).

Brevoord, E., Pouwels, A. C., Olthof, F. P. P., Wijngaards, H. N. J., and O'Connor P., ACS Symposium Series, **634**, 340 (1996).

Brunauer, S., Emmett, P. H., Teller, E., J. Amer. Chem. Soc. **60**, 309 (1938)

Burk, E. H., Yoo, J. S., Karch, J. A., and Sun, J. Y., U.S Patent 4,101,444, July 18 (1978).

Burk, E. H., Yoo, J. S., Karch, J. A., and Sun, J. Y., U.S Patent 4,163,709, Aug. 7 (1979a).

Burk, E. H., Yoo, J. S., Karch, J. A., and Sun, J. Y., U.S Patent 4,163,710, Aug. 7 (1979b).

Cadet, V., Raatz, F., Lynch, J., and Marcilly, Ch., Appl. Catal. **68**, 263 (1991).

Castillo, C., and Hayes, J. C., U.S Patent 4,364,848, Dec. 21 (1982a).

Castillo, C., and Hayes, J. C., U.S Patent 4,382,015, May 3 (1983a).

Castillo, C., and Hayes, J. C., U.S Patent 4,404,090, Sept. 13 (1983b).

Castillo, C., and Hayes, J. C., U.S Patent 4,361,496, Nov. 30 (1982b).

Chen, I., and Shine, D. W., Ind. Eng. Chem. Res. **27**, 429 (1988).

Chen, N. Y., Proc. Fifth Int. Congr. Catal. **2**, 1343 (1972).

Cheng, W. C., Juskels, M. V., and Suárez, W., Appl. Catal. **103**, 87 (1993).

Chester, A. W., Prepr. Div. Pet. Chem., National Meeting of the Am. Chem. Soc. **26**, 505 (1981).

Chester, A. W., and Stover, W. A., U.S. Patent 4,276,149, June 30 (1981).

Chester, A. W., Chu, P., Huss, A., and Kirker, G. W., U.S. Patent 4,919,787, April 24 (1990).

Ciapetta, F. G. and Henderson, D. S., Oil Gas J. **65**, 88 (1967).

Cimbalo, R. N., Foster, R. L., and Wachtel, S. J., Oil Gas J. **70**, 112 (1972).

Connor, J. E., Rothrock, J. J., Birkhimer, E. R., and Leum, L. V., Ind. Eng. Chem. Res. **49**, 276 (1957).

Crane, H. R., Connor, J. E., and Masologites, G. P., Pet. Refin. **40**, 168 (1961).

Dadyburjor, D. B., Catalysis **9**, 229 (1992).

Dale, G. H., and McKay, D. L., Hydrocarbon Process. **56**, 97 (1977).

Dandekar, A., Baker, R. T. K., and Vannice, M. A., Carbon **36**, 1821 (1998).

Dawoud, S. R., and Syed, A. A., Fuel Sci. Technol. Int. **10**, 141 (1992).

Derouane, E. G., Proceedings of the Ketjen Catalyst Symposium, The Netherlands, paper # G-3, (1986).

Dimitriadis, V. D., Lappas, A. A., and Vasalos, L. A., Fuel. **77**, 1377 (1998).

Doolin, P. K., Hoffman, J. F., and Mitchell, M. M., Appl. Catal. **71**, 233 (1991).

Dougan, T. J., Alkemade, U., Lakhanpal, B., and Boock, L. T., Oil Gas J. **92**, 81(1994).

Dreiling, M. J., and Schaffer, A. M., J. Catal. **56**, 130 (1979).

Duprez, D., Fadili, K., and Barbier, J. Ind. Eng. Chem. Res. **36**, 3180 (1997).

Durante, V. W., Olszanski, D. J., Reagan, W. J., and Brown, S. M., U.S. Patent 4,430,199, Feb. 7 (1984).

Edison R. R., Siemssen, J. O., and Masologites, G. P., Oil Gas J. **74**, 54 (1976).

English, A. R., and Kowalczyk, D. C., Oil Gas J. **82**, 127 (1984).

Erickson, H., US Patent 3,168,462, Feb. 1 (1965).

Farag, H., Ng, Siauw, and de Lasa H., Ind. Eng. Chem Res. **32**, 1071 (1993).

Feng, L., Li, X., Dadyburjor, D. B., and Kugler. E. L., J. Catal. **190**, 1 (2000).

Feron, B., Gallezot, P., and Bourgogne, M., J. Catal. **134**, 469 (1992).

Figueiredo, J. L., Fuel **65**, 1377 (1986).

Fleisch, T. H., Meyers, B. L., Ray, G. J., Hall, J. B., Marshall, C. L., J. Catal. **99**, 117 (1986)

Gall, J. W., Nielsen, R. H., McKay, D. L., and Mitchell, N. W., Presented at the National Petroleum Refiners Association Annual Meeting, San Antonia, TX, paper AM-82-50, (1982).

Gates, B. C., Katzer, J. R., and Schuit, G. C. A., Chemistry of Catalytic Processes, McGraw-Hill Book Company, 1979.

Geisler, H., and Groenenboom C. J., Proceedings of the Akzo Catalysts Symposium, The Netherlands, paper # F-5, (1988).

Germain, J. E., Catalytic Conversions of Hydrocarbons, Academic Press, London, 1969.

Gerritsen, L. A., Wijngaards, H. N. J., Verwoert, J., and O'Connor, P., Akzo Catalyst Symposium, The Netherlands, p.109, (1991).

Ginzel, W., Proceedings of the Katalistiks' 6th Annual Fluid Cat Cracking Symposium, Munich, West Germany, paper #8, (1985).

Goula, M. A., Lemonidou, A. A., and Efstathiou, A. M., J. Catal. **161**, 626 (1996).

Grane, H. R., Connor, J. E., and Masologites, G. P., Petroleum Refiner. **40**, 168 (1961).

Grau, J. M. and Parera, J. M., Appl. Catal. **70**, 9 (1991).

Guisnet, M., and Magnoux, P., Appl. Catal. **54**, 1 (1989).

Haas, A., Suárez, W. and Young, G. W., in " AIChE Symposium Series: Advanced Fluid Catalytic Cracking Technology", (K. C. Chuang, George W. Young and M. Benslay, Eds.), **88**, 133 (1992).

Habib, E. T., Owen, H., Snyder, P. W., Streed, C. W., and Venuto, P. B., Ind. Eng. Chem. Prod. Res. Dev. **16**, 291 (1977).

Harding, R. H., Zhao, X., Qian, K., Kuppuswamy, R., Cheng, W. C., Ind. Eng. Chem. Res. **35**, 2561 (1996)

Harkins, W. D., Jura, G., J. Am. Chem. Soc. **66**, 1362 (1944)

Hayes, J. C., and Castillo, C., U.S Patent 4,447,552, May 8 (1984).

Heite, R. S., English, A. R., and Smith, G. A., Presented at the National Petroleum Refiners Association Annual Meeting, San Antonia, TX, paper AM-90-52, (1990).

Hemler, C. L., and Vermillion, W. L., Oil Gas J. **71**, 88 (1973).

Henriques, C.A., Monteiro, J. L. F., Magnoux, P., and Guisnet, M., J. Catal. **172**, 436 (1997).

Hildebrand, R. E., Huling, G. P., and Ondish, G. F., Oil Gas J. **71**, 112 (1973).

Hirschberg, E. H., Bertolacini, R. J., and Modica, F.S., U.S. Patent 4,363,720, Dec. 14 (1982).

Huling, G. P., McKinney, J. D., and Readal, T. C., Oil Gas J. **73**, 73 (1975).

Hurst, N. W., Gentry, S. J., Jones, A., and McNicol, B. D., Cat. Rev. -Sci. Eng. **24**, 233 (1982).

Jaras, S., Appl. Catal. **2**, 207 (1982).

Jouguet, B., Gervasini, A., and Auroux, A., Chem. Eng. Technol. **18**, 243 (1995).

Kelemen, S. R., Freund, H. and Mims, C. A., J. Catal. **97**, 228 (1986).

Kennedy, J. V., and Jossens, L. W., Presented at AIChE Spring National Meeting, Fuels and Petrochemicals Divisions, New FCC Technology: additives; Orlando, FL, paper 60A, (1990).

Koh, D. J., Chung, J. –S., Kim, Y. G., Lee, J. S., Nam, I. –S., and Moon, S. H., J. Catal. **138**, 630 (1992)

Koranne, M. M., Goodwin, J. G. Jr., and Marcelin, G., J. Catal. **148**, 369 (1994).

Kugler, E. L., and Leta, D. P., J. Catal. **109**, 387 (1988).

Lampert, J. K., Koermer, G. S., Macaoay, J. M., Chabala, J. M., Levi-Setti, R., Appl. Surf. Sci., 55, 149 (1992).

Larocca, M., Farag, H., Siauw, Ng and de Lasa H., Ind. Eng. Chem. Res. **29**, 2181 (1990).

Larson, O. A., and Beuther, H., Prepr. Div. Pet. Chem., Am. Chem. Soc. **11**, B-95, (1966).

Larsson, M., Jansson, J., and Asplund, S., J. Catal. **178**, 49 (1998).

Lee, F. M., Ind. Eng. Chem. Res. **28**, 920 (1989).
Lerner, B. A., and Himpsi F. L., Oil Gas J. **95**, 61 (1997).

Letzsch, W. S., Ritter, R. E., and Vaughan, D. E. W., Oil Gas J. **74**(4), 130 (1976).

Li, C. -P., and Chen, Y.W., Thermochim Acta **256**, 457 (1995).

Li, C., and Brown, T. C., Energy Fuels **13**, 888 (1999).

Li, C., Minh. C. L., and Brown, T. C., J. Catal. **178**, 275 (1998).

Lippens, B. C., deBoer, J. H., J. Catal. **4**, 319 (1965).

Logwinuk, A. K., and Murphy, J. R., NPRA Annual Meeting, San Antonio, TX, March 29-31, Paper AM-81-29, (1981).

Mandal, S., Das A. K., and Ghosh, S., Ind. Eng. Chem. Res. **32**, 1018 (1993).

Mark, H. W., Bertus, B. J., Robert, J. S., McKay, D. L., and Fenska, L. E., U.S. Patent 4,459,366, July 10 (1984).

Mark, H.W., and Ernest, A. Z., U.S. Patent 4,326,990, April 27 (1982).

Martinez, N. P., Lujano, J. A., Kizer, O., P. de Golia, and Cuears M. A., Proceedings of the Ketjen Catalysts Symposium '86, The Netherlands, Paper # F-7, (1986).

Martinez, N., Lujano, J., Alvarez, N., Lubinkowski, J., and McEven, W., U.S. Patent 5,401,384, March 28 (1995).

Maselli, J. M., and Peters, A. W., Cat. Rev. -Sci. Eng. **26**, 525 (1984).

Masologites, G. P., and Beckberger, L. H., Oil Gas J. **71**, 49 (1973).

Masologites, G. P., and Jacobs, H. E., Oil Gas J. **73**, 94 (1975).

McCarty, J.G., and Wise, H., J. Catal. **57**, 406 (1979).

McCulloch, D. C., Oil Gas J. **73**, 53 (1975).

McGovern, S. J., Schatz, K. W., and Zrinscak, F. S., U.S. Patent 4,176,083, Nov. 27 (1979).

McKay, D. L., U.S. Patent 4,025,458, May 24 (1977a).

McKay, D. L., U.S. Patent 4,031,002, June 21 (1977b).

McKay, D. L., U.S. Patent 4,178,267, Dec. 11 (1979c).
McKay, D. L., U.S. Patent 4,111,845, Sept. 5 (1978).

McKay, D. L., U.S. Patent 4,141,858, Feb. 27 (1979a).

McKay, D. L., Bertus, B. J., U.S. Patent 4,166,806, Sept. 4 (1979b).

Menon, P. G., J. Mol. Catal. **59**, 207 (1990).

Minh, C. L., Jones, R. A., Craven, I. E., and Brown, T. C., Energy Fuels **11**, 463 (1997).

Mitchell, B. R., and Vogel, R. F., U.S. Patent 4,707,461, Nov. 17 (1987).

Moljord, K., Magnoux, P., and Guisnet, M., Catal. Lett. **25**, 141 (1994).

Montgomery, J. A., Catalagram **39**, 3 (1973).

Morozov, B. F., Danilova, R. A., Masagutov, R. M., and Berg, G. A., Ind. Chem. Eng. **13**, 324 (1973).

Murphy, J. R., Oil Gas J. **68**, 72 (1970).

Murthy, I. A. P. S., and Swamy, C. S., Journal of Materials Science **28**, 1194 (1993).

Nielsen, R. H., McKay, D. L., and Dale, G. H., U.S. Patent 4,148,712, April 10 (1979).

Occelli, M. L., and Gould, S. A. C., Chemtech May 24 (1994).

Occelli, M. L., Kalwei, M., Wölker, A., Eckert, H., Auroux, A., Gould, S. A. C. J. Catal. **196**, 134 (2000).

Occelli, M. L., Catal. Rev.- Sci. Eng. **33**, 241 (1991).

Occelli, M. L., and Kennedy, J. V., U.S. Patent 4,465,779, Aug. 14 (1984).

Occelli, M. L., Psaras, D., and Suib, S. L., J. Catal. **96**, 363 (1985).

Oh, E. S., Park, Y. C., Lee, I. C., and Rhee, H. K., J. Catal. **172**, 314 (1997).

Otake, Y., and Jenkins, R. G., Carbon **31**, 109 (1993).

Oudar, J., and Wise, H., Deactivation and Poisoning of Catalysts, Marcel Decker, Inc., New York, 1985.

Owen, H., and Venuto, P. B., U.S. Patent 4,035,285, July 12 (1977).

Ozawa, J. K., Porter, R. F., and Humble, J. R., Oil Gas J. **62**, 101 (1964).

Phelps, J .M., Oil Gas J. **55**, 8 (1957).

Pieck, C. L., Jablonski, E. L., Parera, J., Frety, R., and Lefebvre, F., Ind. Eng. Chem. Res. **31**, 1017 (1992).

Plank, C. J., and Rosinski, E. J., Chem. Eng. Prog. Symp. Ser. **73**, 26 (1967).

Plank, C. J., Rosinski, E. J., and Hawthorne, W. P., Ind. Eng. Chem. Prod. Res. Dev. **3**, 165 (1964).

Pohlenz, J. B., Oil Gas J. **61**, 124 (1963).

Pompe, R., Jaras, S., and Vamerberg, N., Appl. Catal. **13**, 171 (1984).

Querini, C. A., and Fung, S. C., Catalysis Today **37**, 277 (1997).

Readal, T., McKinney, J. D., and Titmus, R. A., U.S. Patent 3,977,963, Aug. 31 (1976).

Reichle, A. D., Proceedings of the Akzo Catalyst Symposium, The Netherlands, paper # G-2, (1988).

Rene Bos, A. N., Tromp, Peter J. J., and Akse, H. N., Ind. Eng. Chem. Res. **34**, 3808 (1995).

Ritter, R. E., Oil Gas J. **73**, 41 (1975).

Ritter, R. E., and Young, J. W., Davison Catalogram **68**, 1 (1984).

Ritter, R. E., Blazek, J. J., and Wallace, D. N., Oil Gas J. **72**, 99 (1974).

Ritter, R. E., Welsh, W. A., Rheaume, L., and Magee, J. S., NPRA Annual Meeting, San Antonio, TX, paper AM-81-44, (1981).

Rothrock, J. J., Ind. Eng. Chem. **49**, 272 (1957).

Rudesill, J. A., and Peters, A. W., in Fluid Cracking Catalysts, Occelli, M. L., and O'Connor, P., editors, p. 71, Marcel-Decker, (1998).

Rush, J. B., NPRA Annual Meeting, San Antonio, TX, paper AM-81-43, (1981a).

Rush, J. B., Chemical Engineering Progress **77**, 29 (1981b).

Samyratov, S. T., Salibaev, T. O., Ponomarev, V. D., (1967) in: Yoo, J. S., Burk, E. H., Karch, J. A., and Voss, A. P., Ind. Eng. Chem. Res. **29**, 1183 (1990).
Sandford, R. A., Erickson, H., Gossett, E. C., and Van Petten, S. L., Oil Gas J. **60**, 92 (1962).

Sato, T., and Ito, Y., (1970): in Yoo, J. S., Burk, E. H., Karch, J. A., and Voss, A. P., Ind. Eng. Chem. Res. **29**, 1183 (1990).

Sax, N. I., Dangerous Properties of Industrial Materials, Van Nostrand Reinhold Company, New York, 1979.

Scherzer, J., Octane-Enhancing FCC catalysts, Marcel Dekker Inc., New York, 1990.

Schwartz, A. B., US Patent 3,147,228, April 10 (1963).

Senn, D. R., U.S. Patent 5,389,233, Feb. 14 (1995a).

Senn, D. R., U.S. Patent 5,378,349, Jan. 3 (1995b).

Speronello, B. K., and Reagan, W. J., Oil Gas J. **82**, 139 (1984).

Srivastava, R. D., Stiles, A. B., Jones, G. A., J. Catal. **77**, 192 (1982).

Stine, L. O., and Richter, S. I., U.S Patent 4,268,416, May 19 (1981)

Stobbe-Kreemers, A. W., van Leerdam, G. C., Jacobs, J. P., Brongersmu, H. H., and Scholten,J. J. F., J. Catal. **152**, 130 (1995).

Stratiev, von D., Minkov, D., and Haas, A., Erdol and Kohle Erdgas, Petrochem., **113**, 436 (1997).

Stuntz, G. F., and Bearden, R., U.S. Patent 4,280,895, July 28 (1981a).

Stuntz, G. F., and Bearden, R., U.S. Patent 4,372,841, Feb. 8 (1983).

Stuntz, G. F., and Reid, T. A., U.S. Patent 4,504,380, March 12 (1985b).

Stuntz, G. F., and Schucker, R. C., U.S. Patent 4,504,379, March 12 (1985a).

Subramanian, R. B., Effect of Molecular Type on Catalytic Cracking Performance, M.SChE Thesis, West Virginia University, (1993).

Suggitt, R. M., Paull, P.L., U.S Patent 4,013,546, March 22 (1977).

Tatterson, D. F., and Ford, W. D., U.S Patent 4,298,459, Nov. 3 (1981a).

Tatterson, D. F., and Mieville, R. L., Ind. Eng. Chem. Res. **27**, 1595 (1988).

Tatterson, D. F., and Vasalos, I. A., U.S Patent 4,280,898, July 28 (1981b).

Teixeira, S. V. L. S., Frety, R., and Schmal, M., Ind. Eng. Chem. Res. **33**, 1692 (1994).

Tu, H., U.S. Patent 4,295,955, Oct. 20 (1981).

Tu, H., U.S. Patent 4,364,847, Dec. 21 (1982).

Upson, L. L., Hydrocarbon Process. **60**, 253 (1981).

Valkoric, V., Trace Elements in Petroleum, The Petroleum Publishing Co., Tulsa, Oklahoma, pp. 72-73, (1978).

Van Doorn, J., Verheul, R. C. S., Singoredjo, L., Moulijn, J. A., Fuel **65**, 1383 (1986).

Van Doorn, J., Barbolina, H. A. A., and Moulijn, J. A., Ind. Eng. Chem. Res. **31**, 101 (1992).

Venuto, P. B., and Habib, E. T., Fluid Catalytic Cracking with Zeolite Catalysts, Marcel Dekker Inc., New York, 1979.

Voge, H. H., Catalysis, Volume 6, (Emmet, P. H. Ed.) Reinhold, New York, 1958.

Wachtel, S. J., Baillie, L. A., Foster, R. L., and Jacobs, H. E., Prepr. Div. Pet. Chem., Am. Chem. Soc. **16,** A-55, (1971).

Wallenstein, D., Kanz, B., Haas, A., Appl. Catal. **192**, 105 (2000).

Weisz, P. B., Pure Appl. Chem. **52**, 2091 (1980).

Weisz, P. B., U.S. Patent 3,413,212, Nov. 26 (1968).

Woltermann, G. M., Dodwell, G., and Lerner, B., Presented at the National Petroleum Refiners Association Annual Meeting, San Antonia, TX, paper AM-96-46, (1996).

Wormsbecher, R. F., Peters, A. W., and Maselli, M., J. Catal. **100**, 130 (1986).

Wrammerfors, Å., and Anderson, B., J. Catal. **147**, 82 (1994).

Xu, W. Q., Yin, Y. G., Suib, S. L., and O'Young, C. L., J. Phys. Chem. **99**, 758 (1995).

Yanik, S. J., and O'Connor, P., Chem. Eng. World **32**, 47 (1997).

Yen, L. C., Wrench, R. E. and Kuo, C. M., Oil Gas J. **83**, 87 (1985).

Yoo, J. S., U.S. Patent 4, 319,983, March 16 (1982).
Yoo, J. S., Burk, E. H., Karch, J. A., and Voss, A. P., Ind. Eng. Chem. Res. **29**, 1183 (1990).

Yoo, J. S., Karch, J. A., and Burk, E. H., Ind. Eng. Chem. Res. Dev. **25**, 549 (1986)

Yoshinura, Y., and Furimsky, E., Fuel **65**, 1388 (1986).

Zeuthen, P., and Cooper, B. H., Ind. Eng. Chem. Res. **134**, 755 (1995).

Zrinscak, Sr., Fred, S., and Karsner, G. G., U.S. Patent 4,162,213, July 24 (1979).

12.0 APPENDICES

A. Separation of Lighter Gases

Gas chromatograph: VARIAN 3600

Detectors used: Flame Ionization Detector (FID) & Thermal Conductivity Detector (TCD)

Detector temperatures: 350 ℃

Injector temperature: 220 ℃

Carrier gas: Nitrogen

Carrier gas flow rate: 30 cc/min

Columns used: PLOT, HAYESEP

Temperature programming:

40 ℃ for two minutes
40 ℃ _150 ℃ at 20 ℃ per minute
150 ℃ for zero minute
150 ℃ _220 ℃ at 10 ℃ per minute
220 ℃ for six minutes

B. Conditions for Simulated Distillation

Gas chromatograph: VARIAN 3400

Detectors used: Flame Ionization Detector (FID)

Detector temperatures: 350 ℃

Injector temperature: 220 ℃

Carrier gas: Nitrogen

Cooling medium: Liquid Nitrogen

Carrier gas flow rate: 30 cc/min

Columns used: Supelco Petrocol B packed column

Sample size injected: 0.2-05 : 1

Temperature programming:

- 35 ℃ for two minutes
-35 ℃ _350 ℃ at 10 ℃ per minute
350 ℃ for zero minute

Steps involved: Calibration standard run, reference oil mix run, MAT sample run

C. Data Analysis

Mass balance:

The decision about the acceptance of performed test will be determined by calculating the recovery as follows:

$$R \ (recovery) = \frac{W_g + W_L + W_c}{W_F}$$

Where W_g is the weight of gaseous product, W_L is the weight of liquid product, W_c is the weight of the coke obtained. The recovery value should be within 97% to 103% for the run to be accepted.

Raw Yields:

Gas components: (H_2-C_4's)

$$Y_i = \frac{W_i}{W_F} * 100$$

Where i represents the ith gaseous product.

Gasoline:

$$Y_g = \frac{(X_g * W_L)}{W_F} * 100$$

Where X_g is the mass fraction of gasoline in the combined liquid products.

Light Cycle Oil (LCO):

$$Y_{LCO} = \frac{(X_{LCO} * W_{L)}}{W_F} * 100$$

Where X_{LCO} is the mass fraction of LCO in the combined liquid products.

Heavy Cycle Oil (HCO):

$$Y_{HCO} = \frac{(X_{HCO} * W_L)}{W_F} * 100$$

Where X_{HCO} is the mass fraction of HCO in the combined liquid products.

Coke:

$$Y_{coke} = \frac{W_c}{W_F} * 100$$

Where W_c is the weight of coke formed.

$$Conversion(wt\%) = \frac{W_F - (1 - X_g) * W_L}{W_F} * 100$$

D. Safety Provisions

The gases needed for the equipment are supplied by safely installed stainless steel tubing lines throughout the laboratory. The connection points of these lines will be checked for possible leaks at regular intervals. Gas cylinders are securely chained or strapped to a bench, wall or other means of stable support. All chemicals, which will be used in this research, are stored in a closet having suitable signs indicating the chemicals are stored there and this closet is just below the hood. All the gases used in the experiments are vented into a hood in the laboratory. The wastes such as oil leftover in the syringe, solvent used for washing etc. are stored in a container, which is labeled as oil waste and this container is kept closed under the hood.

Protective equipment such as gloves, goggles or face shields and respiratory protection are available in the laboratory. A fully buttoned lab coat is always used in the laboratory eye protection, preferably a face shield and proper type of protective gloves are used when working with hazardous chemicals. Respiratory protection is used in situations involving hazardous dust or high atmospheric concentration of toxic chemicals. The properties of chemicals involved in this research are given in Table D.1. The specific emergency procedures are already posted next to the equipment. These sheets explain the steps to be followed in case of a malfunction, fire or a leak. An eye wash fountain, fire extinguisher and a safety shower are present in the laboratory. The list of persons to be notified in case of an emergency is also placed at the entrance. Detailed information to maintain a safe laboratory environment can be found in "*Safety Manual: Start-Up and Safety Procedures*" prepared by West Virginia University Department of Chemical Engineering Safety Committee in 1994.

Table D.1 Safety Properties of Chemicals (from Sax, N. L., 1979)

Chemical[*]	Toxicity	Fire Hazard	Explosion/Disaster Hazard	To Fight Fire
Carbon disulfide (CS_2)	Capable of causing death or permanent injury via oral and inhalation mode of exposure;incapacitating and poisonous.	Dangerous,when exposed to heat, flame, sparks or friction.	Severe;when exposed to heat or flame, reacts with Al, Cl_2, azides, C_sN_3,ClO, ethylamine diamine, ethylene imine, F_2, $Pb(N_3)_2$, LiN_3, NO, N_2O_4, (H_2SO_4 + permangates), K, KN_3, RbN_3, NaN_3, Zn. Dangerous; when heated to decompose emits highly toxic fumes of SO_x; can react vigorously with oxidizing materials.	Water, CO_2, dry chemical, fog, mist.
n-hexadecane ($C_{16}H_{34}$)	Unknown,insufficient data or experience recorded or available to permit a statement.	Low, when exposed to heat or flame.	Not available	Water spray mist, CO_2, dry chemical, foam
Gas Oil	Unknown,insufficient data or experience recorded or available to permit a statement.	Moderate, when exposed to heat or flame; can react with oxidizing materials.	Moderate, when exposed to heat or flame	Foam, CO_2, dry chemical
Acetone (C_3H_6O)	May cause reversible or irreversible changes to exposed tissue, not permanent injury or death; can cause considerable discomfort.	Dangerous, when exposed to heat or flame or oxidizers.	Moderate, when vapor is exposed to flame. Dangerous; due to fire and explosion hazard, can react vigorously with oxidizing materials.	CO_2, dry chemical, alcohol foam